6.11 Tectonic Models for the Evolution of Sedimentary Basins

S. Cloetingh, Vrije Universiteit, Amsterdam, The Netherlands

P. A. Ziegler, University of Basel, Basel, Switzerland

6.11.1 Introduction

In this chapter we review the formation and evolution of sedimentary basins in their lithospheric context. To this purpose, we follow a natural laboratory approach, selecting some well-documented basins of Europe. We begin with a brief outline of the evolution of tectonic modeling of sedimentary basin systems since its inception in the late 1970s. We subsequently review key features of the tectonics of rifted and compressional basins in Section 6.11.2. These include the classification of extensional basins into Atlantic type, back-arc, syn- and postorogenic rifts. This is followed by a discussion of thermal thinning of the lithosphere, doming and flood basalts, aspects of particular importance to volcanic rifted margins. We discuss the record of vertical motions during and after rifting in the context of stretching models developed to quantify rifted basin formation. As discussed in Section 6.11.2.1.5., the finite strength of the lithosphere has an important effect on the formation of extensional basins. This applies both to the geometry of the basin shape as well as to the record of vertical motions during and after rifting. We also address the tectonic control on postrift evolution of extensional basins. The concept of strength of the lithosphere has also important consequences for compressional basins. The latter include foreland basins as well as basins formed by lithospheric folding.

In Section 6.11.3, we focus on thermomechanical aspects of sedimentary basin formation in the context of large-scale models for the underlying lithosphere. We highlight the connection between the bulk rheological properties of Europe's lithosphere and the evolution of some of Europe's main sedimentary basins.

In Section 6.11.4, we investigate thermomechanical controls on continental breakup and associated basin migration processes using the NW European margin as a natural laboratory. We specifically address relationships between rift duration and extension velocities, thermal evolution, and the role of mantle plumes and melts. This is followed by a brief discussion of compressional reactivation and its consequences for postrift inversion, borderland uplift, and denudation.

In Section 6.11.5, we further develop the treatment of polyphase deformation of extensional basins taking the Black Sea Basin as a natural laboratory. We concentrate on rheological controls on basin formation affecting the large-scale basin stratigraphy and rift shoulder dynamics. We also discuss the role of intraplate stresses and lithospheric strength evolution during the postrift phase and consequences for neotectonic reactivation of the Black Sea basin system.

In Section 6.11.6, we give an overview on the interplay of extension and compression in the Pannonian–Carpathian basin system of Central Eastern Europe. We begin with a review of temporal and lateral variations in lithospheric strength in the region and its effects on late-stage basin deformation. This is followed by summary of models proposed for the development of the Pannonian–Carpathian system. We also present results of three-dimensional (3-D) modeling approaches investigating the role of 3-D distributions of load and lithospheric strength in orogenic arcs. In doing so, we focus on implications of these models for a better understanding of polyphase subsidence in the Carpathian foredeep.

For our discussion of lithospheric folding as a mode of basins formation, and for the interplay between lithosphere and surface processes in a compressional setting, we have selected the Iberian microcontinent, located within the Africa–Europe collision zone. In the first part of Section 6.11.7, we review constraints on vertical motions, present-day stress regime and interaction between surface

transport and vertical motions for Iberia at large. This is followed by a more detailed treatment of tectonic controls on drainage systems using the Ebro basin system of NE Iberia as a natural laboratory.

The closing section, Section 6.11.8, draws general conclusions and addresses future perspectives.

The origin of sedimentary basins is a key element in the geological evolution of the continental lithosphere. During the last decades, substantial progress was made in the understanding of thermomechanical processes controlling the evolution of sedimentary basins and the isostatic response of the lithosphere to surface loads such as sedimentary basins. Much of this progress stems from improved insights into the mechanical properties of the lithosphere, from the development of new modeling techniques, and from the evaluation of new, high-quality datasets from previously inaccessible areas of the globe. The focus of this chapter is on tectonic models processes controlling the evolution of sedimentary basins.

After the realization that subsidence patterns of Atlantic-type margins, corrected for effects of sediment loading and palaeo-bathymetry, displayed the typical time-dependent decay characteristic of ocean-floor cooling (Sleep, 1971), a large number of studies were undertaken aimed at restoring the quantitative subsidence history of basins on the basis of well data and outcropping sedimentary sections. With the introduction of backstripping analysis algorithms (Steckler and Watts, 1982; Bond and Kominz, 1984), the late 1970s and early 1980s marked a phase during which basin analysis essentially stood for backward modeling, namely reconstructing the tectonic subsidence from sedimentary sequences. These quantitative subsidence histories provided constraints for the development of conceptually driven forward basin models. For extensional basins this commenced in the late 1970s, with the appreciation of the importance of the lithospheric thinning and stretching concepts in basin subsidence (Salveson, 1976). After initiation of mathematical formulations of stretching concepts in forward extensional basin modeling (McKenzie, 1978), a large number of basin fill simulations focused on the interplay between thermal subsidence, sediment loading, and eustatic sea-level changes. To arrive at commonly observed more episodic and irregular subsidence curves the smooth postrift subsidence behaviour was modulated by changes in sediment supply and eustatic sea-level fluctuations. Another approach frequently followed was to input a subsidence curve, thus rendering the basin modeling package essentially a tool to fill in an adopted accommodation space (Burton *et al.*, 1987; Lawrence *et al.*, 1990). For the evolution of extensional basins this approach made a clear distinction between their syn-rift and postrift stage, relating exponentially decreasing postrift tectonic subsidence rates to a combination of thermal equilibration of the lithosphere–asthenosphere system and lithospheric flexure (Watts *et al.*, 1982).

A similar set of assumptions were made to describe the syn-rift phase. In the simplest version of the stretching model (McKenzie, 1978), lithospheric thinning was described as resulting from more or less instantaneous extension. In these models a component of lithosphere mechanics was obviously lacking. On a smaller scale, tilted fault block models were introduced for modeling of the basin fill at the scale of half-graben models. Such models essentially decouple the response of the brittle upper crust from deeper lithospheric levels during rifting phases (see, e.g., Kusznir *et al.*, 1991).

A noteworthy feature of most modeling approaches was their emphasis on the basin subsidence record and their very limited capability to handle differential subsidence and uplift patterns in a process-oriented, internally consistent manner (see, e.g., Kusznir and Ziegler, 1992; Larsen *et al.*, 1992; Doré *et al.*, 1993).

To a large extent the same was true for most of compressional basin modeling. The importance of the lithospheric flexure concept, relating topographic loading of the crust by an overriding mountain chain to the development of accommodation space, was recognized as early as 1973 by Price in his paper on the foreland of the Canadian Rocky Mountains thrust belt (Price, 1973). Also, here it took several years before quantitative approaches started to develop, investigating the effects of lithospheric flexure on foreland basin stratigraphy (Beaumont, 1981). The success of flexural basin stratigraphy modeling, capable of incorporating subsurface loads related to plate tectonic forces operating on the lithosphere (e.g., Van der Beek and Cloetingh, 1992; Peper *et al.*, 1994) led to the need to incorporate more structural complexity in these models, also in view of implications for the simulation of thermal maturation and fluid migration (e.g., Parnell, 1994). The necessary understanding of lithospheric mechanics and basin deformation was developed after a bridge was established between researchers studying deeper lithospheric processes and those who analyzed the record of vertical motions, sedimentation, and erosion in basins. This permitted the development of

basin analysis models that integrate structural geology and lithosphere tectonics.

The focus of modeling activities in 1990s was on the quantification of mechanical coupling of lithosphere processes to the near-surface expression of tectonic controls on basin fill (Cloetingh *et al.*, 1995a, 1995b, 1996, 1997). This invoked a process-oriented approach, linking different spatial and temporal scales in the basin record. Crucial in this was the testing and validation of modeling predictions in natural laboratories for which high-quality databases were available at deeper crustal levels (deep reflection- and refraction-seismic) and the basin fill (reflection-seismic, wells, outcrops), demanding a close cooperation between academic and industrial research groups (see Watts *et al.*, 1993; Sassi *et al.*, 1993; Cloetingh *et al.*, 1994; Roure *et al.*, 1996b).

Figure 1 displays the global distribution of sedimentary basins (Laske and Masters, 1997; see also: Bally and Snelson, 1980, Schlumberger, 1991). **Figure 2** gives the location of extensional and compressional basins in Europe that were selected as examples to discuss advances in data-interactive quantitative basin modeling. Applying a consistent modeling approach to different basins provides an opportunity to compare in this chapter important key parameters of basin evolution (**Table 1**), shedding light on the tectonic controls underlying observed similarities and differences in basin histories.

In the following, we review recent advances in modeling the initiation and evolution of sedimentary basins in their lithospheric context on a global and more regional scale. To the latter purpose we follow a natural laboratory approach selecting some well-documented basins of Europe. Below we first start with a summary of key features of the tectonics of rifted basins on a global scale. In doing so, we introduce in Section 6.11.2 basic concepts for the tectonics of basin formation. We begin with a review of the dynamics of extensional basin systems. First we discuss the genetic types of extensional basins followed by an overview of characteristics of thermal thinning of the lithosphere, doming and flood basalt extrusion, aspects of particular importance to volcanic rifted margins. We examine the record of vertical motions during and after rifting in the context of stretching models developed to quantify rifted basin development. In this section we proceed with thermomechanical aspects of extensional sedimentary basin development in the context of large-scale models for the underlying lithosphere. We also address the tectonic control on postrift evolution of extensional basins. In Section 6.11.2.2 we review the development and evolution of compressional basins in a lithospheric context. We focus on foreland basins and basins that evolved as a result of large-scale compressional folding of intraplate continental lithosphere. Specifically, we address the role of flexure in compressional basin evolution and the interplay between lithosphere dynamics and topography in compressional basin systems.

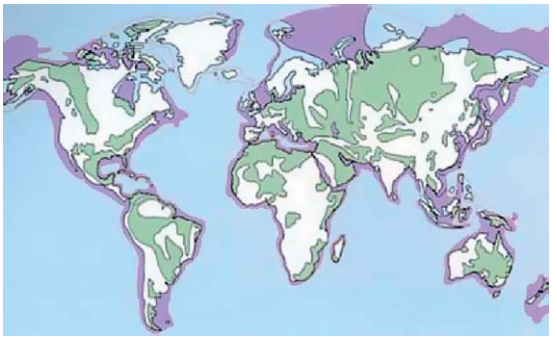

Figure 1 Sedimentary basins of the World. Onshore basins are shown in green, offshore basins are lavender and shown for a maximum water depth of 1000 m. Modified from Schlumberger (1991). World oil reserves – charting the future. Middle East Well Evaluation Reivew 10: 7–15.

In Section 6.11.3, we highlight the connection between the bulk rheological properties of the lithosphere and the evolution of some of Europe's main sedimentary basins. These include some of the best-documented sedimentary basin systems of the world. As discussed in Section 6.11.2, the finite strength of the lithosphere plays an important role in the development of extensional and compressional basins. This applies both to the geometry of the basin shape as well as to the record of vertical motions during and after rifting. As pointed out above, the concept of strength of the lithosphere also has important consequences for compressional basins. The latter include foreland basins as well as basins formed in response to lithospheric folding.

Section 6.11.3 sets the stage for Sections 6.11.4–6.11.7 in which basin modeling studies carried out in a number of selected natural laboratories are described. In each of these sections a particular aspect of tectonic processes controlling the evolution of sedimentary basins is examined. In this way, a review of recent advances and data interactive modeling, integrating process modeling with geological and geophysical data is given, covering key aspects of passive-margin evolution, back-arc basins, foreland basins and basins formed by lithospheric folding. As will become clear from these sections, polyphase evolution of basin systems is the rule rather than an exception.

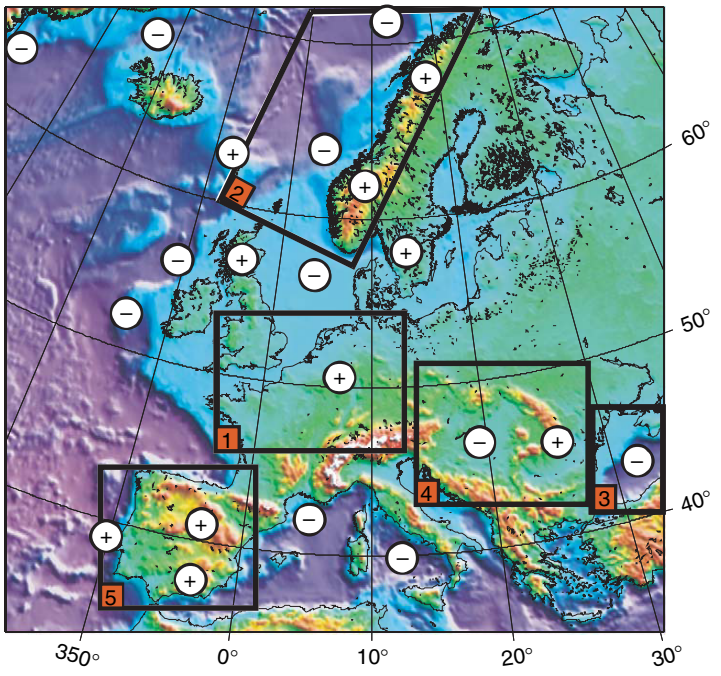

Figure 2 Topographic map of Europe, showing intraplate areas of Late Neogene uplift (circles with plus symbols) and subsidence (circles with minus symbols). Boxes show sedimentary basin systems discussed in this chapter. (1) European Cenozoic rift system and adjacent areas (Section 6.11.2); (2) Northwest European continental margin (Section 6.11.4); (3) Black Sea Basin (Section 6.11.5); (4) Carpathian–Pannonian Basin System (Section 6.11.6); (5) Iberian microcontinent (Section 6.11.7).

Table 1 Key parameters of basin evolution

Symbol	Name	Value
a	Initial lithosphere thickness	100 km
c	Initial crustal thickness	30 km
T_a	Asthenospheric temperature	1333°C
k	Thermal diffusivity	$10^{-6}\,m^2\,s^{-1}$
ρ_c	Surface crustal density	$2800\,kg\,m^{-3}$
ρ_m	Surface mantle density	$3300\,kg\,m^{-3}$
ρ_w	Water density	$1030\,kg\,m^{-3}$
ρ_s	Sediment densities	$2100–2650\,kg\,m^{-3}$
α	Thermal expansion factor	$3.2 \times 10^{-5}\,K^{-1}$
δ	Crustal stretching factor	
β	Subcrustal stretching factor	

In Section 6.11.4, we investigate thermomechanical controls on continental breakup and associated basin migration processes using the NW European margin as a natural laboratory. The volcanic rifted margins of the northern Atlantic are probably the best documented in the world as a result of a major concentrated effort by academia and industry, the latter in the context of hydrocarbon exploration and production. A particularly striking feature is the very long duration of the rifting phases prior to continental breakup. This margin system also allows the quantification of controls on rifted margin topography and compressional reactivation during the post breakup phase. In doing so, we specifically address relationships between rift duration and extension velocities, thermal evolution and the role of mantle plumes and melts. This is followed by a brief discussion on compressional reactivation and its consequences for postrift inversion, borderland uplift and denudation.

In Section 6.11.5, we further develop the treatment of polyphase deformation of extensional basins taking the Black Sea Basin as a natural laboratory. An intriguing feature of this basin system is the concentration of postrift deformation at its margins, without affecting the basin center. We concentrate on rheological controls on basin formation and its consequences for large-scale basin stratigraphy and rift shoulder dynamics. We also discuss the role of intraplate stresses and lithospheric strength evolution during the postrift phase and implications for neotectonic reactivation of the Black Sea Basin system.

In Section 6.11.6, we give an overview on the interplay between extension and compression in the

Pannonian–Carpathian basin system of Central Eastern Europe. This area is the site of pronounced contrasts of lithospheric strength between the Pannonian area, which is probably underlain by the hottest and weakest lithosphere of Europe, and the particularly strong East-European Platform lithosphere bounding the Carpathian arc to the East. Noteworthy features of the Pannonian system are the short duration of rifting phases in a back-arc setting affected by extensional collapse and subsequent compressional reactivation. The Carpathian arc is associated with probably one of the deepest foredeeps of the world, the Focşani Basin that developed in front of the bend zone of the Carpathians in an area that is strongly affected by neotectonics and seismicity. This basin contains more than 9 km of Neogene sediments. This system offers also a unique opportunity to study basin evolution in the aftermath of continental collision. We begin with a review of temporal and lateral variations in lithospheric strength in this region and its effects on late-stage basin deformation. This is followed by a summary of models proposed for the development of the Pannonian–Carpathian system. In the second part of Section 6.11.6, we present the results of 3-D modeling approaches investigating the role of 3-D distribution of loads and lithospheric strength in orogenic arcs. In doing so, we focus on implications of these models for a better understanding of polyphase subsidence in the Carpathian foredeep.

For our discussion on lithospheric folding as a mode of basins development, and for the interplay between lithosphere and surface processes in a compressional setting, we have selected the Iberian microcontinent, located within the Africa–Europe collision zone. In the first part of Section 6.11.7, we review constraints on vertical motions, present-day stress regime and interaction between surface transport and vertical motions for Iberia at large. This is followed by a more detailed treatment of tectonic controls on drainage systems using the Ebro Basin system of NE Iberia as a natural laboratory.

6.11.2 Tectonics of Extensional and Compressional Basins: Concepts and Global-Scale Observations

6.11.2.1 Extensional Basin Systems

Tectonically active rifts, palaeo-rifts and passive margins form a group of genetically related extensional basins that play an important role in the spectrum of sedimentary basin types (Bally and Snelson, 1980; Ziegler and Cloetingh, 2004; *see also* Buck, this volume (Chapter 6.08)). Extensional basins cover large areas of the globe and contain important mineral deposits and energy resources. A large number of major hydrocarbon provinces are associated with rifts (e.g., North Sea, Sirt and West Siberian basins, Dniepr–Donets and Gulf of Suez grabens) and passive margins (e.g., Campos Basin, Gabon, Angola, Mid-Norway and NW Australian shelves, Niger and Mississippi deltas; Ziegler, 1996a,b). On these basins, the petroleum industry has acquired large databases that document their structural styles and allow detailed reconstruction of their evolution. Academic geophysical research programs have provided information on the crustal and lithospheric configuration of tectonically active rifts, palaeo-rifts, and passive margins. Petrologic and geochemical studies have advanced the understanding of rift-related magmatic processes. Numerical models, based on geophysical and geological data, have contributed at lithospheric and crustal scales toward the understanding of dynamic processes that govern the evolution of rifted basins. Below we summarize basic concepts on dynamic processes that control the evolution of extensional basins.

A natural distinction can be made between tectonically active and inactive rifts, and rifts that evolved in continental and oceanic lithosphere. Tectonically active intracontinental (intraplate) rifts, such as the Rhine Graben, the East African Rift, the Baikal Rift and the Shanxi Rift of China, correspond to important earthquake and volcanic hazard zones. The globe-encircling mid-ocean ridge system forms an immense intraoceanic active rift system that encroaches onto continents in the Red Sea and the Gulf of California. Rifts that are tectonically no longer active are referred to as palaeo-rifts, aulacogens, inactive or aborted rifts and failed arms, in the sense that they did not progress to crustal separation. Conversely, the evolution of successful rifts culminated in the breakup of continents, the opening of new oceanic basins and the development of conjugate pairs of passive margins.

In the past, a genetic distinction was made between 'active' and 'passive' rifting (Sengör and Burke, 1978; Olsen and Morgan, 1995). 'Active' rifts are thought to evolve in response to thermal upwelling of the asthenosphere (Dewey and Burke, 1975; Bott and Kusznir, 1979), whereas 'passive' rifts develop in response to lithospheric extension driven by far-field stresses (McKenzie, 1978). It is, however,

questionable whether such a distinction is justified as the study of Phanerozoic rifts revealed that rift-related volcanic activity and doming of rift zones is basically a consequence of lithospheric extension and is not the main driving force of rifting. The fact that rifts can become tectonically inactive at all stages of their evolution, even if they have progressed to the Red Sea stage of limited sea-floor spreading (e.g., Bay of Biscay-Pyrenean rift), supports this concept. However, as extrusion of large volumes of rift-related subalkaline tholeiites must be related to a thermal anomaly within the upper mantle, a distinction between 'active' and 'passive' rifting is to a certain degree still valid, though not as 'black and white' as originally envisaged.

Rifting activity, preceding the breakup of continents is probably governed by forces controlling the movement and interaction of lithospheric plates. These forces include plate boundary stresses, such as slab pull, slab roll-back, ridge push and collisional resistance, and frictional forces exerted by the convecting mantle on the base of the lithosphere (Forsyth and Uyeda, 1975; Bott, 1993; Ziegler, 1993; *see also* Wessel and Müller, this volume (Chapter 6.02)).

On the other hand, deviatoric tensional stresses, inherent to the thickened lithosphere of young orogenic belts, as well as those developing in the lithosphere above upwelling mantle convection cells and mantle plumes (Bott, 1993) do not appear to cause, on their own, the breakup of continents. However, if such stresses interfere constructively with plate boundary and/or mantle drag stresses, the yield strength of the lithosphere may be exceeded, thus inducing rifting (**Figure 3**).

It must be understood that mantle drag forces are exerted on the base of a lithospheric plate if its velocity and direction of movement differs from the velocity and direction of the mantle flow. Mantle drag can constructively or destructively interfere with plate boundary forces, and thus can either contribute towards plate motion or resist it. Correspondingly, mantle drag can give rise to the buildup of extensional as well as compressional intraplate stresses (Forsyth and Uyeda, 1975; Bott, 1993; Artemieva and Mooney, 2002). Although the present lithospheric stress field can be readily explained in terms of plate boundary forces (Cloetingh and Wortel, 1986; Richardson, 1992; Zoback, 1992), mantle drag probably contributed significantly to the Triassic–Early Cretaceous breakup of Pangea, during which Africa remained nearly stationary and straddled an evolving upwelling and radial outflowing mantle convection cell (Pavoni, 1993; Ziegler, 1993; Ziegler *et al.*, 2001). Mechanical stretching of the lithosphere and thermal attenuation of the lithospheric mantle are associated with the development of local deviatoric tensional stresses, which play an increasingly important role during advanced rifting stages (Bott, 1992; Ziegler, 1993). This has led to the development of the concept that many rifts go through an evolutionary cycle starting with an initial 'passive' phase that is followed by a more 'active' stage during which magmatic processes play an increasingly important role (Wilson, 1993a; Burov and Cloetingh, 1997; Huismans *et al.*, 2001a). However, nonvolcanic rifts must be considered as purely 'passive' rifts.

6.11.2.1.1 Modes of rifting and extension

6.11.2.1.1.(i) Atlantic-type rifts Atlantic-type rift systems evolve during the breakup of major continental masses, presumably in conjunction with a reorganization of the mantle convection system (Ziegler, 1993). During early phases of rifting, large areas around future zones of crustal separation can be affected by tensional stresses, giving rise to the development of complex graben systems. In time, rifting activity concentrates on the zone of future crustal separation, with tectonic activity decreasing and ultimately ceasing in lateral graben systems. In time and as a consequence of progressive lithospheric attenuation and ensuing crustal doming, local deviatoric tensional stresses play an important secondary role in the evolution of such rift systems. Upon crustal separation, the diverging continental margins (pericontinental rifts) and the 'unsuccessful' intracontinental branches of the respective rift system become tectonically inactive. However, during subsequent tectonic cycles, such aborted rifts can be tensionally as well as compressionally reactivated (Ziegler *et al.*, 1995, 1998, 2001, 2002). Development of Atlantic-type rifts is subject to great variations mainly in terms of duration of their rifting stage and the level of volcanic activity (Ziegler, 1988, 1990b, 1996b).

6.11.2.1.1.(ii) Back-arc rifts Back-arc rifts are thought to evolve in response to a decrease in convergence rates and/or even a temporary divergence of colliding plates, ensuing steepening of the subduction slab and development of a secondary upwelling system in the upper plate mantle wedge above the subducted lower plate lithospheric slab (Uyeda and McCabe, 1983). Changes in convergence rates between colliding plates are probably an expression of changes in plate interaction. Back-arc rifting can

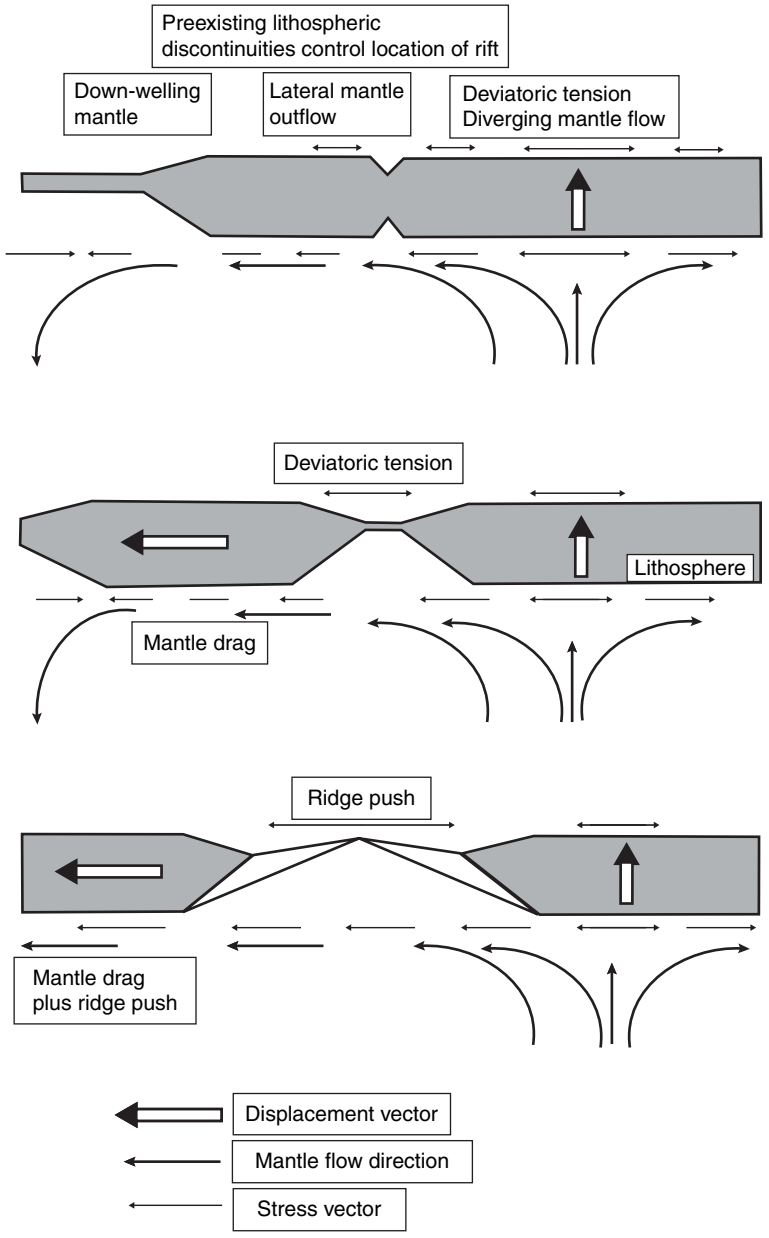

Figure 3 Diagram illustrating the interaction of shear-traction exerted on the base of the lithosphere by asthenospheric flow, deviatoric tension above upwelling mantle convection cells and ridge push forces. Modified from Ziegler PA, Cloetingh S, Guiraud R, and Stampfli GM (2001). Peri-Tethyan platforms: constraints on dynamics of rifting and basin inversion. In: Ziegler PA, Cavazza W, Robertson AHF, and Crasquin-Soleau S (eds.) *Mémoires du Museum National d'Histoire Naturelle* 186: *Peri-Tethys Memoir 6: Peri-Tethyan Rift/Wrench Basins and Passive Margins*, pp. 9–49. Paris: Commission for the Geological Map of the World.

progress to crustal separation and the opening of limited oceanic basins (e.g., Sea of Japan, South China Sea, Black Sea). However, as convergence rates of colliding plates are variable in time, back-arc extensional basins are generally short-lived. Upon a renewed increase in convergence rates, back-arc extensional systems are prone to destruction by back-arc compressional stresses (e.g., Variscan Rheno-Hercynian Basin, Sunda Arc and East China rift systems, Black Sea domain; Uyeda and McCabe, 1983; Cloetingh *et al.*, 1989; Jolivet *et al.*, 1989; Ziegler, 1990a; Letouzey *et al.*, 1991; Nikishin *et al.*, 2001).

6.11.2.1.1.(iii) Syn-orogenic rifting and wrenching Syn-orogenic rift/wrench deformations can be related to indenter effects and ensuing escape tectonics, often involving rotation of intramontane stable blocks (e.g., Pannonian Basin: Royden and Horváth, 1988; Late Carboniferous Variscan fold belt: Ziegler, 1990b), as well as to lithospheric overthickening in orogenic belts, resulting in uplift and extension of their axial parts (Peruvian and Bolivian Altiplano: Dalmayrac and Molnar, 1981, Mercier *et al.*, 1992). Furthermore, collisional stresses exerted on a craton may cause far-field tensional or transtensional reactivation of preexisting fracture systems and thus the development of rifts and pull-apart basins. This model may apply to the Late Carboniferous development of the Norwegian–Greenland Sea rift in the foreland of the Variscan Orogen, the Permo-Carboniferous Karoo rifts in the hinterland of the Gondwanan Orogen, the Cenozoic European rift system in the Alpine foreland and the Neogene Baikal rift in the hinterland of the Himalayas (Ziegler *et al.*, 2001; Dèzes *et al.*, 2004). Under special conditions, extensional structures can also develop in forearc basins (e.g., Talara Basin, Peru; see Ziegler and Cloetingh, 2004).

6.11.2.1.1.(iv) Postorogenic extension Extensional disruption of young orogenic belts, involving the development of grabens and pull-apart structures, can be related to their postorogenic uplift and the development of deviatoric tensional stresses inherent to orogenically overthickened crust (Stockmal *et al.*, 1986; Dewey, 1988; Sanders *et al.*, 1999). The following mechanisms contribute to postorogenic uplift: (1) locking of the subduction zone due to decay of the regional compressional stress field (Whittaker *et al.*, 1992); (2) roll-back and ultimately detachment of the subducted slab from the lithosphere (Fleitout and Froidevaux, 1982; Bott, 1993; Andeweg and Cloetingh, 1998); and (3) retrograde metamorphism of the crustal roots, involving, in the presence of fluids, the transformation of eclogite to less dense granulite (Le Pichon *et al.*, 1997; Straume and Austrheim, 1999). Although tensional collapse of an orogen can commence shortly after its consolidation (e.g. the Variscan Orogen: Ziegler, 1990b; Ziegler *et al.*, 2004), it may be delayed by as much as 30 My, as in the case of the Appalachian-Mauretanides (Ziegler, 1990b). The Permo-Triassic West Siberian Basin that is superimposed on the juncture of the Uralides and Altaides is an example of a postorogenic tensional basin that began to subside shortly after the consolidation of these orogens (Nikishin *et al.*, 2002; Vyssotski *et al.*, 2006). In addition, modifications in the convergence direction of colliding continents and the underlying stress reorientation can give rise to the development of wrench fault systems and related pull-apart basins, controlling early collapse of an orogen, such as the Devonian collapse of the Arctic–North Atlantic Caledonides (Ziegler, 1989b; Ziegler and Dèzes, 2006) or the Stephanian–Early Permian disruption of the Variscan fold belt (Ziegler *et al.*, 2004).

The Basin and Range Province of North America is a special type of postorogenic rifting. Oligocene and younger collapse of the US Cordillera is thought to be an effect of the North American craton having overridden at about 28 Ma the East Pacific Rise in conjunction with rapid opening of the Atlantic Ocean (Verall, 1989). In the area of the southwestern US Cordillera, regional compression waned during the late Eocene and the orogen began to collapse during late Oligocene with main extension occurring during the Miocene and Pliocene (Parsons, 1995). By contrast, the Canadian Cordillera remained intact. During the collapse of the US Cordillera, the heavily intruded, at middle and lower levels ductile crust of the Basin and Range Province was subjected to major extension at high strain rates, resulting in uplift of ductilely deformed core complexes by 10–20 km. The area affected by extension, crustal thinning, volcanism, and uplift measures 1500×1500 km (Wernicke, 1990). The Eo-Oligocene magmatism of the Basin and Range Province bears a subduction-related signature, suggestive of an initial phase of back-arc extension, whereas lithospheric mantle- and asthenosphere-derived magmas play an increasingly important role from Miocene times onward, presumably due to the opening of asthenospheric windows in the Farralon slab during its detachment from in the lithosphere and gradual sinking into the mantle (Parsons, 1995).

6.11.2.1.2 Thermal thinning and stretching of the lithosphere: concepts and models

Mechanical stretching of the lithosphere, triggering partial melting of its basal parts and the upper asthenosphere, is followed by segregation of melts and their diapiric rise into the lithosphere, an increase in conductive and advective heat flux and consequently an upward displacement of the thermal asthenosphere–lithosphere boundary. Small-scale convection in the evolving asthenospheric diapir may contribute to mechanical thinning of the lithosphere by facilitating

lateral ductile mass transfer (**Figure 4**) (Richter and McKenzie, 1978; Mareschal and Gliko, 1991). Progressive thermal and mechanical thinning of the higher-density lithospheric mantle and its replacement by lower-density asthenosphere induces progressive doming of rift zones. At the same time, deviatoric tensional stresses developing in the lithosphere contribute to its further extension (Bott, 1992).

Although major hot-spot activity is thought to be related to a thermal perturbation within the asthenosphere caused by a deep mantle plume, smaller-scale 'plume' activity may also be the consequence of lithospheric stretching triggering by adiabatic decompression partial melting in areas characterized by an anomalously volatile-rich asthenosphere/lithosphere (Wilson, 1993a; White and McKenzie, 1989). In this context, it is noteworthy that extension-induced development of a partially molten asthenospheric diapir that gradually rises into the lithosphere causes by itself further decompression of the underlying asthenosphere and consequently more extensive partial melting and melt segregation at progressively deeper levels. Thus, the evolving diapir may not only grow upward but also downward. Similarly, acceleration of plate divergence and the ensuing increase in sea-floor spreading rates probably causes at spreading axes partial melting and melt segregation at progressively deeper asthenospheric levels reaching down to 80–100 km, as imaged seismic tomography (Anderson *et al.*, 1992).

Melts, which intrude the lithosphere and pond at the crust–mantle boundary, provide a further mechanism for thermal doming of rift zones (**Figure 4**). Emplacement of such asthenoliths, consisting of a mixture of indigenous subcrustal mantle material and melts extracted from deeper lithospheric and upper asthenospheric levels, may cause temporary doming of a rift zone and a reversal in its subsidence pattern, such as for instance the Mid-Jurassic Central North Sea arch (Ziegler, 1990b) or the Neogene Baikal arch (Suvorov *et al.*, 2002).

Depending on the applicability of the 'pure-shear' (McKenzie, 1978) or the 'simple-shear' model (Wernicke, 1985), or a combination thereof (Kusznir *et al.*, 1991), the zone of upper crustal extension, corresponding to the subsiding rift, may coincide with the zone of lithospheric mantle attenuation (pure- and combined-shear) or may be laterally offset from it (simple-shear, see **Figure 5**). Under conditions of

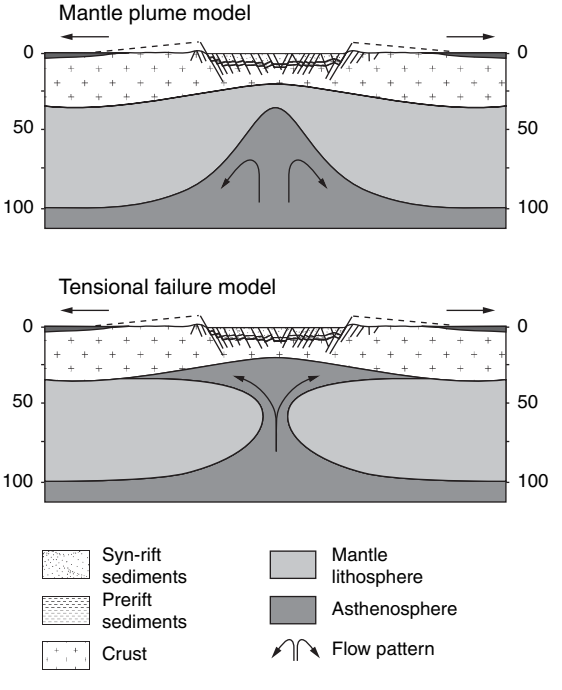

Figure 4 Rift models.

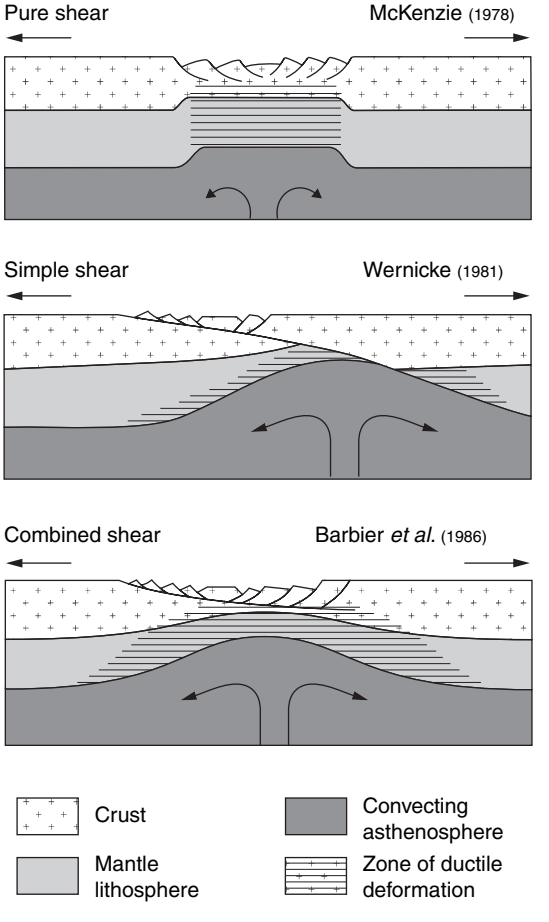

Figure 5 Lithospheric shear models.

pure-shear lithospheric extension, magmatic activity should be centered on the rift axis where in time mid-oceanic ridge basalt (MORB) type magmas can be extruded after a high degree of extension has been achieved. By contrast, under simple-shear conditions, magmatic activity is asymmetrically distributed with respect to the rift axis and MORB-type extrusives may occur on one of the rift flanks (e.g., the Basin and Range Province (Jones *et al.*, 1992), the Red Sea (Favre and Stampfli, 1992), and the Ethiopian Rift (Kazmin, 1991).

A modification to the pure-shear model is the 'continuous depth-dependent' stretching model which assumes that stretching of the lithospheric mantle affects a broader area than the zone of crustal extension (**Figure 6**) (Rowley and Sahagian, 1986). In both models it is assumed that the asthenosphere wells up passively into the space created by mechanical attenuation of the lithospheric mantle. In depth-dependent stretching models this commonly gives rise to flexural uplift of the rift shoulders, and in the flexural cantilever model, which assumes ductile deformation of the lower crust, this produces footwall uplift of the rift flanks and intrabasin fault blocks (Kusznir and Ziegler, 1992). By the same mechanism, the simple-shear model predicts asymmetrical doming of a rift zone or even flexural uplift of an arch located to one side of the zone of upper crustal extension (Wernicke, 1985). A modification to the simple-shear model envisages that massive upper crustal extensional unloading of the lithosphere causes its isostatic uplift and passive inflow of the asthenosphere (Wernicke, 1990).

The structural style of rifts, as defined at upper crustal and syn-rift sedimentary levels, is influenced by the thickness and thermal state of the crust and lithospheric mantle at the onset of rifting, by the amount of crustal extension and the width over which it is distributed, the mode of crustal extension (orthogonal or oblique, simple- or pure-shear) and the lithological composition of the pre- and syn-rift sediments (Cloetingh *et al.*, 1995b; Ziegler, 1996b).

A major factor controlling the structural style of a rift zone is the magnitude of the crustal extensional strain that was achieved across it and the distance over which it is distributed (δ factor). Although quantification of the extensional strain and of the stretching factor δ is of basic importance for the understanding of rifting processes, there is often a considerable discrepancy between estimates derived from upper crustal extension by faulting, the crustal configuration and quantitative subsidence analyses (Ziegler and Cloetingh, 2004).

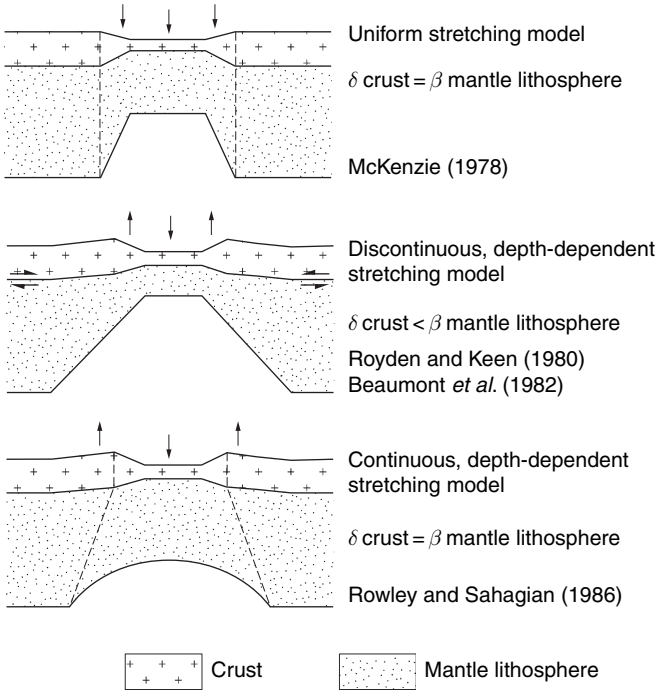

Figure 6 Lithospheric stretching models.

6.11.2.1.3 Syn-rift subsidence and duration of rifting stage

The balance of two mechanisms controls the syn-rift subsidence of a sedimentary basin. First, elastic/isostatic adjustment of the crust to stretching of the lithosphere and its adjustment to sediment loading causes subsidence of the mechanically thinned crust (**Figures 5** and **6**) (McKenzie, 1978; Keen and Boutilier, 1990). Depending on the depth of the lithospheric necking level, this is accompanied by either flexural uplift or down warping of the rift zone (**Figure 7**) (Braun and Beaumont, 1989; Kooi, 1991; Kooi *et al.*, 1992). Second, uplift of a rift zone is caused by upwelling of the asthenosphere into the space created by mechanical stretching of the lithosphere, thermal upward displacement of the asthenosphere–lithosphere boundary, thermal expansion of the lithosphere and intrusion of melts at the base of the crust (**Figure 4**) (Turcotte and Emermann, 1983). Thus, the geometry of a rifted basin is a function of the elastic/isostatic response of the lithosphere to its mechanical stretching and related thermal perturbation (Van der Beek *et al.*, 1994).

The duration of the rifting stage of intracontinental rifts (aborted) and passive margins (successful rifts) is highly variable (**Figures 8** and **9**) (Ziegler, 1990b, Ziegler *et al.*, 2001, Ziegler and Cloetingh, 2004). Overall, it is observed that, in time, rifting activity concentrates on the zone of future crustal separation with lateral rift systems becoming inactive. However, as not all rift systems progress to crustal separation, the duration of their rifting stage is obviously a function of the persistence of the controlling stress field. On the other hand, the time required to achieve crustal separation is a function of the strength (bulk rheology) of the lithosphere, the buildup rate, magnitude and persistence of the extensional stress field, constraints on lateral movements of the diverging blocks (on-trend coherence, counteracting far-field compressional stresses), and apparently not so much of the availability of preexisting crustal discontinuities that can be tensionally reactivated.

Crustal separation was achieved in the Liguro-Provençal Basin after 9 My of crustal extension and in the Gulf of California after about 14 My of rifting, whereas opening of the Norwegian–Greenland Sea was preceded by an intermittent rifting history spanning some 280 My (Ziegler, 1988; Ziegler and Cloetingh, 2004). There appears to be no obvious correlation between the duration of the rifting stage (R) of successful rifts (**Figure 9**), which are superimposed on orogenic belts (Liguro-Provençal Basin, Pyrenees $R = 9$ My; Gulf of California, Cordillera $R = 14$ My; Canada Basin, Inuitian fold belt $R = 35$ My; Central Atlantic, Appalachians $R = 42$ My; Norwegian–Greenland Sea, Caledonides $R = 280$ My) and those which developed within stabilized cratonic lithosphere (southern South Atlantic $R = 13$ My; northern South Atlantic $R = 29$ My; Red Sea $R = 29$ My; Baffin Bay $R = 70$ My; Labrador Sea $R = 80$ My). This suggests that the availability of crustal discontinuities, which regardless of their age (young orogenic belts, old Precambrian shields) can be tensionally reactivated, does not play a major role in the time required to achieve crustal separation. However, by weakening the crust, such discontinuities play a role in the localization and distribution of crustal strain. Moreover, by weakening the lithosphere, they

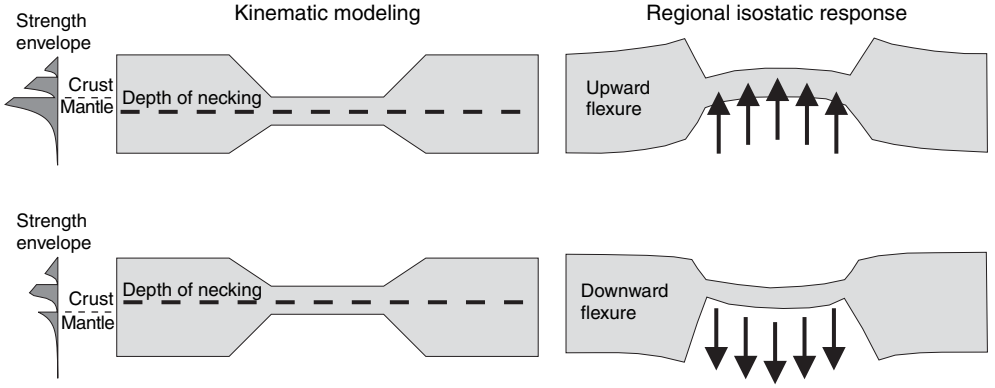

Figure 7 Concept of lithospheric necking. The level of necking is defined as the level of no vertical motions in the absence of isostatic forces. Left panel: kinematically induced configuration after rifting for different necking depths. Right panel: subsequent flexural isostatic rebound.

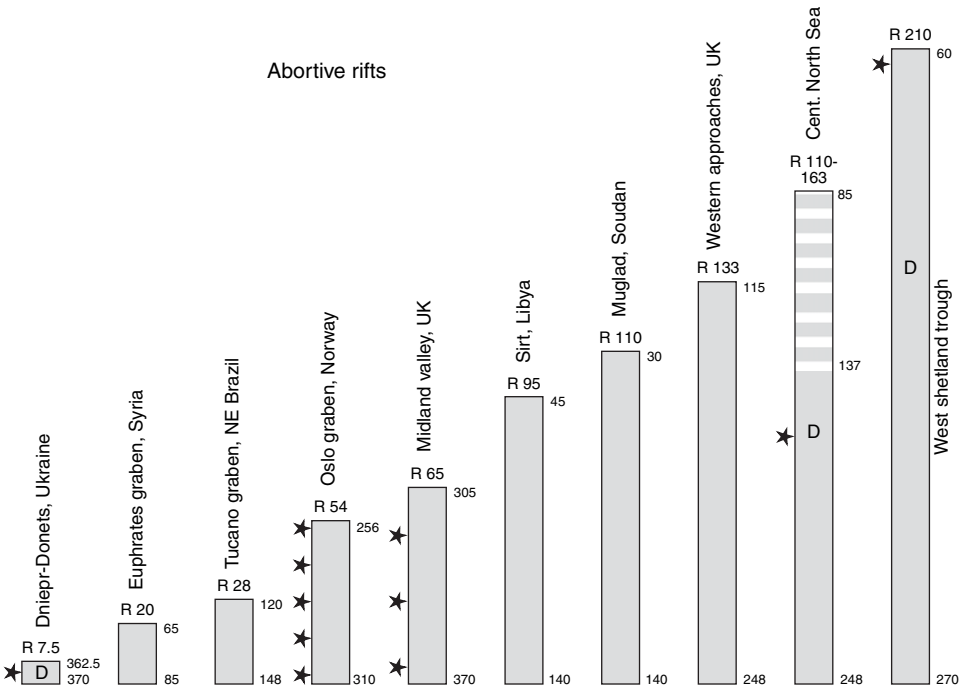

Figure 8 Duration of rifting stage of 'abortive' rifts (palaeo-rifts, failed arms). Vertical columns in My; numbers on side of vertical columns indicate onset and termination of rifting stage in My; numbers under R on top of each column give the duration of rifting stage in My; stars indicate periods of main volcanic activity; D indicates periods of doming. Modified from Ziegler PA and Cloetingh S (2004). Dynamic processes controlling evolution of rifted basins. *Earth-Science Reviews* 64: 1–50.

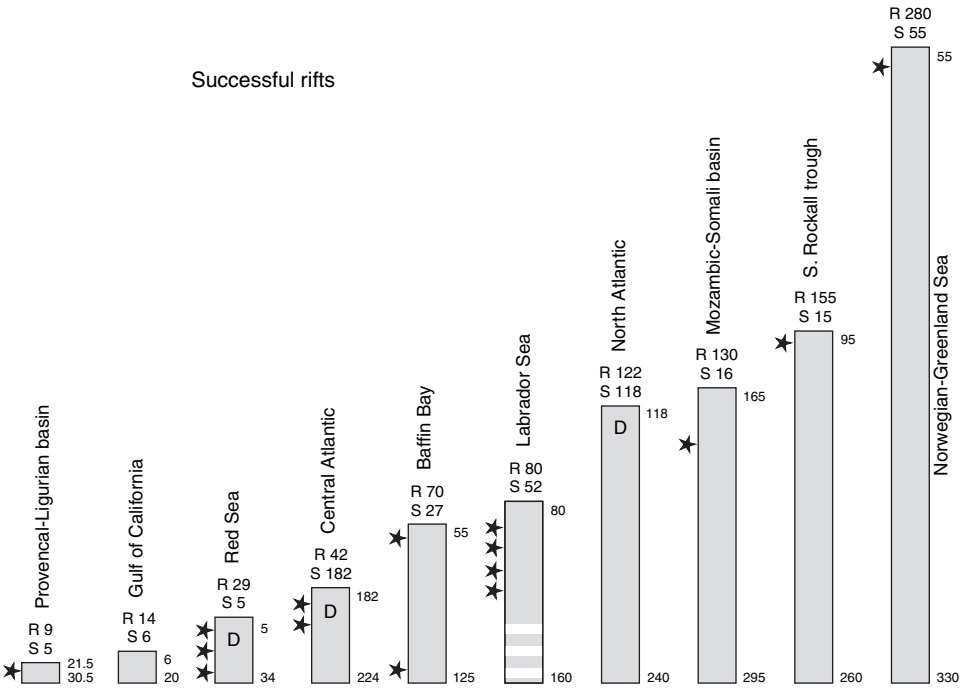

Figure 9 Duration of rifting stage of 'successful' rifts. Legend same as **Figure 8**. Numbers beside letter 'S' indicate duration of seafloor spreading stage in My. Modified from Ziegler PA and Cloetingh S (2004). Dynamic processes controlling evolution of rifted basins. *Earth-Science Reviews* 64: 1–50.

contribute to the preferential tensional reactivation of young as well as old orogenic belts (Janssen *et al.*, 1995; Ziegler *et al.*, 2001).

6.11.2.1.4 Postrift subsidence

Similar to the subsidence of oceanic lithosphere, the postrift subsidence of extensional basins is mainly governed by thermal relaxation and contraction of the lithosphere, resulting in a gradual increase of its flexural strength, and by its isostatic response to sedimentary loading. Theoretical considerations indicate that subsidence of postrift basins follows an asymptotic curve, reflecting the progressive decay of the rift-induced thermal anomaly, the magnitude of which is thought to be directly related to the lithospheric stretching value (Sleep, 1973; McKenzie, 1978; Royden *et al.*, 1980; Steckler and Watts, 1982; Beaumont *et al.*, 1982; Watts *et al.*, 1982). During the postrift evolution of a basin, the thermally destabilized continental lithosphere reequilibrates with the asthenosphere (McKenzie, 1978; Steckler and Watts, 1982; Wilson, 1993b). In this process, in which the temperature regime of the asthenosphere plays an important role (ambient, below, or above ambient), new lithospheric mantle, consisting of solidified asthenospheric material, is accreted to the attenuated old continental lithospheric mantle (Ziegler *et al.*, 1998). In addition, densification of the continental lithosphere involves crystallization of melts that accumulated at its base or were injected into it, subsequent thermal contraction of the solidified rocks and, under certain conditions, their phase transformation to eclogite facies. The resulting negative buoyancy effect is the primary cause of postrift subsidence. However, in a number of basins, significant departures from the theoretical thermal subsidence curve are observed. These can be explained as effects of compressional intraplate stresses and related phase transformations (Cloetingh and Kooi, 1992; Van Wees and Cloetingh, 1996; Lobkovsky *et al.*, 1996).

6.11.2.1.4.(i) Shape and magnitude of rift-induced thermal anomalies

The shape and dimension of rift-induced asthenosphere–lithosphere boundary anomalies essentially controls the geometry of the evolving postrift thermal-sag basin (**Figure 5**). Thermal sag basins associated with aborted rifts are broadly saucer-shaped and generally overstep the rift zone, with their axes coinciding with the zone of maximum lithospheric attenuation.

Pure-shear-dominated rifting gives rise to the classical 'steer's head' configuration of the syn- and postrift basins (White and McKenzie, 1989) in which both basin axes roughly coincide, with the postrift basin broadly overstepping the rift flanks. This geometric relationship between syn- and postrift basins is frequently observed (e.g., North Sea Rift: Ziegler, 1990b; West Siberian Basin: Artyushkov and Baer, 1990; Dniepr-Donets Graben: Kusznir *et al.*, 1996, Stephenson *et al.*, 2001; Gulf of Thailand: Hellinger and Sclater, 1983; Watcharanantakul and Morley, 2000; Sudan rifts: McHargue *et al.*, 1992). Such a geometric relationship is compatible with discontinuous, depth-dependent stretching models that assume that the zone of crustal extension is narrower than the zone of lithospheric mantle attenuation (**Figure 6**). The degree to which a postrift basin oversteps the margins of the syn-rift basin is a function of the width difference between the zone of crustal extension and the zone of lithospheric mantle attenuation (White and McKenzie, 1988) and the effective elastic thickness (EET) of the lithosphere (Watts *et al.*, 1982).

Conversely, simple-shear dominated rifting gives rise to a lateral offset between the syn- and postrift basin axes. An example is the Tucano Graben of northeastern Brazil, which ceased to subside at the end of the rifting stage, whereas the coastal Jacuipe–Sergipe–Alagoas Basin, to which the former was structurally linked, was the site of crustal and mantle-lithospheric thinning culminating in crustal separation and subsequent major postrift subsidence (Karner *et al.*, 1992; Chang *et al.*, 1992). Moreover, the simple-shear model can explain the frequently observed asymmetry of conjugate passive margins and differences in their postrift subsidence pattern (e.g., Central Atlantic and Red Sea: Favre and Stampfli, 1992). Discrepancies in the postrift subsidence of conjugate margins are attributed to differences in their lithospheric configuration at the crustal separation stage. At the end of the rifting stage, a relatively thick lithospheric mantle supports lower plate margins, whereas upper plate margins are underlain by a strongly attenuated lithospheric mantle and partly directly by the asthenosphere. Correspondingly, lower plate margins are associated at the crustal separation stage with smaller thermal anomalies than upper plate margins (Ziegler *et al.*, 1998; Stampfli *et al.*, 2001). These differences in lithospheric configuration of conjugate simple-shear margins have repercussions on their rheological structure, even after full thermal relaxation of the lithosphere, and their compressional reactivation potential (see further ahead; Ziegler *et al.*, 1998) (**Table 2**).

Table 2 Rheological and thermal parameters of crust and lithospheric materials, adopted for the rheological models shown in **Figure 11**

Layer	Rheology	Conductivity ($W\,m^{-1}\,K^{-1}$)	Heat production ($10^{-6}\,W\,m^{-3}$)
Sediments (models A,B,C)	Quartzite	2	0.2
Sediments (model D)	Quartzite	1.4	1.8
Upper crust	Quartzite	2.6	1.88
Lower crust	Diorite	2.6	0.5
Lithospheric mantle	Olivine	3.1	0

The magnitude of postrift tectonic subsidence of aborted rifts and passive margins is a function of the thermal anomaly that was introduced during their rifting stage and the degree to which the lithospheric mantle was thinned. Most intense anomalies develop during crustal separation, particularly when plume assisted and asthenospheric melts well up close to the surface. The magnitude of thermal anomalies induced by rifting that did not progress to crustal separation depends on the magnitude of crustal stretching (δ-factor) and lithospheric mantle attenuation (β-factor), the thermal regime of the asthenosphere, the volume of melts generated and whether these intruded the lithosphere and destabilized the Moho (**Figure 4**).

After 60 My, about 65%, and after 180 My about 95% of a deep-seated thermal anomaly associated with a major pullup of the asthenosphere–lithosphere boundary have decayed (mantle-plume model (**Figure 4**)). Thermal anomalies related to intralithospheric intrusions (tensional-failure model (**Figure 4**)) have apparently a faster decay rate. For instance, the Mid-Jurassic North Sea rift dome had subsided below the sea level, 20–30 My after its maximum uplift, that is, well before crustal extension had terminated (Ziegler, 1990b; Underhill and Partington, 1993).

6.11.2.1.4.(ii) Stretching factors derived from quantitative subsidence analyses The thickness of the postrift sedimentary column that can accumulate in passive margin basins and in thermal-sag basins above aborted rifts is not only a function of the magnitude of the lithospheric mantle and crustal attenuation factors β and δ, but also of the crustal density and the water depth at the end of their rifting stage, as well as of the density of the infilling postrift sediments (carbonates, evaporites, clastics). Moreover, it must be kept in mind that during the postrift cooling process the flexural rigidity of the lithosphere increases gradually, resulting in the distribution of the sedimentary load over progressively wider areas.

Quantitative postrift subsidence analyses of extensional basins, neglecting intraplate stresses, are thought to give a measure of the thermal contraction of the lithosphere and, conversely, of lithospheric stretching factors, as suggested by the McKenzie (1978) model and its early users (e.g., Sclater and Christie, 1980; Barton and Wood, 1984). Such analyses, assuming Airy isostasy, yield often considerably larger δ-factors than indicated by the populations of upper crustal faults (Ziegler, 1983, 1990b; Watcharanantakul and Morley, 2000). This discrepancy is somewhat reduced when flexural isostasy is assumed (Roberts *et al.*, 1993). However, as, during rifting, attenuation of the lithosphere is not only achieved by its mechanical stretching but also by convective and thermal upward displacement of the asthenosphere–lithosphere boundary, the magnitude of a thermal anomaly derived from the postrift subsidence of a basin cannot be directly related to a mechanical stretching factor. Moreover, intraplate compressional stresses and phase transformations in the lower crust and lithospheric mantle have an overprinting effect on postrift subsidence and can cause significant departures from a purely thermal subsidence curve (Cloetingh and Kooi, 1992; Van Wees and Cloetingh, 1996; Lobkovsky *et al.*, 1996).

Furthermore, during rifting the ascent of mantle-derived melts to the base of the crust can cause destabilization of the Moho, magmatic inflation of the crust and its metasomatic reactivation and secondary differentiation (Morgan and Ramberg, 1987; Mohr, 1992; Stel *et al.*, 1993; Watts and Fairhead, 1997). For instance, lower crustal velocities of 6.30–7.2 $km\,s^{-1}$ and densities of $3.02 \times 10^{-3}\,kg\,m^{-3}$ characterize the highly attenuated crust of the Devonian Dniepr-Donets rift almost up to the base of its syn-rift sediments, probably owing to its syn-rift permeation by mantle-derived melts (Yegorova *et al.*, 1999; Stephenson *et al.*, 2001).

Moreover, accumulation of very thick postrift sedimentary sequences can cause phase transformation of crustal rocks to granulite facies, with the resulting densification of the crust accounting for accelerated basin subsidence. This process can be amplified in the

cases of eclogite transformation of basaltic melts that were injected into the lithospheric mantle or that had accumulated at its base (Lobkovsky *et al.*, 1996). However, it is uncertain whether large-scale eclogite formation can indeed occur at crustal thicknesses of 30–40 km (Carswell, 1990; Griffin *et al.*, 1990). Although phase transformations, entailing an upward displacement of the geophysical Moho, are thought to occur under certain conditions at the base of very thick Proterozoic cratons (increased confining pressure due to horizontal intraplate stresses and/or ice load, possible cooling of asthenosphere, Cloetingh and Kooi, 1992), it is uncertain whether physical conditions conducive to such transformations can develop in response to postrift sedimentary loading of palaeorifts and passive margins as, for example, suspected for East Newfoundland Basin (Cloetingh and Kooi, 1992) and the West Siberian Basin (Lobkovsky *et al.*, 1996).

As rifting processes can take place intermittently over very long periods of time (e.g., Norwegian–Greenland Sea rift: Ziegler, 1988), thermal anomalies introduced during early stretching phases start to decay during subsequent periods of decreased extension rates. Thus, the thermal anomaly associated with a rift may not be at its maximum when crustal stretching terminates and the rift becomes inactive. Similarly, late rifting pulses and/or regional magmatic events may interrupt and even reverse lithospheric cooling processes (e.g., Palaeocene thermal uplift of northern parts of Viking Graben due to Iceland plume impingement: Ziegler, 1990a, 1990b; Nadin and Kusznir, 1995). Therefore, analyses of the postrift subsidence of rifts that have evolved in response to multiple rifting phases spread over a long period need to take their entire rifting history into account.

Intraplate compressional stress, causing deflection of the lithosphere in response to lithospheric folding, can seriously overprint the thermal subsidence of postrift basins. The example of the Plio-Pleistocene evolution of the North Sea shows that the buildup of regional compressional stresses can cause a sharp acceleration of postrift subsidence (**Figure 10**) (Cloetingh, 1988; Cloetingh *et al.*, 1990; Kooi and Cloetingh, 1989; Kooi *et al.*, 1991; Van Wees and Cloetingh, 1996). Similar contemporaneous effects are recognized in North Atlantic passive-margin basins (Cloetingh *et al.*, 1987, 1990) as well as in the Pannonian Basin (Horváth and Cloetingh, 1996). Also the late Eocene accelerated subsidence of the Black Sea Basin can be attributed to the buildup of a regional compressional stress field (Robinson *et al.*, 1995; Cloetingh *et al.*, 2003).

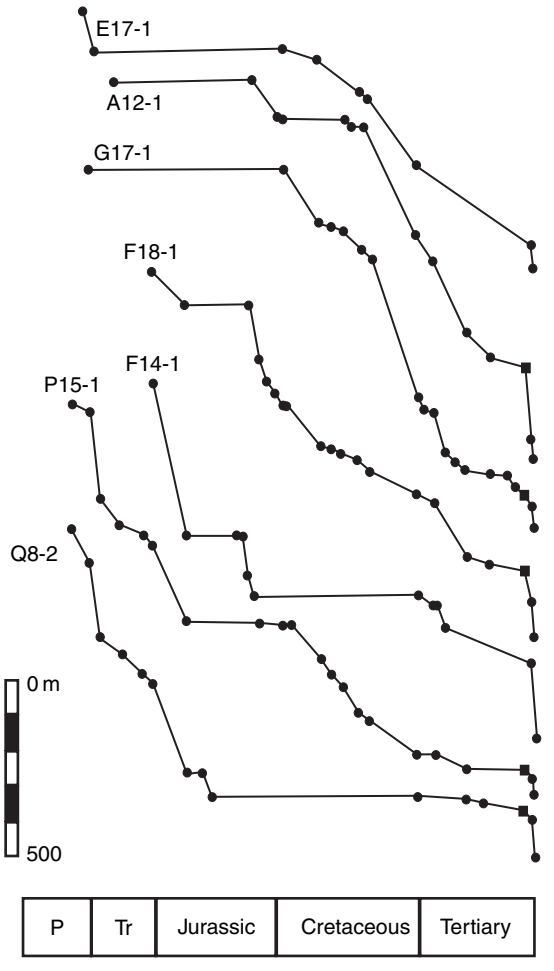

Figure 10 Tectonic subsidence curves of southern North Sea, showing accelerated subsidence during Plio-Pleistocene. Postrift stage starts during the Cretaceous. Modified from Kooi H, Hettema M, and Cloetingh S (1991). Lithospheric dynamics and the rapid Pliocene-Quaternary subsidence in the North Sea basin. *Tectonophysics* 192: 245–259.

At present, many extensional basins are in a state of horizontal compression as documented by stress indicators summarized in the World Stress Map (Zoback, 1992) and the European Stress Map (e.g., Gölke *et al.*, 1996). The magnitude of stress-induced vertical motions of the lithosphere during the postrift phase, causing accelerated basin subsidence and tilting of basin margins, depends on the ratio of the stress level and the strength of the lithosphere inherited from the syn-rift phase. Moreover, horizontal stresses in the lithosphere strongly affect the development of salt diapirism, accounting for local subsidence anomalies (Cloetingh and Kooi, 1992) and have a strong impact on the hydrodynamic regime of rifted basins

(Van Balen and Cloetingh, 1993, 1994) by contributing to the development of overpressure, as seen in parts of the Pannonian Basin (Van Balen *et al.*, 1999). Glacial loading and unloading can further complicate postrift lithospheric motions, a better insight into the nature of which is required (Solheim *et al.*, 1996).

These considerations indicate that stretching factors derived from the subsidence of postrift basins must be treated with reservations. Nevertheless, quantitative subsidence analyses, combined with other data, are essential for the understanding of postrift subsidence processes by giving a measure of the lithospheric anomaly that was introduced during the rifting stage of a basin and by identifying deviations from purely thermal cooling trends.

6.11.2.1.4.(iii) Postrift compressional reactivation potential Palaeo-stress analyses give evidence for changes in the magnitude and orientation of intraplate stress fields on time scales of a few million years (Letouzey, 1986; Philip, 1987; Bergerat, 1987; Dèzes *et al.*, 2004). Thus, in an attempt to understand the evolution of a postrift basin, the effects of tectonic stresses on subsidence must be separated from those related to thermal relaxation of the lithosphere (Cloetingh and Kooi, 1992).

In response to the buildup of far-field compressional stresses, rifted basins, characterized by a strongly faulted and thus permanently weakened crust, are prone to reactivation at all stages of their postrift evolution, resulting in their inversion (Ziegler, 1990a; Ziegler *et al.*, 1995, 1998, 2001). Only under special condition can gravitational forces associated with topography around a basin cause its inversion (Bada *et al.*, 2001).

Rheological considerations indicate that the lithosphere of thermally stabilized rifts, lacking a thick postrift sedimentary prism, is considerably stronger than the lithosphere of adjacent unstretched areas (Ziegler and Cloetingh, 2004). This contradicts the observation that rift zones and passive margins are preferentially deformed during periods of intraplate compression (Ziegler *et al.*, 2001). However, burial of rifted basins under a thick postrift sequence contributes by thermal blanketing to weakening of their lithosphere (Stephenson, 1989; Van Wees, 1994), thus rendering it prone to tectonic reactivation.

In order to quantify this effect and to assess the reactivation potential of conjugate simple-shear margins during subduction initiation, their strength evolution was modeled and compared to that of oceanic crust (Ziegler *et al.*, 1998). By applying a 1-D two-layered lithospheric stretching model, incorporating the effects of heat production by the crust and its sedimentary thermal blanketing (**Table 2**), the thermomechanical evolution of the lithosphere was analyzed in an effort to predict its palaeo-rheology (Van Wees *et al.*, 1996; Bertotti *et al.*, 1997).

For modeling purposes, a time frame of 100 My was chosen. Of this, the first 10 My (between 100 and 90 My in **Figure 11**) correspond to the rifting stage, culminating in separation of the conjugate upper and lower plate margins, and the following 90 My to the seafloor spreading stage during which oceanic lithosphere is accreted to the diverging plates. For modeling purposes it was assumed that the prerift crustal and mantle-lithosphere thickness are 30 and 70 km, respectively, and that at the end of the rifting stage the upper plate margin has a crustal thickness of 15 km ($\delta = 2$) and a remaining lithospheric mantle thickness of 7 km ($\beta = 10$) (δ and β are, respectively, the crustal and subcrustal stretching factor (Royden and Keen, 1980)), whilst the lower plate margin has a crustal thickness of 10 km ($\delta = 3$) and a lithospheric mantle thickness of 63.6 km ($\beta = 1.1$) (**Figures 11(a)** and **11(b)**). Results show that through time the evolution of strength envelopes for lower and upper plate passive margins differs strongly. In principle, during rifting, increased heating of the lithosphere causes its weakening; this effect is most pronounced at the moment of crustal separation. However, upper and lower plate margins show a very different evolution, both during the rifting and postrift stage.

At the moment of crustal separation, upper plate margins are very weak due to strong attenuation of the mantle-lithosphere and the ascent of the asthenospheric material close to the base of the crust. During the postrift evolution of such a margin, having a crustal thickness of 15 km, the strength of the lithosphere increases gradually as new mantle is accreted to its base and cools during the reequilibration of the lithosphere with the asthenosphere (**Figures 11(a)** and **12(a)**). In contrast, the evolution of a sediment starved lower plate margin with a crustal thickness of 10 km is characterized by a syn-rift strength increase due to extensional unroofing of the little attenuated mantle-lithosphere; the strength of such a margin increases dramatically during the postrift stage due to its progressive cooling (**Figures 11(b)** and **12(b)**). At the timeframe of 0 My, a sediment starved lower plate margin is considerably stronger than the conjugate upper plate margin for which a sedimentary cover of about 7 km was assumed. The strength evolution of an upper plate margin is initially controlled

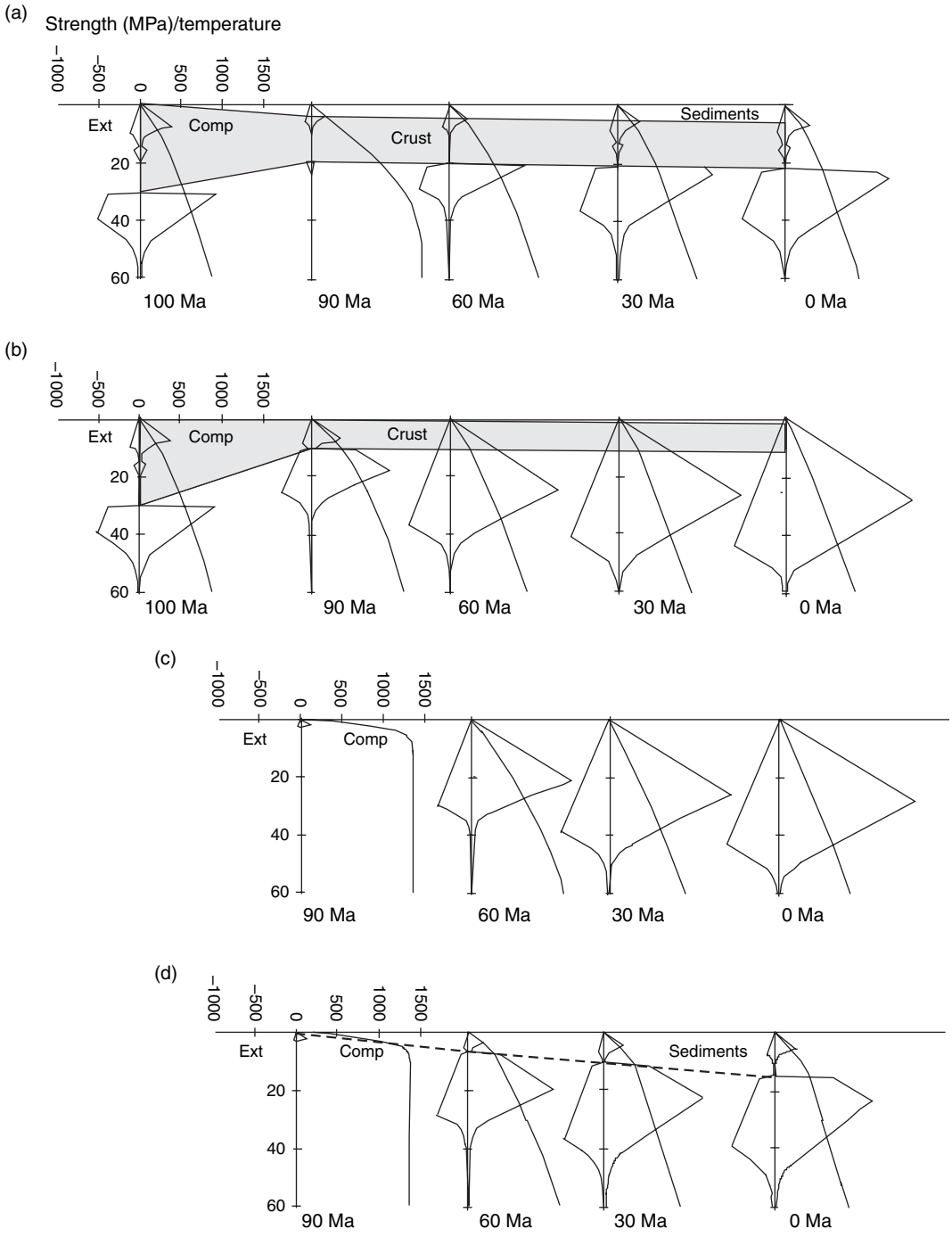

Figure 11 Depth-dependent rheological models for the evolution of lower plate and upper plate passive margins and oceanic lithosphere. For modeling parameters see **Tables 2** and **3**. (a) Upper plate passive margin ($\delta = 2$, $\beta = 10$), characterized at end of postrift phase by complete sediment fill of accommodation space ($\rho_s = 2100\,\mathrm{kg\,m^{-3}}$, 7.084 km sediments). (b) Lower plate passive margin ($\delta = 3$, $\beta = 1.1$), marked by sediment starvation at end of postrift phase (1 km sediments). (c) Oceanic lithosphere with a thin sedimentary cover of 1 km. (d) Oceanic lithosphere with a gradually increasing sedimentary cover reaching a maximum of 15 km. Modified from Ziegler PA, Van Wees J-D, and Cloetingh S (1998). Mechanical controls on collision-related compressional intraplate deformation. *Tectonophysics* 300: 103–129.

by the youthfulness of its lithospheric mantle and its thicker crust, and later by the thermal blanketing effect of sediments infilling the available accommodation space. On the other hand, the strength of oceanic lithosphere, that is covered by thin sediments only, increases dramatically during its 90 My evolution and ultimately exceeds the strength of both margins, even if these are sediment starved (**Figures 11(c)** and **12**). However, the strength of 90 My old oceanic lithosphere that has been progressively covered by very thick sediments is significantly reduced (**Figure 11(d)**) to the point that it approaches the strength of a sediment filled lower plate margin (**Figure 12**).

To test the effects of sediment infill and thermal blanketing on the strength evolution of upper and lower plate passive margins, a wide range of models were run assuming that sediments completely fill the tectonically created accommodation space (sediment overfilled (**Figure 12**)), adopting different sediment densities and corresponding sediment thickness variations (**Table 3**). Results show that a thick syn- and postrift sedimentary prism markedly reduces the integrated strength of a margin. However, despite

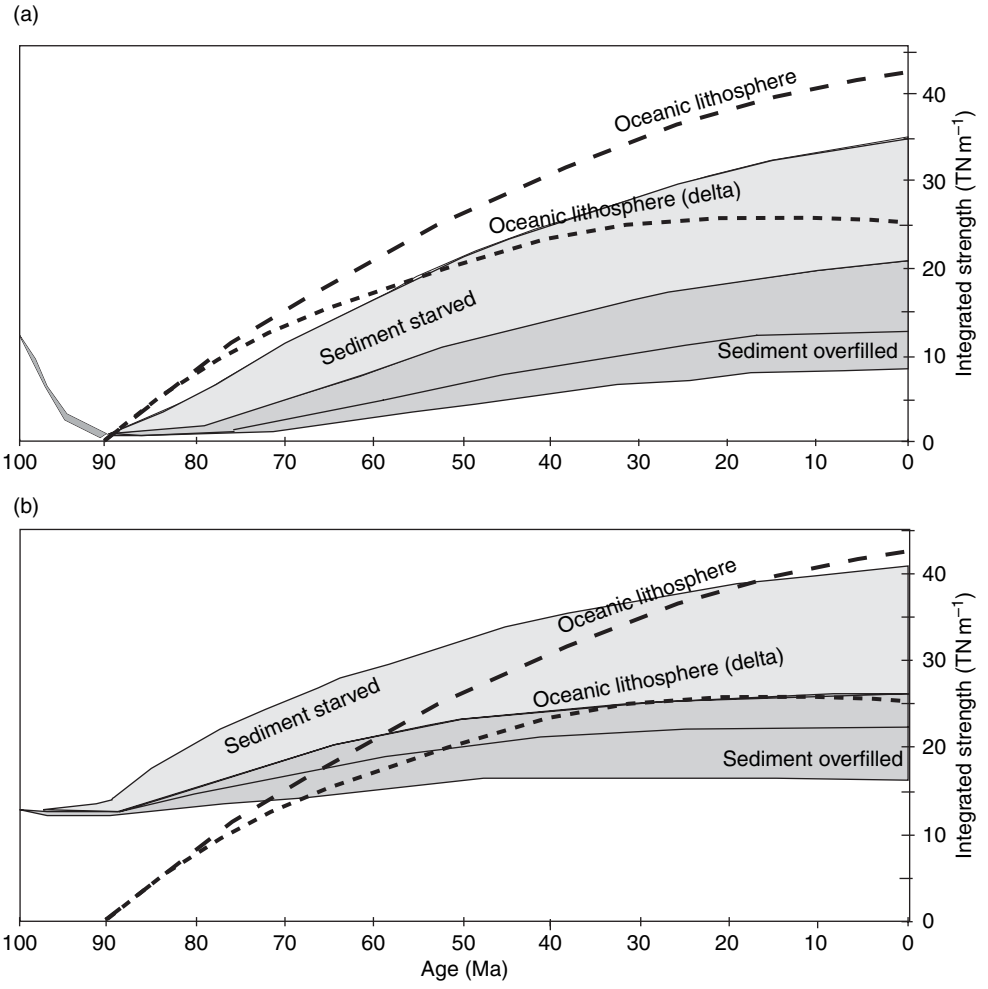

Figure 12 Integrated compressional strength evolution of sediment-starved and sediment-filled (a) upper plate, and (b) lower plate passive margins, compared to the integrated strength evolution of oceanic lithosphere with thin and thick sediment cover as in **Figure 11**. Shaded areas demonstrate strong sensitivity of integrated strength to sediment infilling, ranging from sediment starvation (highest strength values) to complete fill of accommodation space (dark shading, lowest strength values). Curves in dark shaded area correspond to different sediment densities and related range in sediment thickness (see **Table 3**). Modified from Ziegler PA Van, Wees J-D, and Cloetingh S (1998). Mechanical controls on collision-related compressional intraplate deformation. *Tectonophysics* 300: 103–129.

Table 3 Sediment-overfilled scenario (up to water surface), adopted in **Figure 12**

		Tectonic air-loaded subsidence (m)	Accumulated sediment fill (m)		
			$\rho_s = 2100\,kg\,m^{-3}$	$\rho_s = 2500\,kg\,m^{-3}$	$\rho_s = 2650\,kg\,m^{-3}$
Upper plate	Syn-rift	1474	4396	7065	9148
	Postrift	2375	7084	11384	14739
Lower plate	Syn-rift	2599	7752	7752	16130
	Postrift	3332	9939	15972	20679

the strong sediment fill effect on the integrated strength, earlier identified first-order differences between upper and lower plate margins remain. Compared to oceanic lithosphere, both with a 1 km sedimentary cover (**Figures 11(c) and 12**) and a 15 km thick cover (**Figure 11(d)**), a sediment overfilled upper plate margin (applying $\rho_S = 2100\,kg\,m^{-3}$) is characterized by lower integrated strength values throughout its evolution. However, for a lower plate margin conditions are dramatically different. Up to 20–70 My after rifting, the lower plate integrated strength values are significantly higher than those for oceanic lithosphere, both with a thin and a thick sedimentary cover.

From these strength calculations it is evident that at any stage the upper plate margin is weaker than oceanic lithosphere and the conjugate lower plate margin. This suggests that the upper plate margin is the most likely candidate for compressional reactivation and the initiation of a subduction zone. For realistic sediment density and infill values ($\rho_S \leq 2500\,kg\,m^{-3}$), also the upper plate margin tends to grow stronger in time, indicating that after a prolonged postrift stage (>70 My) localization of deformation and subduction along such a margin, instead of on the adjacent continent, should be facilitated by weakening mechanisms that are not incorporated in our standard rheological assumptions for the lithosphere, such as preexisting crustal and mantle discontinuities and the boundaries between old and newly accreted lithospheric mantle.

The modeling shows that the compressional yield strength of passive margins can vary considerably, depending on their lithospheric configuration, sedimentary cover and thermal age. Lower plate margins, at which much of the old continental mantle-lithosphere is preserved, are considerably stronger than upper plate margins at which asthenospheric material has been accreted to the strongly attenuated old mantle-lithosphere. Although mature oceanic lithosphere is characterized by a high compressional yield strength, it can be significantly weakened in areas where thick passive-margin sedimentary prisms or deep-sea fans prograde onto it (e.g., Gulf of Mexico: Worrall and Snelson, 1989; Niger Delta: Doust and Omatsola, 1989; Bengal fan: Curray and Moore, 1971).

6.11.2.1.5 Finite strength of the lithosphere in extensional basin formation

In recent approaches to extensional basin modeling the implementation of finite lithospheric strengths is an important step forward (see Section 6.11.3 for a review). Advances in the understanding of lithospheric mechanics (e.g., Ranalli, 1995; Burov and Diament, 1995) demonstrate that early stretching models which assumed zero lithospheric strength during rifting are not valid. Moreover, the notion of a possible decoupling zone between the strong upper crust and the strong lithospheric upper mantle (see Section 6.11.3.1) is also important in the context of extensional basin formation. During the past decades the relative importance of pure shear (McKenzie, 1978) and simple shear (Wernicke, 1985) mode of extension has been a matter of debate. **Figure 13** suggests that in the presence of a weak lower crustal layer decoupling of the mechanically strong upper

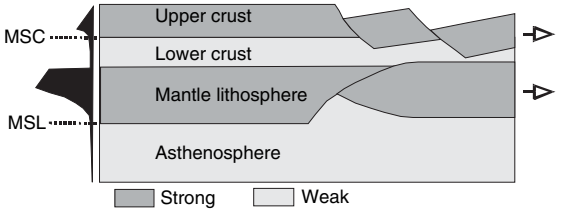

Figure 13 Kinematic model for extension of rheologically stratified lithosphere. See strength profile on left side of diagram. MSC and MSL indicate the base of the mechanically strong crust and mechanically strong lithosphere, respectively. Reston TJ (1990) The lowest crust and the extension of the continental lithosphere; kinematic analysis of BIRPS deep seismic data. *Tectonics* 9: 1235–1248.

crust from the even stronger upper lithospheric mantle, the zone and symmetry of upper crustal extension, does not necessarily have to coincide with the zone and symmetry of lithospheric mantle extension. This is particularly the case if the upper crust is weakened by preexisting discontinuities favouring its simple shear extensional deformation (Ziegler, 1996b). A better appreciation of the role played by rheology during basin formation and the advent of corresponding modeling capabilities during the past few years has increasingly shifted the focus of attention away from these end members of lithospheric extension. Finite element models have explored the large-scale implications of a finite lithospheric strength and particularly its sensitivity to the presence of fluids in the crust and lithospheric mantle (Braun and Beaumont, 1989; Dunbar and Sawyer, 1989; Govers and Wortel, 1993; Bassi, 1995). These dynamic models, which require intensive computing, are expensive to run, and thus are not suitable for an industry user-oriented environment. However, they have provided the background for a more user-friendly class of kinematic models targeted at modeling rift-shoulder uplift and basin fill (Cloetingh *et al.*, 1995c). These kinematic models invoke the concept of lithospheric necking around one of its strong layers during extensional basin formation (see Braun and Beaumont, 1989; Kooi *et al.*, 1992; Spadini *et al.*, 1995b). **Figure 7** illustrates the basic features of these models and their relation to the strength distribution within the lithosphere. In the presence of a strong layer in the subcrustal mantle, the level of lithospheric necking is deep, inducing pronounced rift-shoulder topography. This type of response is to be expected if extension affects cold and correspondingly strong intracontinental lithosphere; it is commonly observed in intracratonic rifts and rifted margin such as, for example, the Red Sea and the Trans-Antarctic Mountains (Cloetingh *et al.*, 1995c).

For Alpine/Mediterranean basins, which developed on a weak lithosphere with a thickened crust, the necking level is generally located at shallower depths (**Figure 14**). An example of such a situation is found in the Pannonian Basin (Van Balen *et al.*, 1995, 1999; Horváth and Cloetingh, 1996) where the necking level is located at depths between 5 and 10 km within the upper crust. In this case the strength of the lithospheric upper mantle has decreased to almost zero (see also **Figure 7**). Important exceptions to this general pattern do occur, however, such as in the Southern Tyrrhenian Sea, for which our modeling indicates a deep necking level to fit observational data (Spadini *et al.*, 1995a, 1995b, Spadini and Podladchikov, 1996). This is primarily attributed to the fact that the Southern Tyrrhenian Basin developed essentially on Hercynian lithosphere with significant bulk strength of its mantle component. In other areas, this concept has led to a better understanding of lateral variations in basin structure and sedimentary fill within one and the same basin. This is exemplified by the Black Sea (see Section 6.11.5), where modeling deciphered important variations in necking level and thermal conditions between its eastern and western sub-basins that can be attributed to differences in the timing and mode of their development (Spadini *et al.*, 1996, 1997, Robinson *et al.*, 1995, Cloetingh *et al.*, 2003).

The interdependence of the necking depth and such parameters as prerift crustal and lithospheric thicknesses, the EET of the lithosphere and strain rates was investigated in a comparative study on several basins, using the same modeling technology (Cloetingh *et al.*, 1995b, 1995c). Results of this study are summarized in **Figure 14**, illustrating that for Alpine/Mediterranean basins the position of the necking level depends primarily on the prerift crustal thickness and strain rate, whereas the key controlling factors in intracratonic rifts appear to be the prerift lithospheric thickness and strain rate. This figure also illustrates where other basin formation processes have played a role. For instance, the Saudi Arabia–Red Sea margin (point 7), is characterized by the presence of plume-related activity in the upper mantle that explains the systematic misfit of this case. The importance of the prerift lithosphere rheology for the subsequent basin geometry and the patterns of vertical motions are evident from these models. Moreover, they demonstrate that the better we are able to constrain the prerift evolution of an area, the greater the chance we have to define the parameter range that has to be to adopted for large-scale syn-rift mechanics.

6.11.2.1.6 Rift-shoulder development and architecture of basin fill

As discussed above, the finite strength of the lithosphere has important implications for the crustal structure of extensional basins and the development of accommodation space in them. The development of significant rift-shoulder topography in response to lithospheric extension has drawn attention to the need to constrain the coupled vertical motion of the shoulders and the subsiding basin (Kusznir and Ziegler, 1992). Whereas the standard approach in basin analysis focused until recently primarily on

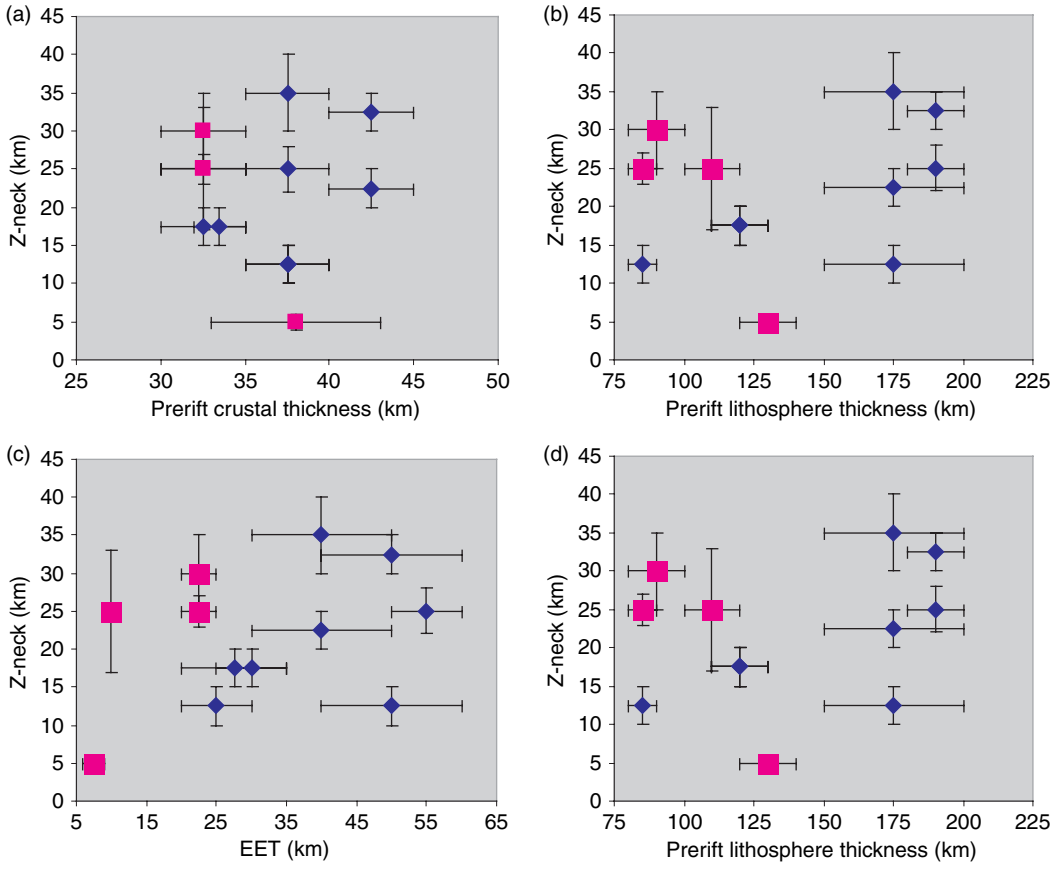

Figure 14 Correlation diagrams for the relationship between: (a) necking depth and prerift crustal thickness; (b) necking depth and prerift lithosphere thickness; (c) EET and necking depth; and (d) necking depth and strain rate. Squares and diamonds indicate data from Alpine/Mediterranean basins and intracratonic rifts, respectively. Numbers refer to the following basins: 1 Gulf of Lion; 2 Valencia trough; 3 southern Tyrrhenian Sea; 4 Pannonian basin; 5 North Sea; 6 Baikal rift; 7 Saudi Arabia Red Sea; 8 Trans-Antarctic Mountains; 9 Barents Sea; 10 East African Rift; 11 western Black Sea; 12 eastern Black Sea. Modified from Cloetingh S, Durand B, and Puigdefabregas C (eds.) (1995d) *Special Issue on Integrated Basin Studies (IBS) – A European Commission (DGXII) project*. Marine and Petroleum Geology 12(8): 787–963.

the subsiding basin, treating sediment supply as an independent parameter, necking models highlight the need for linking sediment supply to the rift-flank uplift and erosion history. To this end, a two-fold approach was followed. The first research line aimed at constraining the predicted uplift histories by geothermochronology. Modeling of the distribution of fission-track length permits to backstack the eroded sediments from their present position in the basin to their source on the rift shoulder in an effort to obtain a better reconstruction of the rift-shoulder geometries (e.g., Van der Beek *et al.*, 1995; Rohrman *et al.*, 1995). This has led to a better understanding of the timing and magnitude of rift-shoulder uplift, for example, on the Norwegian margin, shedding light on the observed relationship between on-shore uplift and the presence of thick Late Cenozoic sedimentary wedges in the adjacent offshore basin (see also Section 6.11.4).

A second research line focused on the development of a model for basin fill simulation, integrating the effects of rift-shoulder erosion through hill-slope transport and river incision with sediment deposition in the basin. As illustrated in **Figure 15** (see Van Balen *et al.*, 1995), these models predict the progradation of sedimentary wedges into extensional basins and the development of hinterland basins having a distinctly different stratigraphic signature than predicted by standard models, which invoke stretching and postrift flexure, and which are commonly applied in the existing packages. Testing of this new model against a number of rifted margins around the world demonstrates that erosion of the rift-shoulder topography, created during extension of a lithosphere

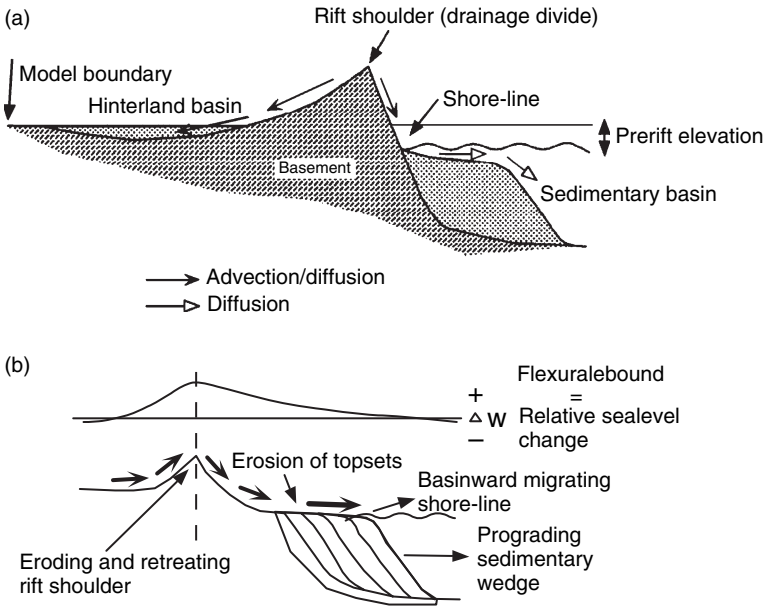

Figure 15 (a) Cartoon of the rift shoulder erosion model. The isostatic response to necking of the lithosphere during extension causes a flexurally supported rift shoulder. In a landward direction the rift shoulder is flanked by a flexural down warp, the hinterland basin. The erosion products of the rift shoulder are transported to the offshore rifted basin and the hinterland basin. When the hinterland basin is completely filled, the sediments are taken out at the location indicated by 'model boundary'. These sediments are reintroduced into the model at the shoreline position in the offshore basin, establishing conservation of mass in the model. (b) Cartoon illustrating the mechanism of initial postrift coastal offlap at passive margins. Flexural rebound in response to erosional unloading at the rift shoulder causes uplift extending far into the offshore basin. The uplift causes erosional truncation of the topsets of the sedimentary wedge. Coastal onlap will occur when the rate of erosion-induced uplift is less than the subsidence caused by sedimentary loading, thermal contraction and the flexural response to the increase in rigidity. Δw shows the instantaneous flexural uplift (+) and subsidence (–) pattern caused by rift shoulder erosion. Modified from Van Balen RT, Van der Beek PA, and Cloetingh S (1995) The effect of rift shoulder erosion on stratal patterns at passive margins: implications for sequence stratigraphy. *Earth and Planetary Science Letters* 134: 527–544.

with a finite strength, eliminates to a large extent the need to invoke eustatic sea-level changes to explain the most commonly encountered large-scale stratigraphic features of rifted basins and associated hinterland basins.

On the scale of individual half-grabens, faulting exerts the main control on the basin architecture. Modeling studies have focused on the coupling of fault block tilting and the flexural behaviour of the extending lithosphere, as illustrated in **Figure 16**. In a first step, modeling technology was developed to quantify the thermal effects of faulting on an extending lithosphere (Ter Voorde and Bertotti, 1994). Subsequently, models were developed that link the evolution of individual half-grabens to the extensional response of the deeper lithospheric (Ter Voorde and Cloetingh, 1996). The second step aimed at validating and testing these models against closely constrained natural examples, such as the well-exposed Mesozoic Southern Alpine rifted margin, where extensive radiometric dating and the application of Ar/Ar laser-probing techniques permitted to constrain with high accuracy the thermal evolution of the extending lithosphere at sub-basin and basin-wide scales (Bertotti and Ter Voorde, 1994). Testing and validation of the stratigraphic modeling component was carried out by a case-history study of the Oseberg field in the Norwegian part of the Viking graben (Ter Voorde *et al.*, 1997). This study demonstrated the need to establish a regional framework, linking the mechanics of the Oseberg block to the crustal evolution of adjacent areas, as a prerequisite for more detailed reservoir modeling.

Considering the notion that in syn-rift basins different spatial and temporal scales are by their very nature linked, ignorance of constraints and structural information on surrounding areas will severely limit the quality of reservoir modeling. Modeling provides a quantitative tool to assess tectonic controls on syn-rift depositional sequences at a sub-basin scale (see also Nottvedt *et al.*, 1995). The amount of footwall uplift of an individual fault block appears to depend

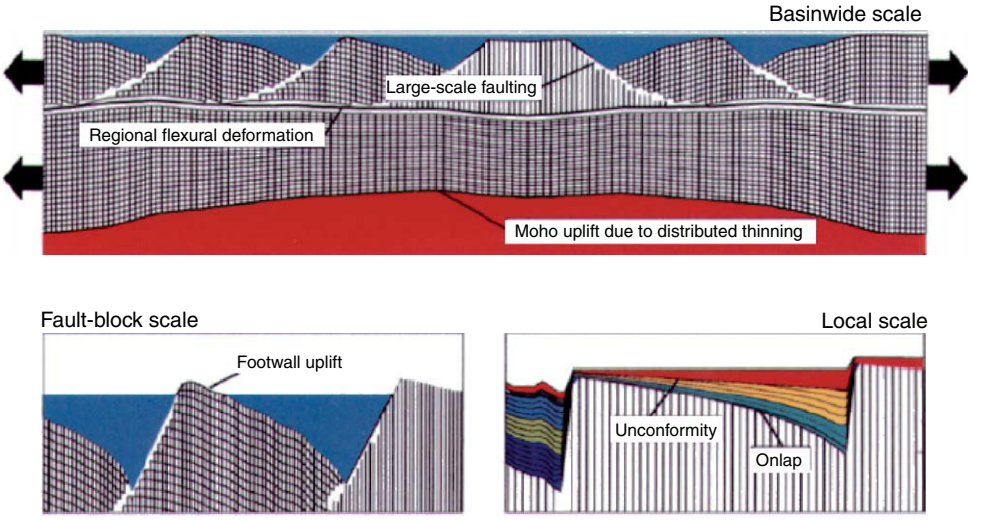

Figure 16 Finite difference model developed for modeling of extensional tilted fault-blocks and large-scale deformation of the lithosphere. Modified from Ter Voorde and Cloetingh S (1996) Numerical modelling of extension in faulted crust: effects of localized and regional deformation on basin stratigraphy. *Geological Society*, *London*, *Special Publications* 99: 283–296.

directly on the lithospheric necking level, controlling the large-scale response of the lithosphere to extension, and, therefore, should not only be attributed to factors restricted to the sub-basin scale.

6.11.2.1.7 Transformation of an orogen into a cratonic platform: the area of the European Cenozoic Rift System

The European Cenozoic Rift System (ECRIS) extends from the shores of the North Sea to the Mediterranean and transects the French and German parts of the Late Palaeozoic Variscan Orogen (**Figure 17**) (Ziegler, 1990b, 1994; Dèzes *et al.*, 2004). In the ECRIS area, the deeply eroded Variscan Orogen was, and partly is still covered by extensive Late Permian and Mesozoic platform sediments. These were disrupted during the evolution of ECRIS owing to rift-related uplift of the Rhenish and Bohemian Massifs, the Vosges-Black Forest Arch and the Massif Central, thus exposing parts of the Variscan Orogen and providing insight into its architecture. This offers a unique opportunity to assess processes controlling the transformation of the Variscan Orogen into a cratonic platform (see Ziegler *et al.*, 2004 for details and comprehensive references).

Main elements of ECRIS are the Lower Rhine (Roer Valley), Hessian, Upper Rhine, Limagne, Bresse, and Eger grabens. The Lower Rhine and Hessian grabens transect the external parts of the Varsican Orogen, the Rheno-Hercynian thrust belt. The Upper Rhine, Bresse, and Limagne grabens cross-cut the internal parts of the Variscan Orogen (**Figure 18**), consisting of the Mid-German Crystalline Rise and the Saxo-Thuringian, Bohemian-Armorican and Moldanubian-Arverno-Vosgian zones, that are characterized by basement-involving nappes and a widespread syn- and postorogenic magmatism. The Eger graben is superimposed on the eastern parts of the Saxo-Thuringian zone.

In the ECRIS area, the depth to Moho varies between 24 and 30 km and increases away from it to 34–36 km and more (**Figure 19**) (Ziegler and Dèzes, 2006). The thickness of the lithosphere decreases from about 100–120 km in the Bohemian Massif and along the southern end of the Upper Rhine Graben to 60–70 km beneath the Rhenish Massif and Massif Central, and appears to increase to some 120 km or more in the Western Netherlands and beneath the Paris Basin (Babuska and Plomerova, 1992, 1993; Sobolev *et al.*, 1997; Goes *et al.*, 2000a, 2000b). Mantle tomography images beneath the ECRIS area a system of upper asthenospheric low velocity anomalies, interpreted as plume heads that have spread out above the 410 km discontinuity (Spakman and Wortel, 2004; Sibuet *et al.*, 2004), and from which secondary, relatively weak plumes rise up under the Rhenish Massif (Ritter *et al.*, 2001) and the Massif Central (Granet *et al.*, 1995).

The present crustal and lithospheric configuration of Western and Central Europe bears no relationship to the major structural units of the Variscan Orogen, but shows close affinities to ECRIS (Ziegler and

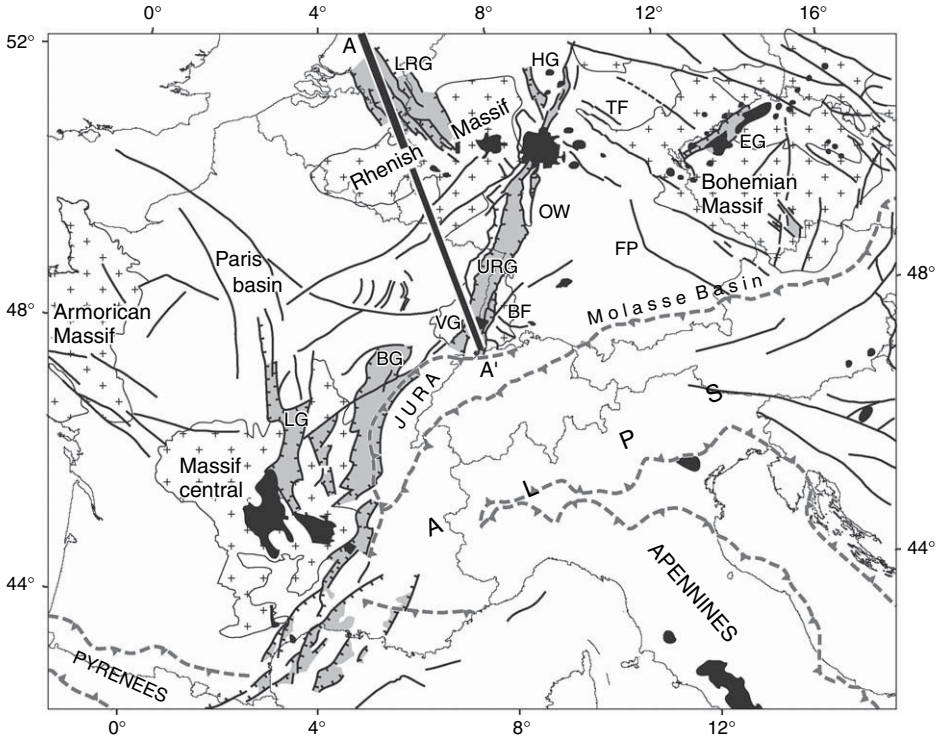

Figure 17 Location map of ECRIS in the Alpine foreland, showing Cenozoic fault systems (black lines), rift-related sedimentary basins (light gray), Variscan massifs (cross pattern) and Cenozoic volcanic fields (black). Interrupted barbed line: Alpine deformation front. BF Black Forest, BG Bresse Graben, EG Eger (Ore) Graben, FP Franconian Platform; HG Hessian grabens, LG Limagne Graben, LRG Lower Rhine (Roer Valley) Graben, URG Upper Rhine Graben, OW Odenwald; VG Vosges. Modified from Dèzes *et al.*, (2004).

Dèzes, 2006). However, development of the Variscan Orogen involved major crustal shortening and subduction of substantial amounts of supra-crustal rocks, continental and oceanic crust and lithospheric mantle (Ziegler *et al.*, 1995, 2004). By analogy with modern examples, such as the Alps (Schmid *et al.*, 1996, 2004; Stampfli *et al.*, 1998), the Variscan Orogen must have been characterized at the time of its end-Westphalian consolidation (305 Ma) by a significantly thickened crust and lithosphere. Subsequently, its orogenically destabilized lithosphere reequilibrated with the asthenosphere so that by Late Mesozoic time cratonic crustal and lithospheric thicknesses of about 28–35 km and 100–120 km, respectively, were established.

Processes controlling postorogenic modification of the Variscan lithosphere have been variably attributed to Permo-Carboniferous slab detachment, delamination of the lithospheric mantle, crustal extension, and plume activity and subsequent thermal relaxation of the lithosphere controlling the subsidence of an intracratonic basin system (Lorenz and Nicholls, 1984; Ziegler, 1990b; Henk, 1999; Henk *et al.*, 2000; Van Wees *et al.*, 2000; Prijac *et al.*, 2000). In order to assess the relative importance of processes contributing toward the postorogenic transformation of the Variscan lithosphere to its craton-like configuration, the evolution of the different Varsican units transected by ECRIS was reviewed, crustal reflection-seismic profiles inspected and quantitative subsidence curves developed for selected wells penetrating the sedimentary cover of the Variscan basement and these compared to a theoretical thermal decay curve.

During the last 310 My, the tectonic setting of the Variscan domain changed repeatedly. Following the late Westphalian (305 Ma) consolidation of the Variscan Orogen its Stephanian–Early Permian collapse (305–280 Ma) was controlled by wrench faulting and associated magmatic activity. During Late Permian to Cretaceous times, large parts of the Variscan domain were incorporated into an intracratonic basin system. This was affected during the latest Cretaceous and Palaeocene by an important pulse of intraplate compression that relates to early phases of the Alpine orogeny. At the same time, an array of

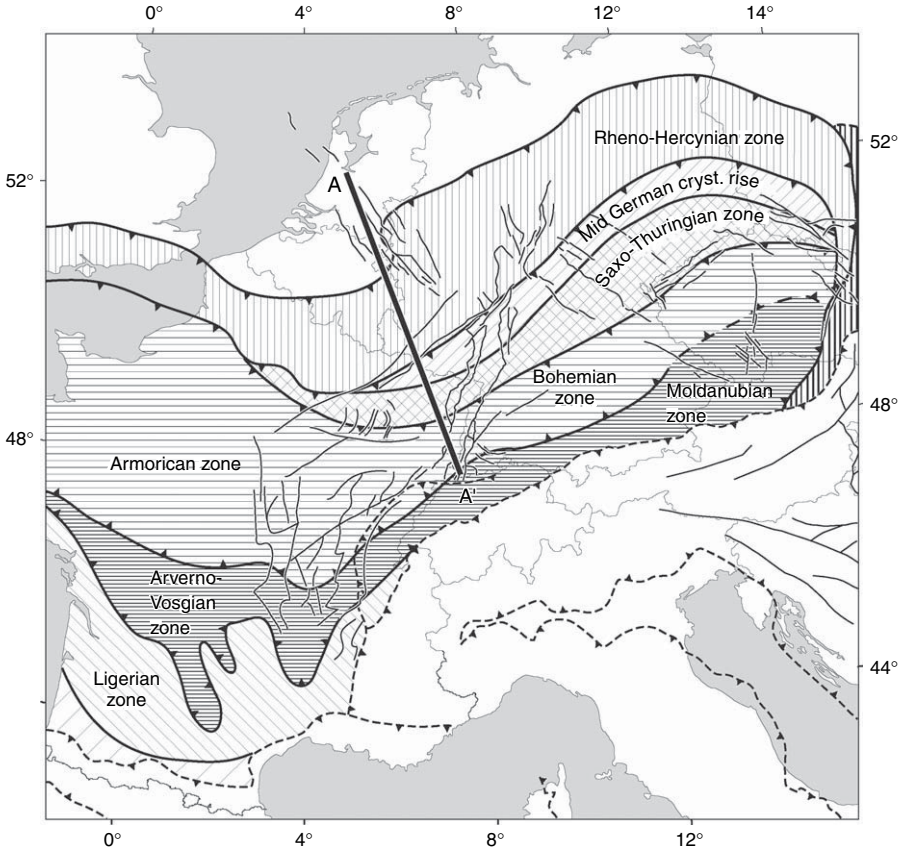

Figure 18 Variscan tectonic framework with superimposed ECRIS fault pattern. Modified from Ziegler PA, Schumacher ME, Dézes P, van Wees J-D, and Cloetingh S (2004) Post-Variscan evolution of the lithosphere in the Rhine Graben area: constraints from subsidence modelling. In: Wilson M, Neumann E-R, Davies GR, Timmerman MJ, Heeremans M, and Larsen BT (eds.) *Geological Society*, *London*, *Special Publications*, 223: *Permo-Carboniferous Magmatism and Rifting in Europe*, pp. 289–317. London: Geological Society, London.

mantle plumes impinged on the lithosphere of Western and Central Europe, such as the NE Atlantic and Iceland plumes and precursors of the Massif Central and Rhenish plumes. The resulting increase in the potential temperature of the asthenosphere caused a renewed destabilization of the lithosphere, as evidenced by Palaeocene injection of mafic dykes in the Massif Central, Vosges-Black Forest and Bohemian Massif, reflecting low-degree partial melting of the lithospheric thermal boundary layer at depths of 60–100 km. Starting in mid-Eocene times, ECRIS developed in the foreland of the evolving Alpine and Pyrenean orogens, with crustal extension and continued plume activity causing further destabilization of its lithosphere–asthenosphere system (Ziegler, 1990b; Dèzes *et al.*, 2004, 2005; Ziegler and Dèzes, 2006, 2007).

In terms of defining boundary conditions for modeling the postorogenic evolution of the Variscan lithosphere, information on its Late Carboniferous (305 Ma), late Early Permian (280 Ma), end-Cretaceous (65 Ma) and present configuration is required. Whilst present crustal thicknesses are closely constrained, control on lithospheric thickness is less reliable. The Late Carboniferous, late Early Permian and end-Cretaceous–Palaeocene lithospheric configurations can, however, only be inferred from circumstantial evidence. In this respect, vertical movements of the crust, derived from its sedimentary cover, provide constraints for assessing the postorogenic evolution of the Variscan lithosphere.

Below the Late Palaeozoic and Mesozoic evolution of the ECRIS area is summarized, results of quantitative and forward modeled subsidence analyses on selected wells presented, and a model proposed for the postorogenic evolution of the lithosphere (see Ziegler *et al.*, 2004). The time scales of Menning *et al.*, (2000) and Menning (1995) were

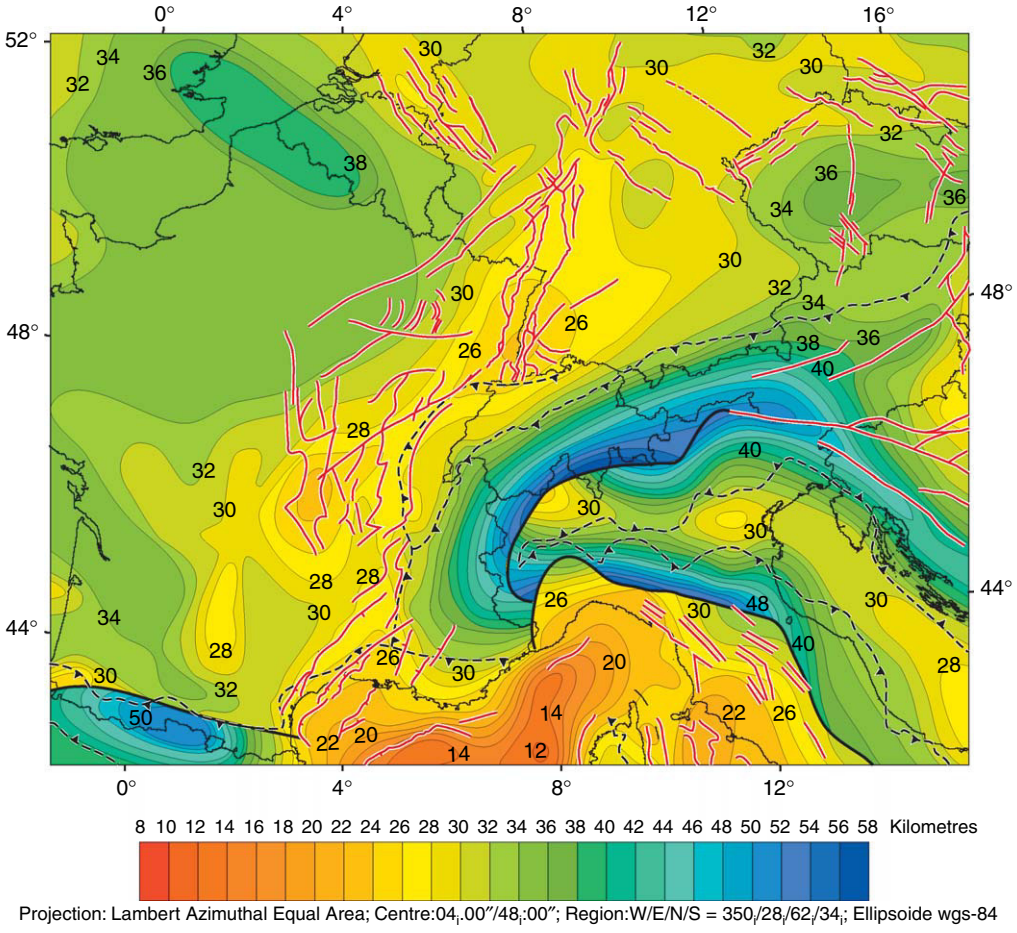

Figure 19 Depth map of Moho discontinuity (2 km contour interval) in the Alpine foreland, constructed by integration of published regional maps. Red lines: superimposed Cenozoic fault systems. Interrupted barbed line: Alpine deformation front. Modified from Dèzes P and Ziegler PA (2004) Moho depth map of western and central Europe. EUCOR-URGENT homepage: http://www.unibas.ch/eucor-urgent (acessed Jul 2007).

adopted for the Carboniferous and Permo-Triassic, respectively, and for later times the scale of Gradstein and Ogg (1996).

6.11.2.1.7.(i) Variscan Orogen Evolution of the Variscan Orogen, which forms part of the Hercynian mega-suture along which Laurussia and Gondwana were welded together, involved the stepwise accretion of a number of Gondwana-derived terranes (e.g., Saxo-Thuringian, Armorican-Bohemian, and Moldanubian terranes) to the southern margin of Laurussia and ultimately the collision of Africa with Europe (Ziegler, 1989a, 1989b, 1990b; Tait *et al.*, 1997). ECRIS transects the suture between the Rheno-Hercynian foreland and the Saxo-Thuringian terrane, and the more internal sutures between the Saxo-Thuringian and Bohemian, and the Bohemian and Moldanubian terranes (**Figure 18**). The triple junction of the Upper Rhine, Roer, and Hessian grabens is superimposed on the south-dipping Rheno-Hercynian/Saxo-Thuringian suture. The Upper Rhine Graben transects the south-dipping Saxo-Thuringian/Bohemian suture in the northern part of the Vosges and Black Forest (Lalaye-Lubin-Baden-Baden zone), and the north-dipping Bohemian/ Moldanubnian suture in the southern part of the Black Forest (Badenweiler-Lenzkirch zone) (Eisbacher *et al.*, 1989; Franke, 2000; Hegner *et al.*, 2001). To the southwest, the latter links up with the Mt. du Lyonnais suture that is cross-cut by the Bresse and Limagne Grabens (Lardeaux *et al.*, 2001). Total Carboniferous lithospheric shortening in the area transected by ECRIS presumably exceeded 600 km.

At the end-Westphalian termination of the Variscan orogeny, the crustal and lithospheric configuration of

the future ECRIS area was heterogeneous and presumably marked by a considerable topographic relief. Whereas the Rheno-Hercynian zone was underlain by continental foreland lithosphere, the Saxo-Thuringian and Moldanubian zones were characterized by an orogenically thickened lithosphere that was thermally destabilized by widespread granitic magmatism. In the internal zones of the Variscan Orogen, crustal thicknesses probably ranged between 45 and 60 km with crustal roots marking the Rheno-Hercynian/Saxo-Thuringian, Saxo-Thuringian/Bohemian, and Bohemian/Moldanubnian sutures. By end-Westphalian times, a major south-dipping continental lithospheric slab extended from the Variscan foreland beneath the Rheno-Hercynian/Saxo-Thuringian suture in the area of the Mid-German Crystalline Rise. Similarly, a north-dipping, partly oceanic subduction slab was probably still associated with the Bohemian/Moldanubnian suture, whereas the south-dipping Saxo-Thuringian/Bohemian slab had already been detached during mid-Visean times (**Figure 20(a)**).

6.11.2.1.7.(ii) Stephanian–Early Permian disruption of the Variscan Orogen End-Westphalian consolidation of the Variscan Orogen was followed by its Stephanian–Early Permian wrench-induced collapse (305–280 Ma), reflecting a change in the Gondwana-Laurussia convergence from oblique collision to a dextral translation (Ziegler, 1989a, 1989b, 1990b). Continental-scale dextral shears, such as the Tornquist-Teisseyre and the Bay of Biscay fractures zones, were linked by secondary sinistral and dextral shear systems. These overprinted and partly disrupted the Variscan Orogen and its northern foreland. Wrench tectonics and associated magmatic activity abated in the Variscan domain and its foreland at the transition to the Late Permian (Ziegler, 1990b; Marx *et al.*, 1995; Ziegler and Stampfli, 2001; Ziegler and Dèzes, 2006). Stephanian–Early Permian wrench-induced disruption of the rheologically weak Variscan Orogen was accompanied by regional uplift, widespread extrusive and intrusive magmatism peaking during the Early Permian, and the development of a multidirectional array of transtensional trap-door and pull-apart basins containing continental clastics (**Figure 21**). Basins developing during this time span underwent a complex, polyphase evolution, including late-stage transpressional deformation controlling their partial inversion. Although Stephanian–Early Permian wrench faulting locally caused uplift of core complexes (e.g., Massif Central, Montagne Noire: Vanderhaeghe and Teyssier, 2001) and subsidence of often narrow, fault-bounded basins, implying high crustal stretching factors, large intervening areas were not significantly extended (Van Wees *et al.*, 2000; Ziegler *et al.*, 2004).

Whilst exhumation of the Variscan Internides had commenced already during the main phases of the Variscan orogeny, regional uplift of the entire orogen and its foreland commenced only after crustal shortening had ceased. Stephanian–Early Permian erosional and tectonic exhumation of the Variscan Orogen, in many areas to formerly mid-crustal levels (Burg *et al.*, 1994; Vigneresse, 1999), can be attributed to a combination of such processes as wrench deformation, heating of crustal roots and related eclogite to granulite transformation (Bousquet *et al.*, 1997; Le Pichon *et al.*, 1997), detachment of subducted slabs, upwelling of the asthenosphere, thermal attenuation of the lithospheric mantle, and magmatic and thermal inflation of the remnant lithosphere (**Figure 20(b)**).

6.11.2.1.7.(ii).(a) Permo-Carboniferous magmatism and lithospheric destabilization The widespread Stephanian–Early Permian (305–285 Ma) alkaline intrusive and extrusive magmatism of the Variscan domain and its foreland is mantle-derived and locally shows evidence of strong crustal contamination (Bonin, 1990; Bonin *et al.*, 1993; Marx *et al.*, 1995; Benek *et al.*, 1996; Breitkreuz and Kennedy, 1999; Neumann *et al.*, 1995, 2004). Melt generation by partial melting of the uppermost asthenosphere and lithospheric thermal boundary layer was probably triggered by a rise in the potential temperature of the asthenosphere and by its localized transtensional decompression. Wrench-induced detachment of subducted lithospheric slabs presumably caused a reorganization of the mantle convection system and upwelling of the asthenosphere. Mantle-derived mafic melts, which had ascended to the base of the crust, underplated it, inducing crustal anatexis, and the intrusion of fractionally crystallized granitic to granodioritic–tonalitic melts into the crust.

Combined with erosional and locally tectonic unroofing of the Variscan crust, interaction of mantle-derived melts with the felsic lower crust contributed to a reequilibration of the Moho at depths of 28–35 km and locally less. By Mid-Permian times (±280 Ma), some 25 My after consolidation of the Variscan Orogen, its crustal roots had disappeared.

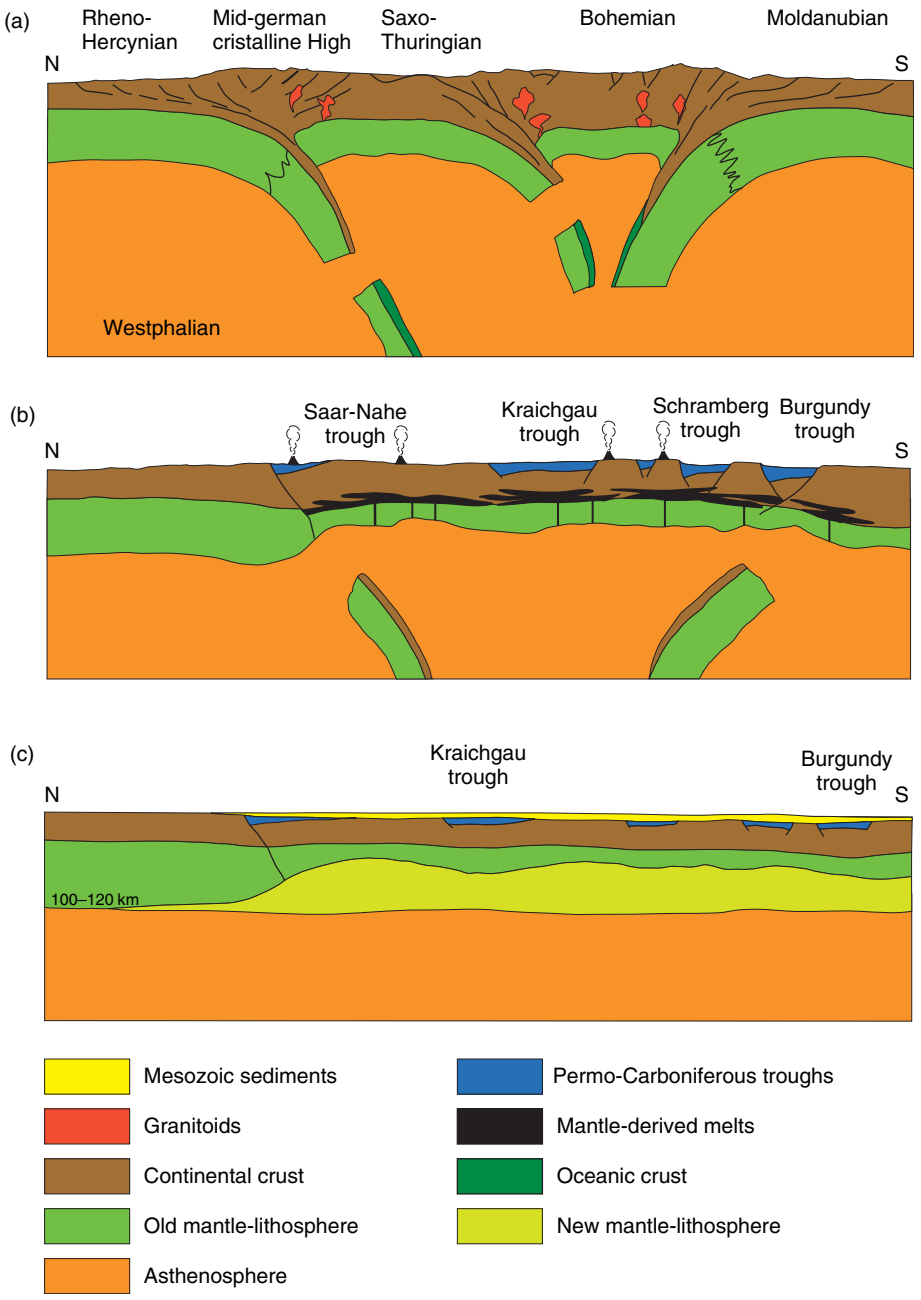

Figure 20 Conceptual model for Late Palaeozoic and Mesozoic evolution of the lithosphere in the ECRIS area along transect A-A'(not to scale). For location of transect see **Figures 17** and **18**. Modified from Ziegler PA, Schumacher ME, Dézes P, van Wees J-D, and Cloetingh S (2004) Post-Variscan evolution of the lithosphere in the Rhine Graben area: constraints from subsidence modelling. In: Wilson M, Neumann E-R, Davies GR, Timmerman MJ, Heeremans M, and Larsen BT (eds.) *Geological Society*, *London*, *Special Publications*, 223: *Permo-Carboniferous Magmatism and Rifting in Europe*, pp. 289–317. London: Geological Society, London.

6.11.2.1.7.(ii).(b) Permo-Carboniferous evolution of the ECRIS Zone During the Stephanian and Early Permian, a system of essentially ENE–WSW trending transtensional intramontane basins developed in the ECRIS area (**Figure 21**). Subsidence of these basins, which contain thick continental clastics and volcanics, involved reactivation of the Variscan structural grain, predominantly by dextral shear. The Saar-Nahe Trough is superimposed on the Rheno-Hercynian/Saxo-Thuringian and partly on

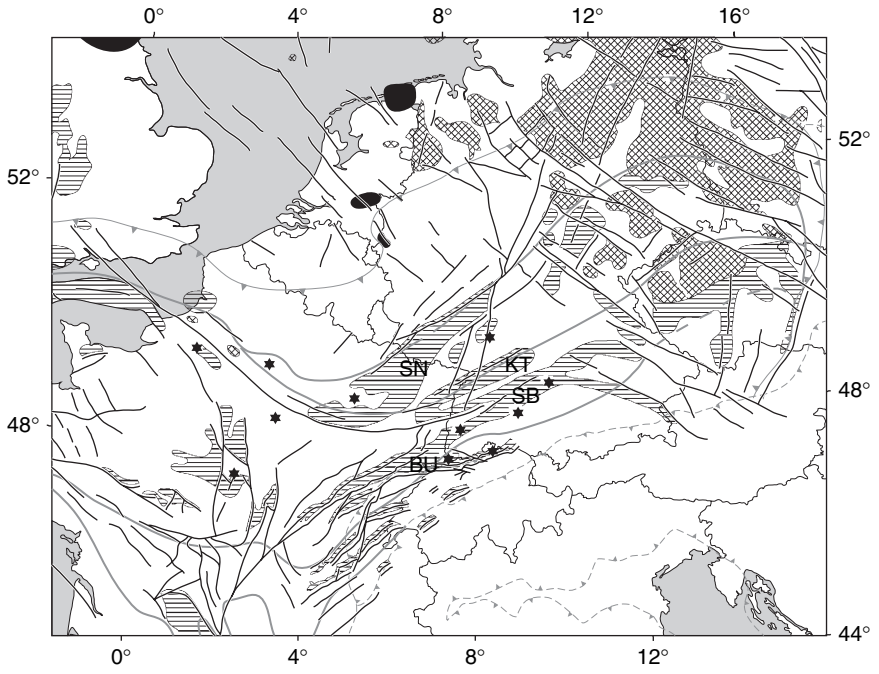

Figure 21 Stephanian–Early Permian tectonic framework of ECRIS area, showing sedimentary basins (horizontally hatched), major volcanic fields (cross hatched), major sills (black) and fault systems with superimposed Variscan tectonic units (solid lines) and Alpine deformation front (interrupted barbed line). Abbreviations: BU Burgundy Trough, KT Kraichgau Trough, SB Schramberg Trough, SN Saar-Nahe Trough. Black dots show location of analysed wells. Modified from Ziegler PA, Schumacher ME, Dézes P, van Wees J-D, and Cloetingh S (2004). Post-Variscan evolution of the lithosphere in the Rhine Graben area: constraints from subsidence modelling. In: Wilson M, Neumann E-R, Davies GR, Timmerman MJ, Heeremans M, and Larsen BT (eds.) *Geological Society*, *London*, *Special Publications*, 223: *Permo-Carboniferous Magmatism and Rifting in Europe*, pp. 289–317. London: Geological Society, London.

the Saxo-Thuringian/Bohemian sutures. The Kraichgau Trough broadly reflects reactivation of the Saxo-Thuringian/Bohemian Lalaye–Lubin–Baden–Baden suture, whereas the Schramberg and Burgundy troughs are associated with the Bohemian/Moldanubnian Lenzkirch–Badenweiler–Mt. du Lyonnais suture. Subsidence of these basins was coupled with uplift and erosion of intervening highs, amounting, for instance, at the margin of the Saar-Nahe Trough to as much as 10 km. At the same time, NNE–SSW trending Variscan shear zones were sinistrally reactivated, partly outlining the Cenozoic Upper Rhine and Hessian grabens.

In the area of the Variscan Internides, the widespread occurrence of a reflection-seismically laminated 10–15 km thick lower crust is mainly attributed to Permo-Carboniferous injection of mantle-derived basic sills. Moreover, truncation of the crustal orogenic fabric by the Moho (Meissner and Bortfeld, 1990) speaks for contemporaneous magmatic destabilization of the crust–mantle boundary. In the internal Variscan zones, no mantle reflectors related to subducted crustal material (Ziegler *et al.*, 1998) could be detected despite dedicated surveys (Meissner and Rabbel, 1999). This is thought to reflect delamination and/or strong thermal thinning of the lithospheric mantle (**Figure 20(b)**).

Combined with widespread magmatic activity, these phenomena testify to a major thermal surge that can be related to the detachment of the subducted south-dipping continental Rheno-Hercynian lithospheric slab beneath the Mid-German Crystalline Rise and the north-dipping Moldanubian slab in the area of the Lenzkirch–Badenweiler–Mt. du Lyonnais suture, causing upwelling of the asthenosphere into the space formerly occupied by these slabs (**Figure 20(b)**). This triggered partial melting of the asthenosphere and remnant lithospheric mantle, ascent of melts to the base of the crust and anatexis of lower crustal rocks (model of Davies and Von Blanckenburg, 1996). In conjunction with the ensuing reorganization of mantle flow patterns, a not-very-active mantle plume apparently welled up to the base of the lithosphere in the eastern parts of the future Southern Permian Basin, causing strong thermal attenuation of the lithospheric

mantle and Moho destabilization (Bayer *et al.*, 1999; Van Wees *et al.*, 2000; Ziegler *et al.*, 2004).

6.11.2.1.7.(iii) Late Permian and Mesozoic thermal subsidence and rifting By late Early Permian times (±280 Ma), magmatic activity abated and thermal anomalies introduced during the Permo-Carboniferous began to decay. Combined with progressive degradation of the remnant topography and cyclically rising sea levels, this accounted for the subsidence of increasingly larger areas below the erosional base level and the development of a new intracratonic basin system. However, in large parts of Western and Central Europe thermal reequilibration of the lithosphere–asthenosphere system was overprinted and partly interrupted by the Triassic onset of a new rifting cycle that preceded and accompanied the step-wise breakup of Pangea. Major elements of this breakup system are the southward propagating Arctic–North Atlantic and the westward propagating Neotethys rift systems. Simultaneously, a multidirectional rift system developed in Western and Central Europe, comprising the North Sea rift, the Danish–Polish Trough and the graben systems of the Atlantic shelves. Stress fields controlling their evolution changed repeatedly during the Jurassic and Early Cretaceous (Ziegler, 1988, 1990b; Ziegler *et al.*, 2001; Ziegler and Dèzes, 2006).

Although the ECRIS area was only marginally affected by Mesozoic rifting, minor diffuse crustal stretching probably contributed towards the subsidence of the Kraichgau, Nancy-Pirmasens, Burgundy, and Trier troughs (**Figure 22**). Triassic and Jurassic reactivation of Permo-Carboniferous faults, controlling subtle lateral facies and thickness changes, is also evident in the Paris Basin and in the area of the Burgundy Trough. On the other hand, Mesozoic crustal extension played a more important role in the subsidence of the West Netherlands Basin and in the lower Rhône Valley.

In an effort to quantify in the wider ECRIS area Late Permian and Mesozoic vertical crustal movements, tectonic subsidence curves were constructed for selected wells of the Paris Basin, Upper Rhine Graben, and

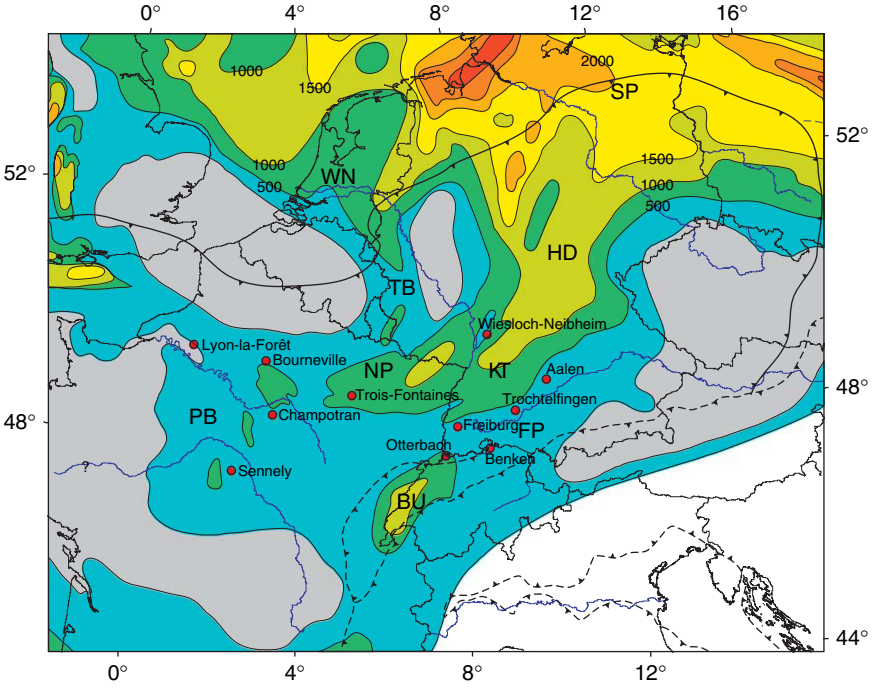

Figure 22 Isopach map of restored Triassic series, contour interval 500 m, showing location of analyzed wells and Variscan (solid barbed line) and Alpine (interrupted barbed line) deformation fronts. White: areas of nondeposition; horizontally hatched: not mapped area. Abbreviations: BU Burgundy Trough, FP Franconian Platform, GG Glückstadt Graben, HD Hessian Depression, KT Kraichgau Trough, NP Nancy-Pirmasens Trough, PB Paris Basin, PT Polish Trough, SP Southern Permian Basin, TB Trier Basin, WN West Netherlands Basin. Modified from Ziegler PA, Schumacher ME, Dézes P, van Wees J-D, and Cloetingh S (2004) Post-Variscan evolution of the lithosphere in the Rhine Graben area: constraints from subsidence modelling. In: Wilson M, Neumann E-R, Davies GR, Timmerman MJ, Heeremans M, and Larsen BT (eds.) *Geological Society*, *London*, *Special Publications*, 223: *Permo-Carboniferous Magmatism and Rifting in Europe*, pp. 289–317. London: Geological Society, London.

Franconian Platform (Ziegler *et al.*, 2004), applying the back stripping method of Sclater and Christie (1980). These curves, similar to those by Loup and Wildi (1994), Prijac *et al.*, (2000) and Van Wees *et al.*, (2000), show that reequilibration of the lithosphere with the asthenosphere commenced during the late Early Permian (±280 Ma) and continued throughout Mesozoic times. Moreover, they show superimposed on the long-term thermal subsidence trends intermittent and generally local Mesozoic subsidence accelerations (**Figure 23**). These are interpreted as reflecting either tensional reactivation of Permo-Carboniferous fault systems or compressional deflection of the lithosphere (Cloetingh, 1988) under stress fields related to far-field rifting and wrench activity.

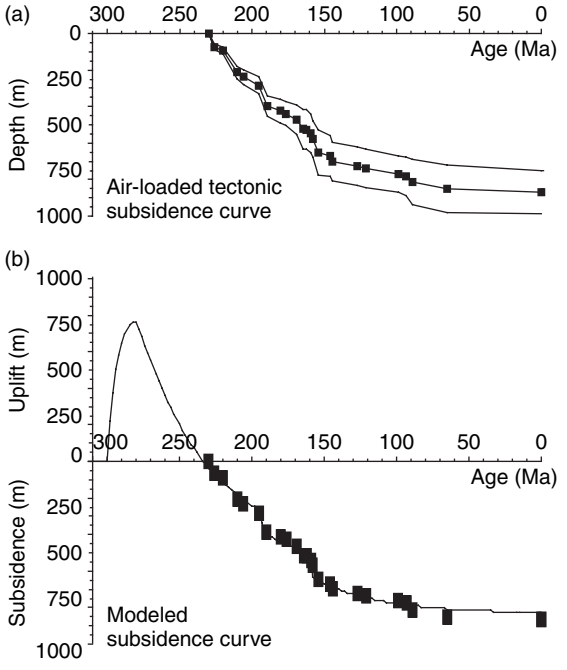

Figure 23 (a) Air-loaded tectonic subsidence curve and (b) modeled subsidence curve for well Bourneville, Paris Basin. For locations see **Figure 22**. Black squares: control points derived from penetrated sedimentary sequence. The positive part of the modeled subsidence curve reflects uplift of the crust in response to thermal thinning and/or delamination of the mantle-lithosphere; its negative part reflects thermal subsidence of the crust during re-equilibration of the lithosphere/asthenosphere system. Modified from Ziegler PA, Schumacher ME, Dézes P, van Wees J-D, and Cloetingh S (2004) Post-Variscan evolution of the lithosphere in the Rhine Graben area: constraints from subsidence modelling. In: Wilson M, Neumann E-R, Davies GR, Timmerman MJ, Heeremans M, and Larsen BT (eds.) *Geological Society, London, Special Publications*, 223: *Permo-Carboniferous Magmatism and Rifting in Europe*, pp. 289–317. London: Geological Society, London.

Temporal and spatial variations in these subsidence accelerations relate to differences in the orientation of preexisting crustal discontinuities and changes in the prevailing stress field. Nevertheless, overall subsidence patterns reflect long-term reequilibration of the lithosphere–asthenosphere system.

6.11.2.1.7.(iv) Tectonic subsidence modeling To define the end-Early Permian configuration of the lithosphere, the tectonic subsidence curves were compared to a theoretical thermal decay curve, applying a numerical forward/backward modeling technique which automatically finds the best-fit stretching parameters for the observed subsidence data (Van Wees *et al.*, 1996, 2000).

Forward/backward modeling of tectonic subsidence is based on lithospheric stretching assumptions (δ = crustal stretching factor, β = lithospheric mantle stretching factor) under which the lithosphere is represented by a plate with constant temperature boundary conditions, adopting a fixed basal temperature (McKenzie, 1978; Jarvis and McKenzie, 1980; Royden and Keen, 1980). For thermal calculations, a 1-D numerical finite difference model was used, adopting parameters as given by Van Wees *et al.*, (2000), that allows for incorporation of finite and multiple stretching phases, as well as for crustal heat production effects and conductivity variations (Van Wees *et al.*, 1992, 1996, 2000; Van Wees and Stephenson, 1995). Differential stretching of the crust and lithospheric mantle can be applied to simulate thermal attenuation of the latter. Input parameters for forward/backward modeling of the observed subsidence curves include the prerift crustal and present lithospheric thickness, and for each stretching phase its timing, duration and mode of lithospheric extension (uniform $\delta = \beta$ (McKenzie, 1978); two-layered $\delta < \beta$ (Royden and Keen, 1980)). In iterative steps modeling parameters are changed until a good fit is obtained between the observed and modeled subsidence curves. Best-fit stretching parameters thus determined give a measure of the thermal perturbation of the lithosphere during the Permo-Carboniferous and subsequent tensional events that interfered with the reequilibration of the asthenosphere–lithosphere system.

Modeling of the lithosphere evolution in the ECRIS area is based on the concept that after the Permo-Carboniferous thermal surge (300–280 Ma) the temperature of the asthenosphere returned rapidly to ambient levels (1300°C), at which it remained until the end-Cretaceous renewed flareup

of plume activity. In the forward/backward model lithospheric thicknesses of 100–120 km were adopted that, according to Babuska and Plomerova (1992, 1993), are representative for areas not affected by Cenozoic rifting. Furthermore, as most of the analyzed wells are located outside Permo-Carboniferous troughs, initial crustal thicknesses were assumed to be close to the present values.

The subsidence curves were modeled with Permo-Carboniferous differential crustal and lithospheric mantle extension (attenuation), allowing β factors to attain significantly greater values than δ factors. The high β factors represent the effects of delamination and thermal thinning of the lithospheric mantle. On the other hand, the temporary Mesozoic subsidence accelerations were successfully modeled with uniform lithospheric extension ($\delta = \beta$). The modeled subsidence curves (**Figure 24**) demonstrate that, after an initial uplift phase between 300 and 280 Ma, which gives a measure of Stephanian–Early Permian lithospheric thinning, the subsequent evolution of the lithosphere was governed by the long-term decay of thermal anomalies introduced during the Permo-Carboniferous tectonomagmatic cycle. This is in accordance with the assumption that the temperature of the asthenosphere had returned to ambient levels around 280 Ma.

Good fits between observed and modeled tectonic subsidence curves were obtained, assuming initial crustal thicknesses of 30–35 km, final lithospheric thicknesses of 100–120 km, and a Permo-Carboniferous 'stretching' phase that spanned 300–280 Ma and involved decoupled crustal extension and attenuation of the lithospheric mantle. This assumption is compatible with the concept that during the Permo-Carboniferous reequilibration of the crust–mantle boundary crustal extension played only locally a significant role. In this respect it is noteworthy that the important Permo-Carboniferous troughs, which occur on the Massif Central and the Bohemian Massif and beneath the Franconian Platform, do not coincide with major Late Permian and Mesozoic depocenters, whereas no major Permo-Carboniferous basins are located under the Southern Permian Basin and Paris Basin depocenters (Ziegler, 1990b). Indeed, no obvious relationship is evident between the distribution and orientation of Permo-Carboniferous troughs and the geometry of the superimposed Late Permian-Mesozoic thermal-sag basins (cf. **Figures 21** and **22**). This suggests that during the Permo-Carboniferous tectonomagmatic cycle, uniform and/or depth-dependent lithospheric extension was, on a regional scale, only a contributing but not the dominant mechanism of

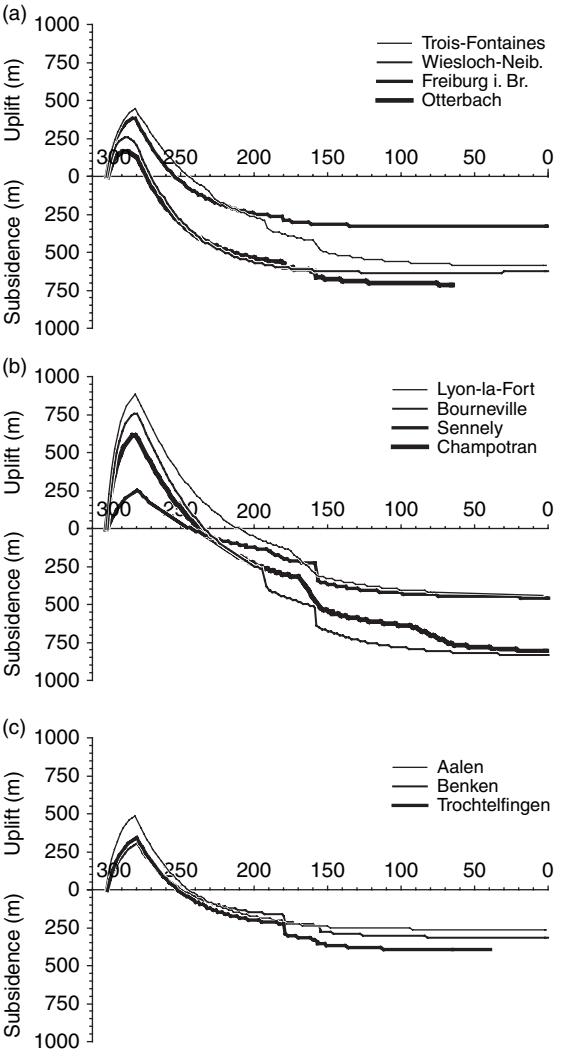

Figure 24 Modeled subsidence curves for (a) Upper Rhine Graben and Lorraine area, (b) Paris Basin, and (c) Franconian platform. For location of wells see **Figure 22**. Modified from Ziegler PA, Schumacher ME, Dézes P, van Wees J-D, and Cloetingh S (2004) Post-Variscan evolution of the lithosphere in the Rhine Graben area: constraints from subsidence modelling. In: Wilson M, Neumann E-R, Davies GR, Timmerman MJ, Heeremans M, and Larsen BT (eds.) *Geological Society, London, Special Publications*, 223: *Permo-Carboniferous Magmatism and Rifting in Europe*, pp. 289–317. London: Geological Society, London.

crustal and lithospheric mantle thinning, as advocated for the Paris Basin by Prijac *et al.*, (2000). By contrast, lithospheric stretching may have played a somewhat more important role in the evolution of the Hessian Depression, Nancy-Pirmasens and Burgundy system of Late Permian and Mesozoic basins that is superimposed on a Basin-and-Range type array of Permo-Carboniferous troughs (**Figures 21** and **22**).

Modeled subsidence curves indicate that during the Permo-Carboniferous tectonomagmatic cycle the lithospheric mantle was significantly attenuated and that β factors attained values in the range of 1.8–10. As these values are subject to large lateral variations, they reflect that thinning of the lithospheric mantle was heterogeneous and generally more intense in areas that evolved into Mesozoic depocenters than in areas marginal to them. Similarly, in areas that remained positive features throughout much of Mesozoic times, such as the Bohemian and Armorican Massifs, the lithospheric mantle was apparently not significantly thinned during the Permo-Carboniferous and retained a thickness of 70–100 km, as well as an orogen (subduction)-related anisotropy (Babuska and Plomerova, 2001; Judenherc *et al.*, 2002). Sensitivity studies indicate that best fits between observed and modeled subsidence curves are obtained when the thickness of the thermal lithosphere at its end-Mesozoic equilibration with the asthenosphere is set at 100 or 120 km. Yet, even at these values, Permo-Carboniferous β factors and the end-Early Permian thickness of the remnant lithospheric mantle (RLM) vary significantly (e.g., Trochtelfingen: 100 km lithosphere: $\beta = 3.02$, RLM 23.2 km; 120 km lithosphere: $\beta = 1.96$, RLM 43.3 km). For the Paris Basin, the best fit between observed and modeled subsidence curves was achieved with a lithosphere thickness of 120 km, whereas for the Upper Rhine Graben and the Franconian Platform best fits were obtained with a lithosphere thickness of 100 km. Whereas a 100 km lithosphere thickness is compatible with the Palaeocene plume-related segregation depth of olivine-melilitic partial melts in the Vosges, Black Forest, and Bohemian Massif (Wilson *et al.*, 1995), the apparently greater lithosphere thickness beneath the Paris Basin remains enigmatic.

In view of the above, values given in **Table 1** for the end-Early Permian thickness of the RLM ought to be regarded as rough approximations. Nevertheless, it is evident that substantial Permo-Carboniferous thinning of the lithospheric mantle provided the principal driving mechanism for the Late Permian and Mesozoic subsidence of thermal-sag basins that developed in the ECRIS area. On a regional scale, modeled Permo-Carboniferous crustal extension was relatively low. Under the assumption of initial crustal thicknesses of 30–35 km, automated modeling yielded δ factors of 1.04–1.13 and crustal thicknesses close to present values.

The minor, intra-Mesozoic subsidence accelerations, which overprint the long-term thermal subsidence curves, were successfully modeled by uniform lithospheric extension with cumulative $\delta = \beta$ values in the range of 1.01–1.07. As corresponding extensional faulting is generally poorly documented, stress-induced deflections of the lithosphere (Cloetingh, 1988) may have contributed to some of these subsidence anomalies.

Summarizing, in the wider ECRIS area the following sequence of dynamic processes controlled the transformation of the overthickened crust and lithosphere of the Variscan Orogen to present-day crustal and lithospheric thicknesses:

(1) Stephanian–Early Permian wrench faulting caused disruption of the Variscan Orogen, detachment of subducted lithospheric slabs and upwelling of the asthenosphere, giving rise to widespread mantle-derived magmatic activity. During this thermal surge, partial delamination and thermal thinning of the lithospheric mantle, thermal inflation of the remnant lithosphere and interaction of mantle-derived partial melts with the lower crust accounted for the destruction of the 45–60 km deep crustal roots of the Variscan Orogen and its regional uplift. By end-Early Permian times the crust was thinned down on a regional scale to 27–35 km, mainly by magmatic processes and erosional unroofing and only locally by mechanical stretching, whilst the thickness of the mantle-lithosphere was reduced to 9–40 km in areas that evolved into Late Permian to Mesozoic depocentres, whereas it retained a thickness of 40–90 km beneath slowly subsiding areas and persisting highs. There is no relationship between the degree of lithospheric thinning and the different Variscan tectonic units.

(2) During the late Early Permian the temperature of the asthenosphere returned rapidly to ambient levels. With this, reequilibration of the lithosphere with the asthenosphere commenced and persisted during the Mesozoic, controlling the subsidence of a system of intracratonic thermal-sag basins. As there is no clear relationship between the distribution of Permo-Carboniferous troughs and the geometry of the superimposed intracratonic Late Permian to Mesozoic thermal-sag basins, Permo-Carboniferous thermal thinning and delamination of the lithospheric mantle provided the principal driving mechanism for their subsidence. Minor intra-Mesozoic tensional events hardly disturbed the asthenosphere–lithosphere system of the ECRIS area where by end-Cretaceous times the lithosphere had reequilibrated with the asthenosphere at depths of 100–120 km.

(3) The lithosphere–asthenosphere system of the ECRIS area became destabilized again at the transition from the Cretaceous to the Palaeocene in conjunction with a phase of major intraplate compression that was accompanied by the impingement of mantle plumes. With the late Eocene activation of ECRIS, crustal extension, and particularly Neogene increased plume activity, caused further destabilization of its lithosphere–asthenosphere system (Dèzes *et al.*, 2004). As a result, the present thickness of the lithosphere decreases from 100–120 km in areas flanking ECRIS to 60–70 km beneath parts of the Rhenish Massif and the Massif Central (Babuska and Plomerova, 1993).

6.11.2.2 Compressional Basins Systems

Below we discuss basic concepts and observations for large-scale compressional basin systems. In doing so, we focus on foreland basins and basins initiated by lithospheric folding.

6.11.2.2.1 Development of foreland basins

Foreland basins owe their existence to the capacity of the lithosphere to support loads, such as the topography of orogenic wedges or subducted lithospheric slabs. The lithosphere deforms by flexurally bending downwards over areas often exceeding the spatial scale of these loads. The width of the resulting depression, the foreland basin, provides information on the mechanical strength of the underlying lithosphere. Under an imposed load, a zero-strength lithosphere would simply sink vertically into the mantle (Airy isostasy), thus not accounting for the development of a foreland basin. By contrast, a mechanically strong lithosphere, characteristic of cratonic forelands, allows for the subsidence of wide and relatively shallow foreland basins (flexural isostasy). Such wide foreland basins are associated with the Canadian Rocky Mountains of Alberta and British Columbia and the Appalachian fold-and-thrust belts that are superimposed on the North American Proterozoic cratonic crust (e.g., Beaumont, 1981; Quinlan and Beaumont, 1984). By contrast, the much narrower Alpine foreland basins of Europe (Mascle *et al.*, 1998) developed on considerably younger lithosphere that equilibrated with the asthenosphere after the Variscan orogeny and was modified by Mesozoic rifting activity. The time elapsed between rifting and the syn-orogenic flexural deformation of this foreland lithosphere was very variable (Pyrenees: ca. 30 Ma; Apennines: ca. 130 Ma). The relatively modest widths of the foreland basins of the Carpathians (Zoetemeijer *et al.*, 1999; Maţenco *et al.*, 1997b), Pyrenees (Millan *et al.*, 1995), the Betic Cordillera (Van der Beek and Cloetingh, 1992), the Apennines (Zoetemeijer *et al.*, 1993), and the eastern Alps (Andeweg and Cloetingh, 1998) reflect a relatively weak lithosphere.

In addition to topographic loading by orogenic wedges and loading by the sedimentary fill of the foreland basins, additional forces operate on the lithosphere, such as slab-pull, slab-detachment and slab roll-back, and play an important role in shaping the geometry of prowedge and retrowedge foreland basins (**Figure 25**) (e.g., Millan *et al.*, 1995; Ziegler *et al.*, 2002). Moreover, depending on mechanical coupling/decoupling of the orogenic wedge and the foreland lithosphere, horizontal compressional stresses can be exerted onto the latter, influencing the geometry of an evolving flexural foreland basin (Ziegler *et al.*, 2002).

In a first generation of flexural foreland basin models, the different loading components and forces were

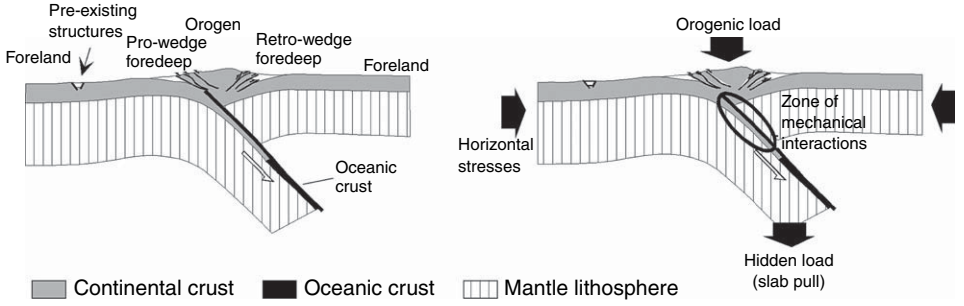

Figure 25 Conceptual model illustrating forces controlling the subsidence of retro- and pro-wedge foreland basins and showing zone of potential mechanical coupling between the upper and lower plate. Modified from Ziegler PA, Bertotti G, and Cloetingh S (2002). Dynamic processes controlling foreland development – the role of mechanical (de)coupling of orogenic wedges and forelands. In: Bertotti G, Schulmann K, and Cloetingh SAPL (eds.) *EGU St. Mueller Special Publication Series*, 1: *Continental Collision and the Tectono-Sedimentary Evolution of Forelands*, pp. 17–56. EGU.

represented by a system of vertical loads, shear forces, and bending moments (Royden, 1988, 1993). This approach is illustrated in **Figure 26**. A characteristic feature of these models is that horizontal stresses were neglected. Nevertheless, these have been shown to play a potentially important role in the geometry of foreland basins and the architecture of their sedimentary fill (Peper *et al.*, 1994). These models were utilized to extract information on the mechanical properties of the lithosphere that was treated as an elastic plate rather than as a depth-dependent rheologically stratified beam. Consequently, the models yielded rough estimates for the effective elastic thickness of the lithosphere and a first approximation for the bulk rheology of the continents. This approach permitted to examine the effect of the time elapsed since the last thermal perturbation of the lithosphere (generally a rifting phase) on its deflection during the subsequent foreland basin development phase. In this respect, Desegaulx *et al.*, (1991) explained the rapid Cenozoic subsidence of the Aquitaine foreland basin (SW France) in terms of preorogenic syn-rift extensional thinning and associated thermal perturbation of the lithosphere and its postrift thermal subsidence and sedimentary loading.

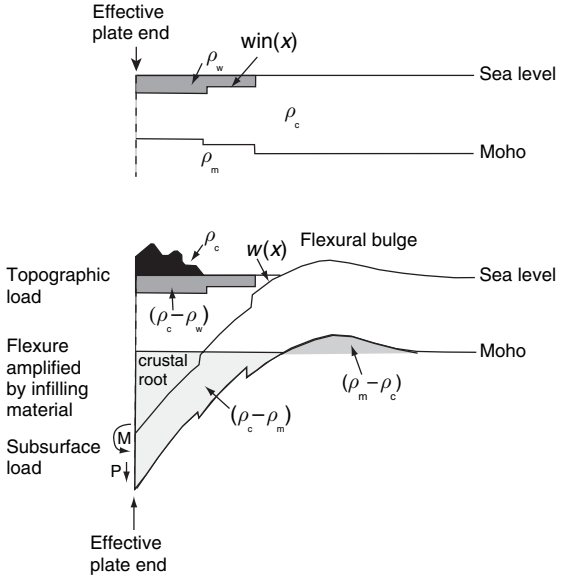

Figure 26 Concept of lithospheric flexure during foreland basin evolution. Deflection of the subducting lower plate lithosphere is the combined result of topographic loading by the mountain chain of the upper plate, the weight of the sediments in the foreland basin, and the weight of the subducted slab. The shape of the flexural foreland depression is controlled by the interplay between the lithospheric strength of the lower plate, the magnitude of the differential loads imposed on it, and the level of collision-related compressional stresses transmitted into it. Modified from Royden (1993); see also Ziegler *et al.*, (2002).

The thermomechanical age concept provides the framework for effective elastic thickness (EET) estimates of the lithosphere. **Figure 27** was constructed on the basis of a large data set for Eurasian foreland basins (Cloetingh and Burov, 1996) and illustrates the general trend of increasing elastic plate thickness with increasing thermomechanical age. Also plotted in **Figure 27** are predictions for the bulk rheology of the lithosphere based on extrapolations from rock mechanical data, constrained by crustal geophysical data and thermal models. A characteristic feature of these models is the incorporation of a quartz-dominated upper crustal rheology and an olivine-controlled mantle rheology (see also **Figure 11**). These models are cast in terms of the depth to the base of the mechanically strong upper part of the crust (MSC) and the mechanically strong part of the upper mantle lithosphere (MSL). Analysis of **Figure 27** demonstrates that the mechanical properties of the crust are little affected by its age-dependent cooling, whereas the thickness and strength of the lithospheric mantle is very strongly age dependent. Depth- and temperature-dependent rheological models for the lithosphere show that the mechanically weak lower crust separates the mechanically strong upper crust and upper lithospheric mantle (e.g., Watts and Burov, 2003). The EET bands for the mechanically strong upper crust and upper lithospheric mantle describe the integrated EET of the lithosphere that has a bearing on its response to loads imposed on it. The degree of coupling and/or decoupling between these two mechanically strong layers and the scatter of data points reflects, to a large extent, the importance of mechanical weakening of the lower crust by tectonic stresses (Cloetingh and Burov, 1996).

At the same time it was realized that rheological decoupling of the upper crust and lithospheric mantle plays an important role in the structural style of intraplate compressional deformations (e.g., Rocky Mountains and Bohemian Massif; Ziegler *et al.*, 1995, 2002).

6.11.2.2.2 Compressional basins: lateral variations in flexural behaviour and implications for palaeotopography

Modeling of compressional basins followed essentially the same philosophy as the modeling of extensional basins. Initial lithosphere-scale models focused on the role of flexural behaviour of the lithosphere during foreland basin development (e.g., Zoetemeijer *et al.*,

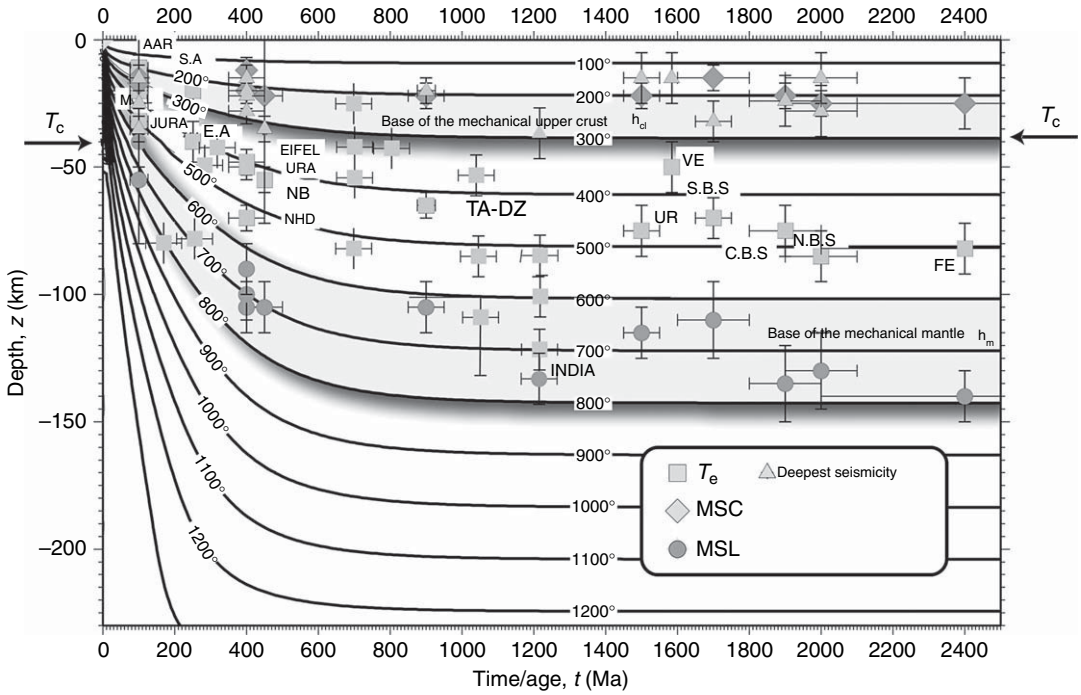

Figure 27 Compilation of observed and predicted values of effective elastic thickness (EET), depth to bottom of mechanically strong crust (MSC), and depth to bottom of mechanically strong lithospheric mantle (MSL) plotted against the age of the continental lithosphere at the time of loading and comparison with predictions from thermal models of the lithosphere. Labeled contours are isotherms. Isotherms marked by 'solid lines' are for models that account for additional radiogenic heat production in the upper crust. 'Dashed lines' correspond to pure cooling models for continental lithosphere. The equilibrium thermal thickness of the continental lithosphere is 250 km. 'Shaded bands' correspond to depth intervals marking the base of the mechanical crust (MSC) and the mantle portion of the lithosphere (MSL). 'Squares' correspond to EET estimates, 'circles' indicate MSL estimates, and 'diamonds' correspond to estimates of MSC. 'Bold letters' correspond to directly estimated EET values derived from flexural studies on, for example, foreland basins, 'Thinner letters' indicate indirect rheological estimates derived from extrapolation of rock-mechanics studies. The data set includes (I): Old thermo-mechanical ages (1000–2500 Ma): northernmost (N.B.S.), central (C.B.S.), and southernmost Baltic Shield (S.B.S.); Fennoscandia (FE); Verkhoyansk plate (VE); Urals (UR); Carpathians; Caucasus, (II): Intermediate thermo-mechanical ages (500–1000 Ma): North Baikal (NB); Tarim and Dzungaria (TA-DZ); Variscan of Europe: URA, NHD, EIFEL; and (III): Younger thermo-mechanical ages (0–500 Ma): Alpine belt: JURA, MOLL (Molasse), AAR; southern Alps (SA) and eastern Alps (EA); Ebro Basin; Betic rifted margin; Betic Cordilleras. Modified from Cloetingh S and Burov E (1996) Thermomechanical structure of European continental lithosphere: constraints from rheological profiles and EET estimates. *Geophysical Journal International* 124: 695–723.

1990; Van der Beek and Cloetingh, 1992). These studies drew on data sets consisting of wells, gravity data, and deep seismic profiling, such as the ECORS profiles through the Pyrenees, completed in the 1980s. Roure *et al.*, (1994, 1996a) and Ziegler and Roure (1996) give a detailed discussion on constraints provided by deep seismic data on the bulk geometry of Alpine belts. Flexural modeling was backed up by large-scale studies on the rheological evolution of continental lithosphere (Cloetingh and Burov, 1996) that demonstrated in compressional settings a direct link between the mechanical properties of the lithosphere, its thermal structure, and the level of regional intraplate stresses.

The inferences drawn from large-scale flexural modeling provided feedback for subsequent analysis on sub-basin scales. For example, modeling predictions for the presence of weak lithosphere in the Alpine belt invoke steep downward deflection of the lithosphere, favouring the development of upper crustal flexure-induced synthetic and antithetic tensional faults (Ziegler *et al.*, 2002). Such fault systems are observed on reflection-seismic profiles in the Alpine Molasse Basin of Germany and Austria (Ziegler, 1990b) and in the Carpathian foreland basin of Poland (Oszczypko, 2006), the Ukraine (Izotova and Popadyuk, 1996), and Romania (Maţenco *et al.*, 1997a). This flexure-induced upper crustal normal faulting has caused weakening of the lithosphere. Integrated flexural analysis of a set of profiles across the Ukranian Carpathians and their

foreland has demonstrated an extreme deflection of the lithosphere, leading almost to its failure, and very pronounced offsets on upper crustal normal faults (see **Figure 28**) (Zoetemeijer *et al.*, 1999).

Following studies on the palaeorheology of the lithosphere, constrained by high-quality thermochronology in the Central Alps (Okaya *et al.*, 1996) and Eastern Alps (Genser *et al.*, 1996), the importance of large lateral variations in the mechanical strength of mountain belts became evident. This pertains particularly to a pronounced strength reduction from the external part of an orogen towards its internal parts. As a result, foreland basins will develop in the external zone with its stronger lithosphere, whereas in the internal zones of the orogens pull-apart basins will develop on low-strength lithosphere (Nemes *et al.*, 1997, Cloetingh *et al.*, 1992). The consequences of lateral flexural strength variations of the lithosphere were explored by a modeling study that was carried out along a transsect through the NE Pyrenees that is well constrained by crustal-scale seismic control and an extensive field-derived database (Vergés *et al.*, 1995). Apart from investigating the present configuration of foreland basin and quantifying the present-day mechanical structure of the lithosphere underlying the southern Pyrenees fold-and-thrust belt, the relationship between palaeotopography and flexural evolution of the orogen was analyzed (Millan *et al.*, 1995). This novel approach led to a set of testable predictions on palaeotopography (**Figure 29**) and sediment supply to the foreland basin.

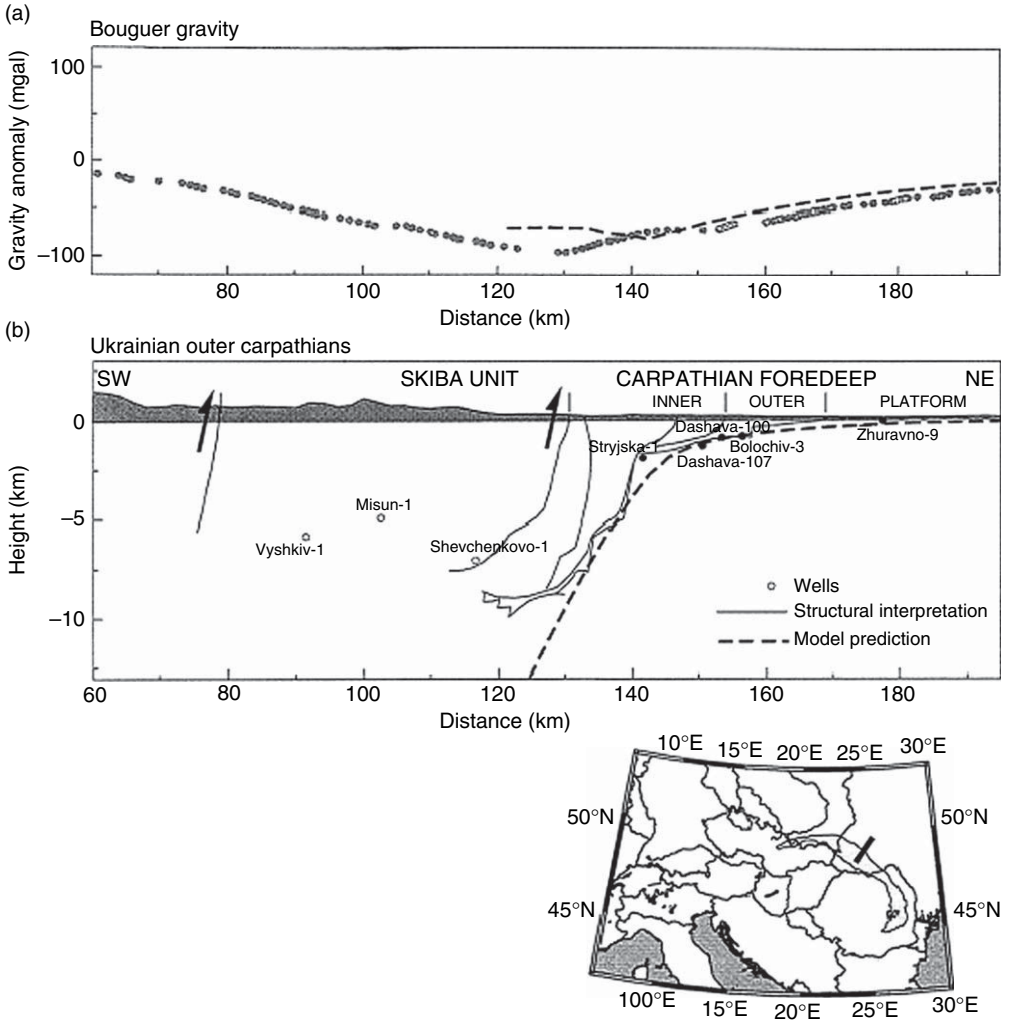

Figure 28 Cross section illustrating (a) Bouguer gravity anomaly and (b) steep down bending (*b*) of the East-European platform lithosphere beneath the Ukranian segment of the Carpathian fold-and-thrust belt. The extreme curvature of the downbent lithosphere is associated with major upper crustal normal faulting. Narrow foreland basins are characteristic for foreland flexures involving weak lithosphere. Modified from Zoetemeijer *et al.*, (1999).

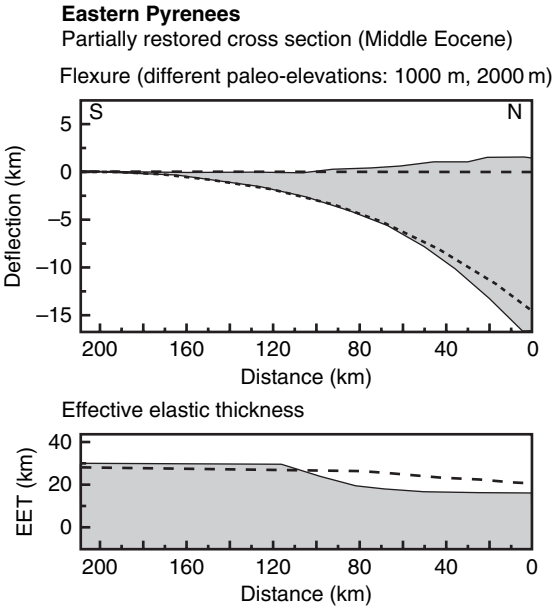

Figure 29 Modeled flexure for a partly restored section (Middle Eocene) in the eastern Pyrenees. Top: Lithospheric flexure computed for low (1000 m) and moderate palaeo-topographic elevations (2000 m). Dots represent observed deflection of the lithosphere. Dashed line: Fit obtained for 1000 m elevation, bending moment $M = 7 \times 10^{16}$ N and shear force $V = 1.6 \times 10^{11}$ N m^{-1}. Solid line: Fit obtained for 2000 m elevation, bending moment $M = 5 \times 10^{16}$ N and shear force $V = 1 \times 10^{11}$ N m^{-1}. Increasing elevations are accompanied by decreasing subduction forces. Bottom: EET values for the model with the best flexural fit. An overall thicker EET is required for moderate to low estimates of palaeo-elevation. Modified from Millan H, Den Bezemer T, Vergés J, *et al.*, (1995) Paleo-elevation and EET evolution at mountain ranges: inferences from flexural modelling in the eastern Pyrenees and Ebro basin. *Marine and Petroleum Geology* 12: 917–928.

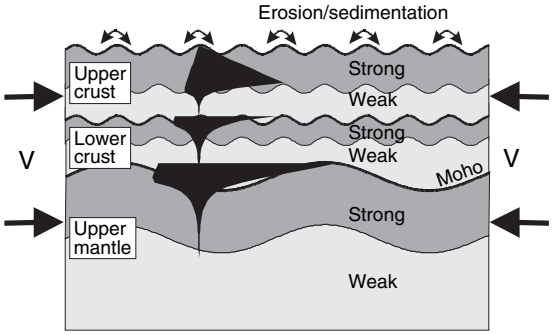

Figure 30 Schematic diagram illustrating decoupled lithospheric mantle and crustal folding, and consequences of vertical motions and sedimentation at the Earth's surface. *V* is horizontal shortening velocity; upper crust, lower crust, and mantle layers are defined by corresponding rheologies and physical properties. A typical brittle-ductile strength profile (in black) for decoupled crust and upper mantle–lithosphere, adopting a quartz–diorite–olivine rheology, is shown for reference.

6.11.2.2.3 Lithospheric folding: an important mode of intraplate basin formation

Folding of the lithosphere, involving its positive as well as negative deflection (see **Figure 30**), appears to play a more important role in the large-scale neotectonic deformation of Europe's intraplate domain than hitherto realized (Cloetingh *et al.*, 1999). The large wavelength of vertical motions associated with lithospheric folding necessitates integration of available data from relatively large areas (Elfrink, 2001), often going beyond the scope of regional structural and geophysical studies that target specific structural provinces. Recent studies on the North German Basin have revealed the importance of its neotectonic structural reactivation by lithospheric folding (Marotta *et al.*, 2000). Similarly, the Plio-Pleistocene subsidence acceleration of the North Sea Basin (**Figure 10**) is attributed to stress-induced buckling of its lithosphere (Van Wees and Cloetingh, 1996). Moreover, folding of the Variscan lithosphere has been documented for Brittany (Bonnet *et al.*, 2000), the adjacent Paris Basin (Lefort and Agarwal, 1996), and the Vosges–Black Forest arch (Dèzes *et al.*, 2004; Ziegler and Dèzes, in press). Lithospheric folding is a very effective mechanism for the propagation of tectonic deformation from active plate boundaries far into intraplate domains (e.g., Stephenson and Cloetingh, 1991; Burov *et al.*, 1993; Ziegler *et al.*, 1995, 1998, 2002).

At the scale of a microcontinent that was affected by a succession of collisional events, Iberia provides a well-documented natural laboratory for lithospheric folding and the quantification of the interplay between neotectonics and surface processes (Cloetingh *et al.*, 2002). An important factor in favour of a lithosphere-folding scenario for Iberia is the compatibility of the thermotectonic age of its lithosphere and the wavelength of observed deformations.

Well-documented examples of continental lithospheric folding also come from other cratonic areas. A prominent example of lithospheric folding occurs in the Western Goby area of Central Asia, involving a lithosphere with a thermotectonic age of 400 Ma. In this area, mantle and crustal wavelengths are 360 km and 50 km, respectively, with a shortening rate of ~10 mm yr^{-1} and a total amount of shortening of, 200–250 km during 10–15 My (Burov *et al.*, 1993; Burov and Molnar, 1998).

Quaternary folding of the Variscan lithosphere in the area of the Armorican Massif (Bonnet *et al.*, 2000) resulted in the development of folds with a

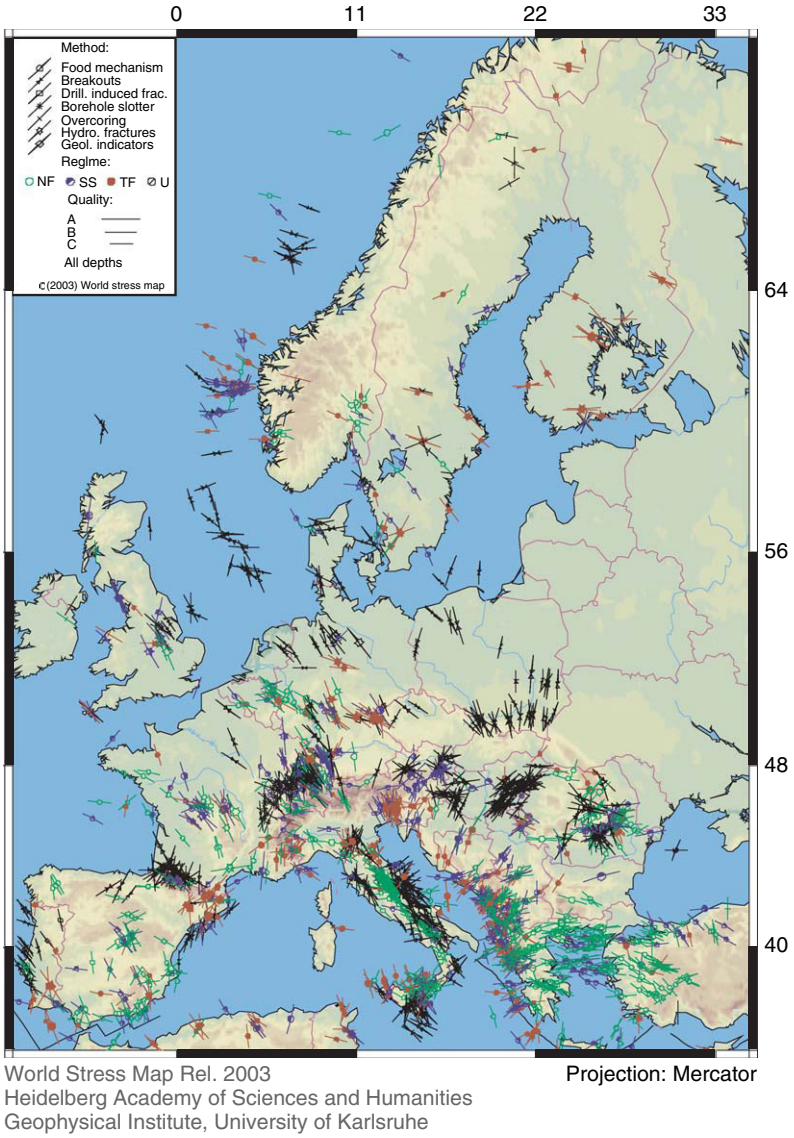

Figure 31 Present-day stress map of Europe showing orientation of maximum horizontal stress axes (S_{Hmax}). Different symbols stand for different stress indicators; their length reflects the data quality, 'A' being highest. Background shading indicates topographic elevation (brown high, green low). This map was derived from the World Stress Map database (http://www.world-stress-map.org/).

wavelength of 250 km, pointing to a mantle-lithospheric control on deformation. As the timing and spatial pattern of uplift inferred from river incision studies in Brittany is incompatible with a glacio-eustatic origin, Bonnet *et al.*, (2000) relate the observed vertical motions to deflection of the lithosphere under the present-day NW–SE directed compressional intraplate stress field of NW Europe (**Figure 31**). Stress-induced uplift of the area appears to control fluvial incision rates and the position of the main drainage divides. The area located at the western margin of the Paris Basin and along the rifted Atlantic margin of France has been subject to thermal rejuvenation during Mesozoic extension related to North Atlantic rifting (Ziegler and Dèzes, 2006; Robin *et al.*, 2003) and subsequent compressional intraplate deformation (Ziegler *et al.*, 1995), also affecting the Paris Basin (Lefort and Agarwal, 1996). Leveling studies in this area (Lenôtre *et al.*, 1999) also point towards its ongoing deformation.

The inferred wavelength of these neotectonic lithosphere folds is consistent with the general relationship

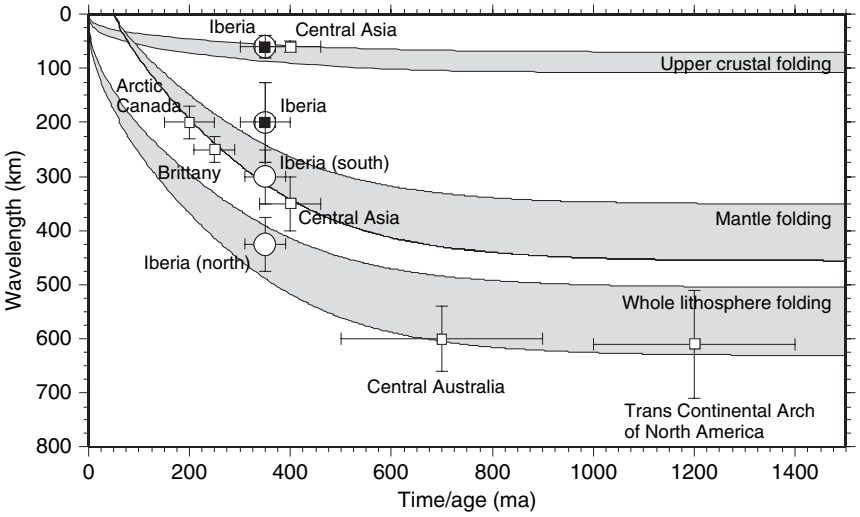

Figure 32 Comparison of observed (solid squares) and modeled (open circles) wavelengths of crustal, lithospheric mantle and whole lithospheric folding in Iberia (Cloetingh *et al.*, 2002) with theoretical predictions (Cloetingh *et al.*, 1999) and other estimates (open squares) for wavelengths documented from geological and geophysical studies (Stephenson and Cloetingh, 1991; Nikishin *et al.*, 1993; Ziegler *et al.*, 1995; Bonnet *et al.*, 2000). Wavelength is given as a function of the thermo-tectonic age at the time of folding. Thermo-tectonic age corresponds to the time elapsed since the last major perturbation of the lithosphere prior to folding. Note that neotectonic folding of Variscan lithosphere has recently also been documented for Brittany (Bonnet *et al.*, 2000). Both Iberia and Central Asia are characterized by separate dominant wavelengths for crust and mantle folds, reflecting decoupled modes of lithosphere folding (Cloetingh *et al.*, 2005). Modified from Cloetingh S, Burov E, Beekman F, Andeweg B, Andriessen PAM, Garcia-Castellanos D, de Vicente G, and Vegas R (2002) Lithospheric folding in Iberia. *Tectonics* 21(5): 1041 (doi:10.1029/2001TC901031).

that was established between the wavelength of lithospheric folds and the thermotectonic age of the lithosphere on the base of a global inventory of lithospheric folds (**Figure 32**) (see also Cloetingh and Burov, 1996; Cloetingh *et al.*, 2005). In a number of other areas of continental lithosphere folding, smaller wavelength crustal folds have also been detected, for example, in Central Asia (Burov *et al.*, 1993; Nikishin *et al.*, 1993).

Thermal thinning of the mantle-lithosphere, often associated with volcanism and doming, enhances lithospheric folding and appears to control the wavelength of folds. Substantial thermal weakening of the lithospheric mantle is consistent with higher folding rates in the European foreland as compared to folding in Central Asia (Nikishin *et al.*, 1993), which is marked by pronounced mantle strength (Cloetingh *et al.*, 1999).

6.11.3 Rheological Stratification of the Lithosphere and Basin Evolution

6.11.3.1 Lithosphere Strength and Deformation Mode

The strength of continental lithosphere is controlled by its depth-dependent rheological structure in which the thickness and composition of the crust, the thickness of the lithospheric mantle, the potential temperature of the asthenosphere, and the presence or absence of fluids, as well as strain rates play a dominant role. By contrast, the strength of oceanic lithosphere depends on its thermal regime, which controls its essentially age-dependent thickness (Kusznir and Park, 1987; Cloetingh and Burov, 1996; Watts, 2001; *see also* Watts, this volume (Chapter 6.01) and Burov, this volume (Chapter 6.03)). **Figure 33** gives synthetic strength envelopes for three different types of continental lithosphere and for oceanic lithosphere at a range of geothermal gradients (Ziegler and Cloetingh, 2004). These theoretical rheological models indicate that thermally stabilized continental lithosphere consists of the mechanically strong upper crust, which is separated by a weak lower crustal layer from the strong upper part of the mantle–lithosphere that in turn overlies the weak lower mantle–lithosphere. By contrast, oceanic lithosphere has a more homogeneous composition and is characterized by a much simpler rheological structure. Rheologically, thermally stabilized oceanic lithosphere is considerably stronger than all types of continental lithosphere. However, the strength of oceanic lithosphere can be

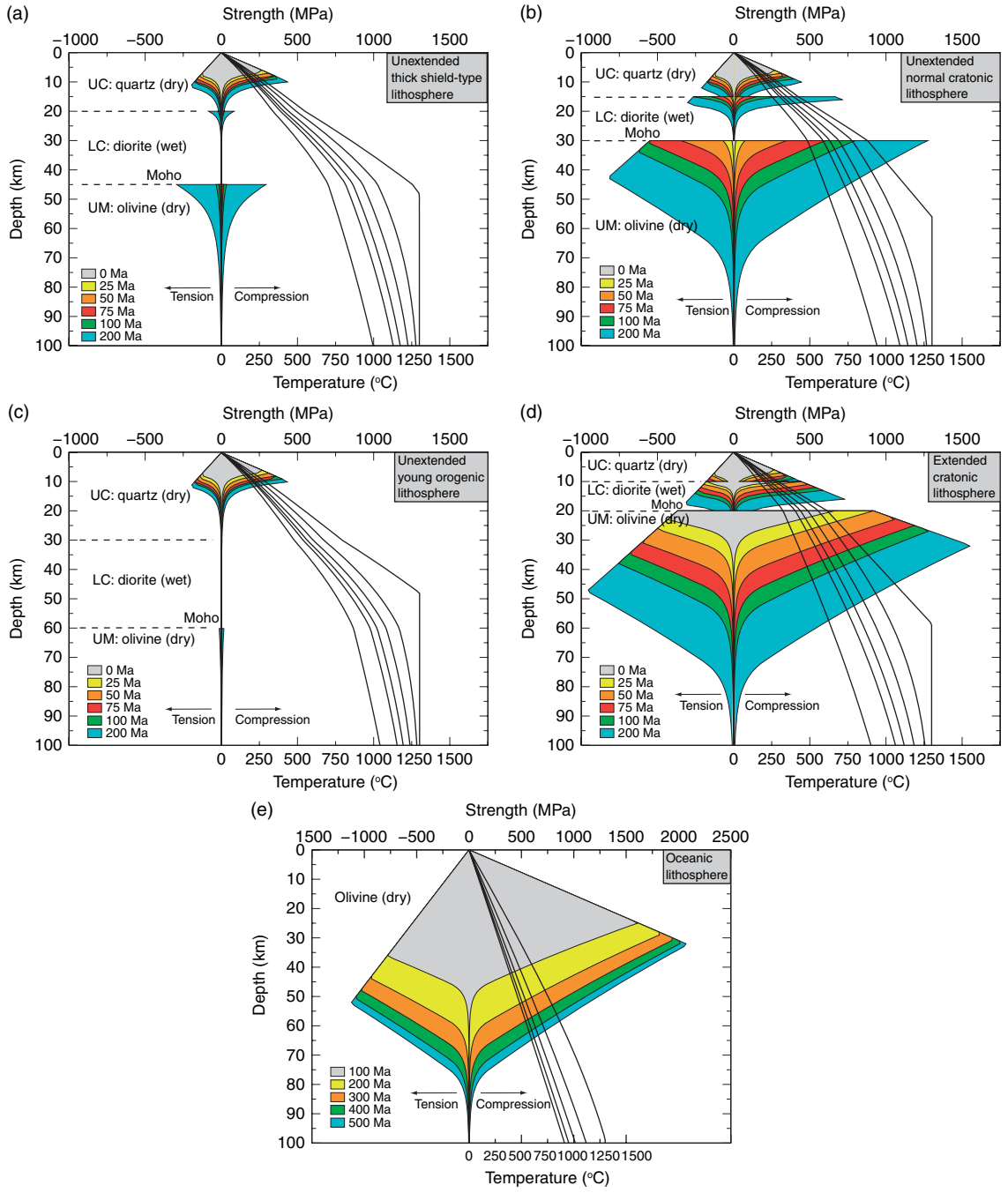

Figure 33 Depth-dependent rheological models for various lithosphere types and a range of geothermal gradients, assuming a dry quartz/diorite/olivine mineralogy for continental lithosphere (Ziegler, 1996a; Ziegler *et al.*, 2001). (a) Unextended, thick-shield-type lithosphere with a crustal thickness of 45 km and a lithospheric mantle thickness of 155 km. (b) Unextended, 'normal' cratonic lithosphere with a crustal thickness of 30 km and a lithospheric mantle thickness of 70 km. (c) Unextended, young orogenic lithosphere with a crustal thickness of 60 km and a lithospheric mantle thickness of 140 km. (d) Extended, cratonic lithosphere with a crustal thickness of, 20 km and a lithospheric mantle thickness of 50 km. (e) Oceanic lithosphere. Modified from Ziegler PA, Cloetingh S, Guiraud R, and Stampfli GM (2001) Peri-Tethyan platforms: constraints on dynamics of rifting and basin inversion. In: Ziegler PA, Cavazza W, Robertson AHF, and Crasquin-Soleau S (eds.) *Mémoires du Museum National d'Histoire Naturelle* 186: *Peri-Tethys Memoir 6: Peri-Tethyan Rift/Wrench Basins and Passive Margins*, pp. 9–49. Paris: Commission for the Geological Map of the World.

seriously weakened by transform faults and by the thermal blanketing effect of thick sedimentary prisms prograding onto it (e.g., Gulf of Mexico, Niger Delta, Bengal Fan; Ziegler *et al.*, 1998; see also **Figure 13**).

The strength of continental crust depends largely on its composition, thermal regime and the presence of fluids, and also on the availability of preexisting crustal discontinuities (*see also* Burov, this volume (Chapter 6.03)). Deep-reaching crustal discontinuities, such as thrust- and wrench-faults, cause significant weakening of the otherwise mechanically strong upper parts of the crust. As such discontinuities are apparently characterized by a reduced frictional angle, particularly in the presence of fluids (Van Wees, 1994), they are prone to reactivation at stress levels that are well below those required for the development of new faults. Deep reflection-seismic profiles show that the crust of Late Proterozoic and Palaeozoic orogenic belts is generally characterized by a monoclinal fabric that extends from upper crustal levels down to the Moho at which it either soles out or by which it is truncated (**Figure 34**) (see Ziegler and Cloetingh, 2004). This fabric reflects the presence of deep-reaching lithological inhomogeneities and shear zones.

The strength of the continental upper lithospheric mantle depends to a large extent on the thickness of the crust but also on its age and thermal regime (*see* Jaupart and Mareschal, this volume (Chapter 6.05)). Thermally stabilized stretched continental lithosphere with a 20 km thick crust and a lithospheric mantle thickness of 50 km is mechanically stronger than unstretched lithosphere with a 30 km thick crust and a 70 km thick lithospheric mantle (compare **Figures 33(b) and 33(d)**). Extension of stabilized continental crustal segments precludes ductile flow of the lower crust and faults will be steep to listric and propagate towards the hanging wall, that is, towards the basin center (Bertotti *et al.*, 2000). Under these conditions, the lower crust will deform by distributing ductile shear in the brittle–ductile transition domain. This is compatible with the occurrence of earthquakes within the lower crust and even close to the Moho (e.g., southern Rhine Graben: Bonjer, 1997; East African rifts: Shudofsky *et al.*, 1987).

On the other hand, in young orogenic belts, which are characterized by crustal thicknesses of up to 60 km and an elevated heat flow, the mechanically strong part of the crust is thin and the lithospheric mantle is also weak (**Figure 33(c)**). Extension of this type of lithosphere, involving ductile flow of the lower and middle crust along pressure gradients away from areas lacking upper crustal extension into zones of major upper crustal extensional unroofing, can cause crustal thinning and thickening, respectively. This deformation mode gives rise to the development of core complexes with faults propagating toward the hanging wall (e.g., Basin and Range Province: Wernicke, 1990; Buck, 1991; Bertotti *et al.*, 2000). However, crustal flow will cease after major crustal thinning has been achieved, mainly due to extensional decompression of the lower crust (Bertotti *et al.*, 2000).

Generally, the upper mantle of thermally stabilized, old cratonic lithosphere is considerably stronger than the strong part of its upper crust (**Figure 33(a)**) (Moisio *et al.*, 2000). However, the

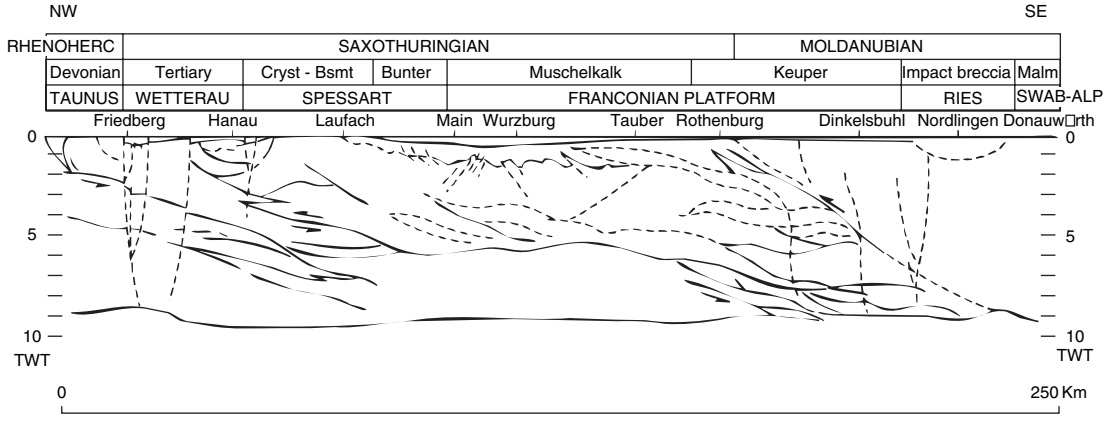

Figure 34 Crustal fabric of the Variscan Orogen as imaged by the DEKORP 2-S reflection–seismic line, South Germany. Modified from Behr HJ and Heinrichs T (1987) Geological interpretation of DEKORP 2 –S: A deep seismic reflection profile across the Saxothuringian and possible implications for late Variscan structural evolution of Central Europe. Tectonophysics 142: 173–202.

occurrence of upper mantle reflectors, which generally dip in the same direction as the crustal fabric and probably are related to subducted oceanic and/or continental crustal material, suggests that the continental lithospheric mantle is not necessarily homogenous but can contain lithological discontinuities that enhance its mechanical anisotropy (Vauchez *et al.*, 1998; Ziegler *et al.*, 1998). Such discontinuities, consisting of eclogitized crustal material, can potentially weaken the strong upper part of the lithospheric mantle. Moreover, even in the face of similar crustal thicknesses, the heat flow of deeply degraded Late Proterozoic and Phanerozoic orogenic belts is still elevated as compared to adjacent old cratons (e.g., Pan African belts of Africa and Arabia; Janssen, 1996). This is probably due to the younger age of their lithospheric mantle and possibly also to a higher radiogenic heat generation potential of their crust. These factors contribute to weakening of former mobile zones to the end that they present rheologically weak zones within a craton, as evidenced by their preferential reactivation during the breakup of Pangea (Ziegler, 1989a, 1989b; Janssen *et al.*, 1995; Ziegler *et al.*, 2001).

From a rheological point of view, the thermally destabilized lithosphere of tectonically active rifts, as well as of rifts and passive margins that have undergone only a relatively short postrift evolution (e.g., 25 Ma), is considerably weaker than that of thermally stabilized rifts and of unstretched lithosphere (**Figures 33** and **35**, Ziegler *et al.*, 1998). In this respect, it must be realized that, during rifting, progressive mechanical and thermal thinning of the lithospheric mantle and its substitution by the upwelling asthenosphere is accompanied by a rise in geotherms causing progressive weakening of the

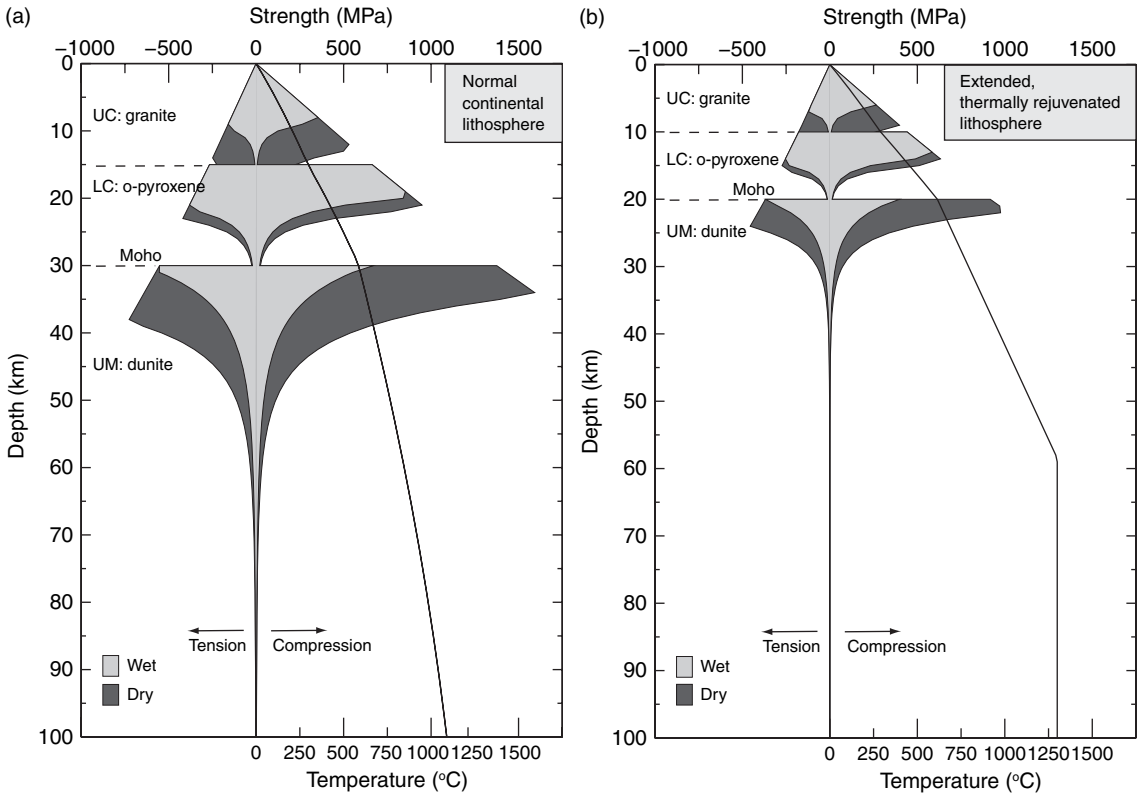

Figure 35 Depth-dependent rheological models for dry and wet, unextended 'normal' cratonic lithosphere and stretched, thermally attenuated lithosphere, assuming a quartz/diorite/olivine mineralogy. (a) Unextended, cratonic lithosphere with a crustal thickness of 30 km and a lithospheric mantle thickness of 70 km. (b) Extended, thermally destabilized cratonic lithosphere with a crustal thickness of, 20 km and a lithospheric mantle thickness of 38 km. Modified from Ziegler PA, Cloetingh S, Guiraud R, and Stampfli GM (2001) Peri-Tethyan platforms: constraints on dynamics of rifting and basin inversion. In: Ziegler PA, Cavazza W, Robertson AHF, and Crasquin-Soleau S (eds.) *Mémoires du Museum National d'Histoire Naturelle* 186: *Peri-Tethys Memoir 6: Peri/Tethyan Rift/Wrench Basins and Passive Margins*, pp. 9–49. Paris: Commission for the Geological Map of the World.

extended lithosphere. In addition, its permeation by fluids causes its further weakening (**Figure 35**). Upon decay of the rift-induced thermal anomaly, rift zones are, rheologically, considerably stronger than unstretched lithosphere (**Figure 33**). However, accumulation of thick syn- and postrift sedimentary sequences can cause by thermal blanketing a weakening of the strong parts of the upper crust and lithospheric mantle of rifted basins (Stephenson, 1989). Moreover, as faults permanently weaken the crust of rifted basins, they are prone to tensional as well as compressional reactivation (Ziegler *et al.*, 1995, 1998, 2001, 2002).

In view of its rheological structure, the continental lithosphere can be regarded under certain conditions as a two-layered viscoelastic beam (**Figure 13**) (Reston, 1990, ter Voorde *et al.*, 1998). The response of such a system to the buildup of extensional and compressional stresses depends on the thickness, strength and spacing of the two competent layers, on stress magnitudes and strain rates and the thermal regime (Zeyen *et al.*, 1997; Watts and Burov, 2003). As the structure of continental lithosphere is also areally heterogeneous, its weakest parts start to yield first, once tensional as well as compressional intraplate stress levels equate their strength.

6.11.3.2 Mechanical Controls on Basin Evolution: Europe's Continental Lithosphere

Studies on the mechanical properties of the European lithosphere revealed a direct link between its thermotectonic age and bulk strength (Cloetingh *et al.*, 2005, Cloetingh and Burov, 1996; Pérez-Gussinyé and Watts, 2005). On the other hand, inferences from P- and S-wave tomography (Goes *et al.*, 2000a, 2000b; Ritter *et al.*, 2000, 2001) and thermomechanical modeling (Garcia-Castellanos *et al.*, 2000) point to a pronounced weakening of the lithosphere in the Lower Rhine area owing to high upper mantle temperatures. However, the Late Neogene and Quaternary tectonics of the Ardennes–Lower Rhine area appear to form part of a much wider neotectonic deformation system that overprints the Late Palaeozoic and Mesozoic basins of NW Europe. This is supported by geomorphologic evidence and the results of seismicity studies in Brittany (Bonnet *et al.*, 1998, 2000) and Normandy (Lagarde *et al.*, 2000; Van Vliet-Lanoë *et al.*, 2000), by data from the Ardennes–Eifel region (Meyer and Stets, 1998; Van Balen *et al.*, 2000), the southern parts of the Upper Rhine Graben (Nivière and Winter, 2000), the Bohemian Massif (Ziegler and Dèzes, 2005, in press), and the North German Basin (Bayer *et al.*, 1999). Lithosphere-scale folding and buckling, in response to the buildup of compressional intraplate stresses, can cause uplift or subsidence of relatively large areas at timescales of a few million years and thus can be an important driving mechanism of neotectonic processes. For instance, the Plio-Pleistocene accelerated subsidence of the North Sea Basin is attributed to down-buckling of the lithosphere in response to the buildup of the present-day stress field (Van Wees and Cloetingh, 1996). Similarly, uplift of the Vosges–Black Forest arch, which at the level of the crust–mantle boundary extends from the Massif Central into the Bohemian Massif (**Figure 17**), commenced during the Burdigalian ($\pm$18 Ma) and persisted until at least early Pliocene times. Uplift of this arch is attributed to lithospheric folding controlled by compressional stresses originating at the Alpine collision zone (Ziegler *et al.*, 2002; Dèzes *et al.*, 2004; Ziegler and Dèzes, 2005, in press).

An understanding of the temporal and spatial strength distribution in the NW European lithosphere may offer quantitative insights into the patterns of its intraplate deformation (basin inversion, up-thrusting of basement blocks), and particularly into the pattern of lithosphere-scale folding and buckling.

Owing to the large amount of high-quality geophysical data acquired during the last 20 years in Europe, its lithospheric configuration is rather well known, though significant uncertainties remain in many areas about the seismic and thermal thickness of the lithosphere (Babuska and Plomerova, 1992; Artemieva and Mooney, 2001; Artemieva, 2006). Nevertheless, available data help to constrain the rheology of the European lithosphere, thus enhancing our understanding of its strength.

So far, strength envelopes and the effective elastic thickness of the lithosphere have been calculated for a number of locations in Europe (e.g., Cloetingh and Burov, 1996). However, as such calculations were made for scattered points only, or along transects, they provide limited information on lateral strength variations of the lithosphere. Although lithospheric thickness and strength maps have already been constructed for the Pannonian Basin (Lankreijer *et al.*, 1999) and the Baltic Shield (Kaikkonen *et al.*, 2000), such maps were until recently not yet available for all of Europe.

As evaluation and modeling of the response of the lithosphere to vertical and horizontal loads requires

an understanding of its strength distribution, dedicated efforts were made to map the strength of the European foreland lithosphere by implementing 3-D strength calculations (Cloetingh *et al.*, 2005).

Strength calculations of the lithosphere depend primarily on its thermal and compositional structure and are particularly sensitive to thermal uncertainties (Ranalli and Murphy, 1987; Ranalli, 1995; Burov and Diament, 1995). For this reason, the workflow aimed at the development of a 3-D strength model for Europe was twofold: (1) construction of a 3-D compositional model and (2) calculating a 3-D thermal cube. The final 3-D strength cube was obtained by calculating 1-D strength envelopes for each lattice point (x, y) of a regularized raster covering NW Europe (**Figure 36**). For each lattice point, the appropriate input values were obtained from a 3-D compositional and thermal cube. A geological and geophysical geographic database was used as reference for the construction of the input models.

For continental realms, a 3-D multilayer compositional model was constructed, consisting of one mantle-lithosphere layer, 2–3 crustal layers and an overlying sedimentary cover layer, whereas for oceanic areas a one-layer model was adopted. For the depth to the different interfaces several regional or European-scale compilations were available that are based on deep seismic reflection and refraction or surface wave dispersion studies (e.g., Panza, 1983; Calcagnile and Panza, 1987; Suhadolc and Panza, 1989; Blundell *et al.*, 1992; Du *et al.*, 1998; Artemieva *et al.*, 2006). For the base of the lower crust, we strongly relied on the European Moho map of Dèzes and Ziegler (2004) (**Figure 37**). Regional compilation maps of the seismogenic lithosphere thickness were used as reference to the base of the thermal lithosphere in subsequent thermal modeling (Babuska and Plomerova, 1993, 2001; Plomerova *et al.*, 2002).

Figure 38(a) shows the integrated strength under compression of the entire lithosphere of Western and

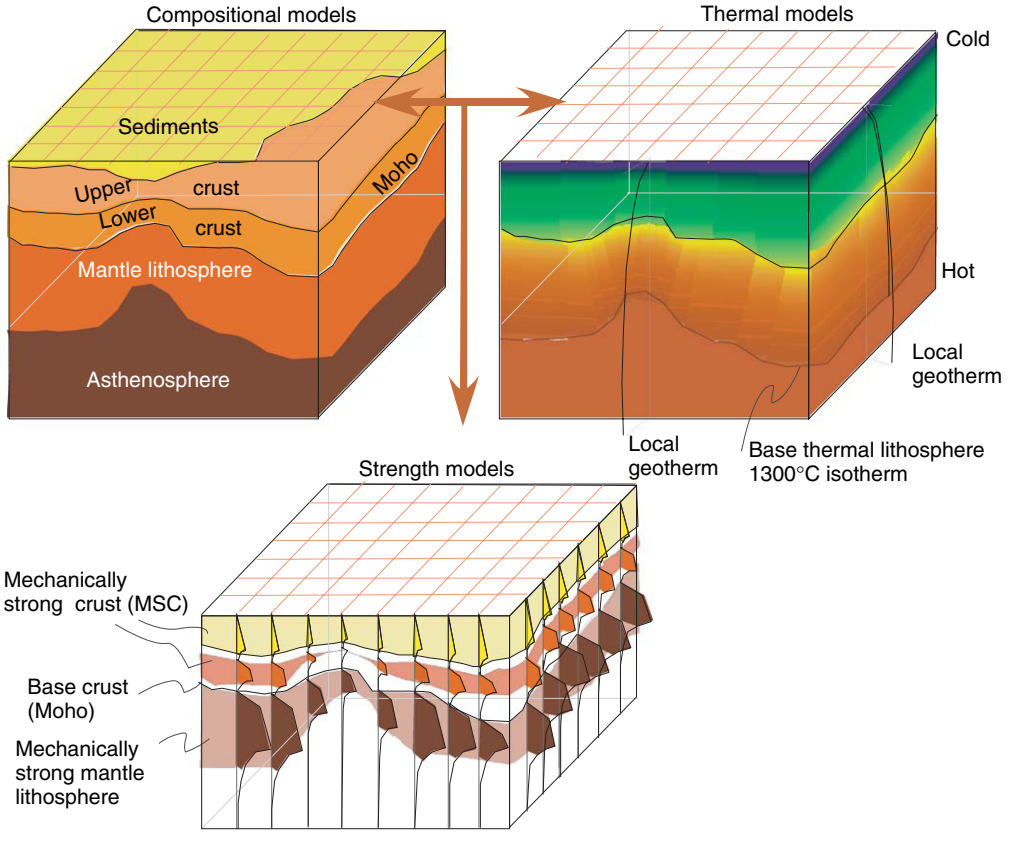

Figure 36 From crustal thickness (top left) and thermal structure (top right) to lithospheric strength (bottom): conceptual configuration of the thermal structure and composition of the lithosphere, adopted for the calculation of 3-D strength models. Modified from Cloetingh S, Ziegler PA, Beekman F, Andriessen PAM, Maţenco L, Bada G, Garcia-Castellanos D, Hardebol N, Dézes P, and Sokoutis D (2005) Lithospheric memory, state of stress and rheology: Neotectonic controls on Europe's intraplate continental topography. *Quaternary Science Reviews* 24: 241–304.

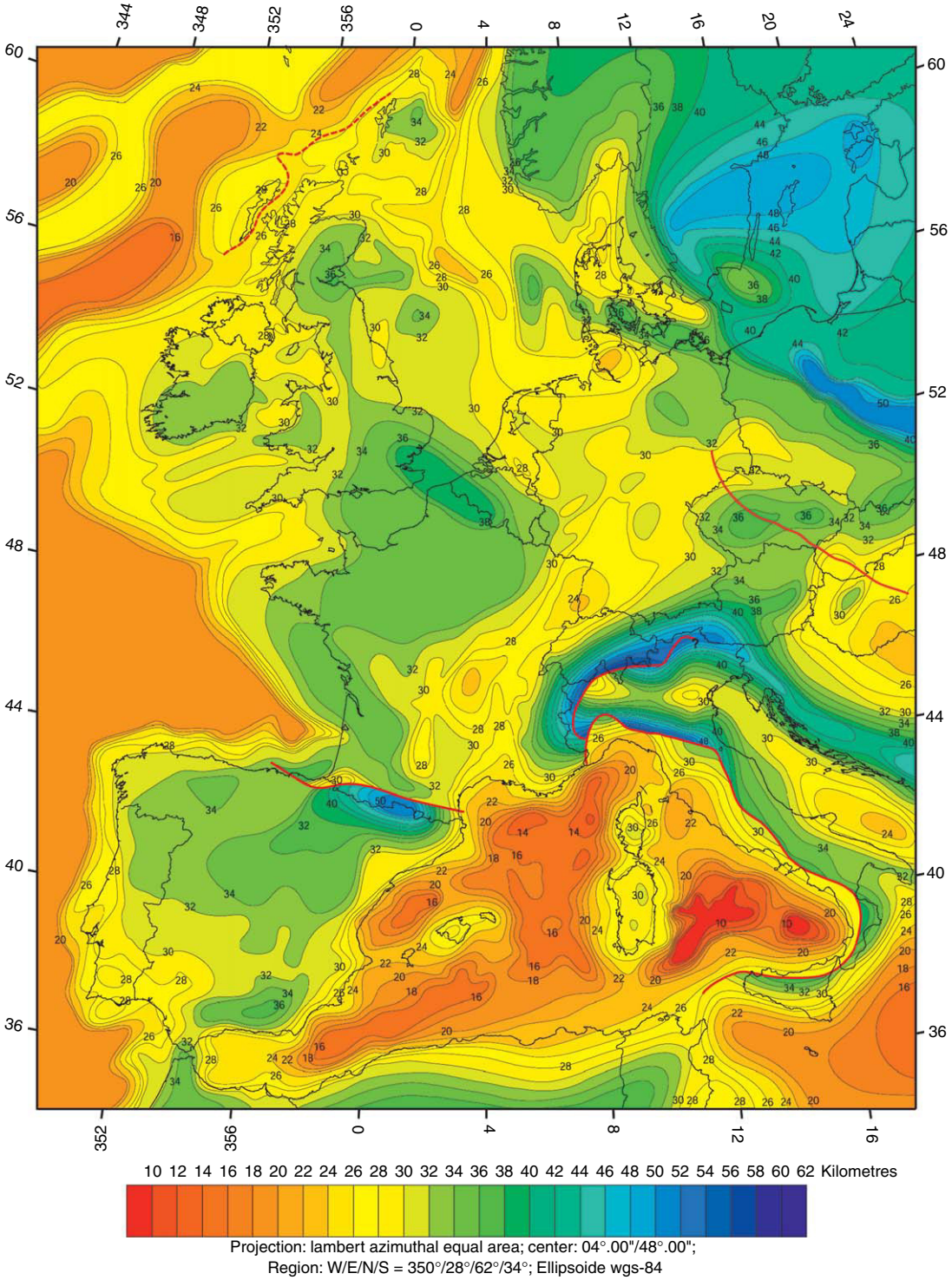

Figure 37 Depth map of Moho discontinuity (2 km contour interval) for Western Europe, constructed by integration of published regional maps. For data sources, see http://comp1.geol.unibas.ch/. Red lines (solid and stippled) show offsets of the Moho discontinuities. Modified from Dèzes P and Ziegler PA (2004) Moho depth map of western and central Europe. EUCOR-URGENT homepage: http://www.unibas.ch/eucor-urgent (acessed Jul 2007).

Central Europe, whereas **Figure 38(b)** displays the integrated strength of the crustal part of the lithosphere. As is evident from **Figure 38**, Europe's lithosphere is characterized by major spatial mechanical strength variations, with a pronounced contrast between the strong Proterozoic lithosphere of the East-European Platform to the east of the Teisseyre–Tornquist line and the relatively weak Phanerozoic lithosphere of Western Europe.

A similar strength contrast occurs at the transition from strong Atlantic oceanic lithosphere to the relatively weak continental lithosphere of Western Europe. Within the Alpine foreland, pronounced NE–SE trending weak zones are recognized that coincide with such major geologic structures as the Rhine Graben System and the North Danish–Polish Trough, which are separated by the high-strength North German Basin and the Bohemian Massif. Moreover, a broad zone of weak lithosphere characterizes the Massif Central and surrounding areas.

The presence of thickened crust in the area of the Teisseyre–Tornquist suture zone (**Figure 37**) gives rise to a pronounced mechanical weakening of the lithosphere, particularly of its mantle part.

Whereas the lithosphere of Fennoscandia is characterized by a relatively high strength, the North Sea rift system corresponds to a zone of weakened lithosphere. Other areas of high lithospheric strength are the Bohemian Massif and the London–Brabant Massif both of which exhibit low seismicity (**Figure 39**).

A pronounced contrast in strength can also be noticed between the strong Adriatic indenter and the weak Pannonian Basin area (see also **Figure 38**). Comparing **Figure 38(a)** with **Figure 38(b)** reveals that the lateral strength variations of Europe's

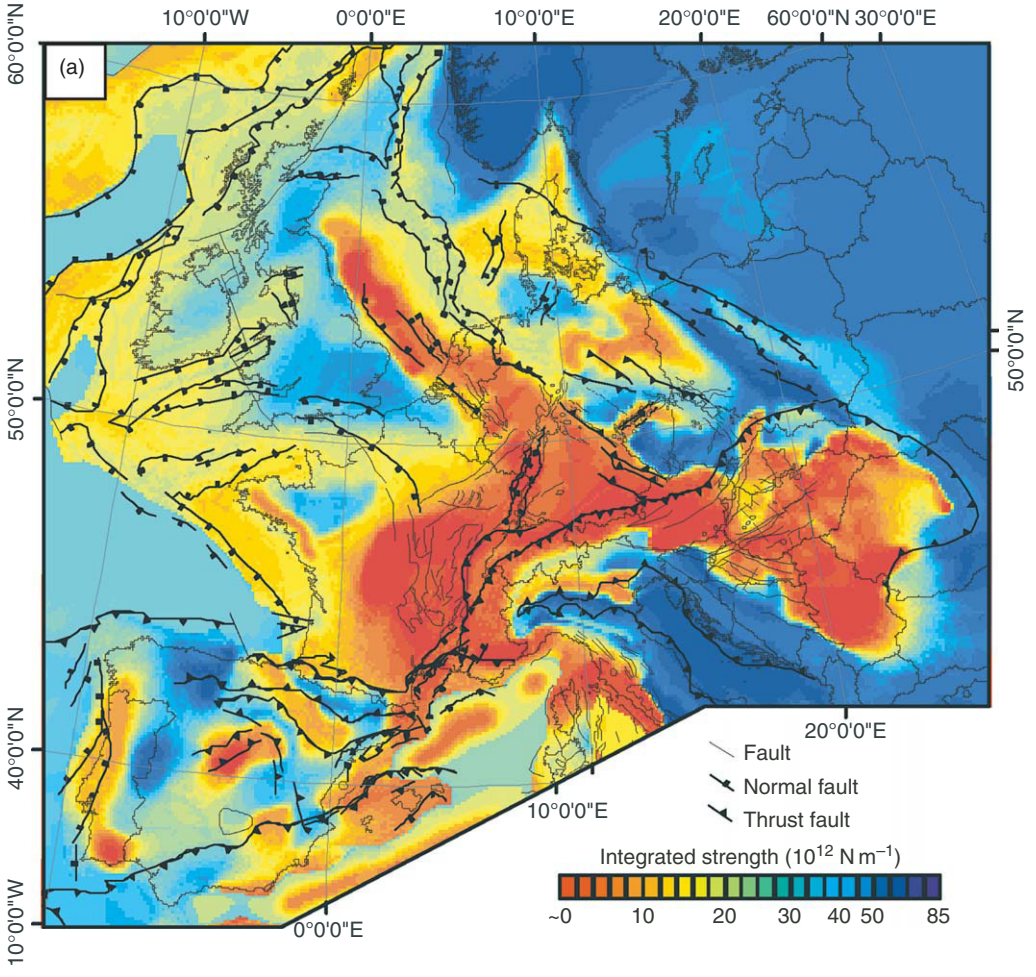

Figure 38 (*Continued*)

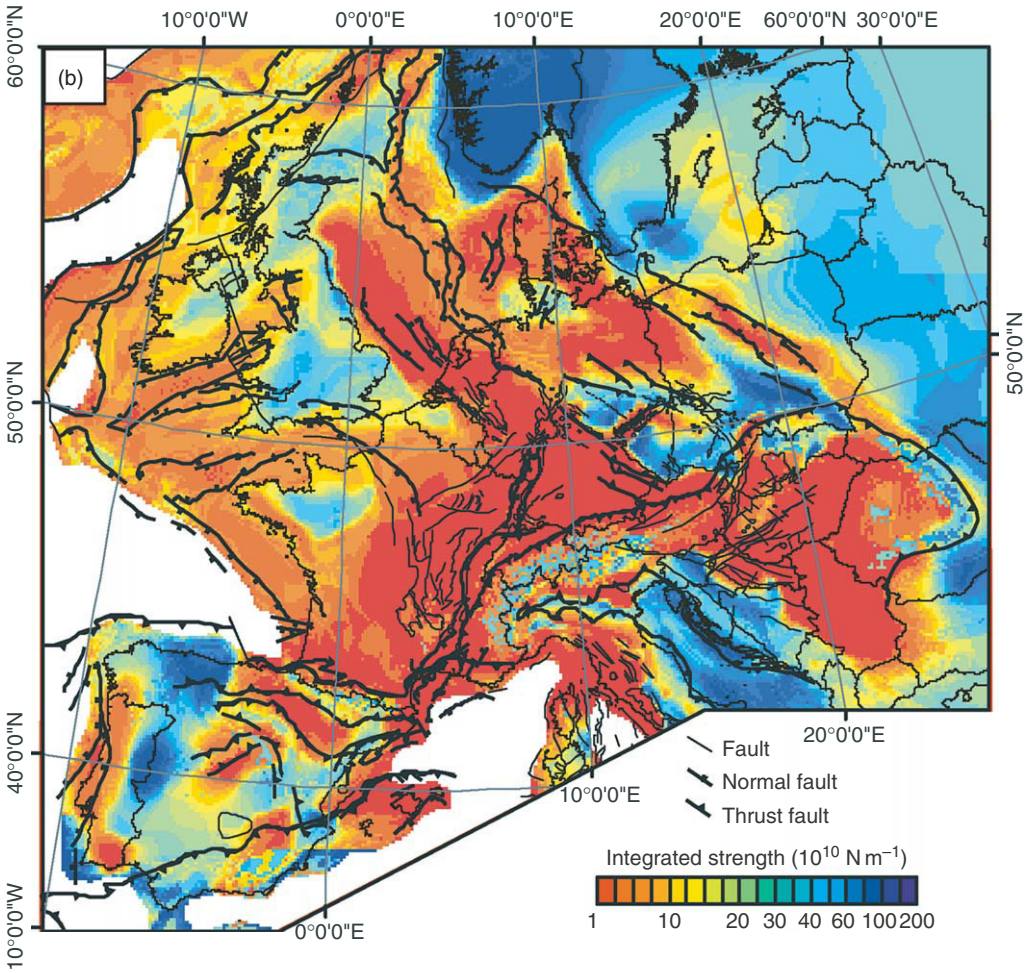

Figure 38 Integrated strength maps for intraplate Europe. Contours represent integrated strength in compression for (a) total lithosphere and (b) crust. Adopted composition for upper crust, lower crust, and mantle is based on a wet quartzite, diorite, and dry olivine composition, respectively. Rheological rock parameters are based on Carter and Tsenn (1987) The adopted bulk strain-rate is $10^{-16}\,s^{-1}$, compatible with constraints from GPS measurements (see text). The main structural features of Europe are superimposed on the strength maps. Modified from Cloetingh S, Ziegler PA, Beekman F, Andriessen PAM, Matenco L, Bada G, Garcia-Castellanos D, Hardebol N, Dézes P, and Sokoutis D (2005) Lithospheric memory, state of stress and rheology: Neotectonic controls on Europe's intraplate continental topography. *Quaternary Science Reviews* 24: 241–304.

intraplate lithosphere are primarily caused by variations in the mechanical strength of the lithospheric mantle, whereas variations in crustal strength appear to be more modest. The variations in lithospheric mantle strength are primarily related to variations in the thermal structure of the lithosphere that can be related to thermal perturbations of the sub-lithospheric upper mantle imaged by seismic tomography (Goes *et al.*, 2000a), with lateral variations in crustal thickness playing a secondary role, apart from Alpine domains which are characterized by deep crustal roots. High strength in the East-European Platform, the Bohemian Massif, the London–Brabant Massif and the Fennoscandian Shield reflects the presence of old, cold, and thick lithosphere, whereas the European Cenozoic Rift System coincides with a major axis of thermally weakened lithosphere within the Northwest European Platform. Similarly, weakening of the lithosphere of southern France can be attributed to the presence of tomographically imaged plumes rising up under the Massif Central (Granet *et al.*, 1995; Wilson and Patterson, 2001).

The major lateral strength variations that characterize the lithosphere of extra-Alpine Phanerozoic Europe are largely related to its Late Cenozoic

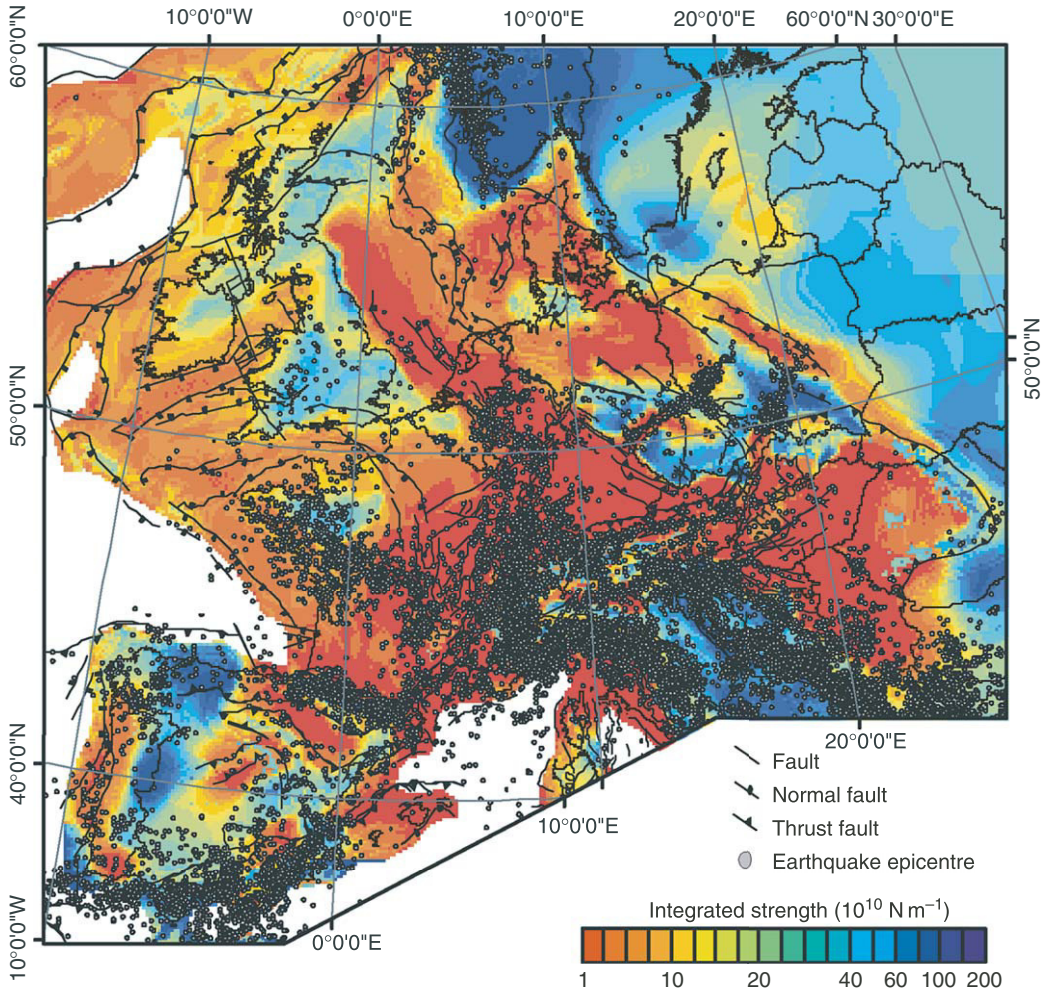

Figure 39 Distribution of crustal seismicity superimposed on map of integrated strength for the European crust (see **Figure 38b**). Earthquake epicenters from the NEIC data center (NEIC, 2004), queried for magnitude >2 and focal depths <35 km.

thermal perturbation as well as to Mesozoic and Cenozoic rift systems and intervening stable blocks, and not so much to the Caledonian and Variscan orogens and their accreted terranes (Dèzes *et al.*, 2004, Ziegler and Dèzes, 2006). These lithospheric strength variations (**Figure 38(a)**) are primarily related to variations in the thermal structure of the lithosphere and, therefore, are compatible with inferred variations in the EET of the lithosphere (see Cloetingh and Burov, 1996; Pérez-Gussinyé and Watts, 2005).

The most important strong inliers in the lithosphere of the Alpine foreland lithosphere correspond to the Early Palaeozoic London–Brabant Massif and the Variscan Armorican, Bohemian and West-Iberian Massifs. The strong Proterozoic Fennoscandian–East-European Craton flanks the weak Phanerozoic European lithosphere to the northeast, whereas the strong Adriatic indenter contrasts with the weak lithosphere of the Mediterranean collision zone.

Figure 39 displays on the background of the crustal strength map the distribution of seismic activity, derived from the NEIC global earthquake catalogue (USGS). As is obvious from this figure, crustal seismicity is largely concentrated on the presently still active Alpine plate boundaries, and particularly on the margins of the Adriatic indenter. In the Alpine foreland, seismicity is largely concentrated on zones of low lithospheric strength, such as the European Cenozoic rift system, and areas where preexisting crustal discontinuities are reactivated under the presently prevailing NW-directed stress field, such as

the South Armorican shear zone (Dèzes *et al.*, 2004; Ziegler and Dèzes, in press) and the rifted margin of Norway (Mosar, 2003).

It should be noted that the strength maps presented in **Figure 38** do not incorporate the effects of spatial variations in the composition of crustal and mantle layers. Future work will address the effects of such second-order strength perturbations, adopting constraints on the composition of several crustal and mantle layers provided by seismic velocities (Guggisberg *et al.*, 1991; Aichroth *et al.*, 1992) and crustal and upper-mantle xenolith studies (Mengel *et al.*, 1991; Wittenberg *et al.*, 2000).

6.11.4 Northwestern European Margin: Natural Laboratory for Continental Breakup and Rift Basins

The Atlantic margin of Mid-Norway (**Figure 40**) is one of the best documented continental margins of the world owing to the availability of a wealth of high-quality industry data and intense research collaboration between industrial, governmental, and academic institutions (Torné *et al.*, 2003; Mosar, 2003). For this reason, the Mid-Norway margin serves as a natural laboratory for studying process controlling the development of a passive margin, the crustal separation phase of which was accompanied by extensive magmatic activity. Moreover, it permits to analyze, for passive margins, enigmatic features such as its post-breakup partial inversion and erosional truncation in near-shore areas in conjunction with uplift of the Norwegian Caledonides, the controlling mechanisms of which have since long been debated.

Studies on the North Atlantic margins have led to the development of a new generation of models for controls on continental breakup and the subsequent evolution of ocean–continent boundary zones, quantification of melting processes, lateral migration of rifting activity and associated vertical motions (**Figure 41**) (see also Cloetingh *et al.*, 2005). It appears that breakup processes have set the stage for subsequent tectonic reactivation of the margin under a compressional stress regime and overprinting upper-mantle thermal anomalies (Ziegler and Cloetingh, 2004). Systematic quantification of uplift and erosion of the marginal Caledonian highlands by thermogeochronology and other techniques (**Figure 42**) has revealed pronounced along-strike variations in the magnitude of their late-stage uplift and related geomorphologic development.

6.11.4.1 Extensional Basin Migration: Observations and Thermomechanical Models

In the literature, several examples of extensional basins have been described in which the locus of extension shifted in time toward the zone of future crustal separation (e.g., Bukovics and Ziegler, 1985; Ziegler, 1988, 1996b; Lundin and Doré, 1997). These basins typically consist of several laterally adjacent fault-controlled sub-basins the main sedimentary fill of which often differs by several tens of millions of years. As such, they reflect lateral changes in their main subsidence phases that can be attributed to a temporal lateral shift of the centers of lithosphere extension.

A well-documented example of this phenomenon is the Mid-Norway passive continental margin. Prior to the final Late Cretaceous–Early Tertiary rifting event that culminated in continental breakup, the Mid-Norway Vøring margin was affected by several rifting events (Ziegler, 1988; Bukovics and Ziegler, 1985; Skogseid *et al.*, 1992). These resulted in the subsidence of a sequence depocenters located between the Norwegian coast and the continent–ocean boundary (**Figure 43**). On a basin-wide scale, this passive margin consists of the Late Palaeozoic–Triassic Trøndelag Platform, located in the east, the Jurassic–Early Cretaceous Vøring Basin in the central part of the shelf, and adjacent to the continent–ocean boundary the marginal extended zone that was active during the final stretching event preceding continental breakup at the Paleocene–Eocene transition (Lundin and Doré, 1997; Reemst and Cloetingh, 2000; Skogseid *et al.*, 2000; Osmundsen *et al.*, 2002). The Nordland Ridge is a classical footwall uplift that is associated with the border fault of the Vøring Basin, whilst the Vøring Marginal High is associated with the continent–ocean boundary. Although there is still considerable uncertainty about the age of the oldest syn-rift sedimentary sequences involved in the different deep-seated fault blocks of the Mid-Norway margin and the width of the area that was affected by the pre-Jurassic extensional phases (Gabrielsen *et al.*, 1999; Mosar *et al*, 2002), it is generally agreed that in time extension shifted westward, away from the Trøndelag Platform towards the Vøring Basin and ultimately centered on the continental breakup axis (e.g., Bukovics and Ziegler, 1985; Lundin and Doré, 1997; Reemst and Cloetingh, 2000).

Other areas in which extensional strain concentrated in time toward the rift axis or the future

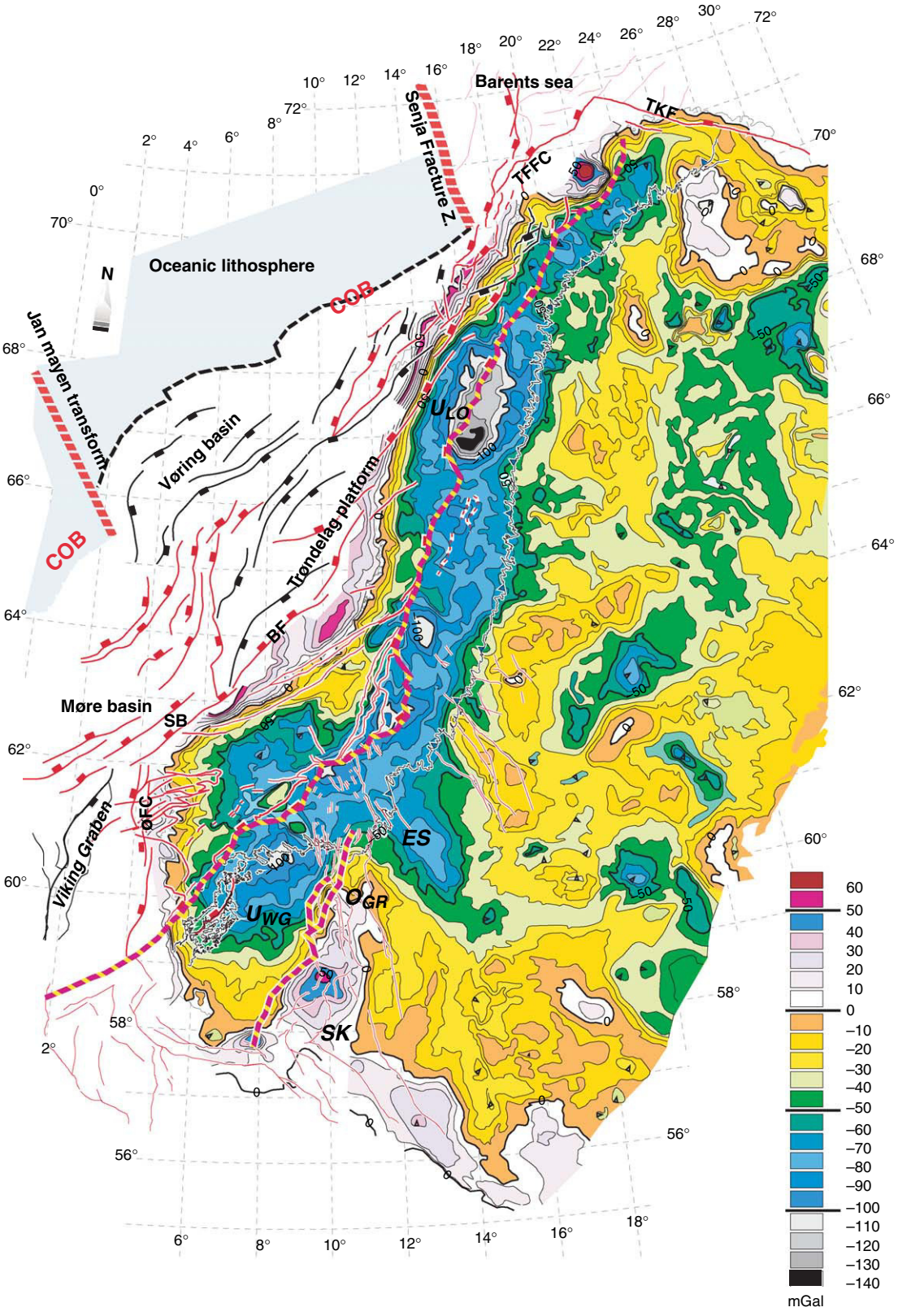
Barents sea
Senja Fracture Z.
TKF
TFFC
Oceanic lithosphere
COB
COB
Jan mayen transform
Vøring basin
Trøndelag platform
BF
Møre basin
SB
øFC
Viking Graben
ULO
ES
OGR
UWG
SK
N
mGal
60
50
40
30
20
10
0
−10
−20
−30
−40
−50
−60
−70
−80
−90
−100
−110
−120
−130
−140

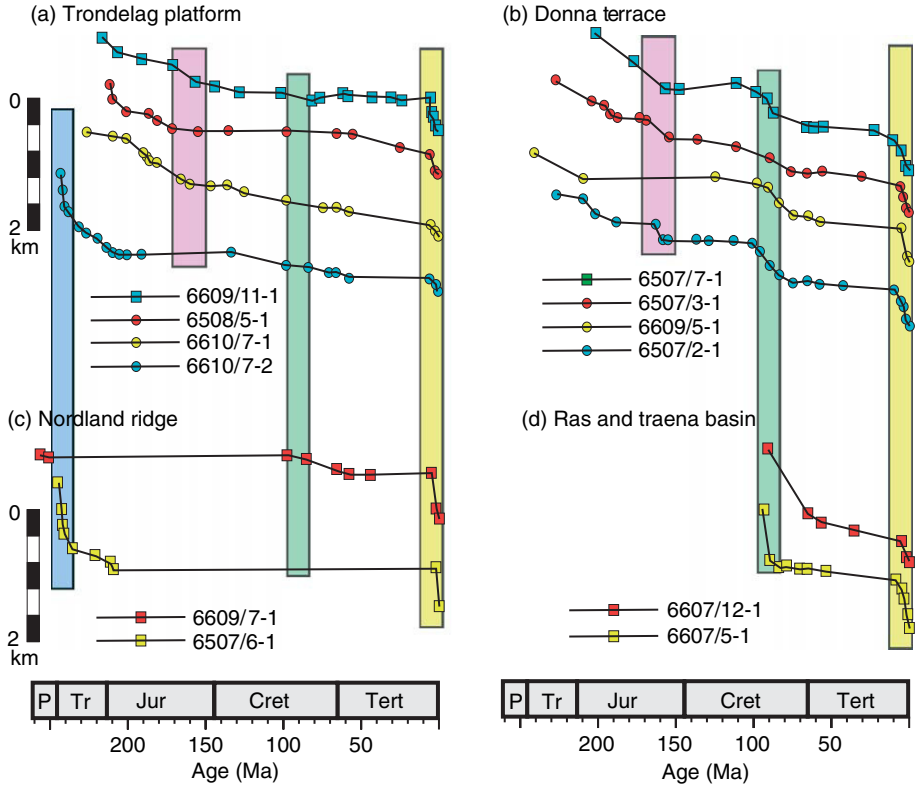

Figure 41 Tectonic subsidence curves for four sub-basins and platforms of the Mid-Norwegian margin. Note the simultaneously occurring subsidence accelerations (colored bars). The Mesozoic subsidence accelerations reflect pronounced rift-related tectonic phases, whereas the Late Neogene subsidence acceleration (light yellow bar) coincides with a major reorganization of the Northern Atlantic stress field. Modified from Reemst, P (1995) Tectonic modeling of rifted continental margins; Basin evolution and tectono-magmatic development of the Norwegian and NW Australian margin. PhD thesis, Vrije Universiteit, Amsterdam, 163p.

breakup axis are, for instance, the Viking Graben of the North Sea (Ziegler, 1990b), the nonvolcanic Galicia margin and the passive rifted ancient South Alpine margin (e.g., Manatschal and Bernoulli, 1999; Bertotti *et al.*, 1997).

Several hypotheses have been proposed to explain this rift migration by invoking the principle that rifting occurs where the lithosphere is weakest (Steckler and Ten Brink, 1986). A mechanism for limiting extension at a given location was studied, for example, by England (1983), Houseman and England (1986), and Sonder and England (1989), who found that cooling of the continental lithosphere during stretching may increase its strength, so that deformation shifts to a previously low strain region (Sonder and England, 1989). With this mechanism, other effects such as changes in plate boundary forces are not required to explain basin migration.

Migration of the extension locus has also been attributed to temporally spaced multiple stretching phases, separated by periods during which the lithosphere is not subjected to extension. Under such a scenario, the lithosphere that was weakened during an earlier stretching phase needs sufficient time to cool and regain its strength and to become indeed stronger than the adjacent unextended area before

Figure 40 Bouguer gravity anomaly map of the onshore parts of the Scandinavian North Atlantic passive margin, showing superimposed rift-related normal fault systems. The width of the passive margin between the continent-ocean boundary (COB), marked by the dashed fat black line, and the innermost boundary fault system (IBF), marked by the dashed fat red line, ranges from 550 km in the south to over 700 km in Mid-Norway to 165 km north of Lofoten. Note the onshore extension of the rift system. The wiggly black barbed line marks the position of the Caledonian Thrust Front. Modified from Mosar J (2003). Scandinavia's North Atlantic passive margin. *Journal of Geophysical Research* 108: 2630.

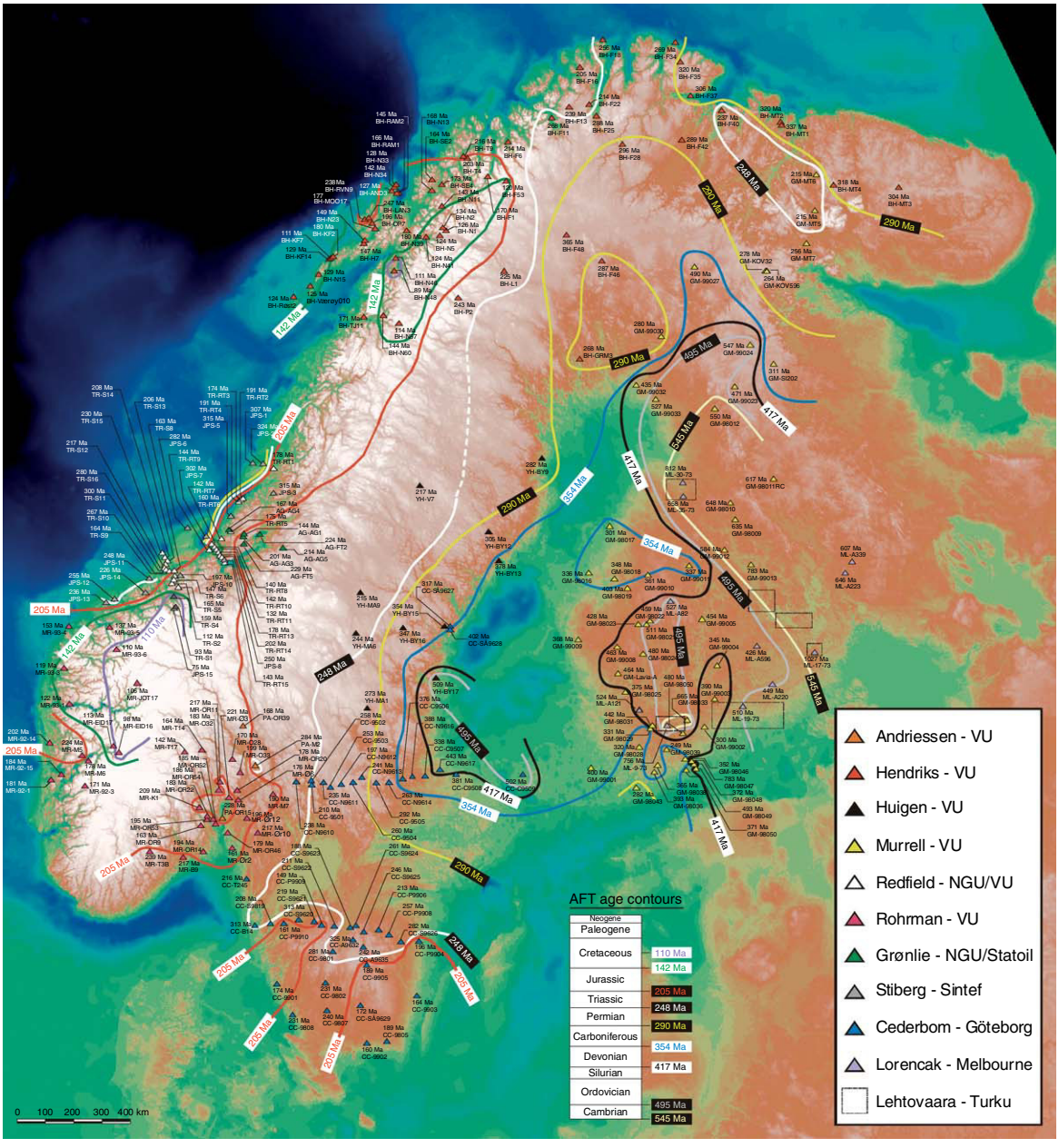

Figure 42 Digital elevation model of Scandinavia. Contour lines show vertical motions in My derived from AFT analyses.

the onset of the next stretching event. Obviously, this concept requires a long period of tectonic quiescence between successive rifting events. Bertotti *et al.*, (1997) showed in a model for the thermomechanical evolution of the South Alpine rifted margin that its strongly thinned parts indeed could have been stronger than the remainder of the margin. This is compatible with rheological considerations which suggest that stretched and thermally stabilized lithosphere, characterized by a thinned crust and a considerably stronger lithospheric mantle, is considerably stronger than unextended lithosphere (**Figure 33**) (Bertotti *et al.*, 1997). This hypothesis requires sudden time-dependent changes in the magnitude and possibly the orientation of intraplate stress fields, controlling the different stretching and nonstretching phases. Nevertheless, evidence for tensional reactivation of rifts which were abandoned millions of years ago suggests that crustal-scale faults permanently weaken their lithosphere to the degree

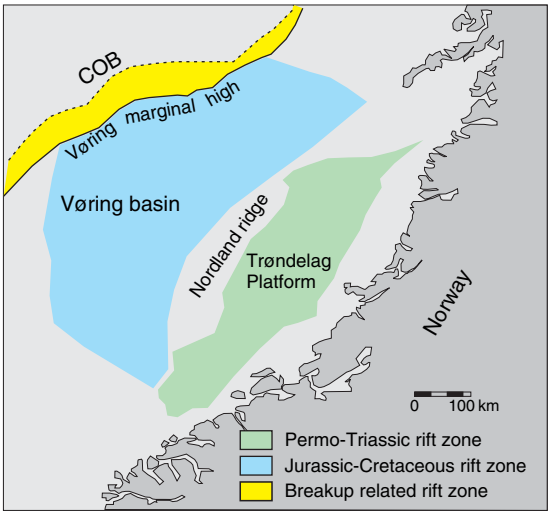

Figure 43 Sketch map of rift zones on the Mid-Norwegian margin showing timing of main rift activity. Modified from Skogseid J and Eldholm O (1995) Rifted continental margin off mid-Norway. In: Banda E, Talwani E, and Torné M (eds.) *Rifted Ocean-Continent Boundaries*, pp. 147–153. Dordrecht: Kluwer Academic.

that under given conditions they are prone to tensional and compressional reactivation (Ziegler and Cloetingh, 2004).

Sawyer and Harris (1991) and Favre and Stampfli (1992) have described for the evolution of the Central Atlantic rift a gradual concentration of extensional strain towards the future zone of crustal separation. This phenomenon is attributed to the syn-rift gradual rise of the lithospheric isotherms and a commensurate upward shift of the lithospheric necking level and the intracrustal brittle/ductile deformation boundary. As a result of this, extensional strain concentrates in time on the thermally more intensely weakened part of the lithosphere, generally corresponding to the rift axis, thus causing narrowing of the rift and abandonment of its lateral graben systems (Ziegler and Cloetingh, 2004). In the case of the Central Atlantic, this process was enhanced by the impingement of a short-lived, though major, mantle plume at the Triassic–Jurassic transition (Wilson, 1997; Nikishin *et al.*, 2002). In the following, we discuss the implications of a viscoelastic plastic finite element model for extension of a lithosphere with an initially symmetric upper-mantle weakness (for details see Van Wijk and Cloetingh, 2002). When large extension rates are applied, focusing of deformation takes place, causing lithospheric necking and eventually continental breakup. Hereafter, this will be referred to as 'standard' rifting. A different evolution of deformation localization takes place when the lithosphere is extended at low strain rates. In this case, the necking area may start to migrate laterally, and hence prevent continental breakup. Modeling results will be compared to observations on basin migration at the Mid-Norway, Galicia and ancient South Alpine margins.

The modeled domain consists of an upper and lower crust and a lithospheric mantle (**Figure 44**) to which the rheological parameters of granite, diabase and olivine, respectively, have been assigned (see **Table 4**) (Carter and Tsenn, 1987). In order to facilitate deformation localization, the crust was thickened by 2 km in the center of the domain, forming a linear feature parallel to the future rift axis. This

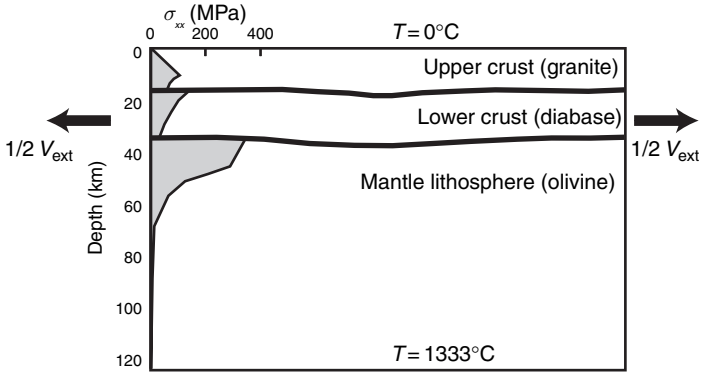

Figure 44 Pre-extensional configuration of the lithospheric model and horizontal deviatoric stress field. v_{ext} is extension velocity. Note thicker crust in the central part of the model domain. Upon volume preserving stretching of the lithosphere, the width of the model domain increases while its thickness decreases. Modified from Van Wijk JW and Cloetingh S (2002) Basin migration caused by slow lithospheric extension. *Earth and Planetary Science Letters* 198: 275–288.

Table 4 Material parameter values for the numerical modeling results presented in **Figures 45–51**

Parameter	Layer	Value
Density	Upper crust	$2700\,kg\,m^{-3}$
	Lower crust	$2800\,kg\,m^{-3}$
	Mantle lithosphere	$3300\,kg\,m^{-3}$
Thermal expansion		$10^{-5}\,K^{-1}$
Crustal heat production		$10^{-6}\,W\,m^{-3}$
Specific heat		$1050\,J\,kg^{-1}\,K^{-1}$
Conductivity	Crust	$2.6\,W\,m^{-1}\,K^{-1}$
	Mantle lithosphere	$3.1\,W\,m^{-1}\,K^{-1}$
Bulk modulus	Crust	$3.3\,10^{10}$ Pa
	Mantle lithosphere	$12.5\,10^{10}$ Pa
Shear modulus	Crust	$2\,10^{10}$ Pa
	Mantle lithosphere	$6.5\,10^{10}$ Pa
Power law exponent '*n*'	Upper crust	3.3
	Lower crust	3.05
	Mantle lithosphere	3.0
Activation energy '*Q*'	Upper crust	$186.7\,kJ\,mol^{-1}$
	Lower crust	$276\,kJ\,mol^{-1}$
	Mantle lithosphere	$510\,kJ\,mol^{-1}$
Material constant '*A*'	Upper crust	$3.16\,10^{-26}\,Pa\,n\,s^{-1}$
	Lower crust	$3.2\,10^{-20}\,Pa\,n\,s^{-1}$
	Mantle lithosphere	$7.0\,10^{-14}\,Pa\,n\,s^{-1}$
Internal friction angle		30
Internal dilatation angle		0
Cohesion		$20\,10^{6}$ Pa
(Initial) thickness of model domain *H*		125 km

causes localized weakening of the upper mantle and a corresponding strength reduction of the lithosphere. A lithosphere with this configuration is thought to be typical for orogenic belts after post-orogenic thermal equilibration of their thickened crust (Henk, 1999). The Mid-Norway margin is superimposed on the Caledonian orogen, the crust of which was presumably still thickened prior to the Late Carboniferous onset of rifting (Skogseid *et al.*, 1992).

Appendix 1 discusses fundamental aspects of the adopted dynamical model for slow extension. The model is not prestressed and is subjected to horizontal extension applied at its right and left edges (**Figure 44**). The tested constant extension rates range between ~3 and ~30 mm yr^{-1} and are compatible with present-day plate velocities derived from the Global Positioning System (Argus and Heflin, 1995). The surface of the model is unconstrained whilst for its base a vertical velocity component is prescribed calculated from the principle of volume conservation. Temperatures are calculated using the heat conduction equation. The initial geotherm is in steady state. The temperature at the surface is 0°C, and at the base of the model (125 km depth) it is 1333°C. The heat flow through the right and left sides of the domain is zero. The crustal heat production is constant (**Table 4**).

6.11.4.2 Fast Rifting and Continental Breakup

As rift structures resulting from various high extension rates ('standard necking cases') do not differ significantly, one representative test in which the lithosphere was stretched with a total velocity of about 16 mm yr^{-1} is discussed here. At the onset of lithospheric extension deformation localizes in the center of the domain where the initial mantle weakness was introduced. Thinning of the crust and mantle lithosphere concentrates here, and mantle material starts to well up (**Figure 45**). Thinning of the crust and mantle lithosphere continues, eventually resulting in continental breakup after ~27 My of stretching. Continental breakup is here defined as occurring when the crust is thinned by a factor 20, though another factor or another definition for continental breakup could have been chosen. This definition corresponds to about 40–50% of extension of the model domain at continental breakup. Thinning factors for the crust (β) and

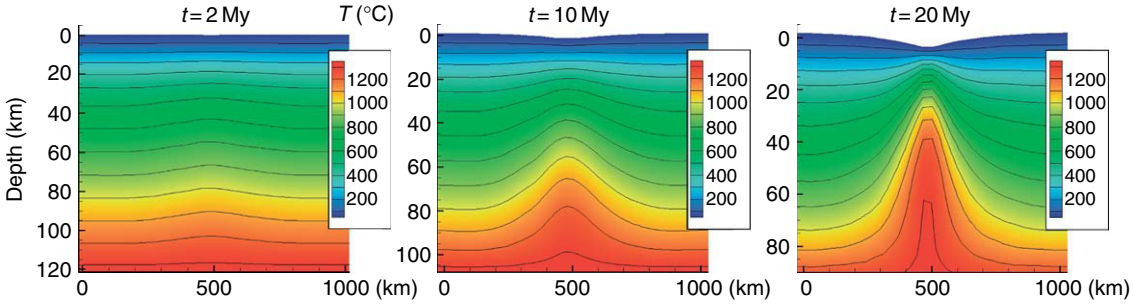

Figure 45 Thermal evolution of the lithosphere 2, 10, and 20 My after the onset of stretching at a rate of $v_{ext} \approx 16\,mm\,yr^{-1}$. Note the changing horizontal and vertical scales in the panels indicating the changing sizes of the model domain upon stretching. Modified from Van Wijk JW and Cloetingh S (2002) Basin migration caused by slow lithospheric extension. *Earth and Planetary Science Letters* 198: 275–288.

lithospheric mantle (δ) are shown in **Figure 46**. The base of the lithospheric mantle is the 1300°C isotherm, and β and δ are defined as the ratio between the initial and the present thickness of the crust or lithospheric mantle, respectively.

The total (integrated) strength of the lithosphere during rifting is shown in **Figure 47**. The center of the model domain, on which the initial mantle weakness was imposed, is the weakest part; this continues to be so until continental breakup. Integrated strength values of the continental lithosphere vary between 10^{12} and $10^{13}\,N\,m^{-1}$ with the higher values characterizing Precambrian shields (Ranalli, 1995; England, 1986). In our model the strength of the lithosphere falls within this range. During rifting, the strength of the lithosphere decreases with time, owing to its thinning and heating as a consequence of its stretching and nonlinear rheology.

In other cases with higher constant extension rates the localization of deformation is comparable to that discussed above. In all cases, deformation concentrates on one zone in which thinning continues until continental breakup is achieved. The duration of the rifting stage preceding continental breakup depends on the extension velocity. When the lithosphere is stretched at grater velocities, it takes less time to reach continental breakup (**Figure 48**). When extension velocities are less than $\sim$8 mm yr^{-1}, stretching of the lithosphere does not lead to continental breakup. The dependence of rift duration on potential mantle temperature is discussed in Van Wijk *et al.*, (2001). The configuration of the rift shows no clear dependence on the tested stretching velocities (see also Bassi, 1995).

The tendency for the lithosphere to neck (or to focus strain) is weaker with decreasing extension velocities. When stresses exerted on the lithosphere

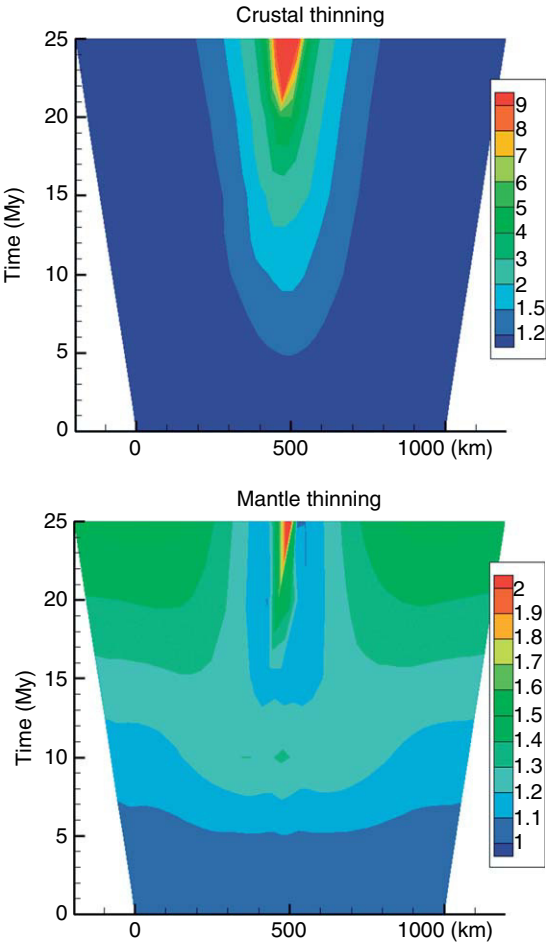

Figure 46 Evolution of thinning factors of crust (β) and mantle lithosphere (δ) for $v_{ext} \approx 16\,mm\,yr^{-1}$. Breakup after $\sim$27 My. Width of the model domain (horizontal axis) vs. time (vertical axis). The width of the model domain increases as the lithosphere is extended. Modified from Van Wijk JW and Cloetingh S (2002) Basin migration caused by slow lithospheric extension. *Earth and Planetary Science Letters* 198: 275–288.

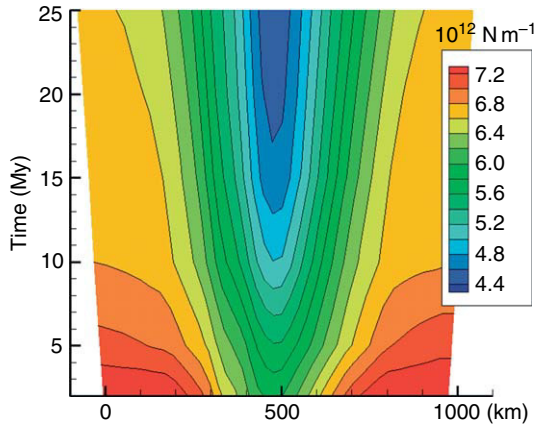

Figure 47 Evolution of lithosphere strength ($\int_0^H \sigma(z)\,dz$), in N m^{-1}, for $v_{ext} \approx 16$ mm yr^{-1}. Modified from Van Wijk JW and Cloetingh S (2002) Basin migration caused by slow lithospheric extension. *Earth and Planetary Science Letters* 198: 275–288.

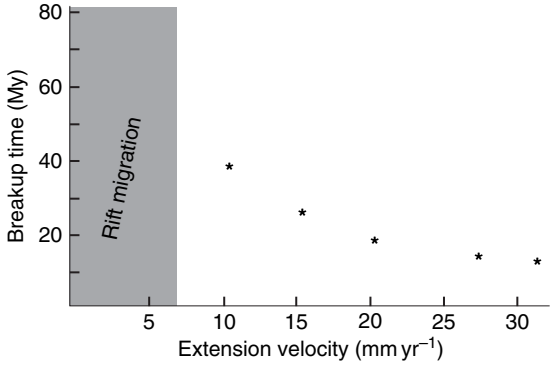

Figure 48 Rift duration until continental breakup as a function of total extension velocity (stars). Rifting at larger extension rates eventually results in breakup, while at lower rates syn-tectonic cooling prevails causing rift migration before breakup is achieved. Modified from Van Wijk JW and Cloetingh S (2002) Basin migration caused by slow lithospheric extension. *Earth and Planetary Science Letters* 198: 275–288.

are smaller, the rate of strain localization also slows down, mantle upwelling is slower and syn-rift lateral conductive cooling plays a more important role. When the lithosphere is stretched at high rates, upwelling of mantle material is fast (almost adiabatic) with little or no horizontal heat conduction. The fast rise of hot asthenospheric material further reduces the strength of the lithosphere in the central region, with the consequence that lithospheric deformation and thinning accelerates even further. The result is a short rifting stage preceding continental breakup.

6.11.4.3 Thermomechanical Evolution and Tectonic Subsidence During Slow Extension

The lithosphere reacts differently to low extension rates (Van Wijk and Cloetingh, 2002). Results of a representative test with an extension rate of ~6 mm yr^{-1} over a period of 100 My have been selected to illustrate the thermal evolution of the lithosphere (**Figure 49**). During the first 30 My after the onset of stretching, deformation localizes in the center of the model domain where the lithosphere was pre-weakened (**Figure 44**). Mantle material wells up and a sedimentary basin developed. Subsequently, as lithospheric stretching proceeds, temperatures begin to decrease (see panels 45 My and 50 My, **Figure 49**), in contrast to what happened in the standard necking case shown in **Figure 45**. Development of the upwelling zone ceases and the lithosphere cools in the center of the domain. Cooling of the central zone continues while after 70 My increasing temperatures are evident on both sides of the previously extended central zone. As these new upwelling zones develop further (**Figure 49**, 110 My panel) two new basins develop adjacent to the initial, first-stage basin. Temperatures in the lithosphere are now lower below the initial basin as compared to the surrounding lithosphere; a 'cold spot' is present in an area that underwent initial extension (see also **Figure 50**). Surface heat flow values reflect this thermal structure; the surface heat flow values are lower in the first-stage basin (66 mW m^{-2}) than in the surrounding areas (75 mW m^{-2}) at 110 My.

Thinning factors for the crust and mantle lithosphere are shown in **Figure 50**. Thinning of the crust starts, as expected, in the central weakness zone of the domain where a single basin forms, with a maximum thinning factor of ~1.85 for the crust. Crustal thinning in the central basin continues until about 65 My after the onset of stretching, at which time the locus of thinning shifts towards both sides of the initial basin. The zones of second-stage maximum thinning are located at a distance of about 500 km from the center of the initial rift. Although stretching of the lithosphere continues after 65 My, extensional strain is no longer localized in the initial rift basin but is centred on the two flanking new rifted basins. The thinning factor of the mantle lithosphere reflects this behaviour. During the first ~45 My of stretching upwelling mantle material causes δ to be larger in the central zone of the domain than in its surroundings. Thereafter, however, temperatures decrease rapidly in the central zone (see also **Figure 49**) as

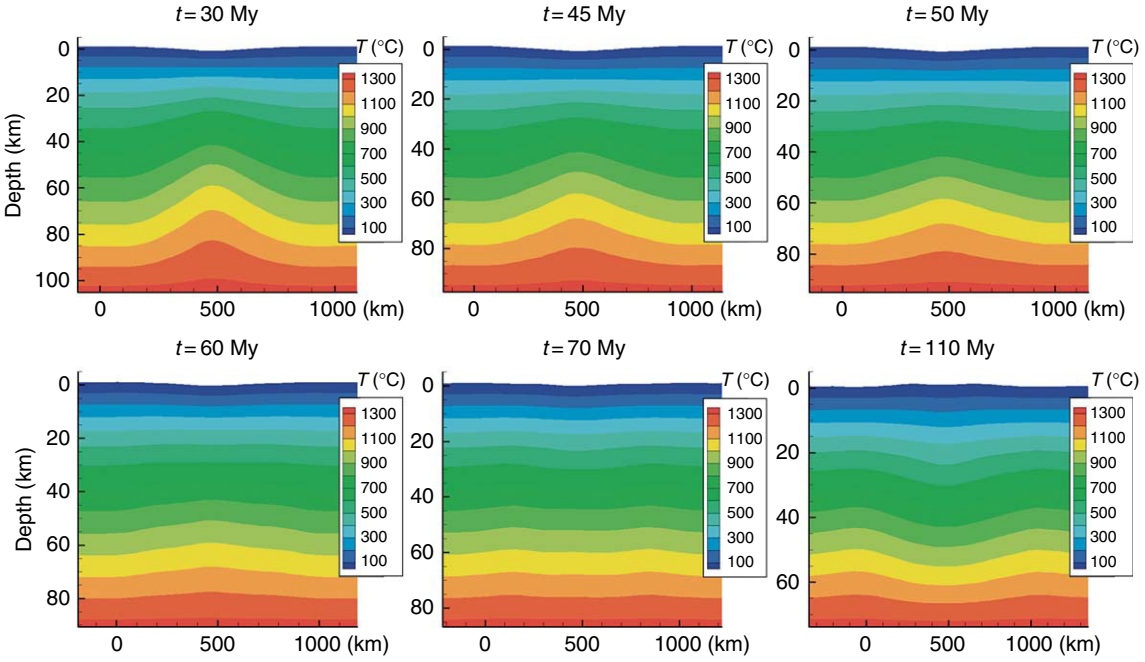

Figure 49 Thermal evolution of the lithosphere for a migrating rift at an extension rate of $v_{ext} \approx 6\,mm\,yr^{-1}$, times in My after the onset of stretching. Modified from Van Wijk and Cloetingh (2002).

new upwelling zones develop on its flanks with δ decreasing in the area of the first basin and increasing beneath the new basins.

Figure 51 gives, for the modeling domain, the evolution of its surface topography as well as synthetic tectonic subsidence curves for its three rifted basins. After ~35 My of stretching, the central basin reaches a maximum depth of about 760 m that would be amplified by sediment loading. Subsequently, the two lateral basins begin to subside whilst the central basin is uplifted. Ziegler (1987) defined basin inversion as the reversal of the subsidence patterns of a sedimentary basin in response to the buildup of compressional or transpressional stresses. According to this definition, no basin inversion takes place in our model as the lithosphere remains in a tensional setting. The synthetic tectonic subsidence curve for the central basin (right panel in **Figure 51(b)**) shows a clear reversal of its subsidence pattern under a stretching regime. The relative uplift is considerable that, depending on the location within this basin, amounts to approximately 800–1700 m. The left panel in **Figure 51(b)** shows the subsidence curve for one of the second-stage rifts that started to subside after about 50 My. The central panel shows the subsidence curve for the 'transition zone' between the initial basin and the second-stage basin that formed after rift migration. This area displays continuous uplift.

The total strength of the lithosphere, obtained by integrating the stress field over the thickness of the lithosphere (Ranalli, 1995), is shown in **Figure 52**. After the onset of stretching the central part of the model domain progressively weakens, reaching its minimum strength by 30 My. Thereafter its strength increases, but remains lower than the rest of the domain. From 55 My onward, the smallest values of lithospheric strength occur on both sides of the central basin beneath the second-stage rifts. By comparing the strength of the lithosphere with its thermal structure (**Figure 49**), the strong dependence of strength on the temperature is evident.

From this modeling study it is concluded that lateral rift migration may occur under conditions of long-term low-strain-rate lithospheric extension. Whether such a model can be applied to the Mid-Norway margin needs to be further analyzed. This requires a step-wise palinspastic restoration of a set of structurally and stratigraphically closely controlled cross sections through the Mid-Norway margin and its conjugate East Greenland margin, permitting quantification of extensional strain rates through time.

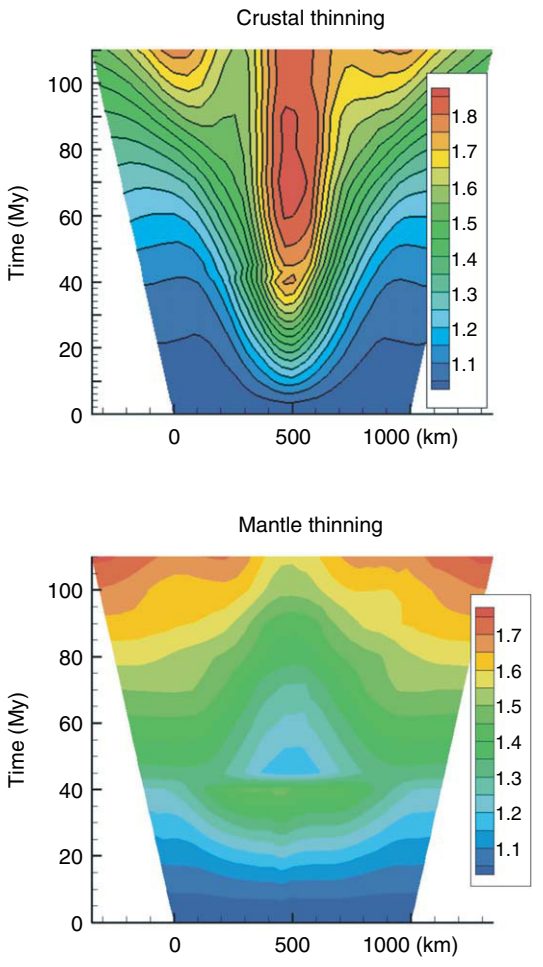

Figure 50 Evolution of thinning factors for the crust (β) and lithospheric mantle (δ) at an extension rate of $v_{ext} \approx 6\,mm\,yr^{-1}$. No continental breakup. The asymmetry (upper panel) is caused by the asymmetry of the finite element grid that was used. We used triangular-shaped elements that resulted in a not perfectly symmetric mesh and initial Moho topography. The wiggles in the lines (lower panel, upper right) are due to interpolation inexactnesses while calculating lithospheric mantle thinning. Modified from Van Wijk JW and Cloetingh S (2002) Basin migration caused by slow lithospheric extension. *Earth and Planetary Science Letters* 198: 275–288.

6.11.4.4 Breakup Processes: Timing, Mantle Plumes, and the Role of Melts

The Mid-Norway margin is a representative part of the Norwegian–Greenland Sea rift along which crustal separation between NW Europe and Greenland was achieved in earliest Eocene times (Mosar *et al.*, 2002; Torsvik *et al.*, 2001). The Norwegian–Greenland Sea rift, which had remained intermittently active for some 280 Ma from the Late Carboniferous until the end of the Paleocene, is superimposed on the Arctic–North Atlantic Caledonides (Ziegler, 1988; Ziegler and Cloetingh, 2004). During the Devonian and Early Carboniferous, orogen-parallel extension controlled the collapse of the Caledonian Orogen, the subsidence of pull-apart basins and uplift of core complexes (Braathen *et al.*, 2002; Eide *et al.*, 2002). During the subsequent rifting stage, tensional reactivation of Caledonian and Devonian–Early Carboniferous crustal discontinuities played an important role in the structuring of the Mid-Norway margin (Mosar, 2003). During the evolution of the Norwegian–Greenland Sea rift, initially a broad zone was affected by crustal extension. In time, rifting activity concentrated progressively on the zone of future crustal separation with lateral elements becoming step-wise abandoned (Ziegler, 1988, 1990b; Mosar *et al.*, 2002; Ziegler and Cloetingh, 2004). On the Mid-Norway margin, syn-rift sediments attain thicknesses of up to 10 km with postrift series reaching thicknesses of 2–3 km (Osmundsen *et al.*, 2002). Whereas Late Carboniferous to early Late Cretaceous crustal extension was not accompanied by volcanic activity, volcanism flared up during the Campanian–Maastrichtian, peaked during the Paleocene and terminated on the Mid-Norway margin upon earliest Eocene crustal separation when it centred on the newly developing system of seafloor spreading axes. The Paleocene development of the Thulean flood basalt province, which was centred on Iceland and had a radius of more than 1000 km, is attributed to the impingement of the Iceland plume on the Norwegian–Greenland Sea rift (Ziegler, 1988; Morton and Parson, 1988; Larsen *et al.*, 1999; Skogseid *et al.*, 2000). Tomographic data image a mantle plume beneath Iceland rising up from near the core–mantle boundary (Bijwaard and Spakman, 1999) (**Figure 53**).

Correspondingly, the Paleocene extrusion and intrusion of large volumes of basaltic rocks on the Mid-Norway margin is generally attributed to a plume-related temperature increase of the asthenosphere. However, the interplay between extension and magmatism during continental breakup is still debated and recent numerical modeling studies suggest that the volumes of melts extruded at volcanic margins may also be generated by 'standard' thermal conditions, provided high extension rates can be implied (**Figure 54**) (Van Wijk *et al.*, 2001).

6.11.4.5 Postrift Inversion, Borderland Uplift, and Denudation

Following Early Eocene crustal separation, the Mid-Norway margin was partly inverted during the Late

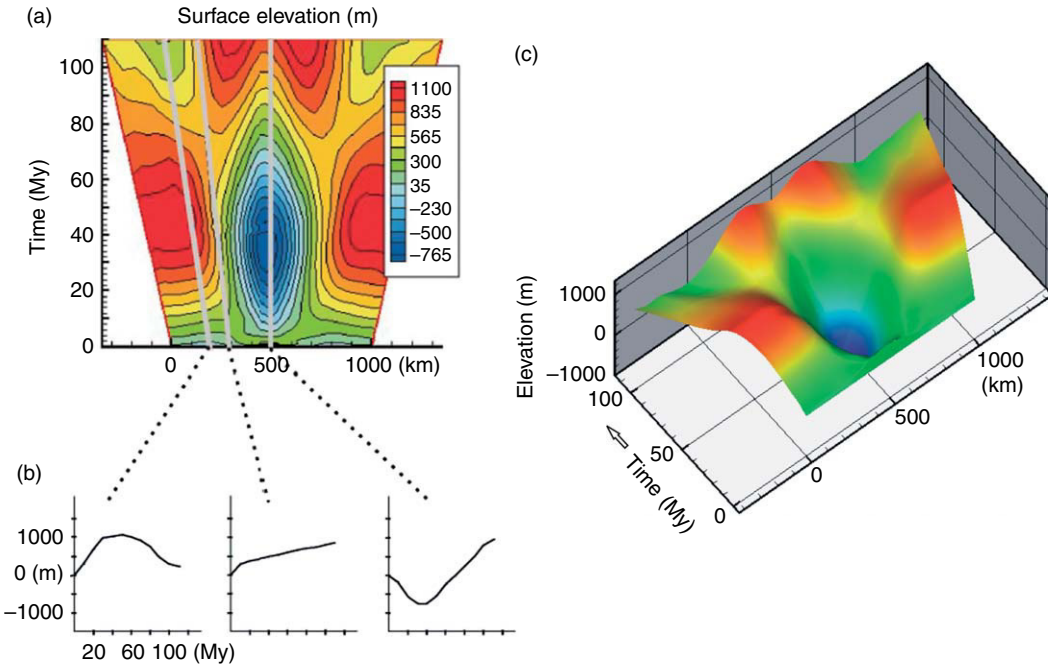

Figure 51 (a) Evolution of relative surface topography for a migrating rift, $v_{ext} \approx 6\,mm\,yr^{-1}$. Gray lines indicate the positions of the corresponding synthetic subsidence curves derived from this panel and shown in (b). (b) Synthetic subsidence curves for three locations indicated in (a): in the first-stage basin (right panel), in the second stage basin (left panel) and in the transition zone separating the two basins (middle panel). (c) Perspective view of the relative surface topography shown in (a). Modified from Van Wijk and Cloetingh 2002.

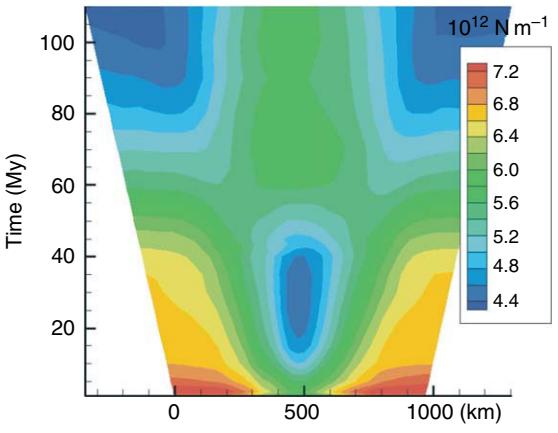

Figure 52 Lithosphere strength evolution for a migrating rift, $v_{ext} \approx 6\,mm\,yr^{-1}$. Modified from Van Wijk JW and Cloetingh S (2002) Basin migration caused by slow lithospheric extension. *Earth and Planetary Science Letters* 198: 275–288.

Eocene–Early Oligocene and Miocene in the prolongation of the Iceland and Jan Mayen fracture zones (Mosar *et al.*, 2002; Doré and Lundin, 1996). Mechanisms controlling the development of these inversion structures remain enigmatic as theoretical models predict the inversion of passive margins in response to the buildup of compressional ridge-push forces only a few tens of million years after crustal separation. Most of the shortening on the Mid-Norway margin was accommodated along preexisting major fault zones (Pascal and Gabrielsen, 2001; Gabrielsen *et al.*, 1999). Compressional structures, such as long-wavelength arches and domes, strongly modified the architecture of the deep Cretaceous basins and controlled sedimentation patterns during Cenozoic (Bukovics and Ziegler, 1985; Vågnes *et al.*, 1998).

From the Oligocene onward, the near-shore parts of the Mid-Norway margin were uplifted and deeply truncated (Doré and Jensen, 1996; Holtedahl, 1953). Mechanisms controlling the observed broad uplift of the inner shelf and the adjacent on-shore areas, as evident all around Norway also remain enigmatic. However, the long-wavelength of the uplifted area is suggestive for mantle processes (Rohrman and Van der Beek, 1996; Rohrman *et al.*, 2002). Olesen *et al.*, (2002) interpreted the long-wavelength component of the gravity field in terms of both Moho topography and large-scale intrabasement density contrasts.

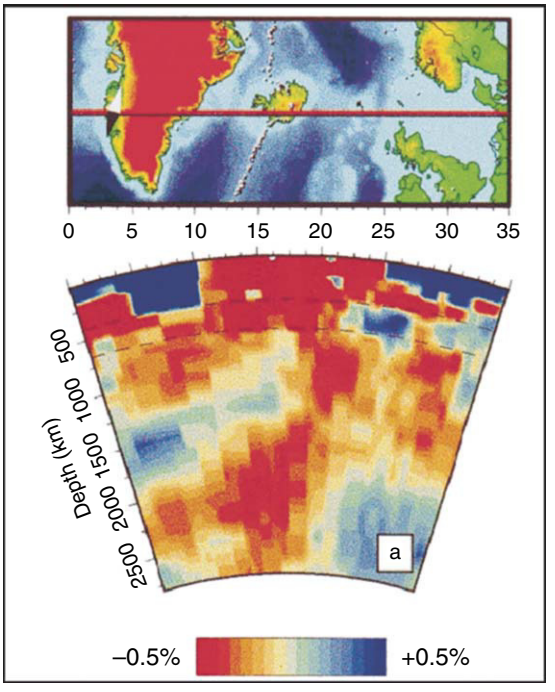

Figure 53 Tomographic cross section showing a large plume-shaped anomaly in the mantle below Iceland. A 0.15% contour is indicated in black for clarity. Dashed lines indicate the 410 and 660 km discontinuities. Modified from Bijwaard H and Spakman W (1999) Fast Kinematic ray tracing of first- and later-arriving global seismic phases. *Geophysical Journal International* 139: 359–369.

Comparing the Bouguer gravity field (**Figure 40**) to the gravity responses from Airy roots at different depths for the northern Scandinavia mountains shows that the compensating masses are located at relatively shallow depths in the upper crust. Consequently, the gravity field of the northern Scandinavian mountains must originate from intra-crustal low-density rocks in addition to Moho depth variations. On the other hand, the mountains of southern Norway appear to be supported by low-density rocks within the mantle (see Cloetingh *et al.*, 2005).

Southwestern Norway was uplifted by as much as to 2 km during Neogene times (**Figure 42**) (Rohrman *et al.*, 1995), as evidenced by the progradation of clastic wedges into the North Sea Basin (Jordt *et al.*, 1995). However, the uplift patterns and timing of southwestern Norway and the northern Scandes differ (Hendriks and Andriessen, 2002). By Late Tertiary times, cold climatic conditions prevailed. The seaward facing side of uplifted land areas was affected by strong glacial erosion, which in turn enhanced their uplift and increased sedimentation and subsidence rates in the flanking basins (**Figure 41**) (Cloetingh *et al.*, 2005). FT analyses along major on-shore lineaments of southern Norway show that preexisting major normal faults, dating back to the Late Palaeozoic and Mesozoic, played a significant role in the Cenozoic uplift pattern (Hendriks and Andriessen, 2002; Cloetingh *et al.*, 2005; Redfield *et al.*, 2005).

Under the presently prevailing northwest-directed compressional stress field the Mid-Norwegian margin and its adjacent highlands are seismically active (Grünthal, 1999) with some faults showing evidence for recent movement (Mörner, 2004). Uplift of the South Norwegian highland continues, whilst the North Sea Basin experiences a phase of accelerated subsidence that began during the Pliocene and that is attributed to stress-induced deflection of the lithosphere (**Figure 10**) (Van Wees and Cloetingh, 1996).

6.11.5 Black Sea Basin: Compressional Reactivation of an Extensional Basin

The Black Sea (**Figure 55**), in which water depths range up to 2.2 km, is underlain by a larger western and a smaller eastern sub-basin that are separated by the Andrusov Ridge. The western basin is floored by oceanic and transitional crust and contains up to 19 km of Cretaceous to recent sediments. The eastern basin is floored by strongly thinned continental crust and contains up to 12 km of Cretaceous and younger sediments. The Andrusov Ridge is buried beneath 5–6 km thick sediments and is upheld by attenuated continental crust. Significantly, the sedimentary fill of the Black Sea basin system is characterized by nearly horizontal layering that is only disturbed along its flanks bordering the orogenic systems of the Balkanides and Pontides in the south, and the Great Caucasus and Crimea in the north and north-east (**Figure 56**).

The Black Sea basin system is thought to have evolved by Aptian–Albian back-arc rifting that progressed in the western sub-basin to crustal separation and Cenomanian–Coniacian seafloor spreading. During the Late Senonian and Paleocene the Black Sea was subjected to regional compression in conjunction with the evolution of

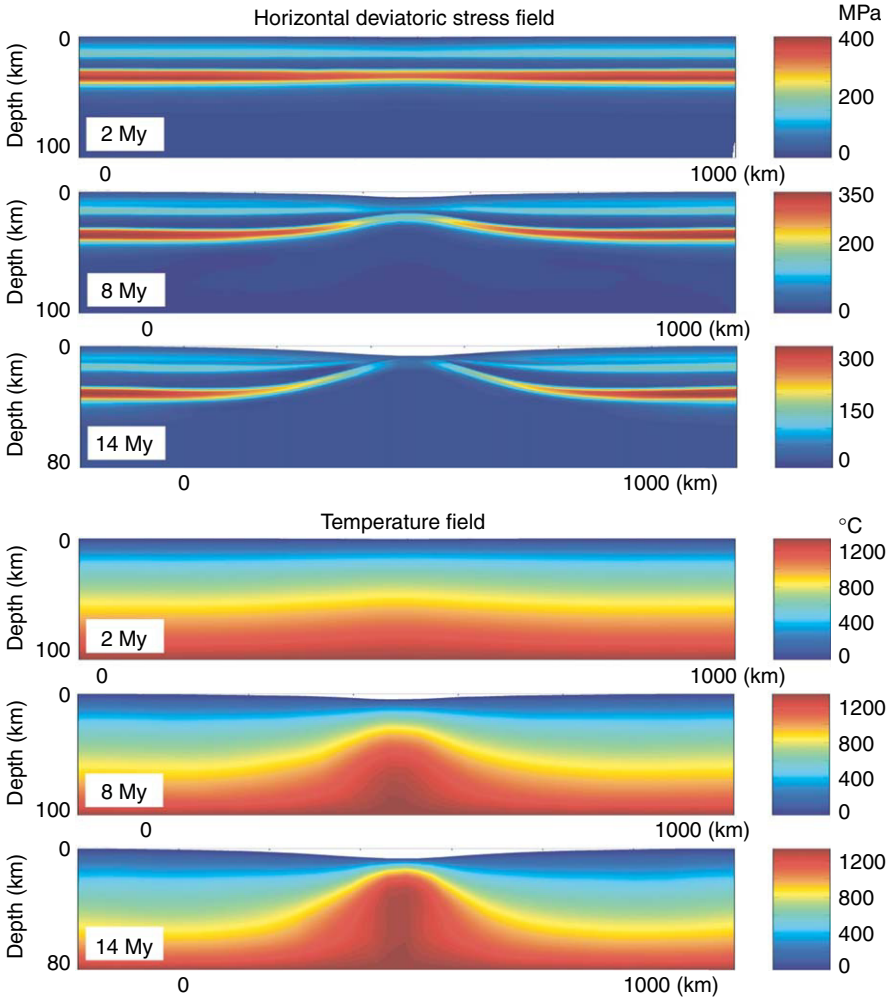

Figure 54 Dynamic numerical model for extension of lithosphere and passive continental margin formation, simulating the evolution of the northern Atlantic volcanic rifted margin. Upper three panels show deviatoric stress field at three subsequent time steps. Lower three panels show temperature field at these time steps. Note the development of melts, usually attributed to mantle plumes, as a direct consequence of lithospheric extension and breakup. Modified from Van Wijk JW, Huismans RS, Ter Voorde M, and Cloetingh S (2001). Melt generation at volcanic continental margins: No need for a mantle plume? *Geophysical Research Letters* 28: 3995–3998.

its flanking orogenic belts. During the Early Eocene major rifting and volcanism affected the eastern Black Sea Basin and the eastward adjacent Acharat–Trialeti Basin. During the Late Eocene and Oligocene, the Pontides thrust belt developed along the southern margin of the Black Sea and inversion of the Great Caucasus Trough and the Acharat–Trialeti rift commenced. The present stress regime of the Black Sea area as deduced from earthquake focal mechanisms, structural, and GPS data is compression dominated, reflecting continued collisional interaction of the Arabian and the Eurasian plates that controls ongoing crustal shortening in the Great Caucasus. In the absence of intrabasinal deformations, the Pliocene and Quaternary accelerated subsidence of the Black Sea Basin is attributed to stress-induced downward deflection of its lithosphere (Nikishin *et al.*, 2001, 2003; Cloetingh *et al.*, 2003).

Although there is general agreement that the Black Sea evolved in response to Late Cretaceous and Eocene back-arc extension, the exact timing and kinematics of opening of its western and eastern subbasins is still being debated (e.g., Robinson *et al.*, 1995;

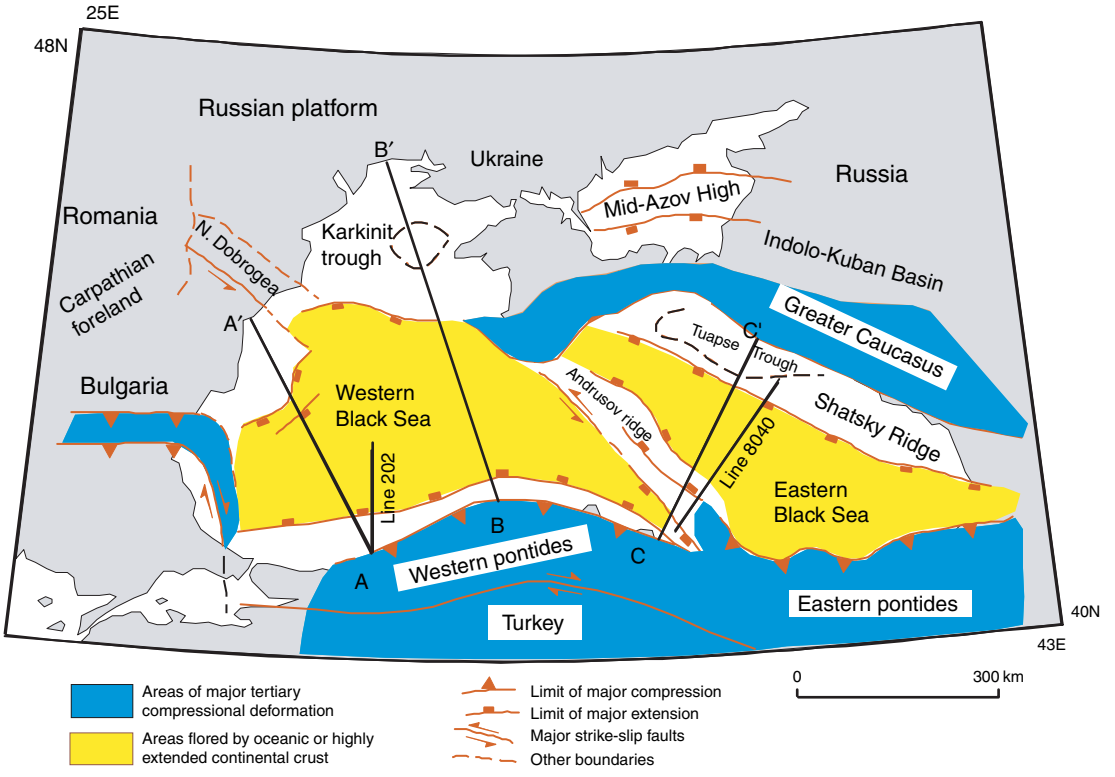

Figure 55 Regional tectonic map of the Black Sea. Modified from Cloetingh S, Spadini G, van Wees JD, and Beekamn F (2003) Thermo-mechanical modelling of Black Sea Basin (de)formation. *Sedimentary Geology* 156: 169–184.

Nikishin *et al.*, 2001, 2003; Cloetingh *et al.*, 2003). This applies particularly to the exact opening timing of the eastern Black Sea for which different interpretations have been advanced varying from Middle to Late Cretaceous (Finetti *et al.*, 1988) to Early Eocene (Robinson *et al.*, 1995) or a combination thereof (Nikishin *et al.*, 2003).

Gravity data show an important difference in the mode of flexural compensation between the western and eastern Black Sea (Spadini *et al.*, 1997). The western Black Sea appears to be in a state of isostatic undercompensation and upward flexure, consistent with a deep level of lithospheric necking. By contrast, for the eastern Black Sea gravity data point toward isostatic overcompensation and a downward state of flexure, compatible with a shallow necking level (**Figure 57**). This is thought to reflect differences in the prerift mechanical properties of the lithosphere of the western and eastern Black Sea sub-basins (Spadini *et al.*, 1996; Cloetingh *et al.*, 1995b).

Below we address the relationship between the prerift finite strength of the lithosphere and geometry of extensional basins and discuss the effects of differences in prerift rheology on the Mesozoic–Cenozoic stratigraphy of the Black Sea basin system. These findings raise important questions on postrift tectonics and on intraplate stress transmission into the Black Sea Basin from its margins. We discuss the results of thermomechanical modeling of the Black Sea Basin along a number of regional cross sections through its western and eastern parts (**Figure 55**), that are constrained by a large integrated geological and geophysical database (see Spadini, 1996; Spadini *et al.*, 1996, 1997).

6.11.5.1 Rheology and Sedimentary Basin Formation

Inferred differences in the mode of basin formation between the western and eastern Black Sea (**Figure 58**), basins can be largely explained in terms of palaeorheologies. The prerift lithospheric strength of the western Black Sea (**Figure 58**) appears to be primarily controlled by the combined mechanical response of a strong upper crust and strong upper mantle (Spadini *et al.*, 1996). The shallow necking level in the eastern Black Sea is compatible with a prerift strength controlled by a strong upper crust decoupled from the weak hot underlying mantle

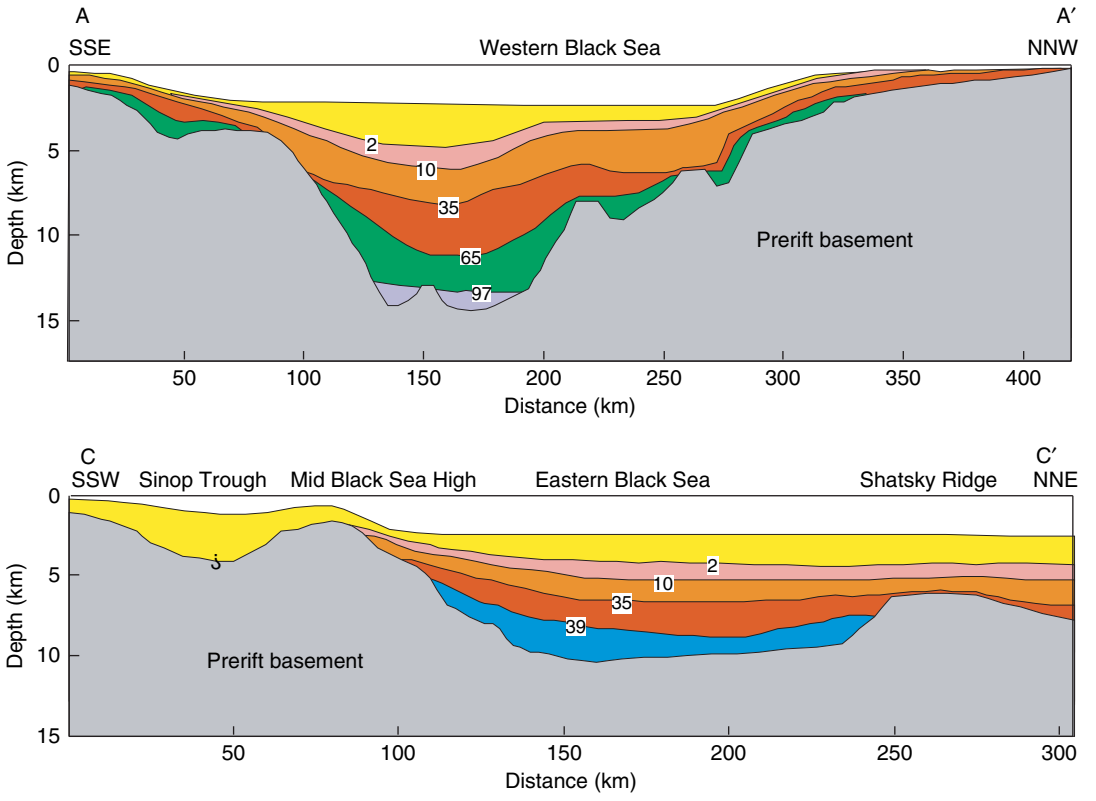

Figure 56 Observed first-order geometry of basement configuration and sediment fill of the Western and Eastern Black Sea. Numbers refer to stratigraphic ages (Ma). Note the substantial thickness of Quarternary sediments. For location of sections A-A′ and C-C′ see **Figure 55**. Modified from Cloetingh S, Spadini G, van Wees JD, and Beekamn F (2003) Thermo-mechanical modelling of Black Sea Basin (de)formation. *Sedimentary Geology* 156: 169–184.

(**Figure 58**). These differences point to important differences in the thermotectonic age of the lithosphere of the two sub-basins (Cloetingh and Burov, 1996). The inferred lateral variations between the western and eastern Black Sea suggest thermal stabilization of the western Black Sea prior to rifting whilst the lithosphere of the eastern Black Sea was apparently already thinned and thermally destabilized by the time of Eocene rifting. The inferred differences in necking level and in the timing of rifting between the western and eastern Black Sea suggest an earlier and more pronounced development of rift shoulders in the western Black Sea Basin as compared to the eastern Black Sea (Robinson *et al*., 1995).

Figures 56 and **59** show observed and modeled stratigraphies along the two selected profiles through the western and eastern Black Sea, respectively (see also **Figure 58**). **Figure 60** illustrates the evolution of basin subsidence and water loaded tectonic subsidence in time (Steckler and Watts, 1978; Bond and Kominz, 1984), calculated for both the Odin (1994) and Harland *et al*., (1990) time scales. Subsidence curves are displayed for locations at the center and the margin of western and eastern Black Sea subbasins, respectively. In the western Black Sea rifting began during the Late Barremian–Aptian and progressed to crustal separation at the transition to the Cenomanian with seafloor spreading ending in the Coniacian. In this deep marine basin up to 12.5 km thick sediments accumulated prior to the late Middle Miocene Sarmatian sea level fall when it was converted into a relatively small up to 800 m deep lake. Late Miocene to recent sediments attains thicknesses of up to 2.5 km (**Figure 59**). The eastern Black Sea basin may have undergone an Aptian–Turonian and a Campanian–Maastrichtian rifting stage prior its Paleocene–Early Eocene rift-related main subsidence and deepening that was accompanied by little flank uplift and erosion. During the Late Eocene, sediment supply from the compressionally active Pontides and Greater Caucasus belts increased and led in the basin center to the deposition of an up to 5 km thick sediments (**Figure 59**). Also the eastern Black Sea remained a deep marine basin until the late

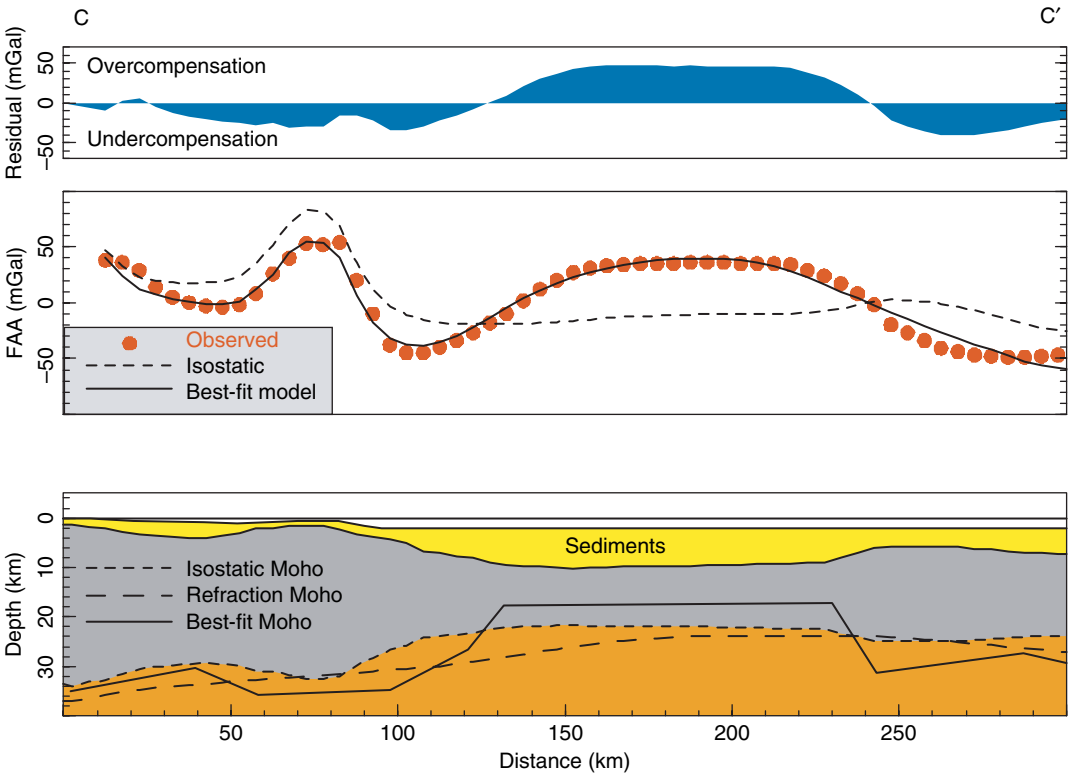

Figure 57 Results of gravity modeling for the Eastern Black Sea, demonstrating isostatic flexural overcompensation in the center of the basin. For location see **Figure 55** line C-C′. Modified from Cloetingh S, Spadini G, van Wees JD, and Beekamn F (2003) Thermo-mechanical modelling of Black Sea Basin (de)formation. *Sedimentary Geology* 156: 169–184.

Middle Miocene Sarmatian when it was converted into a lake. When sea level returned to normal in the Late Miocene, water depth increased dramatically to 2800 m in both the western and eastern Black Sea Basin, presumably in response to the loading effect of the water (Spadini *et al.*, 1996). By the Quaternary, increased sediment supply led to significant subsidence and sediment accumulation, with a modest decrease in water depth to the present-day value of 2200 m. Overall uplift of the margins of the Black Sea commenced in Middle Miocene times (Nikishin *et al.*, 2003). Although the reconstructions by Spadini *et al.*, (1997) and Nikishin *et al.*, (2003) differ in the assumed maximum depth of the basin, its palaeo-bathymetry and sea-level fluctuations during its evolution, the Pliocene–Quaternary subsidence acceleration appears to be a robust (Spadini *et al.*, 1997; Robinson *et al.*, 1995; Nikishin *et al.*, (2003).

6.11.5.2 Role of Intraplate Stresses

Constraints on the present-day stress regime are lacking for the central parts of the Black Sea Basin. However, structural geological field studies and earthquake focal mechanisms in areas bordering the Black Sea (see Nikishin *et al.*, 2001), as well as GPS data (Reilinger *et al.*, 1997) demonstrate that in the collisional setting of the European and Arabian plate the area is subjected to compression. Field studies of kinematic indicators and numerical modeling of present-day and palaeo-stress fields in selected areas (e.g., Gölke and Coblentz, 1996; Bada *et al.*, 1998, 2001) have yielded new constraints on the causes and the expression of intraplate stress fields in the lithosphere. Ziegler *et al.*, (1998) have discussed the key role of mechanical controls on collision related compressional intraplate deformation. These authors discuss the buildup of intraplate stresses in relation to mechanical coupling between an orogenic wedge and its fore- and hinterlands, as well as the implications to the understanding of a number of first-order features in crustal and lithospheric deformation.

Temporal and spatial variations in the level and magnitude of these stresses have a strong impact on the record of vertical motions in sedimentary basins (Cloetingh *et al.*, 1985, 1990; Cloetingh and Kooi,

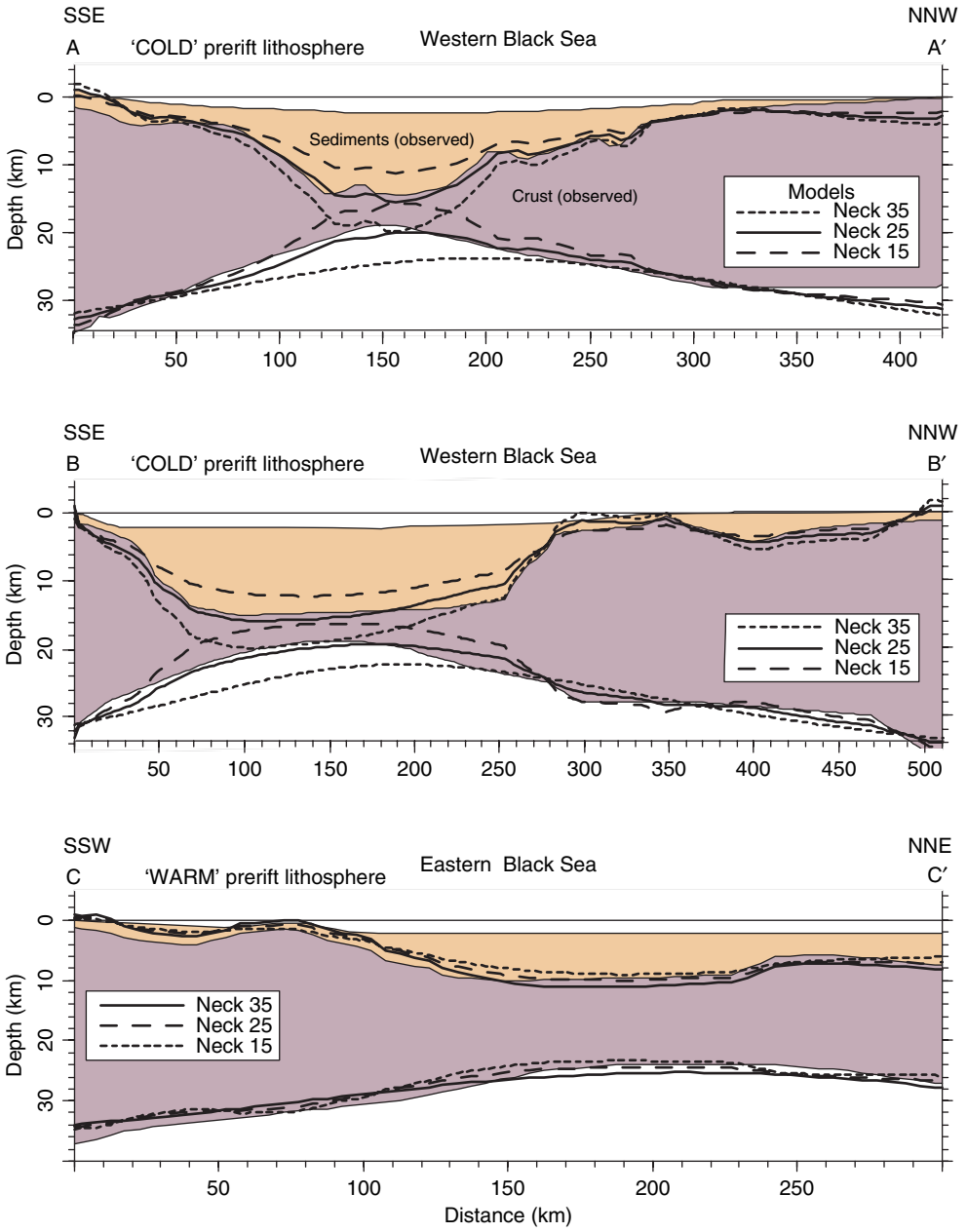

Figure 58 Crustal scale models for extensional basin formation for the Western and Eastern Black Sea. For location of cross sections see **Figure 55**. A comparison of predicted and observed Moho depths provides constraints on levels of necking and thermal regime of the prerift lithosphere. The models support the presence of cold prerift lithosphere compatible with a deep necking level of 25 km in the Western Black Sea. For the Eastern Black Sea, the models suggest the presence of a warm prerift lithosphere with a necking level of 15 km. Modified from Cloetingh S, Spadini G, van Wees JD, and Beekamn F (2003) Thermo-mechanical modelling of Black Sea Basin (de)formation. *Sedimentary Geology* 156: 169–184.

1992; Zoback *et al.*, 1993; Van Balen *et al.*, 1998). Stresses at a level close to lithospheric strength propagating from the margins of the Black Sea Basin into its interior parts had not only a strong effect on their stratigraphic record, but presumably induced by lithospheric folding the observed late-stage subsidence acceleration (Cloetingh *et al.*, 1999), similar to what is recognized in the Pannonian Basin and the North Sea Basin (Horváth and Cloetingh, 1996; Van Wees and Cloetingh, 1996). Over the last few years,

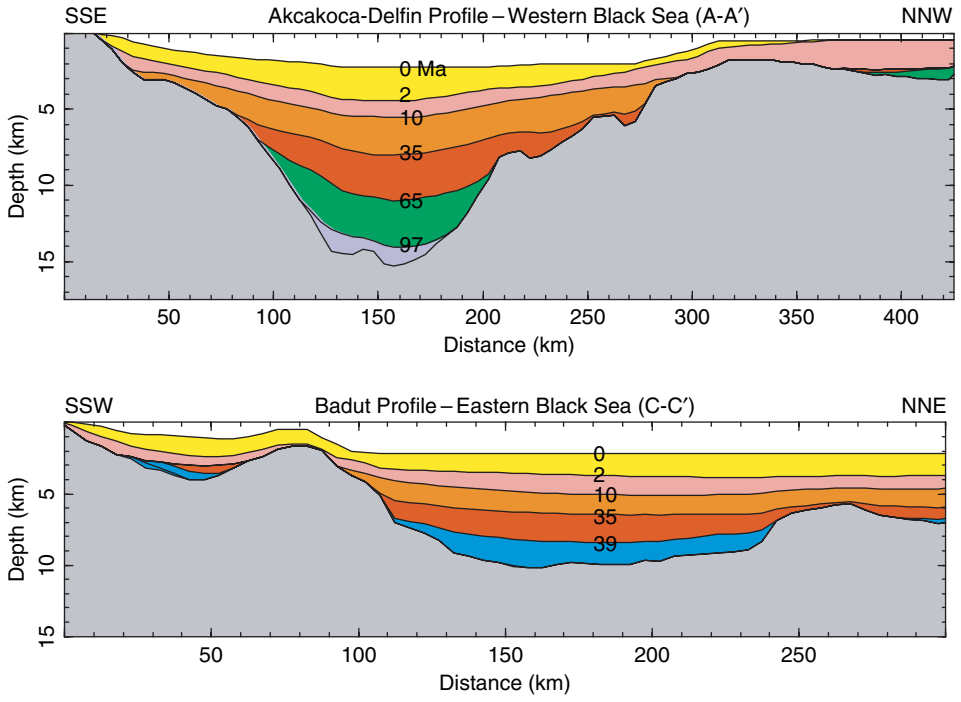

Figure 59 Stratigraphy and basement topography of the Western and Eastern Black Sea modeled along profiles A-A′ and C-C′ (for location see **Figure 55**). Adopted necking levels, constrained by gravity modeling, are 25 km and 15 km for the Western and Eastern Black Sea, respectively. Modified from Cloetingh S, Spadini G, van Wees JD, and Beekamn F (2003). Thermo-mechanical modelling of Black Sea Basin (de)formation. *Sedimentary Geology* 156: 169–184.

increasing attention has been directed to this topic, advancing our understanding of the relationship between changes in plate motions, plate interaction, and the evolution of rifted basins (Janssen *et al.*, 1995; Doré *et al.*, 1997) and foreland areas (Ziegler *et al.*, 1995, 1998, 2001).

A continuous spectrum of stress-induced vertical motions can be expected in the sedimentary record, varying from subtle faulting effects (e.g., **Figure 16**) (Ter Voorde and Cloetingh, 1996; Ter Voorde *et al.*, 1997) and basin inversion (Brun and Nalpas, 1996; Ziegler *et al.*, 1998) to the enhancement of flexural effects and to lithospheric folding induced by high levels of stress approaching lithospheric strengths (Stephenson and Cloetingh, 1991; Nikishin *et al.*, 1993; Burov *et al.*, 1993; Cloetingh and Burov, 1996; Bonnet *et al.*, 1998; Cloetingh *et al.*, 1999).

Crustal and lithospheric folding can be an important mode of basin formation on plates involved in continental collision (Cobbold *et al.*, 1993; Ziegler *et al.*, 1995, 1998; Cloetingh *et al.*, 1999). Numerical models have been developed for simulating the interplay of faulting and folding during intraplate compressional deformation (Beekman *et al.*, 1996; Gerbault *et al.*, 1998; Cloetingh *et al.*, 1999). Models have also been developed to investigate the effects of faulting on stress-induced intraplate deformation in rifted margin settings (Van Balen *et al.*, 1998).

The collisional Caucasus orogeny commenced during the Late Eocene and culminated during Oligocene–Quaternary times. On the other hand, the North Pontides thrust belt was activated during the Late Eocene and remained active until the end of the Oligocene (Nikishin *et al.*, 2001). Correspondingly, the Late Eocene accelerated subsidence of the Black Sea Basin can be attributed to the buildup of a regional compressional stress field (Robinson *et al.*, 1995). The Late Eocene–Quaternary Caucasus orogeny, overprinting back-arc extension in the Black Sea, was controlled by the collisional interaction of the Arabian plate with the southern margin of the East-European craton (Nikishin *et al.*, 2001).

6.11.5.3 Strength Evolution and Neotectonic Reactivation at the Basin Margins during the Postrift Phase

Automated backstripping analyses and comparison of results with forward models of lithospheric stretching

(Van Wees *et al.*, 1998) provide estimates of the integrated lithospheric strength at various syn- and postrift stages. Adopted modeling parameters are listed in **Tables 5** and **6**.

Figure 61 shows a comparison of observed and forward modeled tectonic subsidence curves for the center of the Western Black Sea Basin. Automated backstripping yields a stretching factor β of 6. Modeling fails, however, to predict the pronounced Late Neogene subsidence acceleration, documented by the stratigraphic record that may be attributed to late stage compression. As postrift cooling of the lithosphere leads in time to a significant increase in its integrated strength, its early postrift deformation is favoured. Present-day lithospheric strength profiles calculated for the center and margin of western Black Sea show a pronounced difference. The presence of relatively strong lithosphere in the basin center and weaker lithosphere at the basin margins favours deformation of the latter during late-stage compression. This may explain why observed compressional structures appear predominantly at the edges of the Black Sea Basin and not in its interior (**Figure 55**).

In **Figure 62** the observed and forward modeled tectonic subsidence curves for the center of eastern Black Sea Basin are compared, adopting for modeling a stretching factor β of 2.3 that is compatible with the subsidence data and consistent with geophysical constraints. During the first 10 My of postrift evolution, integrated strengths are low but subsequently increase rapidly owing to cooling of the lithosphere. During the first 10 My after rifting, and in the presence of very weak lithosphere, the strength of which was primarily controlled by the rift-inherited mechanical properties of its upper parts, we expect that this area would be prone to early postrift compressional deformation. It should be noted, however, that with a cooling-related progressive increase of the integrated lithospheric strength, with time increasingly higher stress levels are required to cause large-scale deformation (**Figure 62**). Important in this context is also that, due to substantial crustal thinning, a strong upper mantle layer is present in the central part of the basin at relatively shallow depths.

Based on the present thermomechanical configuration (**Figure 62**) with relatively strong lithosphere in the basin center and relatively weak lithosphere at the basin margins, we predict that a substantial amount of late-stage shortening induced by orogenic activity in the surrounding areas will be taken up along the basin margins, with only minor deformation occurring in the relatively stiff central parts of the basin. The relative difference in rheological strength of the marginal and central parts of the basin is more pronounced in the eastern than in the western Black Sea. These predictions have to be validated by new data focusing on the neotectonics of the Black Sea. High-resolution shallow seismic profiles and acquisition of stress-indicator data could provide the necessary constraints for such future modeling.

Figure 63 gives predictions for basement and surface heat flow in the eastern and western Black Sea and shows markedly different patterns in timing of the rift-related heat flow maximum. The predicted present-day heat flow is considerably lower for the western than for the eastern sub-basin. This is attributed to the presence of more heat producing crustal material in the eastern than in the western Black Sea that is partly floored by oceanic crust. In heat flow modeling studies the effects of sedimentary blanketing were taken into account (Van Wees and Beekman, 2000). Heat flow values vary between $30\,\mathrm{mW\,m^{-2}}$ in the center of the basins up to $70\,\mathrm{mW\,m^{-2}}$ at the Crimean and Caucasus margins (Nikishin *et al.*, 2003). Note the pronounced effect of thermal blanketing in the western Black Sea that contains up to 15 km thick sediments (**Figure 58**). As a result its present-day integrated strength is not that much higher than its initial strength. By contrast, the integrated strength of the eastern Black Sea is much higher than its initial strength as the blanketing effect of its up to 12 km thick sedimentary fill is less pronounced and as water depths are greater.

Figure 32 shows a comparison of theoretical predictions for lithosphere folding of rheologically coupled and decoupled lithosphere, as a function of its thermomechanical age with estimates of folding wavelengths documented in continental lithosphere for various representative areas of the globe (see Cloetingh *et al.*, 1999). The western Black Sea center is marked by a thermomechanical age of around 100 My with rheological modeling indicating mechanical decoupling of the crust and lithospheric mantle (see **Figure 61**). These models imply an EET of at least 40 km (Burov and Diament, 1995) and folding wavelengths of 100–200 km for the mantle and 50–100 km for the upper crust (Cloetingh *et al.*, 1999). For the eastern Black Sea, a probably significantly younger thermomechanical lithospheric age of 55 My implies an EET of no more than 25 km, and indicates mantle folding at wavelengths of ~100–150 km and a crustal folding wavelength

Western Black Sea

Basin margin

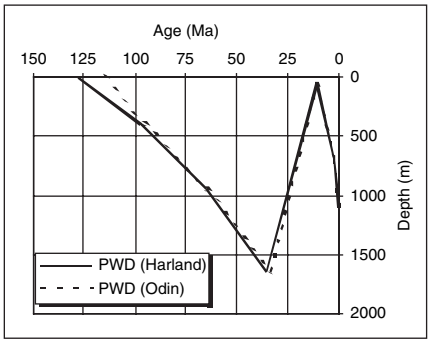

Basin center

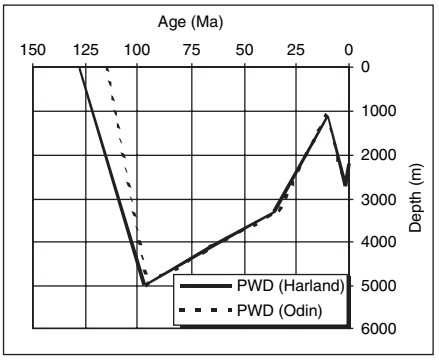

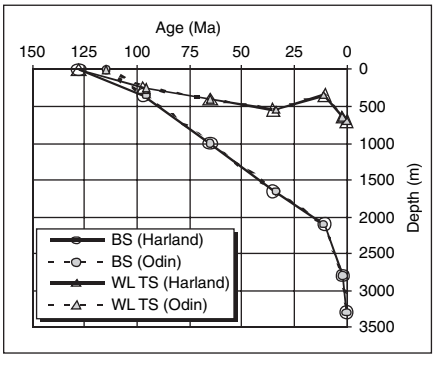

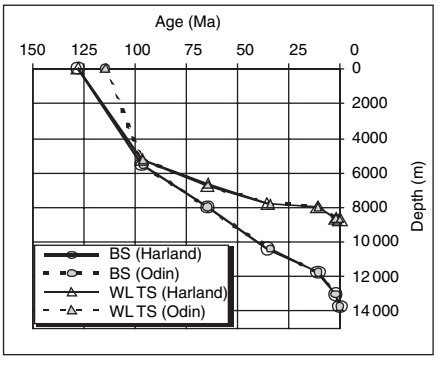

Eastern Black Sea

Basin margin

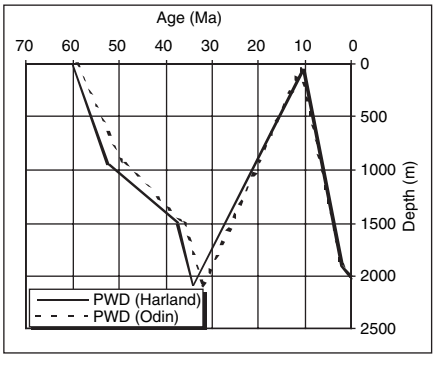

Basin center

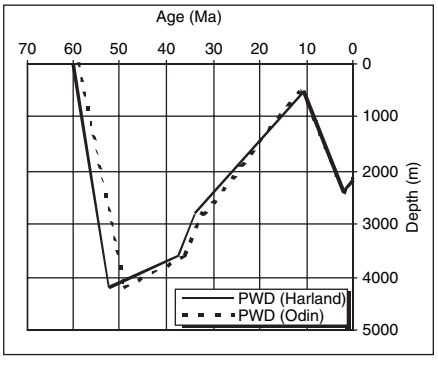

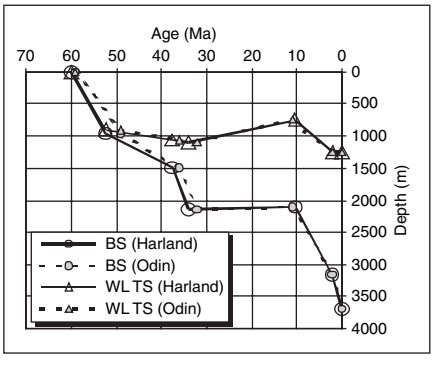

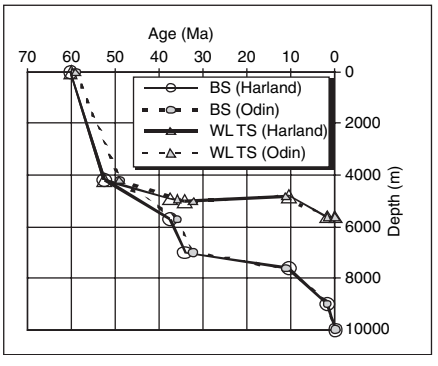

Table 5 Model parameters used to calculate the tectonic subsidence in the rheological models

Symbol	Model parameter	Value
A	Initial lithosphere thickness	120 km (wb), 80 km (eb)
C	Initial crustal thickness	35 km
T_m	Asthenospheric temperature	1333°C
K	Thermal diffusivity	$1 \times 10^{-6}\,m^2\,s^{-1}$
ρ_c	Surface crustal density	$2800\,kg\,m^{-3}$
ρ_m	Surface mantle density	$3400\,kg\,m^{-3}$
ρ_w	Water density	$1030\,kg\,m^{-3}$
α	Thermal expansion coeff.	$3.2 \times 10^{-5}\,K^{-1}$
δ	Crustal stretching factor	6 (wb), 2.3 (eb)
β	Subcrustal stretching factor	6 (wb), 2.3 (eb)

The (eb) and (wb) refer to eastern and western Black Sea, respectively.

Table 6 Default rheological and thermal properties of crust and lithosphere

Layer	Rheology	Conductivity ($W\,m^{-1}\,K^{-1}$)	Heat production ($10^{-6}\,W\,m^{-3}$)
Sediments	Quartzite (d)	1.5	0.5
Upper crust	Quartzite (d)	2.9	2
Lower crust	Diorite (w)	2.9	0.5
Upper mantle	Olivine (d)	2.9	0

The (d) and (w) refer respectively to dry or wet rock samples that contain little or variable amounts of structural water. For more details on the rheological rock properties, see Van Wees and Beekman (2000).

similar to the western Black Sea. A comparison of estimated folding wavelengths with theoretical predictions shows a systematic deviation to larger values. This is characteristic for 'a-typical' folding where the large dimension of the preexisting rift basin causes during the late-stage compressional phase a pronounced increase in the wavelength of the stress-induced down warp (Cloetingh *et al.*, 1999). This effect has been observed in the North Sea Basin (Van Wees and Cloetingh, 1996) and the Pannonian Basin (Horváth and Cloetingh, 1996), both of which are characterized by large sediment loads and a wide rift basin. Such a neotectonic compressional reactivation provides an alternative to previous explanations for recent differential motions in the northern Black Sea Basin (Smolyaninova *et al.*, 1996) that were attributed to convective mantle flow. In view of the recent evidence for crustal shortening in the Black Sea region as a consequence of the Arabian–Eurasian plate interaction (Reilinger *et al.*, 1997), an interpretation in terms of an increased Late Neogene compressional stress level appears to be more likely.

According to modeling results, the eastern Black Sea Basin is much weaker than the western Black Sea. As compared to the western Black Sea, the eastern Black Sea is relatively stronger in the center than at its margins. The margins of the eastern Black Sea appears to be more prone to lithospheric folding, whereas the western Black Sea as a whole is more prone to stress transmission.

6.11.6 Modes of Basin (De)formation, Lithospheric Strength, and Vertical Motions in the Pannonian–Carpathian Basin System

The Pannonian–Carpathian system in Central and Eastern Europe (**Figure 64**) has been the focus of considerable research efforts to integrate a wide range of geophysical and geological data, making it a key area for quantitative basin studies (see Cloetingh *et al.*, 2006; Horváth *et al.*, 2006 for recent reviews). A vast geophysical and geological database has been established during the last decades as a result of a major international research collaboration in this area, largely carried out in the framework of European programs such as the EU Integrated Basin

Figure 60 Results of backstripping analyses for locations at the margins and center of the Western and Eastern Black Sea, respectively. Top panels show palaeo water depth (PWD), bottom panels show basement subsidence (BS) and water loaded tectonic subsidence (WLTS). Each curve is calculated for two different timescales (Odin, 1994; Harland *et al.*, 1990) to illustrate sensitivities. Modified from Cloetingh S, Spadini G, van Wees JD, and Beekamn F (2003) Thermo-mechanical modelling of Black Sea Basin (de)formation. *Sedimentary Geology* 156: 169–184.

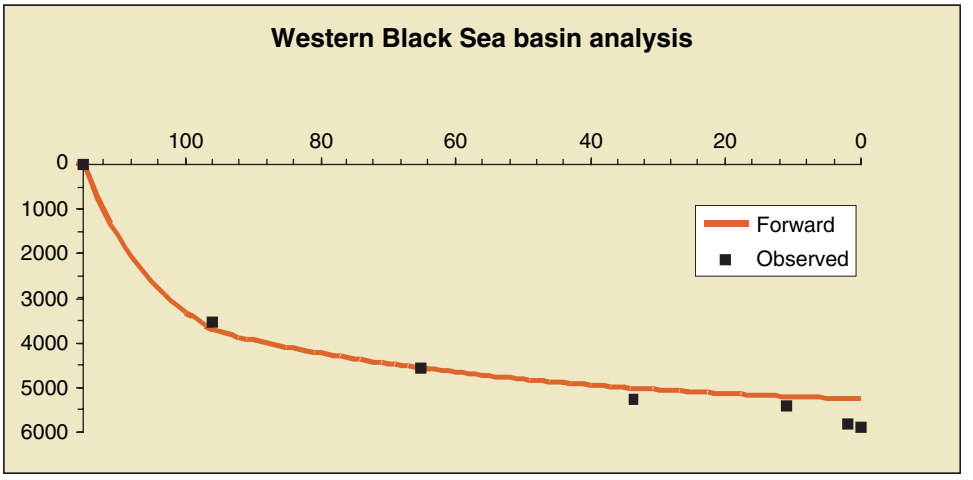
Western Black Sea basin analysis
100
80
60
40
20
0
0
1000
2000
3000
4000
5000
6000
Forward
Observed

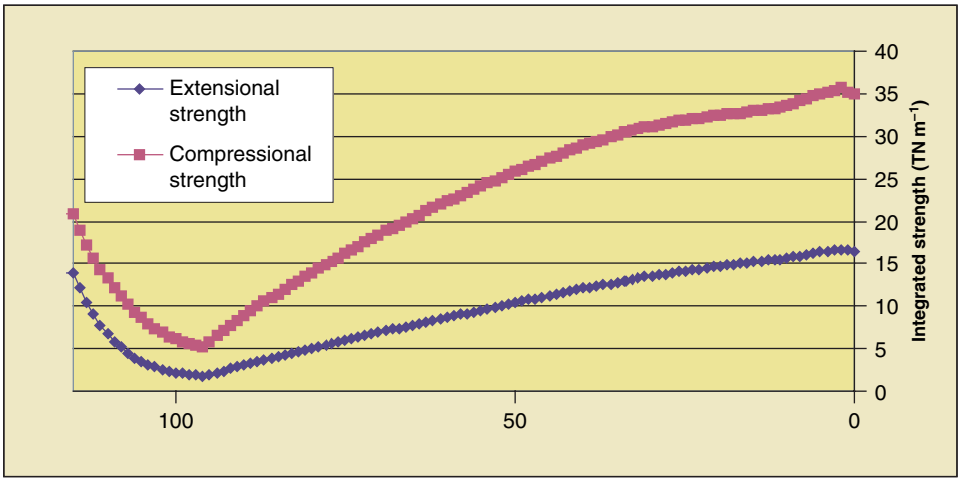
Extensional strength
Compressional strength
40
35
30
25
20
15
10
5
0
Integrated strength (TN m⁻¹)
100
50
0

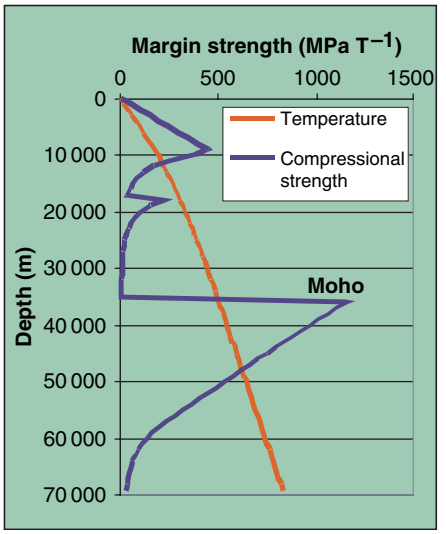
Margin strength (MPa T⁻¹)
0
500
1000
1500
0
10 000
20 000
30 000
40 000
50 000
60 000
70 000
Depth (m)
Temperature
Compressional strength
Moho

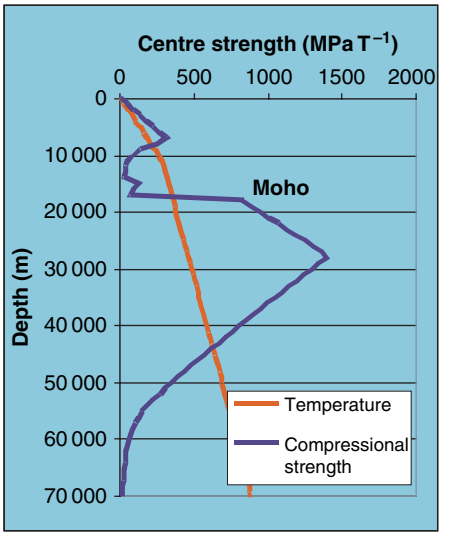
Centre strength (MPa T⁻¹)
0
500
1000
1500
2000
0
10 000
20 000
30 000
40 000
50 000
60 000
70 000
Depth (m)
Moho
Temperature
Compressional strength

Studies project (Cloetingh *et al.*, 1995b; Durand *et al.*, 1999), the ILP-ALCAPA (Cloetingh *et al.*, 1993; Neubauer *et al.*, 1997) and EUROPROBE-PANCARDI (Decker *et al.*, 1998) programs, and the Peri-Tethys program (Ziegler and Horváth, 1996; Brunet and Cloetingh, 2003), partly funded in the context of petroleum exploration. These studies, building on previous land-marking compilations (Royden and Horváth, 1988), marked a major advance in applying basin analysis concepts to the Pannonian–Carpathians system.

An important asset of this natural laboratory is the existence of high-quality constraints on basin evolution obtained through the systematic acquisition of seismic, gravity, heat flow, and magnetotelluric data by various research groups (see Royden and Horváth, 1988; Posgay *et al.*, 1995; Szafián *et al.*, 1997; Tari *et al.*, 1999; Wenzel *et al.*, 1999; Hauser *et al.*, 2001). Extensive industrial reflection-seismic coverage and well data acquired in the context of petroleum exploration and surface studies permitted to construct a high-resolution stratigraphic framework for this area (e.g., Vakarcs *et al.*, 1994; Sacchi *et al.*, 1999; Vasiliev *et al.*, 2004). At the same time, the Carpathian fold and thrust belt has been the focus of concerted efforts, highlighting the connection between lateral variations in structural style, basement characteristics and foreland flexure development in different segments of the Carpathian orogen (Săndulescu, 1988; Roure *et al.*, 1993; Maţenco *et al.*, 1997a, 1997b, 2003; Sanders *et al.*, 1999; Tari *et al.*, 1997; Zoetemeijer *et al.*, 1999) and its hinterland, the Transylvanian Basin (e.g., Ciulavu *et al.*, 2002).

The Pannonian–Carpathian system, therefore, permits to test models for the development of sedimentary basins and their subsequent deformation, and for ongoing continental collision. The lithosphere of the Pannonian Basin is a particularly sensitive recorder of changes in lithospheric stress induced by near-field intraplate and far-field plate boundary processes (Bada *et al.*, 2001). High-quality constraints are available on regional (palaeo)stress fields (Fodor *et al.*, 1999; Gerner *et al.*, 1999) owing to earthquake focal mechanism studies, analyses of borehole breakouts and studies on kinematic field indicators. A close relationship has been established between the timing and nature of stress changes in extensional basins and structural episodes in the surrounding thrust belts, pointing to mechanical coupling between the orogen and its back-arc basin. In parallel, significant efforts have been devoted to reconstruct the spatial and temporal variations in thrusting along the Carpathian orogen (Roure *et al.*, 1993; Schmid *et al.*, 1998; Maţenco and Bertotti, 2000) and its relationship to foredeep depocenters (Meulenkamp *et al.*, 1996; Maţenco *et al.*, 2003; Tărăpoancă *et al.*, 2003), changes in foreland basin geometry and lateral variations in the flexural rigidity of the foreland lithosphere. A general feature of flexural modeling studies carried out on the Carpathian system (e.g., Zoetemeijer *et al.*, 1999; Maţenco *et al.*, 1997b) is the inferred low rigidity of the foreland platform lithosphere that dips beneath the SE Carpathians. Studies constrained by gravity data also point to an important role of the flexural response of the foreland lithosphere to erosional unroofing of the Carpathian mountain chain (Szafián *et al.*, 1997).

Below we present an overview of the tectonic evolution of the Pannonian–Carpathian system in terms of various thermomechanical models. We present a lithospheric strength map of the system that highlights rheological constraints for basin analysis studies and for the reconstruction of the deformation history of this area. We then focus on the development of the system as inferred from subsidence analyses and stretching models of the Pannonian Basin, and the flexural behaviour of the Carpathian foreland lithosphere. The neotectonic reactivation of the region is described in terms of anomalous late-

Figure 61 A comparison of observed and forward modeled tectonic subsidence for the Western Black Sea center. Automated backstripping yields an estimated stretching factor β of 6 (top panel). A pronounced Late Neogene subsidence acceleration (see also **Figure 60**) documented in the stratigraphic record could be an indication of late stage compression. Postrift cooling leads in time to a significant increase in the predicted integrated strength for both compressional and extensional regimes (middle panel; $1\,\mathrm{TN\,m^{-1}} = 10^{12}\,\mathrm{N\,m^{-1}}$). Present-day lithospheric compressional strength profiles calculated for the center and margin of western Black Sea show with depth a pronounced difference (bottom panels). Temperature profiles (in °C) and Moho depth are given for reference. Note the important role of the actual Moho position in terms of mechanical decoupling of the upper crust and mantle parts of the Black Sea lithosphere. Parameters used for modeling of the tectonic subsidence and for rheological strength calculations are listed in **Tables 5** and **6**, respectively. Modified from Cloetingh S, Spadini G, van Wees JD, and Beekamn F (2003) Thermo-mechanical modelling of Black Sea Basin (de)formation. *Sedimentary Geology* 156: 169–184.

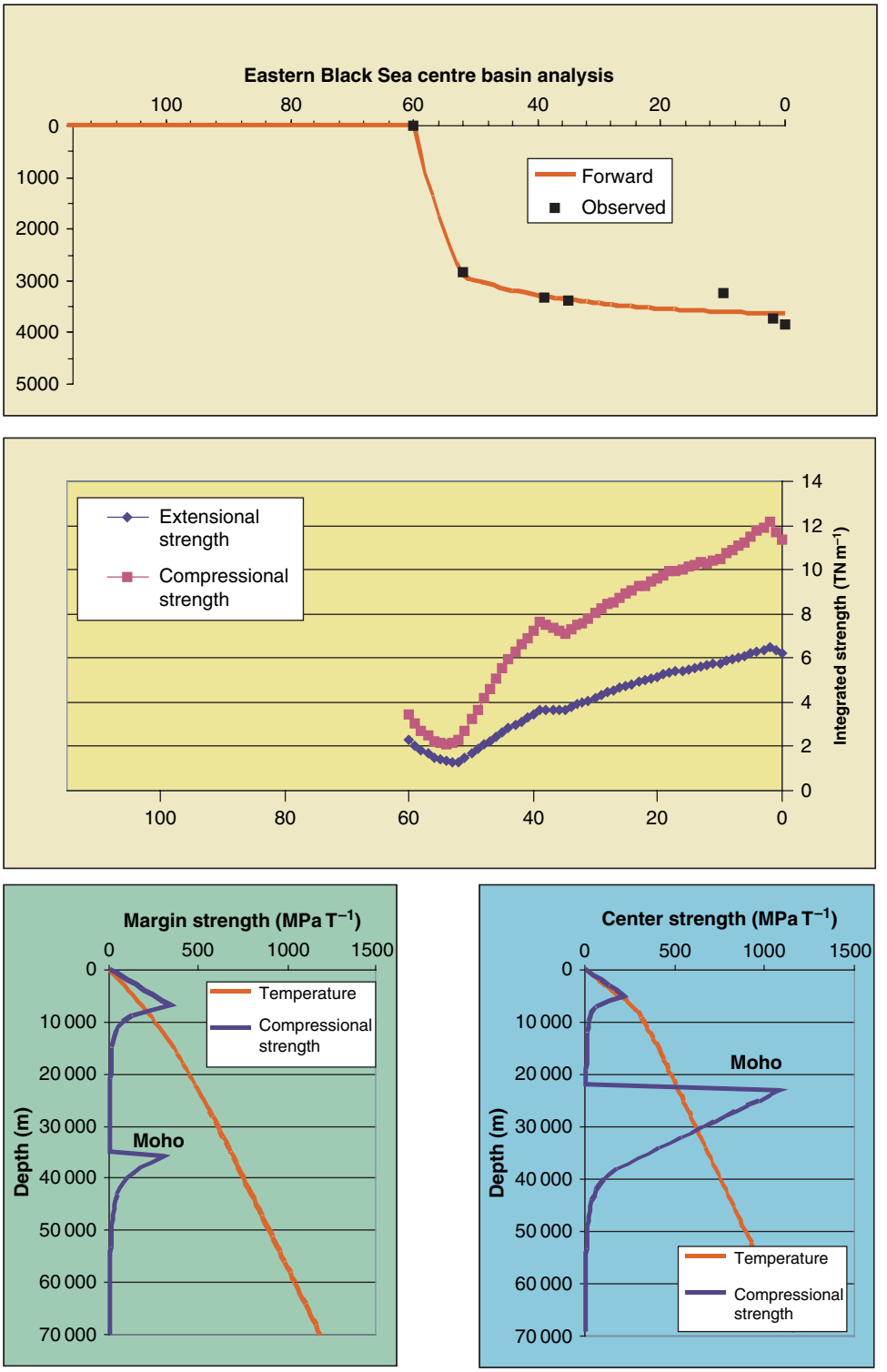

Figure 62 Comparison of observed and forward modeled tectonic subsidence for the Eastern Black Sea center. Automated backstripping yields an estimated stretching factor β of 2.3 (upper panel). Postrift cooling leads in time to a significant increase in the predicted integrated strength for both compressional and extensional regimes (middle panel; $1\,\mathrm{TN\,m^{-1}} = 10^{12}\,\mathrm{N\,m^{-1}}$). Present-day lithospheric strength profiles calculated for the center and margin of the Eastern Black Sea show with depth a pronounced difference (bottom panels). Modified from Cloetingh S, Spadini G, van Wees JD, and Beekamn F (2003) Thermo-mechanical modelling of Black Sea Basin (de)formation. *Sedimentary Geology* 156: 169–184.

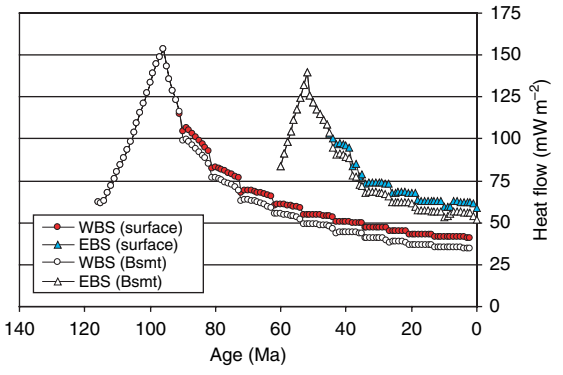

Figure 63 Predictions for basement ('Bsmt') and surface heat flow in the Eastern (triangles) and Western (circles) Black Sea show markedly different patterns in the timing of the heat flow maximum, related to the timing of initial rifting. The predicted present-day heat flow is considerably lower in the Western Black as compared to the Eastern Black Sea. See text for implications for differences in the strength evolution between the Western and Eastern Black Sea. Modified from Cloetingh S, Spadini G, van Wees JD, and Beekamn F (2003). Thermo-mechanical modelling of Black Sea Basin (de)formation. *Sedimentary Geology* 156: 169–184.

stage vertical movements, that is, accelerated subsidence in the center of the Pannonian Basin and fast uplift of the Carpathians orogen due to isostatic rebound in the aftermath of continental convergence and slab detachment. We conclude with a discussion on the thermomechanical aspects of basin inversion, lithospheric folding and related temporal and spatial variations of continental topography in the Pannonian–Carpathian system.

6.11.6.1 Lithospheric Strength in the Pannonian–Carpathian System

The Pannonian–Carpathian system shows remarkable variations in crustal thickness (**Figure 65**) and thermomechanical properties of the lithosphere. Lithospheric rigidity varies in space and time, giving rise to important differences in the tectonic behavior of different parts of the system. As rheology controls the response of the lithosphere to stresses, and thus the formation and deformation of basins and orogens, the characterization of rheological properties and their temporal changes has been a major challenge to constrain and quantify tectonic models and scenarios. This is particularly valid for the Pannonian–Carpathian region where tectonic units with a different history and rheological properties are in close contact.

Figure 66(a) displays three strength envelopes for the western, central and eastern part of the Pannonian lithosphere that were constructed on the basis of extrapolated rock mechanic data, incorporating constraints on crustal and lithospheric structure, and present-day heat flow along the modeled rheological section. These strength profiles show that the average strength of the Pannonian lithosphere is very low (see also Lankreijer, 1998), which is mainly due to high heat flow related to upwelling of the asthenosphere beneath the basin system. The Pannonian Basin, the hottest basin of continental Europe, has an extremely low rigidity lithosphere that renders it prone to repeated tectonic reactivation. This is the result of Cretaceous and Paleogene orogenic phases involving nappe emplacement and crustal accretion, thickening and loading. In this process, the strength of the different Pannonian lithospheric segments gradually decreased, allowing for their tensional collapse under high-level strain localization that lead to the development of the Pannonian Basin. Another essential feature is the present-day lack of lithospheric strength in the lithospheric mantle of the Pannonian Basin. Strength appears to be concentrated in the crustal upper 7–12 km of the lithosphere. This finding is in very good agreement with the depth distribution of seismicity. Earthquake hypocenters are restricted to the uppermost crustal levels, suggesting that brittle deformation of the lithosphere is limited to depth of 5–15 km (Tóth *et al.*, 2002).

Figure 66(b) shows estimates of the total integrated strength (TIS) of the Pannonian–Carpathian lithosphere along section A-A'. Rheology calculations suggest major differences in the mechanical properties of different tectonic units within the system (Lankreijer *et al.*, 1997, 1999). In general, there is a gradual increase of TIS away from the basin center towards the basin flanks in the peripheral areas (see also **Figure 66(c)**). The center of the Pannonian Basin and the Carpathian foreland are the weakest and strongest parts of the system, respectively. The presence of a relatively strong lithosphere in the Transylvanian Basin is due to the absence of large-scale Tertiary extension that prevails in the Pannonian Basin (Ciulavu *et al.*, 2002). The Carpathian arc, particularly its western parts, shows a high level of rigidity apart from the southeastern bend zone where a striking decrease in lithospheric strength is noticed. Calculations for the seismically active Vrancea area indicate the presence of a very weak crust and mantle lithosphere, suggestive of mechanical decoupling between the Transylvanian Basin and the Carpathian Orogen. The pronounced

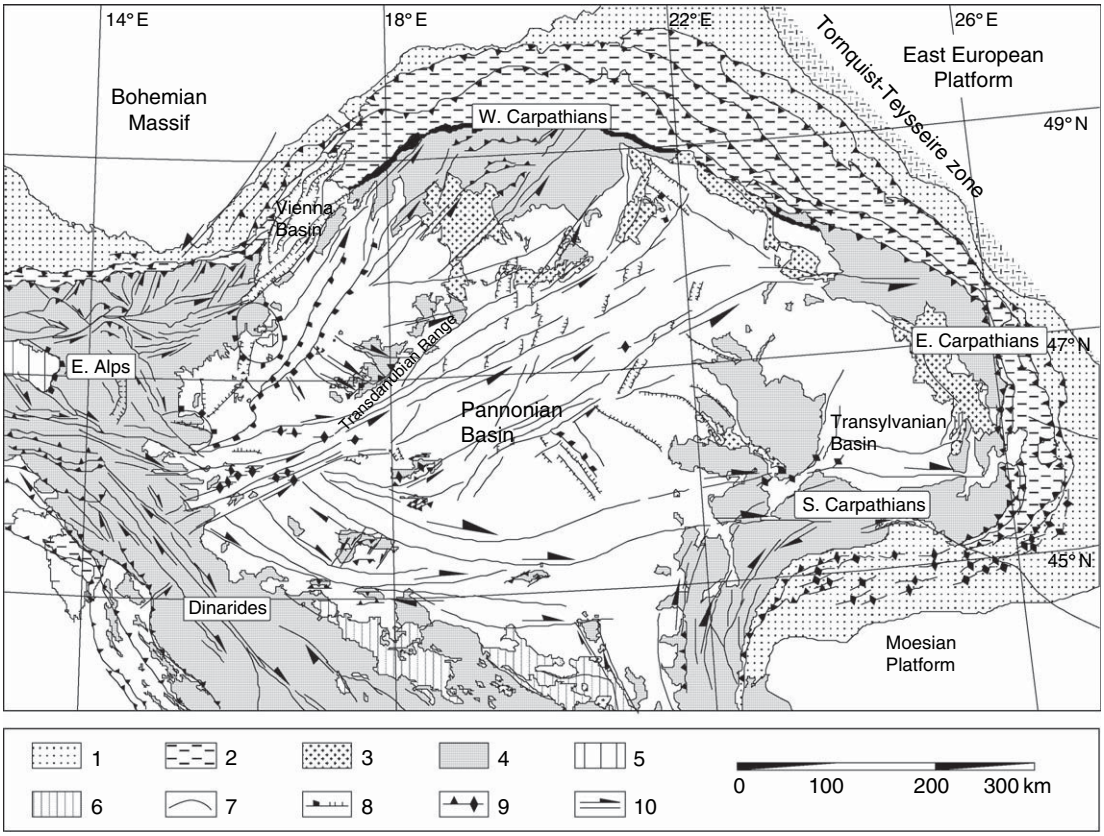

Figure 64 Late Neogene structural pattern in the Pannonian basin system and its vicinity. 1: foreland (molasse) basins; 2: flysch nappes; 3: Neogene vulcanites; 4: pre-Tertiary units on the surface; 5: Variscan basement of the European plate; 6: Dinaric and Vardar ophiolites; 7: tectonic windows in the Eastern Alps; 8: normal and low-angle normal fault; 9: thrust, anticline; 10: strike-slip fault. Modified from Horváth F (1993) Towards a mechanical model for the formation of the Pannonian basin. *Tectonophysics* 226: 333–357.

contrast in TIS between the Pannonian Basin (characterized by TIS $<2.0 \times 10^{12}\,\mathrm{N\,m^{-1}}$) and the Carpathian Orogen and its foreland (characterized by TIS $>3.0 \times 10^{12}\,\mathrm{N\,m^{-1}}$) indicates that recent lithospheric deformation is more likely concentrated in the hot and hence weak Pannonian lithosphere rather than in the surrounding Carpathians.

By conversion of strength predictions to EET values at a regional scale, Lankreijer (1998) mapped the EET distribution for the entire Pannonian–Carpathian system (**Figure 67**). Calculated EET values are largely consistent with the spatial variation of lithospheric strength of the system. Lower values are characteristic for the weak central part of the Pannonian Basin (5–10 km), whereas EET increases toward the Dinarides and Alps (15–30 km) and particularly toward the Bohemian Massif and Moesian Platform (25–40 km). This trend is in good agreement with EET estimates obtained from flexural studies and forward modeling of extensional basin formation. Systematic differences, however, can occur and may be the consequence of significant horizontal intraplate stresses (e.g., Cloetingh and Burov, 1996) or of mechanical decoupling of the upper crust and uppermost mantle that can lead to a considerable reduction of EET values.

The range of calculated EET values reflects the distinct mechanical characteristics and response of the different domains forming part of the Pannonian–Carpathian system to the present-day stress field. These characteristics can be mainly attributed to the memory of the lithosphere. In this respect it must be kept in mind that the tectonic and thermal evolution of these domains differed considerably during the Cretaceous–Neogene Alpine development of both the outer and intra-Carpathians units and the Neogene extension of the

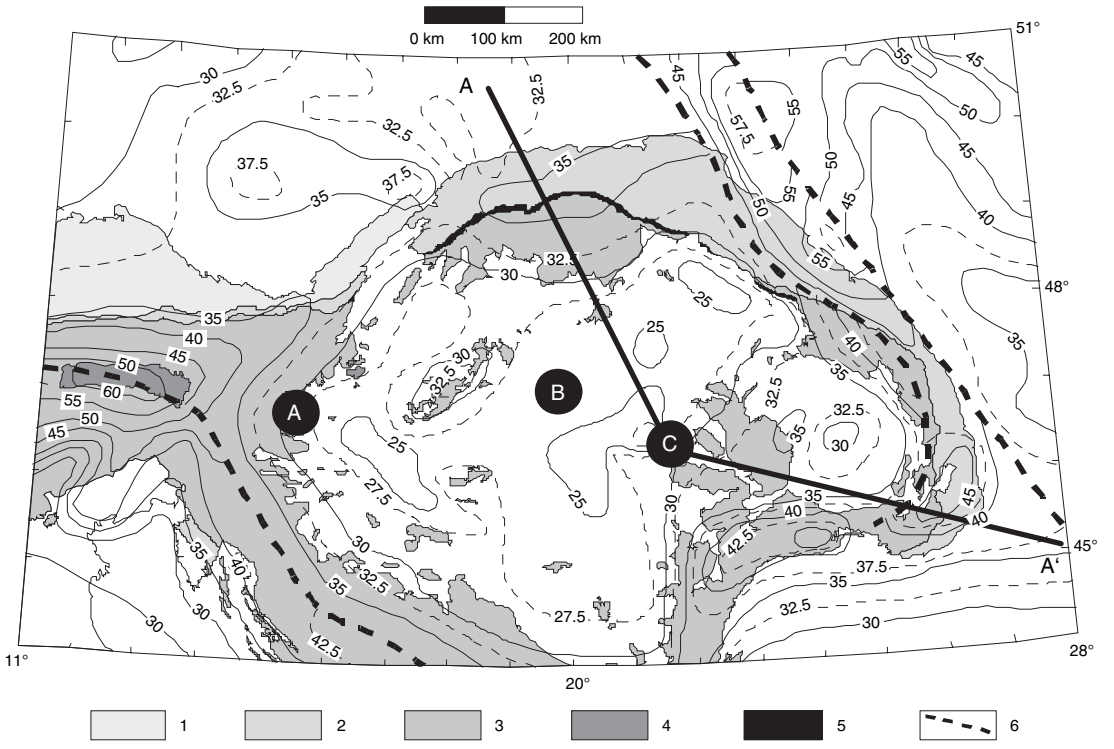

Figure 65 Crustal thickness in the Pannonian Basin and the surrounding mountains. Values are given in km. Letters A, B, and C indicate the location of strength envelopes shown in **Figure 66(a)**. Regional strength profile A-A′ is shown in **Figure 66(b)**. 1: foreland (molasse) foredeep; 2: flysch nappes; 3: pre-Tertiary units on the surface; 4: Penninic windows; 5: Pieniny Klippen Belt; 6: trend of abrupt change in crustal thickness. Modified from Horváth F, Bada G, Szafián P, Tari G, Ádám A, and Cloetingh S (2006) Formation and deofrmation of the Pannonian basin: Constraints from observational data. In: Gee D and Stephenson R (eds.) *Geological Society*, *London*, *Memoirs*, 32: *European Lithosphere Dynamics*, pp. 191–206. London: Geological Society, London.

Pannonian Basin, resulting in a wide spectrum of lithospheric strengths. These, in turn, exert a strong control on the complex present-day pattern of ongoing tectonic activity.

6.11.6.2 Neogene Development and Evolution of the Pannonian Basin

6.11.6.2.1 Dynamic models of basin formation

Following closure of oceanic basins in the Dinarides–Pannonian–Carpathian domain during the Cretaceous and Paleogene continental convergence phases of the Alpine orogeny, the style of tectonic deformation changed fundamentally in the areas of the Pannonian Basin. Whilst in the Carpathian arc large-scale tectonic transport of flysch nappes continued during the Miocene, crustal elements forming its internal parts were disrupted in response to strike–slip motions, extension and rigid body rotations, controlling the early development stages of the Pannonian Basin (e.g., Balla, 1986; Săndulescu, 1988; Csontos *et al.*, 1992; Roure *et al.*, 1993; Kováč *et al.*, 1994; Fodor *et al.*, 1999).

Several models have been proposed to explain the dynamics of Neogene rifting in the Pannonian Basin. An active versus passive mode of rifting has been a matter of continued debate (see Bada and Horváth, 2001) resulting in the proposal of various dynamic models (**Figure 68**) that take into account such prominent features of the Pannonian–Carpathian system as thinned and hot versus thickened and colder lithosphere in its central and peripheral sectors, respectively. For instance, Szádeczky-Kardoss (1967) and, at least in his early works, Stegena (1967) argued for the presence of a mantle diapir beneath the Intra-Carpathian area (**Figure 68(a)**). In this model upwelling of the asthenosphere beneath the Pannonian area caused thinning of the lithosphere and by active rifting subsidence of its central parts, whereas the nappe structure and the roots of surrounding orogens formed above the descending

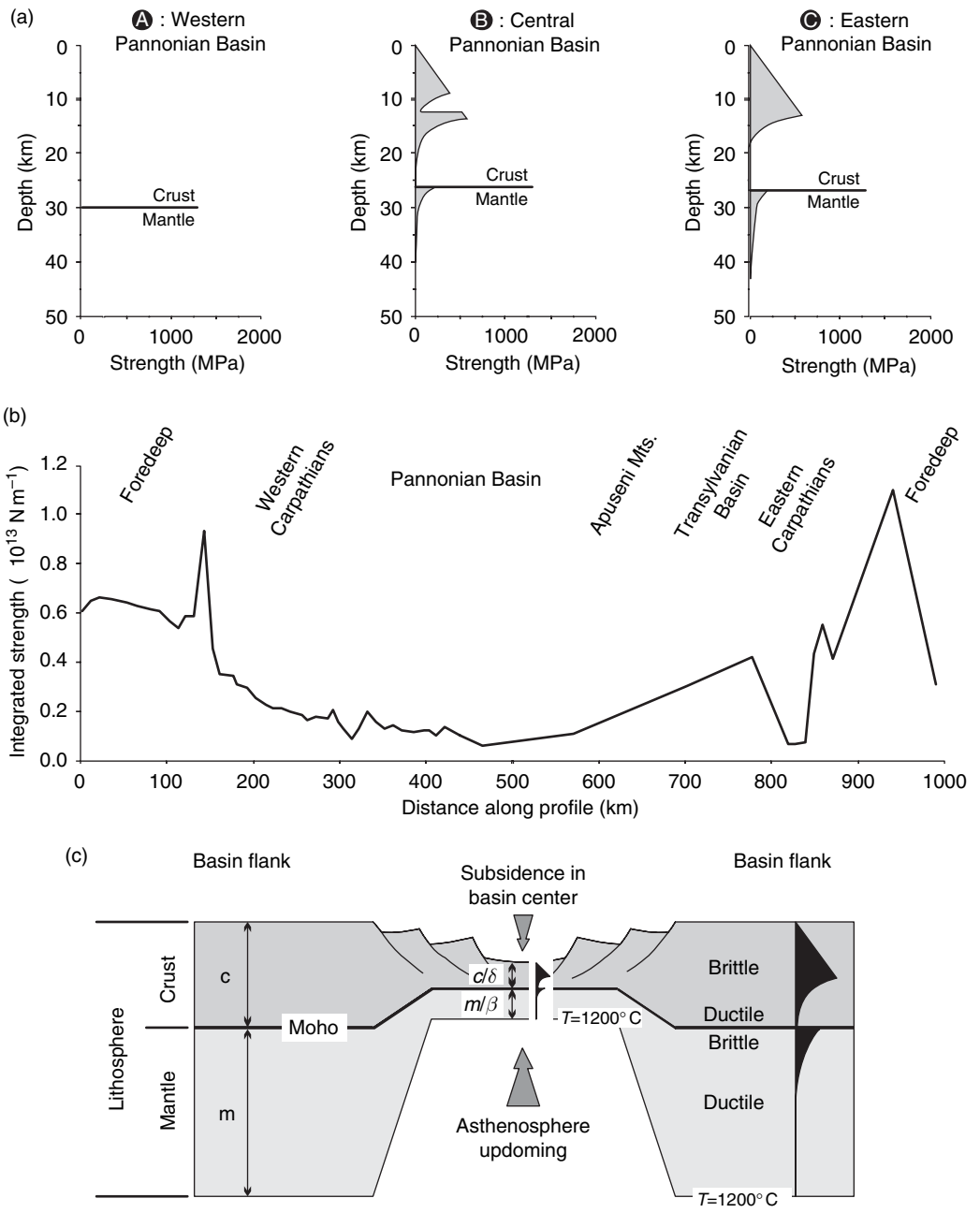

Figure 66 (a) Typical strength envelopes for the western (A), central (B), and eastern (C) parts of the Pannonian Basin. For locations see **Figure 65**. For calculation numerous constraints on the lithospheric structure and petrography, heat flow, strain rate, and stress regime have been adopted (for details, see Lankreijer *et al.*, (1997), Sachsenhofer *et al.*, (1997), Lenkey *et al.*, (2002). Note the nearly complete absence of lithospheric mantle strength predicted by the model. (b) Total integrated lithospheric strength (TIS, in 10^{-13} N m) along a regional profile through the Pannonian–Carpathian system (Lankreijer, 1998). (c) Schematic cross section showing nonuniform stretching of the Pannonian lithosphere and its effect on depth-dependent rheology. In the basin center, the thickness of the crust (c) and lithospheric mantle (m) has been reduced by stretching factors δ and β, respectively. The ascending asthenosphere heats up the system, the isotherms become significantly elevated. As a result, the thinned and hot Pannonian lithosphere became extremely weak and, thus, prone to tectonic reactivation. Modified from Cloetingh S, Bada G, Maţenco L, Lankreijer A, Horváth F, and Dinu C (2006) Thermo-mechanical modelling of the Pannonian-Carpathian system: Modes of tectonic deformation, lithospheric strength and vertical motions. In: Gee D and Stephenson R (eds.) *Geological Society*, *London*, *Memoirs*, 32: *European Lithosphere Dynamics*, pp. 207–221. London: Geological Society, London.

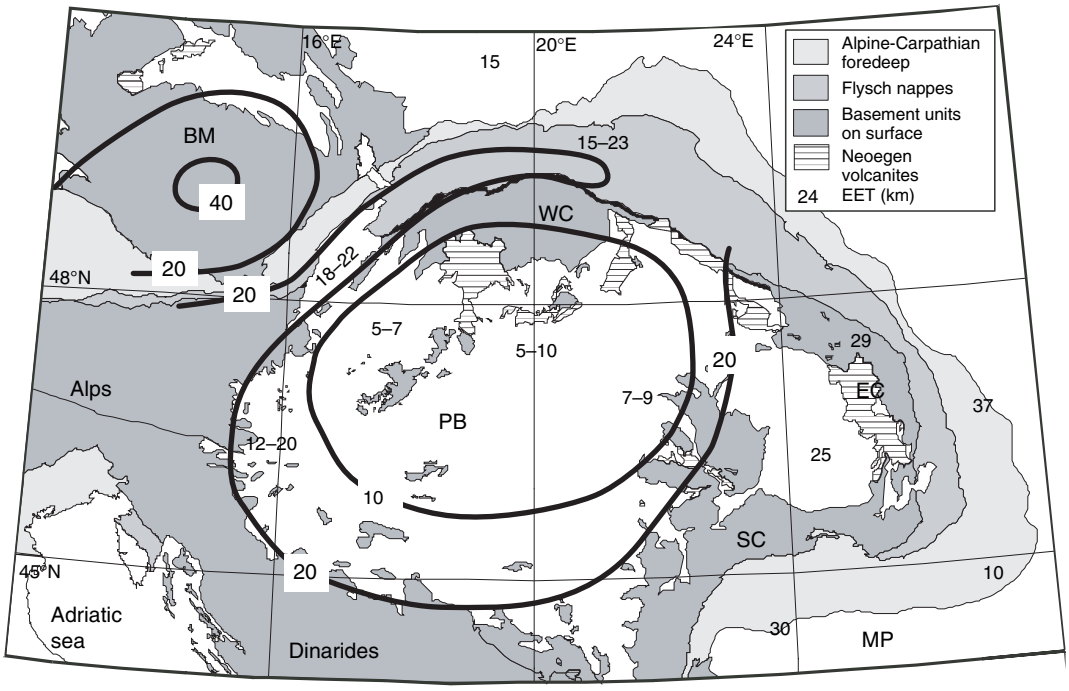

Figure 67 Effective elastic thickness (EET – in km) of the lithosphere in and around the Pannonian Basin predicted from rheological calculations. BM: Bohemian Massif; MP: Moesian Platform; PB: Pannonian basin; EC, SC, WC: Eastern, Southern and Western Carpathians, respectively. Modified from Lankreijer (1998) Rheology and basement control on extensional basin evolution in Central and Eastern Europe: Variscan and Alpine-Carpathian-Pannonian tectonics. PhD thesis, Vrieje Universiteit, Amsterdam, 158p.

branches of this convection cell. Whilst Horváth *et al.*, (1975) and Stegena *et al.*, (1975) also proposed rifting as the driving mechanism for the evolution of the Pannonian Basin, their model applied plate tectonic concepts to the Pannonian region and considered basin subsidence, intense Neogene–Quaternary volcanic activity, extremely high heat flow, and the presence of an anomalous upper mantle and thinned lithosphere as closely related phenomena. These features were attributed to thermal thinning of the Pannonian lithosphere in response to upwelling of the mantle above the subducted European and Adriatic lithospheric slabs that dip beneath the Pannonian domain (**Figure 68(b)**).

Other models stress the back-arc position of the Pannonian domain with respect to the Carpathian arc and postulate that gravity-driven passive roll-back of the subducting European lithospheric slab is the driving force for the tensional subsidence of the Pannonian Basin (**Figure 68(c)**) (e.g., Royden and Karner, 1984; Royden and Horváth, 1988; Csontos *et al.*, 1992; Horváth, 1993; Csontos, 1995; Linzer, 1996). In a modification of this model, eastward mantle flow is thought to control roll back of the subducted slab and related retreat of its hinge line (**Figure 68(d)**) (Doglioni, 1993). Both models account for passive rifting in the Pannonian Basin with tension being exerted on the overriding plate at its contact with the subducting plate by trench suction forces.

Based on thermomechanical finite element modeling Huismans *et al.*, (2001b) were able to simulated temporal changes in rifting style in the Pannonian Basin, suggesting a two-phase evolutionary scheme for the system. According to their model, the initial early Middle Miocene basin subsidence was driven mainly by passive rifting in response to roll-back of the subducted Carpathian slab, involving gravitational collapse of the thickened prerift Pannonian lithosphere. This triggered small-scale convective upwelling of the asthenosphere that has favoured the late-stage thermal subsidence (Horvath, 1993) as well as the compressional inversion of the Pannonian domain during Late Miocene–Pliocene times (e.g., Bada *et al.*, 1999; Fodor *et al.*, 2005).

6.11.6.2.2 Stretching models and subsidence analysis

Efforts to quantify the evolution of the Pannonian Basin started in the early 1980s with the application of classical basin analysis techniques. Due to the

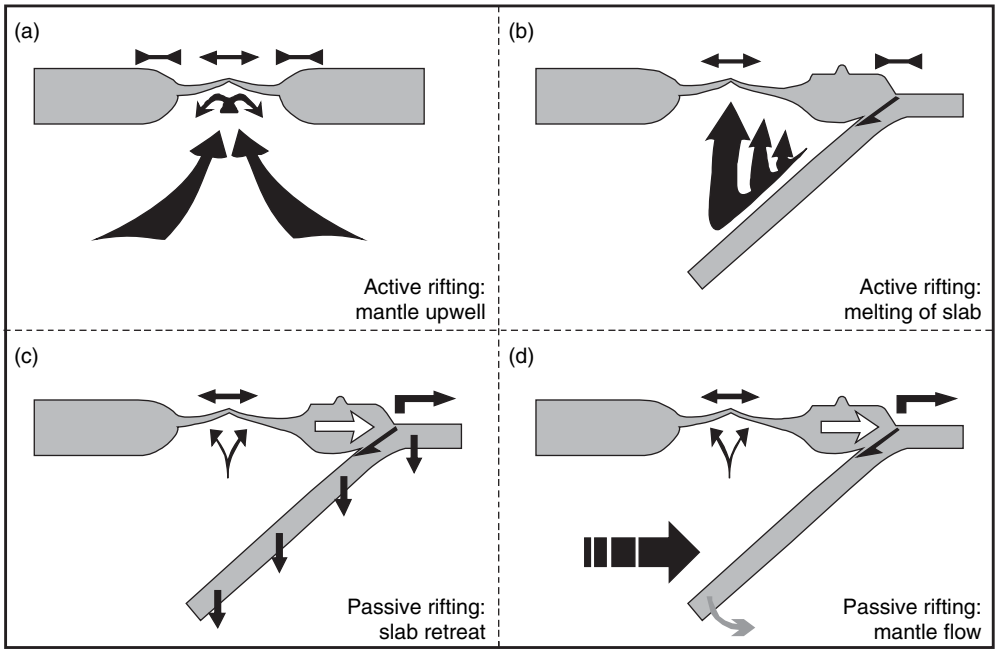

Figure 68 Dynamic models proposed for the evolution of the Pannonian Basin system. (a) Asthenospheric doming results in active rifting of the lithosphere above the central axis of the dome, whereas shortening is taking place in the peripheral areas. (b) Active rifting may also be caused by a subduction generated mantle diapir. (c) Hinge retreat of the subducting European margin driven by the negative buoyancy of the slab induces passive rifting in the overriding plate. (d) The same hinge retreat may be sustained by an eastward mantle flow pushing against the down going slab. Modified from Bada and Horváth (2001).

availability of excellent geological and geophysical constraints, this basin has been a key area for testing stretching models. At the same time, the main characteristics of the Pannonian basin system, such as its extremely high heat flow, the presence of an anomalously thin lithosphere and its position within Alpine orogenic belts, made it particularly suitable and challenging for basin analysis. Research on the Pannonian Basin was triggered by its hydrocarbon potential and addressed local tectonics and regional correlations, as well as studies on its crustal configuration, magmatic activity and related mantle processes.

Sclater *et al.*, (1980) were the first to apply the stretching model of McKenzie (1978) to the intra-Carpathian basins. They found that the development of peripheral basins could be fairly well simulated by the uniform pure shear extension concept with a stretching factor of about 2 ($\beta = 2$). For the more centrally located basins, however, their considerable thermal subsidence and high heat flow suggested unrealistically high stretching factors β up to 5. Thus, they postulated differential extension of the Pannonian lithosphere with moderate crustal stretching (δ factor) and larger stretching of the lithospheric mantle (β factor). Building on this and using a wealth of well data, Royden *et al.*, (1983) introduced the nonuniform stretching concept according to which the magnitude of lithospheric thinning is depthdependent. This concept accounts for a combination of uniform mechanical extension of the lithosphere and thermal attenuation of the lithospheric mantle (Ziegler, 1992, 1996b; Ziegler and Cloetingh, 2004). This is compatible with the subsidence pattern and thermal history of major parts of the Pannonian Basin that suggest a greater attenuation of the lithospheric mantle as compared to the finite extension of the crust. Horváth *et al.*, (1988) further improved this concept by considering radioactive heat generation in the crust, and the thermal blanketing effect of basin-scale sedimentation. By reconstructing the subsidence and thermal history, and by calculating the thermal maturation of organic matter in the central region of the Pannonian Basin (Great Hungarian Plain), a major step forward was made in the field of hydrocarbon prospecting by means of basin analysis techniques.

These studies highlighted difficulties met in explaining basin subsidence and crustal thinning in terms of uniform extension, and point toward the

applicability of anomalous subcrustal mantle thinning. This issue was central to subsequent investigations involving quantitative subsidence analyses (backstripping) of an extended set of Pannonian Basin wells and cross sections and their forward modeling (Lankreijer *et al.*, 1995; Sachsenhofer *et al.*, 1997; Juhász *et al.*, 1999; Lenkey, 1999). Kinematic modeling, incorporating the concept of necking depth and finite strength of the lithosphere during and after rifting (Van Balen *et al.*, 1999), as well as dynamic modeling studies (Huismans *et al.*, 2001b), suggested that the transition from passive to active rifting was controlled by the onset of subcrustal flow and small-scale convection in the asthenosphere. In order to quantify basin-scale lithospheric deformation, Lenkey (1999) carried out forward modeling applying the concept of nonuniform lithospheric stretching and taking into account the effects of lateral heat flow, flexure, and necking of the lithosphere. Calculated crustal thinning factors (δ) indicate large lateral variation of crustal extension in the Pannonian Basin (**Figure 69**). This is consistent with the areal

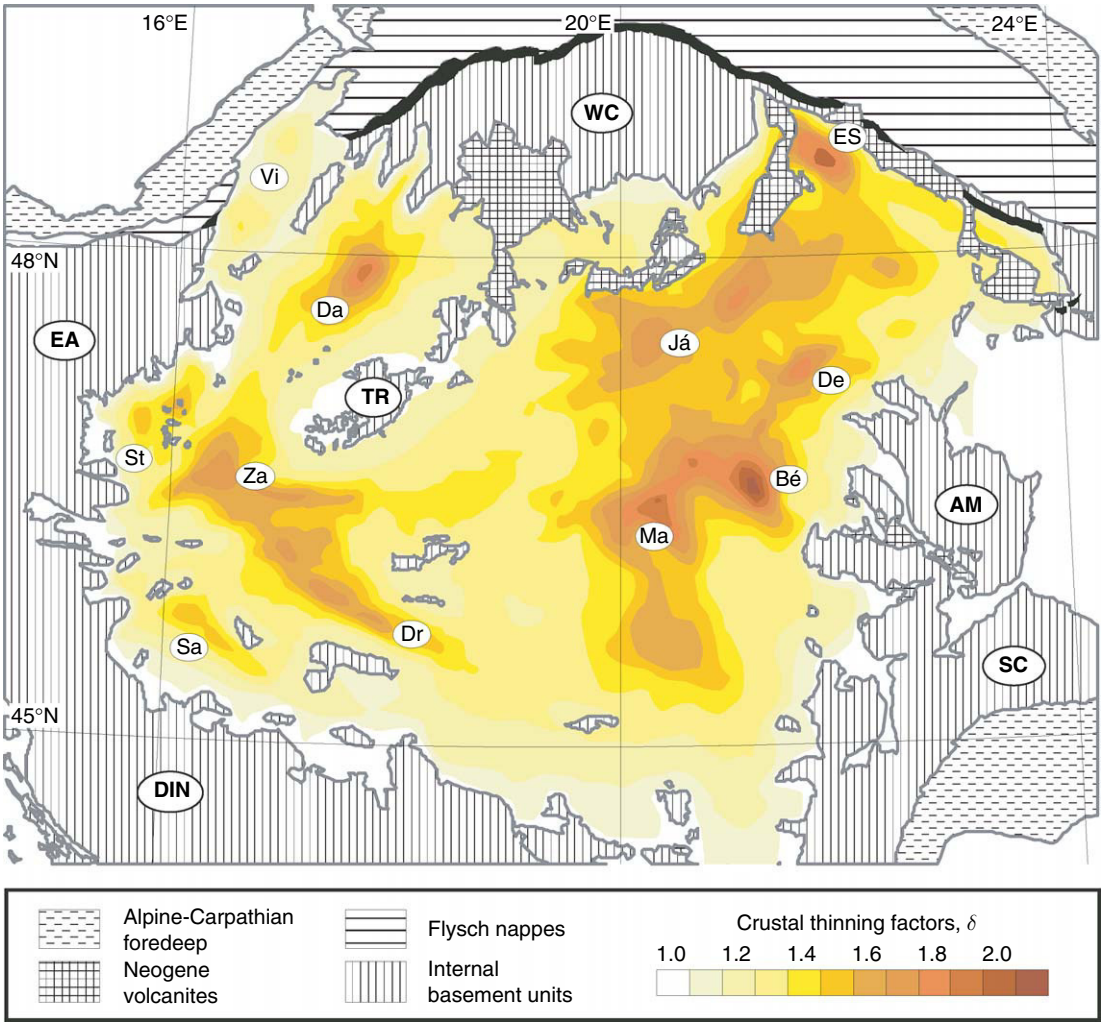

Figure 69 Crustal thinning factors δ calculated by forward modeling for the Pannonian Basin applying the nonuniform stretching concept and taking the effects of lateral heat flow and flexure of the lithosphere into account (after Lenkey, 1999). Note the pronounced lateral variations in crustal extension controlling the development of deep sub-basins separated by areas of limited deformation. AM: Apuseni Mts.; DIN: Dinarides; EA: Eastern Alps; TR: Transdanubian Range; SC, WC: Southern and Western Carpathians, respectively. Local depressions of the Pannonian Basin system: Bé: Békés; Da: Danube; De: Derecske; Dr: Drava; ES: East Slovakian; Já: Jászság; Ma: Makó; Sa: Sava; St: Styrian; Vi: Vienna; Za: Zala. Modified from Cloetingh S, Bada G, Maţenco L, Lankreijer A, Horváth F, and Dinu C (2006) Thermo-mechanical modelling of the Pannonian-Carpathian system: Modes of tectonic deformation, lithospheric strength and vertical motions. In: Gee D and Stephenson R (eds.) *Geological Society*, *London*, *Memoirs*, 32: *European Lithosphere Dynamics*, pp. 207–221. London: Geological Society, London.

pattern of the depth to the pre-Neogene basement (Horváth *et al.*, 2006). The indicated range of crustal thinning factors of 10–100% crustal extension is in good agreement with the prerift palinspastic reconstruction of the Pannonian Basin, and the amount of cumulative shortening in the Carpathian orogen (e.g., Roure *et al.*, 1993; Fodor *et al.*, 1999).

As a major outcome of basin analysis studies, Royden *et al.*, (1983) provided a two-stage subdivision for the evolution of the Pannonian Basin with a syn-rift (tectonic) phase during Early to Middle Miocene times, and a postrift thermal subsidence phase during the Late Miocene–Pliocene. Further development of the stratigraphic database, however, demonstrated the need to refine this scenario. According to Tari *et al.*, (1999), the regional Middle Badenian unconformity, marking the termination of the syn-rift stage, is followed by a postrift phase that is characterized by only minor tectonic activity. Nevertheless, the subsidence history of the Pannonian Basin can be subdivided into three main phases that are reflected in the subsidence curves of selected sub-basins (**Figure 70**). The initial syn-rift phase is characterized by rapid tectonic subsidence, starting synchronously at about 20 Ma in the entire Pannonian Basin. This phase of pronounced crustal extension is recorded everywhere in the basin system and was mostly limited to relatively narrow, fault bounded grabens or sub-basins. During the subsequent postrift phase much broader areas began to subside, reflecting general down warping of the lithosphere in response to its thermal subsidence. This is particularly evident in the central parts of the Pannonian Basin, suggesting that in this area syn-rift thermal attenuation of the lithospheric mantle played a greater role than in the marginal areas (e.g., Sclater *et al.*, 1980; Royden and Dövényi, 1988). The third and final phase of basin evolution is characterized by the gradual structural inversion of the Pannonian Basin system during the Late Pliocene–Quaternary. During these times intraplate compressional stresses gradually built up and caused basin-scale buckling of the Pannonian lithosphere that was associated with late-stage subsidence anomalies and differential vertical motions (Horváth and Cloetingh, 1996). As evident from subsidence curves (**Figure 70**), accelerated late-stage subsidence characterized the central depressions of the Little and Great Hungarian Plains (**Figure 70(b)–(c)**), whereas the peripheral Styrian and East Slovakian sub-basins were uplifted by a few hundred meters after mid-Miocene times (**Figure 70(d)–(e)**) and the Zala Basin during the Pliocene–Quaternary (**Figure 70(f)**). The importance of tectonic stresses, both during the rifting (extension) and subsequent inversion phase (compression), is highlighted by this late-stage tectonic reactivation, as well as by other episodic inversion events in the Pannonian Basin (Horváth, 1995; Fodor *et al.*, 1999).

For the Carpathian foreland, modeling curves (**Figure 70(h)–(j)**) indicate an important Late Miocene (Sarmatian) phase of basin subsidence that relates to tectonic loading of the Eastern and Southern Carpathian foreland by intra-Carpathian terranes. This phase is coeval with the end of syn-rift subsidence of the Pannonian Basin (Horváth and Cloetingh, 1996). Subsidence curves for the Transylvanian Basin (**Figure 70(g)**) indicate for the Badenian–Pannonian a subsidence pattern similar to that of the Carpathian foreland, and for the Pliocene–Quaternary a phase of uplifting that correlated with the inversion of the Pannonian Basin.

6.11.6.3 Neogene Evolution of the Carpathians System

During the last few years, research on the Carpathian system focused on spatial and temporal variations in thrusting, lateral changes in the flexural response of the foreland lithosphere and the development of an unusual foredeep geometry in the Focşani Depression. Reconstruction of orogenic uplift and erosion (e.g., Sanders *et al.*, 1999), coupled with foreland subsidence modeling (Maţenco *et al.*, 2003) elucidated the complex interplay between syn-orogenic deflection of the foreland lithosphere and its lateral variability, subsequent slab-detachment-related isostatic rebound of the orogenic wedge, and increased subsidence in the SE Carpathians corner (Maţenco *et al.*, 1997b; Zoetemeijer *et al.*, 1999; Bertotti *et al.*, 2003; Tărăpoancă *et al.*, 2003, 2004b; Cloetingh *et al.*, 2004).

Tertiary subsidence patterns recorded in the Carpathian foreland units reflect significant vertical motions (e.g., Maţenco *et al.*, 2003; Bertotti *et al.*, 2003 – **Figure 70(h)–(j)**).

In the foreland of the Southern Carpathians, corresponding to the Getic Depression and western Moesian Platform, up to 5 km thick Early Miocene sediments accumulated in a transtensional basin, whilst adjacent platform areas were characterized by nondeposition and/or erosion. Starting in the Middle to Late Miocene, the entier Carpathian foreland subsided flexurally in response to thrust loading. In the evolving foreland basin a major depocenter developed in the Carpathian Bend Zone, corresponding to the Focşani Depression

(**Figure 71**), in which Late Miocene sedimentation rates reached 1500–3000 m My^{-1}. During the Pliocene–Pleistocene, when movements on the Carpathian thrusts had essentially ceased, subsidence of the Focşani Depression continued at sedimentation rates averaging, 200–300 m My^{-1}. Regional subsidence analyses on the Carpathian foreland basin demonstrate that comparable kinematically related episodes of vertical motions occurred simultaneously also in the frontal parts of the Eastern and Southern Carpathians (Maţenco *et al.*, 2003; Bertotti *et al.*, 2003), with limited to no evidence for depocenter migration in the East-Carpathian foreland, contrasting with previous inferences (e.g., Meulenkamp *et al.*, 1996).

6.11.6.3.1 Role of the 3-D distributions of load and lithospheric strength in the Carpathian foredeep

The Focşani Depression, that contains almost 13 km of Middle Miocene to Recent sediments, is located in front of the Carpathian Bend Zone (**Figure 71**), next to the Vrancea seismogenic area. This basin is of great interest insofar as its partly pronounced post-thrusting subsidence and the position of its depocentre in front of the thrust-belt are anomalous in terms of flexural foreland basin development. To explain these phenomena, several models invoked a lithospheric slab that sinks beneath the Focşani Depression into the asthenosphere and accounts for the seismicity of the Vrancea area (**Figure 72**). This slab is interpreted as having formed either by SE-ward roll-back and detachment of the subducted oceanic part of the lower plate (Royden, 1993; Linzer, 1996; Wortel and Spakman, 2000), associated with its tearing along the Trotuş fault (Maţenco and Bertotti, 2000), or by postcollisional delamination of the continental lithospheric mantle from the foreland (Gîrbacea and Frisch, 1998; Chalot-Prat and Gîrbacea, 2000).

The so-called hidden loads have been inferred to affect the SE Carpathians and their foredeep basins (e.g., Royden, 1993). As modeling studies showed that the topographic load of the Carpathians is insufficient to account for the observed foredeep geometry, an extra vertical force had to be applied to the deep end of the subducting plate (Royden and Karner, 1984). Moreover, these models inferred large lateral variations in the rigidity of the Carpathian foreland lithosphere (Maţenco *et al.*, 1997a), possibly inherited from precompressional stages.

The deepest part of the Focşani Depression (**Figure 73**, see also **Figure 82**) is located immediately in front of the Carpathian Bend zone and is limited to the W and NW by the Carpathian thrust front. This basin shallows out rapidly towards the N and SW along the front of the Eastern and Southern Carpathians and SE-ward towards the foreland platform.The 3-D architecture of the Focşani Depression and its evolution through time is well constrained by an extensive reflection-seismic survey. These data show that this basin developed in two stages, namely during the Middle Miocene (Badenian) in response to NE–SW directed extension, and from the Late Miocene onward in response to regional tilting and subsidence that was not accompanied by faulting (Tărăpoancă *et al.*, 2003).

Modeling of the Focşani Depression aimed at assessing how much of its total subsidence can be attributed to syn-rift tectonics and postrift thermal subsidence and whether the remaining subsidence can be explained by foreland flexure in response to 3-D loads in the presence of lateral changes in the flexural strength of the foreland lithosphere (Tărăpoancă *et al.*, 2004).

6.11.6.3.1.(i) Preorogenic extensional basin

Reflection-seismic data define a set of NW–SE trending normal faults along the eastern margin of the Focşani Depression, outlining half-grabens that contain up to 4 km thick Badenian syn-rift sediments and that are bounded by ENE sticking transfer faults (**Figures 73** and **74**). The thickness of Badenian sediments decreases generally toward the eastern shoulder of this graben system that is superimposed on the North Dobrogean orogen. As to the NW and W the Badenian graben system is overridden by the Carpathian nappes, its full extent cannot be reconstructed. The Badenian syn-rift sediments are capped by a nearly regional unconformity that corresponds to the Badenian/Sarmatian boundary and marks the syn- to postrift transition (Tărăpoancă *et al.*, 2004).

Badenian extension in the Carpathians Bend foreland was modeled (Tărăpoancă *et al.*, 2004) using a forward 2-D numerical modeling code that simulates the kinematic and thermal behavior of extending lithosphere (Kooi, 1991). In this model, prerift lithospheric and crustal thicknesses are an input parameter. As in the area of the Carpathian Bend zone present-day lithospheric and crustal thicknesses range between 170 and 190 km, and 30 to 40 km, respectively (Rădulescu, 1988; Horváth, 1993; Nemcok *et al.*, 1998), a prerift lithospheric thickness of 180 m was adopted. Differential stretching factors were then

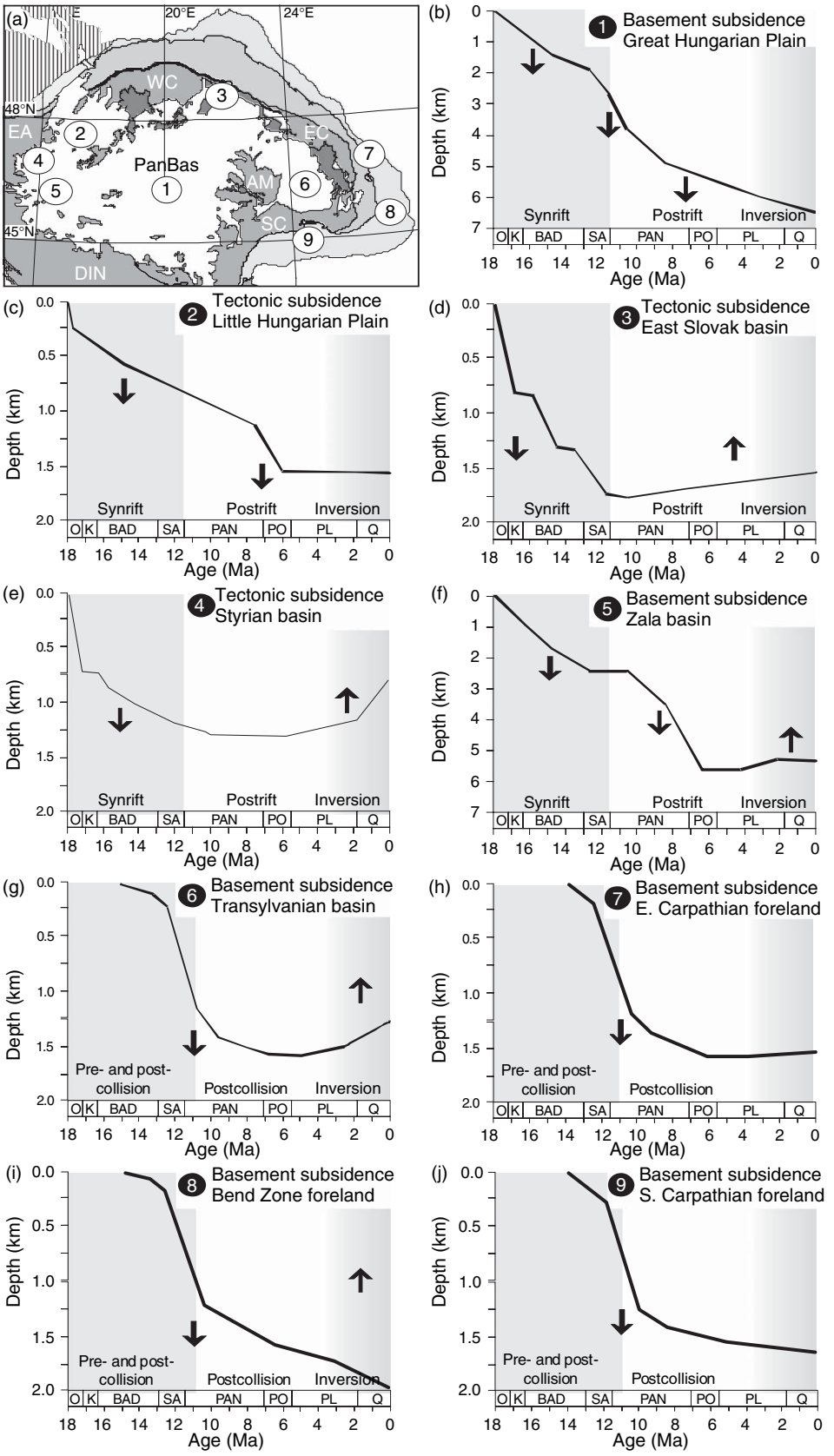
(a)
20°E
24°E
48°N
45°N
WC
EA
EC
PanBas
AM
SC
DIN
1
2
3
4
5
6
7
8
9
(b)
1 Basement subsidence
Great Hungarian Plain
(c)
2 Tectonic subsidence
Little Hungarian Plain
(d)
3 Tectonic subsidence
East Slovak basin
(e)
4 Tectonic subsidence
Styrian basin
(f)
5 Basement subsidence
Zala basin
(g)
6 Basement subsidence
Transylvanian basin
(h)
7 Basement subsidence
E. Carpathian foreland
(i)
8 Basement subsidence
Bend Zone foreland
(j)
9 Basement subsidence
S. Carpathian foreland
Depth (km)
Age (Ma)
Synrift
Postrift
Inversion
Pre- and post-collision
Postcollision
O K BAD SA PAN PO PL Q

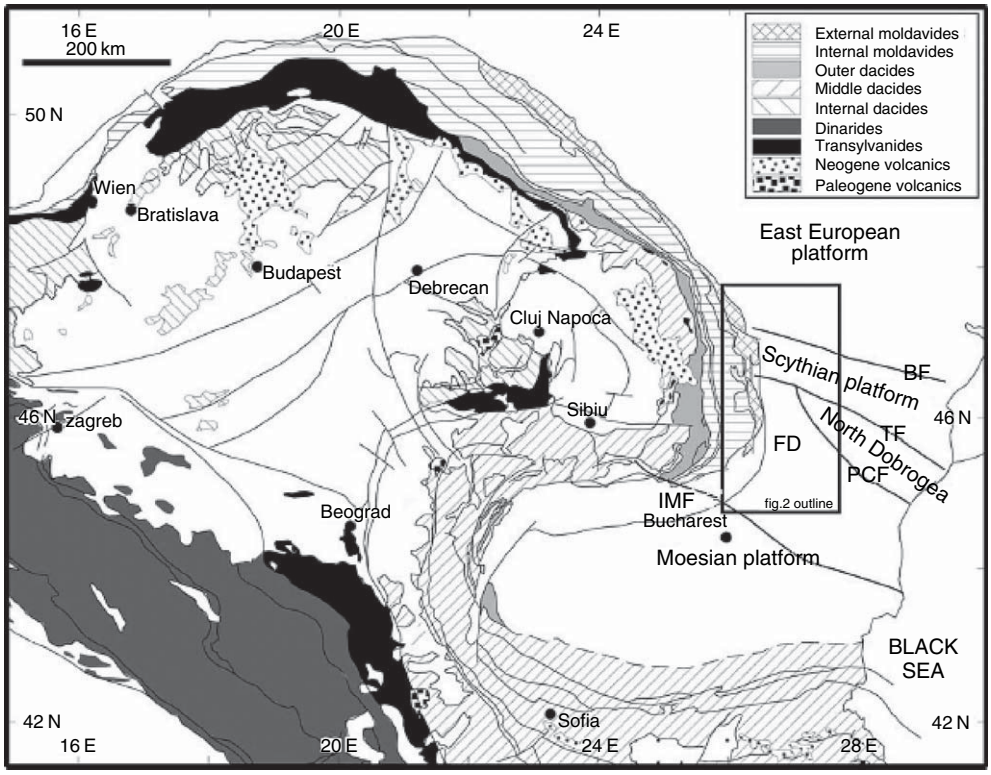

Figure 71 General map of the Carpathian–Pannonian system and location of study area. FD approximate location of Focşani Depression. BF, IMF, PCF, and TF are Bistriţa, Intramoesian, Peceneaga–Camena, and Trotuş faults, respectively, forming the boundaries between different lithospheric domains (platforms) of the Carpathians foreland plate. Modified from Săndulescu M (1984) *Geotectonics of Romania* (in Romanian). Bucharest: Editrons Tehnica.

assigned to the crust and lithospheric mantle to simulate depth-dependent extension whilst basin subsidence was computed for the center of each box.

The cross section chosen for the 2-D modeling is given in **Figure 73**. By flattening the top Badenian marker the configuration of the rifted basin prior to thrusting and flexural loading was restored (**Figures 74** and **75**). For modeling purposes, it was assumed that this basin was filled with sediments up to sea level. Moreover, its fill was decompacted, assuming a silty sand lithology. In order to fit the basin geometry, a range of stretching factors was tested until a good fit between observed and modeled geometries was achieved. The duration of rifting was assumed to be 3 My, corresponding to Badenian times. Further input values are the EET and necking depth of the lithosphere with the former defined either as a constant or being associated with a specific isotherm. Modeling parameters used are summarized in **Table 7** (Tărăpoancă *et al.*, 2004). The modeled profile extends beyond the width of the basin to avoid boundary effects. The best-fit model is shown

Figure 70 Subsidence curves for selected sub-basins of the Pannonian Basin and the Carpathian foreland. Note that after a rapid phase of general subsidence throughout the entire Pannonian Basin, the sub-basins show distinct subsidence histories from Middle Miocene times onward. Arrows indicate generalized vertical movements. Timing of the syn- and postrift phases after Royden *et al.*, (1983). Timing of Carpathians collision after Matenco *et al.*, (2003). For timescale the central Paratethys stages are used. O, K: Ottnangian and Karpatian, respectively (Early Miocene); BAD, SA: Badenian and Sarmatian, respectively (Middle Miocene); PAN, PO: Pannonian and Pontian, respectively (Late Miocene); PL: Pliocene; Q: Quaternary. AM: Apuseni Mts.; DIN: Dinarides; EA: Eastern Alps; PanBas: Pannonian Basin; SC, WC: Southern and Western Carpathians foreland basins, respectively. Modified from Cloetingh S, Bada G, Matenco L, Lankreijer A, Horváth F, and Dinu C (2006) Thermo-mechanical modelling of the Pannonian-Carpathian system: Modes of tectonic deformation, lithospheric strength and vertical motions. In: Gee D and Stephenson R (eds.) *Geological Society*, *London*, *Memoirs*, 32: *European Lithosphere Dynamics*, pp. 207–221. London: Geological Society, London.

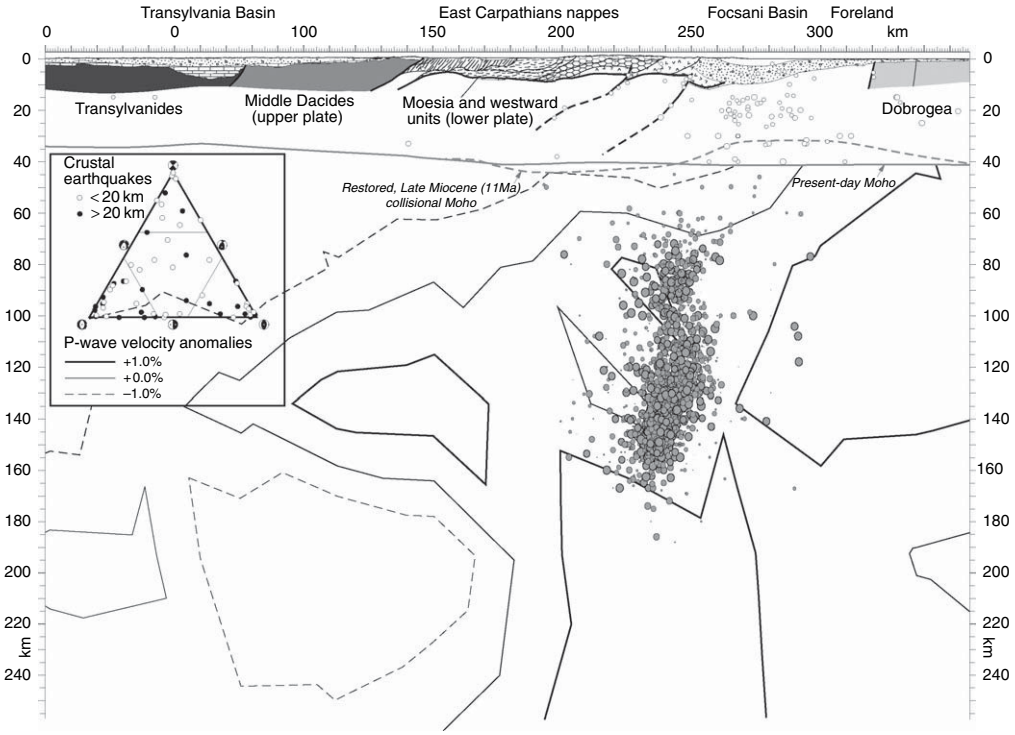

Figure 72 Simplified cross-section through the Romanian Carpathians showing the main tectonic units of the upper and lower tectonic plates and the thin-skinned thrustbelt that developed at their contact. Present-day Moho after Diehl *et al.*, (2005). The Moho surface reconstructed for the moment of collision (~11 Ma, gray dashed line) was constructed by retro-deforming the cumulative postcollisional (latest Miocene–Quaternary) vertical movements. Earthquakes from the SE Carpathians were projected into the cross section as a function of depth and magnitude. Crustal seismicity was projected perpendicular to the cross section (i.e., along the strike of Quaternary folds of the Focşani Basin). Mantle earthquakes were projected along the strike of the NE–SW oriented intermediate Vrancea mantle slab, oblique to the trace of the cross section. The ternary diagram represents the types of focal mechanisms for the crustal earthquakes that apparently do not display any preferred type of fault plane solution. Mantle P-wave velocity anomalies after the regional seismic tomography of Wortel and Spakman (2000). Note that the location and geometry of these anomalies are only qualitative due to the large SE Carpathians zoom. For complete sections at the regional Carpathians scale, see Wortel and Spakman (2000). Modified from Maţenco *et al.*, (2006); see also Schmid *et al.*, (2006).

in **Figure 75**. This model overestimates, however, the uplift of the eastern rift shoulder as the top Badenian marker horizon does not extend across it. Apart from this, a good fit is obtained for most of the profile with minor differences in its westernmost part probably being related to post-Badenian movements along distributed faults (Tărăpoancă *et al.*, 2004). The best-fit model was obtained using an EET of 35 km, a necking depth of 25 km, a prerift crustal thickness of 32 km and assuming uniform extension of the crust and lithospheric mantle. Stretching factors are small and even in the deepest central basin do not exceed 1.1 (**Figure 75**). The rift-induced thermal anomaly is very small due to the low stretching factors and lateral heat dissipation. Correspondingly, the post-Badenian postrift subsidence is less than 100 m or nil (**Figure 76**).

Sensitivity studies showed that changing the prerift crustal thickness from 30 to 40 km had little effect on modeling results. By contrast, changing in the EET and particularly the necking depth caused important changes in results. Assuming the same distribution of stretching factors as in **Figure 75** and a crustal thickness of 32 km, basin geometries for four necking depths and for four EET values, respectively, are shown in **Figure 77**. Due to the small stretching factors, changes in these two parameters affect particularly the depth of the central and central-western part of the basin. As in essence the same basin and the same amount of stretching are obtained, using a lower EET and a shallower necking depth and vice versa, no unique solution can be derived from the basin shape alone.

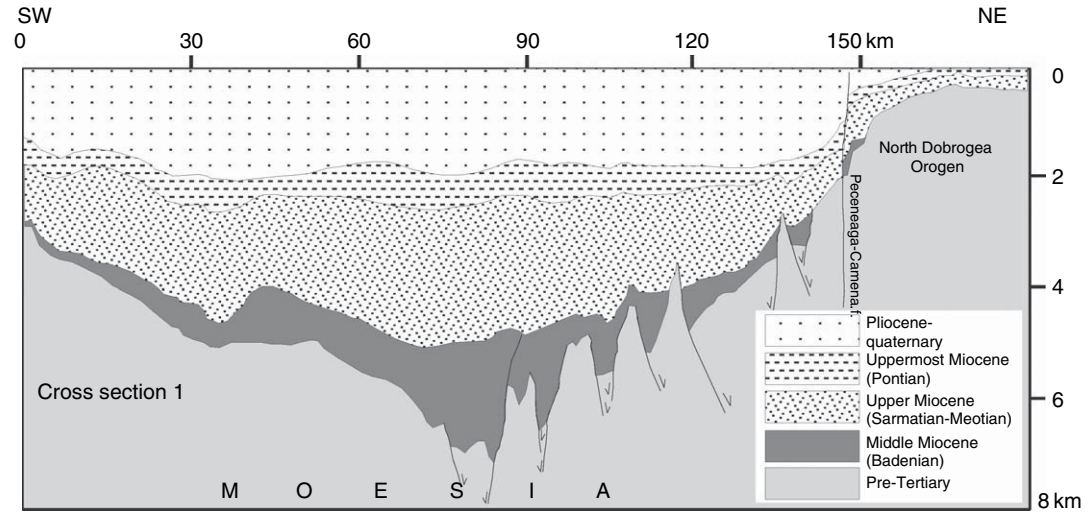

Figure 73 Cross section through southern flank of Focşani Depression showing Badenian extensional basins. Based on maps derived from the interpretation of industrial seismic lines. Modified from Tărapoăncă M, Bertotti G, Maţenco L, Dinu C, and Cloetingh S (2003) Architeccture of the Focsani depression: A 13 km deep basin in the Carpathians bend zone (Romania). *Tectonics* 22: 1074 (doi:10.1029/2002TC001486).

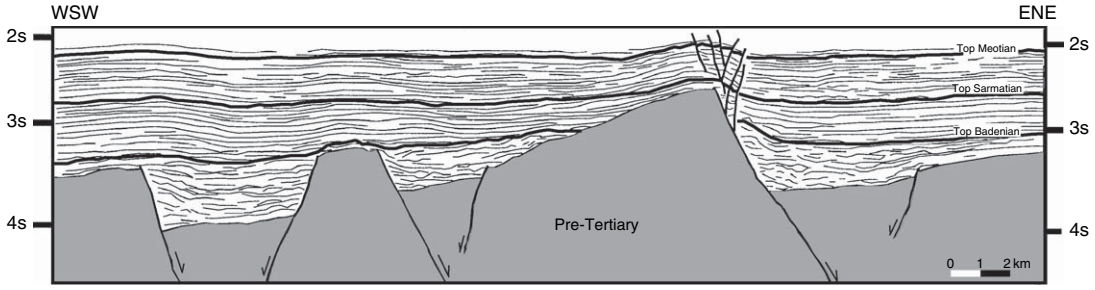

Figure 74 Example of an interpreted seismic line across Badenian fault blocks in the Focşani Depression. Modified after Tărapoăncă M, Dinu C, and Ciulavu D (2004b) Neogene kinematics of the northeastern sector of the Moesian platform (Romania). *American Association of Petroleum Geologists Bulletin* in press.

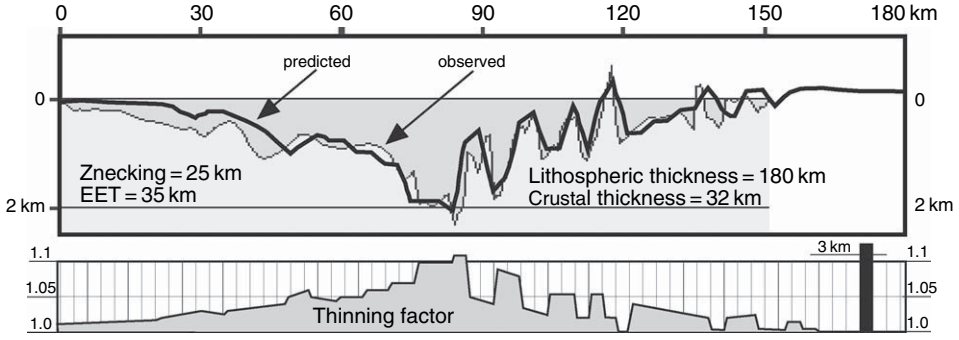

Figure 75 Extensional modeling results for Badenian basins. Upper panel: dark gray field shows configuration of Badenian basins derived from **Figure 73** by flattening the top Badenian marker. Bold line shows best-fit modeled cross section adopting stretching factors given in lower panel. Lower panel: inferred stretching factors (same for crust and lithospheric mantle) plotted for constant 3 km wide steps. Modified from Tărapoăncă *et al.*, (2004a).

Table 7 Parameters used as input data in the extensional modeling of the Focşani depression

Temperature	Surface	0°C
	Asthenosphere	1333°C
Density at surface conditions	Crust	2800 kg m^{-3}
	Lithospheric mantle	3330 kg m^{-3}
Sediment grain density		2660 kg m^{-3}
Thermal expansion coefficient		3.4×10^{-5} K^{-1}
Thermal diffusivity		7.8×10^{-7} m^2 s^{-1}

Nevertheless, as the model predicts almost no postrift subsidence, only a very small part of the observed Sarmatian–Quaternary subsidence can be attributed to Badenian rifting. Moreover, owing to the small amount of stretching, the rift-induced strength reduction of the Moesian Platform is presumably also small.

6.11.6.3.1.(ii) Flexural modeling of the foredeep basin The foredeep basin of the Carpathian Bend Zone is in so far peculiar as its depocenter does not lie beneath this thrust belt, as predicted by simple flexural models. Shallowing of

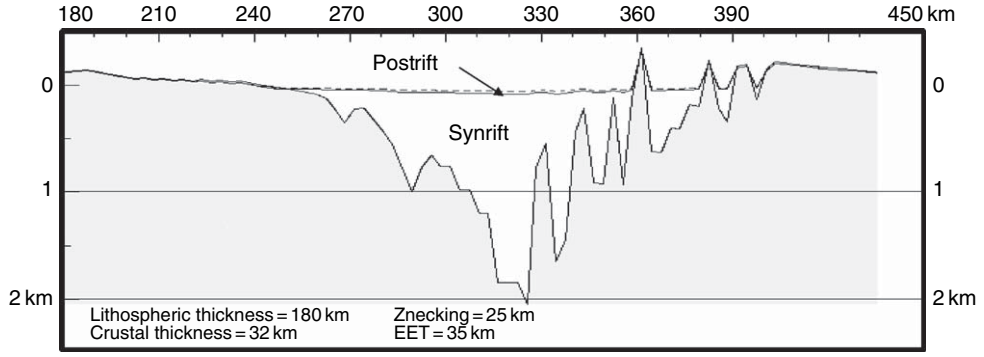

Figure 76 Syn- and postrift subsidence obtained for the best-fit model (see **Figure 75**). Modified from Tărapoăncă M, Garcia-Castellanos D, Bertotti G, Maţenco L, Cloetingh S, and Dinu C (2004a) Role of 3-D distributions of load and lithospheric strength in orogenic arcs: polystage subsidence in the Carpathians foredeep. *Earth and Planetary Science Letters* 221: 163–180.

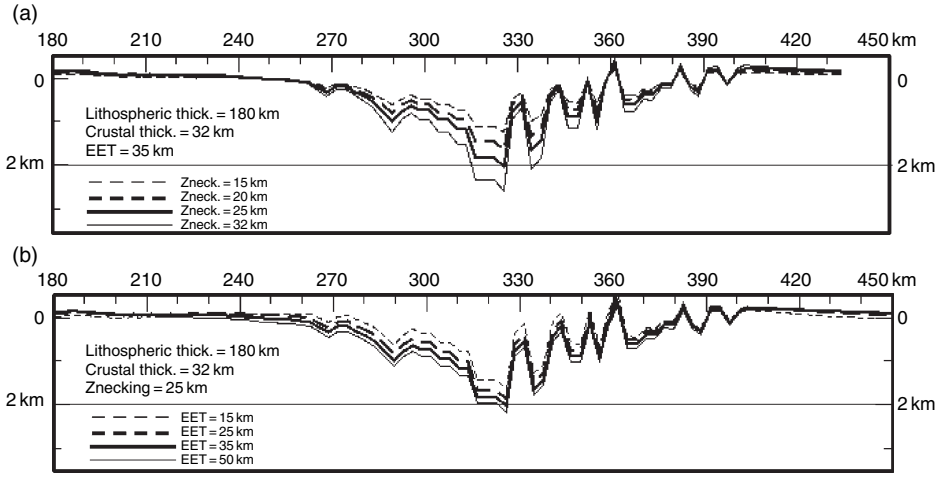

Figure 77 Sensitivity analysis on basin depth for best-fit model (**Figure 75**). Effect of (a) necking depth variations, (b) elastic thickness variations. Modified from Tărapoăncă M, Garcia-Castellanos D, Bertotti G, Maţenco L, Cloetingh S, and Dinu C (2004a) Role of 3-D distributions of load and lithospheric strength in orogenic arcs: polystage subsidence in the Carpathians foredeep. *Earth and Planetary Science Letters* 221: 163–180.

this foredeep towards the thrust belt appears to be associated with the presence of lithospheric blocks characterized by significantly different strengths within the Carpathian domain.

Following an initial cross-section experiment, a planform modeling approach was taken by Tărăpoancă *et al.*, (2004) to test: (1) the effects of a 3-D load distribution and lateral variations in lithospheric strength on the position of the basin, and (2) whether the observed very large subsidence is the effect of 3-D loading rather than of a hidden load.

In the Carpathian Bend zone, flexural subsidence of the foreland in response to nappe emplacement commenced during the early Sarmatian (Săndulescu, 1984, 1988; Maţenco *et al.*, 2003). The thickness of Sarmatian deposits gradually increases from the foreland to about 2.1 km near the present-day thrust front (**Figure 78**). By contrast, the thickness of Meotian deposits decreases from the axial parts of the Focşani Depression towards the Carpathian deformation front (**Figure 78(a)**), indicative for the Late Miocene progressive advance of the latter. During the Early Pliocene, emplacement of the frontal Carpathian thrust elements at their present position involved the development of a typical triangle zone. This resulted in uplift and eastward tilting of the western margin of the Focşani Depression whereas its central parts continued to subside (Maţenco *et al.*, 2003; see their Figure 5 cross section B).

In the deepest parts of the Focşani Depression, which are located in front of the Carpathian thrust front, Pliocene and Quaternary sediments attain a thickness of over 4 km and rest on 4 km thick Late Miocene deposits (**Figure 78(a)**). The eastern flank of the Focşani Depression dips gently towards the basin center whilst its western flank dips steeply eastward with outcropping Late Miocene strata displaying nearly vertical dips (Dumitrescu *et al.*, 1970). Flattening the sedimentary fill of the Focşani Depression at the base-Pliocene level indicates that that this basin was considerably broader during the Late Miocene than at present. To the S of the Focşani Depression, the Late Miocene (Sarmatian) base reaches a depth of ~3.7 km in front of the Carpathians belt and shallows southward with the Pliocene–Quaternary sequence showing roughly

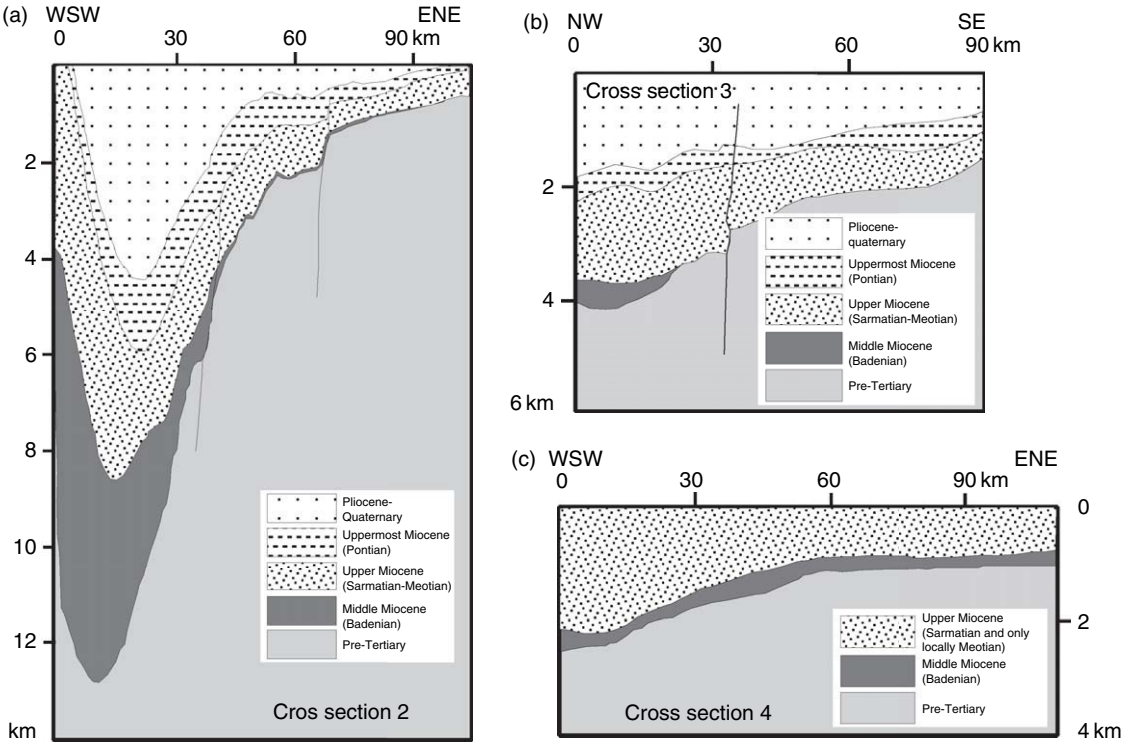

Figure 78 Cross sections through Focşani Depression: (a), central part, (b) southern flank, and (c) northern flank. Modified from Tărapoăncă M, Garcia-Castellanos D, Bertotti G, Maţenco L, Cloetingh S, and Dinu C (2004a) Role of 3-D distributions of load and lithospheric strength in orogenic arcs: polystage subsidence in the Carpathians foredeep. *Earth and Planetary Science Letters* 221: 163–180.

the same thickness as the Late Miocene one (**Figure 78(b)**).

The East-Carpathian orogenic wedge has overridden lithospheric blocks with very different characteristics, namely the East-European Platform, the Dobrogean Orogen and the Moesian Platform, the boundaries of which are sharp and fault controlled (e.g., the Trotuş fault) (**Figure 73**).

To illustrate the effect of lateral strength changes of a loaded plate on the geometry of a flexural basin, the deflection of a 2-D thin elastic plate (e.g., Turcotte and Schubert, 1982) under the weight of a rectangular load was calculated for different EET distributions (**Figure 79**). In these calculations, topography after lithospheric deflection was set to 2 km in the orogen and to zero elsewhere. In the case of a

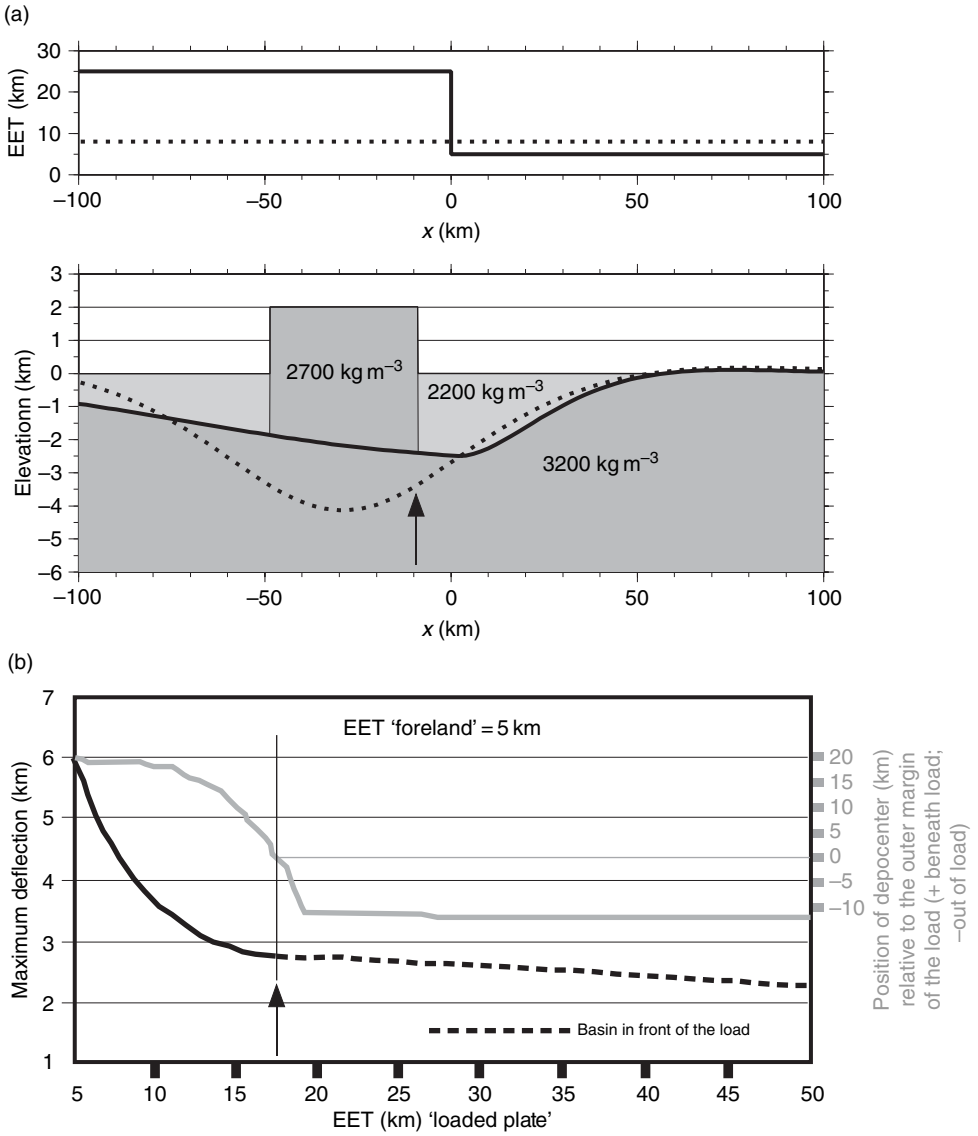

Figure 79 (a) Flexural deflection profiles for two different EET distributions applying the same topographic load. With a uniform EET the maximum deflection occurs beneath the load (dotted line). With a sharp decrease in EET at the right edge of the load the maximum deflection shifts toward the weaker foreland (bold line). (b) Deflection maximum as a function of the strength of the loaded plate (black line) and position of the depocenter relative to the load (gray line). When the EET of the lithosphere is significantly lower in the foreland than beneath the orogen, the deepest part of a foredeep shifts away from the orogen. Modified from Tărapoăncă M, Garcia-Castellanos D, Bertotti G, Maţenco L, Cloetingh S, and Dinu C (2004a) Role of 3-D distributions of load and lithospheric strength in orogenic arcs: polystage subsidence in the Carpathians foredeep. *Earth and Planetary Science Letters* 221: 163–180.

constant EET, the zone of maximum deflection is located directly beneath the imposed load. On the other hand, with a laterally changing EET of the foreland plate and the load being imposed on its stronger part, the maximum deflection tends to shift away from directly beneath the load towards the weaker part of the plate, and, depending on the conditions, can even be separated from the load to the end that the foredeep basin shallows toward the load, as seen in the Focşani Depression. This suggests that the subsidence of the unusually deep SE Carpathians foredeep basin may be related to a reduction of the EET of its substrate, possibly caused by preorogenic extension.

To further investigate the subsidence mechanism of the Focşani Depression, Tărăpoancă *et al.*, (2004) used a flexural model to calculate the deflection of a foreland lithosphere that consists of various blocks with different EET (see, e.g., Van Wees and Cloetingh, 1994 for governing equations) in response to a laterally variable load (see Garcia-Castellanos *et al.*, 2002 for methodology). The load was calculated from the observed topography of the Carpathians region with the evolving flexural basin being filled with constant density material.

For the post-Badenian subsidence of the Focşani Depression, a flexural model was used, taking into account the plan view distribution of topographic loads and lateral variations in the lithospheric strength. Assigning realistic strengths to the different domains of the Carpathian region, a basin is predicted in front of the Carpathians Bend Zone where the deflection of the foreland lithosphere is localized owing to its preexisting extensional weakening and to Quaternary crustal faulting at the transition between the rheologically weak Moesia and the northern more stable blocks (East-Europe/Scythia/North Dobrogea) (Maţenco *et al.*, 2006).

As the deepest modeled basin is only 3.3 km deep (~40% of the observed value), either an additional load is required in the Carpathians Bend Zone or intraplate stresses have to be invoked to explain the geometry and depth of the Focşani Depression.

Additional loads applied to the foreland lithosphere may be attributed to the weight of the steeply dipping Vrancia slab that is located beneath the Focşani Depression (**Figure 72**) or to an unrealistic greater topographic load.

Modeling of the effects of intraplate stresses on the geometry of the Carpathian foredeep (Tărăpoancă *et al.*, 2004), applying an NW–SE directed compressional stress field during postcollisional evolution of the Carpathians, that is, the latest Miocene-Quaternary (see Maţenco and Bertotti, 2000) indicates that with a 500 m topographic load the depth of the Focşani Depression increases to ±6.5 km, corresponding to 75–80% of its post-Badenian subsidence (i.e., postextensional Carpathians thrust loading and postcollisional inversion), whilst with a topographic load of 800 m, its actual depth and depocenter location can be simulated (**Figure 80**). Modifying the magnitude of the intraplate stresses causes in the depocenter depth variations in the order of few hundred meters only. However, similar as models without intraplate stresses, the predicted basin width is larger than the observed one.

Modeling indicates that the previously neglected extensional weakening of the eastern Moesian foreland, combined with compressional intraplate stresses, as well as the 3-D distribution of the topographic load and lithospheric strength variations may play an important role in the subsidence pattern of the SE Carpathian foreland. As such, it suggests a potential alternative to models that exclusively invoke topographic loading and slab pull forces to account for the observed subsidence of this foredeep, and specifically of the Focşani Depression.

6.11.6.4 Deformation of the Pannonian–Carpathian System

The present-day deformation pattern and related topography development in the Pannonian–Carpathian system is characterized by pronounced spatial and temporal variations in the stress and strain fields (**Figure 81**) (see, e.g., Cloetingh *et al.*, 2006). Horváth and Cloetingh (1996) established the importance of Late Pliocene and Quaternary compressional deformation of the Pannonian Basin that explains its anomalous uplift and subsidence, as well as intraplate seismicity. Based on the case study of the Pannonian–Carpathian system, these authors established a novel conceptual model for the structural reactivation of back-arc basins within orogens. At present, the Pannonian Basin has reached an advanced evolutionary stage as compared to other Mediterranean back-arc basins in so far as it has been partially inverted during the last few million years. Inversion of the Pannonian Basin can be related to temporal changes in the regional stress field, from one of tension that controlled its Miocene extensional subsidence, to one of Pliocene–Quaternary compression resulting in deformation, contraction, and flexure of the lithosphere associated with differential vertical motions.

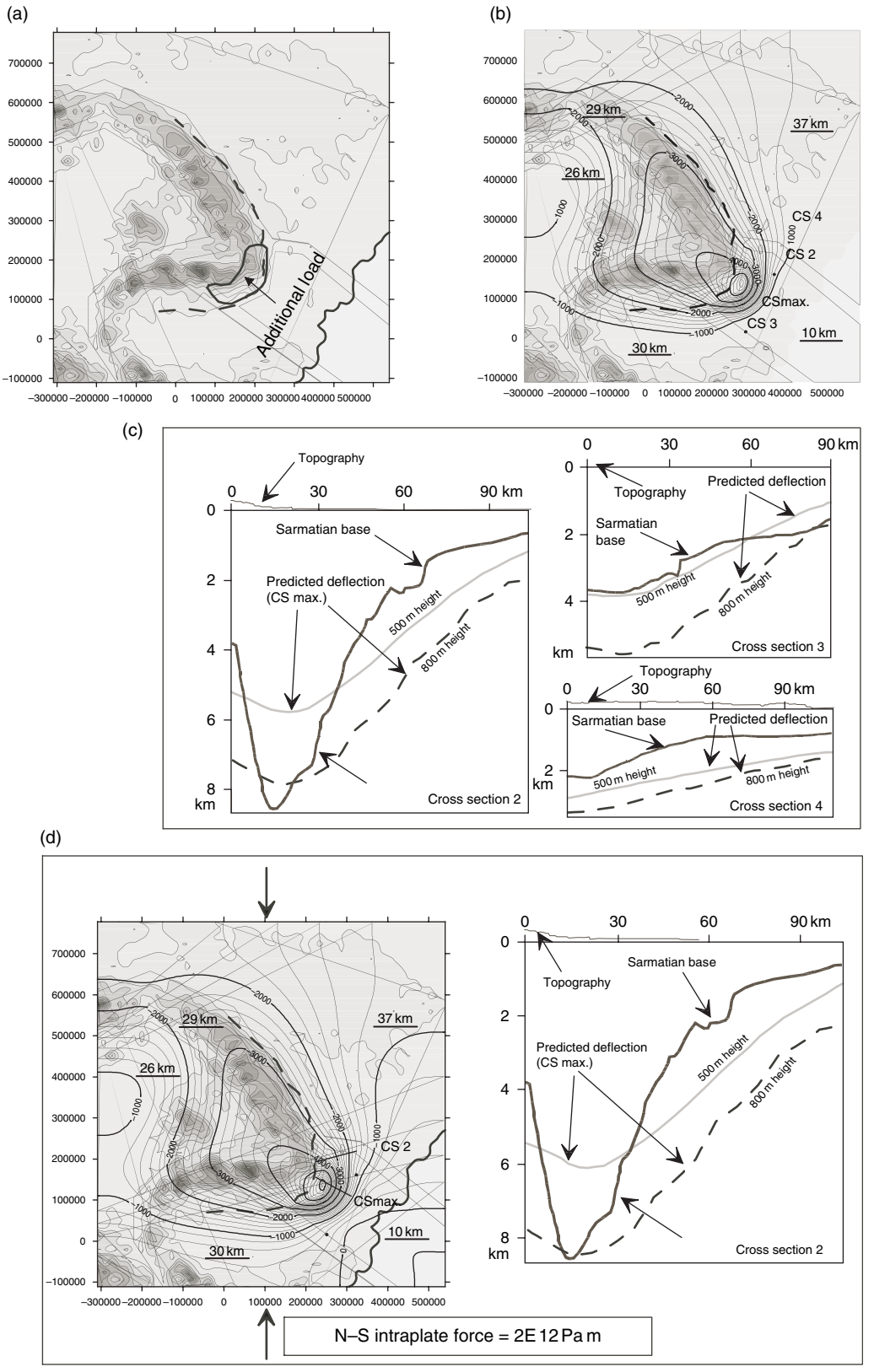
(a)
Additional load
(b)
29 km
37 km
26 km
CS 4
CS 2
CSmax.
CS 3
10 km
30 km
(c)
Topography
Sarmatian base
Predicted deflection
(CS max.)
500 m height
800 m height
Cross section 2
Predicted deflection
Cross section 3
Cross section 4
(d)
N–S intraplate force = 2E 12 Pa m

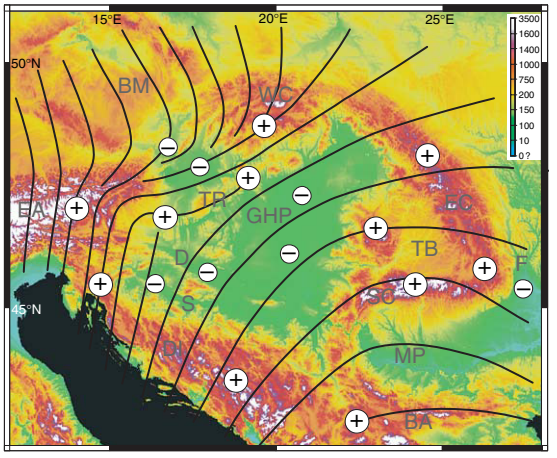

Figure 81 Topography of the Pannonian–Carpathian system showing present-day maximum horizontal stress (S_{Hmax}) trajectories (after Bada *et al.*, 2001). '+' and '−' symbols denote areas of Quaternary uplift and subsidence, respectively. BA: Balkanides; BM: Bohemian Massif; D: Drava Trough; DI: Dinarides; EA: Eastern Alps; EC: Eastern Carpathians; F: Focşani Depression; MP: Moesian Platform; PB: Pannonian Basin; S: Sava Trough; SC: Southern Carpathians; TB: Transylvanian Basin; TR: Transdanubian Range; WC: Western Carpathians. Modified from Cloetingh S, Bada G, Maţenco L, Lankreijer A, Horváth F, and Dinu C (2006). Thermo-mechanical modelling of the Pannonian-Carpathian system: Modes of tectonic deformation, lithospheric strength and vertical motions. In: Gee D and Stephenson R (eds.) *Geological Society, London, Memoirs*, 32: *European Lithosphere Dynamics*, pp. 207–221. London: Geological Society, London.

Therefore, the spatial distribution of uplifting and subsiding areas within the Pannonian Basin can be interpreted as resulting from the buildup of intraplate compressional stresses, causing large-scale positive and negative deflection of the lithosphere at various scales. This includes basin-scale positive reactivation of Miocene normal faults, and large-scale folding of the system leading to differential uplift and subsidence of anticlinal and synclinal segments of the Pannonian crust and lithosphere. Model calculations are in good agreement with the overall topography of the system (**Figure 81**). Several flat-lying, low-elevation areas (e.g., Great Hungarian Plain, Sava and Drava troughs) subsided continuously since the Early Miocene beginning of basin development and contain 300–1000 m thick Quaternary alluvial sequences. By contrast, the periphery of this basin system, as well as the Transdanubian Range, the Transylvanian Basin and the adjacent Carpathian orogen were uplifted and considerably eroded from Late Miocene–Pliocene times onward (see **Figures 70 and 82**). Quantitative subsidence analyses confirm that late-stage compressional stresses caused accelerated subsidence of the central parts of the Pannonian Basin (Van Balen *et al.*, (1999) whilst the Styrian Basin (Sachsenhofer *et al.*, 1997), the Vienna and East Slovak Basins (Lankreijer *et al.*, 1995), and the Transylvanian Basin (Ciulavu *et al.*, 2002) were uplifted by several hundred meters starting in Late Mio–Pliocene times (**Figure 70**). The mode and degree of coupling of the Carpathians with their foreland controls the Pliocene to Quaternary deformation patterns in their hinterland, and particularly interesting, in the Transylvanian Basin (Ciulavu *et al.*, 2002). During their evolution, the Western and Easter Carpathians were intermittently mechanically coupled with the strong European foreland lithosphere, as evidenced by coeval deformations in both the upper and lower plate (Krzywiec, 2001; Maţenco and Bertotti, 2000; Oszczypko, 2006). In terms of coupled deformation, the Carpathian Bend Zone had two distinct periods during its Tertiary evolution, that is, Early–Middle Miocene and Late Miocene–Quaternary. During the first period, the orogen was decoupled from its Moesian lower plate during the Middle Miocene (Badenian) as evidenced by contraction in the upper plate (e.g., Hippolyte *et al.*, 1999) and extensional collapse of the western Moesian Platform (Tărăpoancă *et al.*, 2003). During the Late Miocene collisional coupling

Figure 80 (a) Location of the additional load added to the topography (for discussion see text). (b) Deflection predicted for actual topographic load plus the additional 500 m load. Underlined numbers give the EET for each lithospheric block. Deflection isolines in metres. (c) Cross-sections showing actual and predicted basin depths (for location see (b)). Solid line: observed basin depth; gray line: deflection for 500 m additional topographic load; dashed line: deflection for 800 m additional topographic load. (d) Deflection predicted (map view and cross section) for additional 500 m topographic load combined with an N–S directed intraplate compressional stress of 2×10^{12} N m^{-1}. Solid, gray, and dashed lines as in (c). Modified from Tărapoăncă M, Garcia-Castellanos D, Bertotti G, Maţenco L, Cloetingh S, and Dinu C (2004a) Role of 3-D distributions of load and lithospheric strength in orogenic arcs: polystage subsidence in the Carpathians foredeep. *Earth and Planetary Science Letters* 221: 163–180.

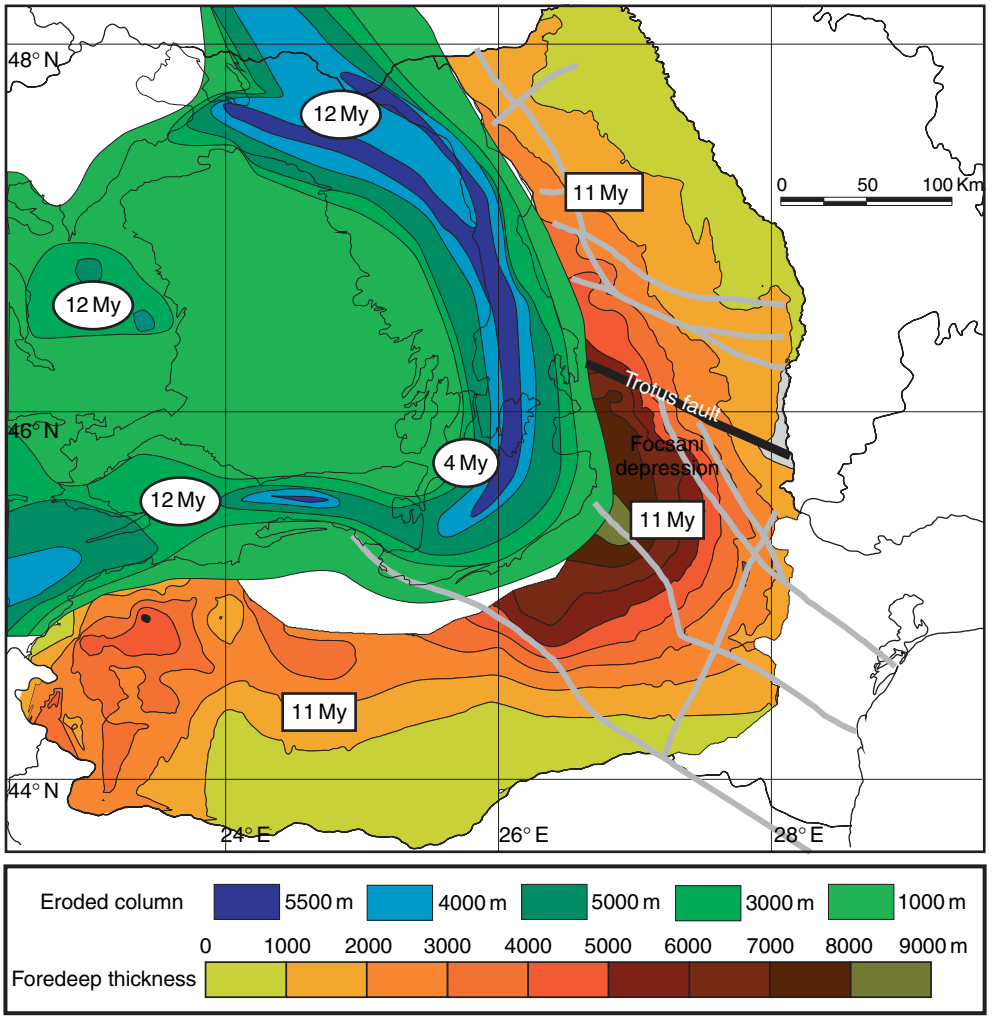

Figure 82 Contours of amount of erosion (km) inferred from fission track analyses in the Romanian Carpathians and Apuseni Mts. (Sanders *et al.*, 1999) and isopachs of sediment thickness in the foreland basin (km). Numbers in elliptic boxes indicate timing of erosion onset in Ma. Numbers in square boxes indicate timing of main subsidence. Note the pronounced lateral differences in uplift ages along the arc, while the main subsidence period is essentially coeval. Modified from Cloetingh S, Bada G, Maţenco L, Lankreijer A, Horváth F, and Dinu C (2006). Thermo-mechanical modelling of the Pannonian-Carpathian system: Modes of tectonic deformation, lithospheric strength and vertical motions. In: Gee D and Stephenson R (eds.) *Geological Society*, *London*, *Memoirs*, 32: *European Lithosphere Dynamics*, pp. 207–221. London: Geological Society, London.

between the orogenic wedge and the foreland increased and persisted to the present (e.g., Bala *et al.*, 2003).

Fission track studies in the Romanian Carpathians demonstrate up to 5 km of erosion that migrated since 12 Ma systematically from their northwestern and southwestern parts towards the Bend area where uplift and erosion was initiated around 4 Ma ago (Sanders *et al.*, 1999) (**Figure 82**). This region coincides with the actively deforming Vrancea zone that is associated with considerable seismic activity at crustal levels and in the mantle (**Figure 72**). These findings can be related to the results of seismic tomography that highlight upwelling of hot mantle material under the Pannonian Basin and progressive detachment of the subducted lithospheric slab that is still ongoing in the Vrancea area (Wortel and Spakman, 2000; Wenzel *et al.*, 2002). Moreover, in the internal parts of the Carpathians, magmatic activity related to slab detachment decreases

systematically in age from 16–14 Ma in their northern parts to 4–0 Ma in the Bend Zone (Nemcok *et al.*, 1998). As such, it tracks the uplift history of the Carpathians that can be related to isostatic rebound of the lower plate upon slab detachment. These rapid differential motions along the rim of the Pannonian Basin and in the adjacent Carpathians had important implications for the sediment supply to depocenters, as well as for the hydrocarbon habitat (Dicea, 1996, Tari *et al.*, 1997, Horváth and Tari, 1999).

In summary, results of forward basin modeling show that an increase in the level of compressional tectonic stress during Pliocene–Quaternary times can explain the first-order features of the observed pattern of accelerated subsidence in the center of the Pannonian Basin and uplift of basins in peripheral areas. Therefore, both observations (see Horváth *et al.*, 2006) and modeling results lead to the conclusion that compressional stresses can cause considerable differential vertical motions in the Pannonian–Carpathian back-arc basin–orogen system.

In the context of basin inversion, the sources of compression were investigated by means of finite element modeling (Bada *et al.*, 1998, 2001). Results suggest that the present stress state of the Pannonian–Carpathian system (**Figure 81**), and particularly of its western part, is controlled by the interplay between plate boundary and intraplate forces. The former include the counterclockwise rotational northward motion of the Adriatic microplate and its indentation into the Alpine-Dinaridic orogen, whereas intraplate buoyancy forces are associated with the elevated topography and related crustal thickness variation of the Alpine–Carpathian–Dinarides belt (**Figure 65**). Model predictions indicate that uplifted regions surrounding the Pannonian basin system can exert compression of about 40–60 MPa on its thinned lithosphere, comparable to values calculated for far-field tectonic stresses (Bada *et al.*, 2001). The analysis of tectonic and gravitational stress sources permitted to estimate the magnitude of maximum horizontal compression, amounting to as much as 100 MPa. These significant compressional stresses are concentrated in the elastic core of the lithosphere, consistent with the ongoing structural inversion of the Pannonian Basin. Such high-level stresses are close to the integrated strength of the system, which may lead to whole lithospheric failure in the form of large-scale folding and related differential vertical motions, and intense brittle deformation in the form of seismo-active faulting.

6.11.7 The Iberia Microcontinent: Compressional Basins within the Africa–Europe Collision Zone

By mid-Cretaceous times, the Iberian microcontinent, including Corsica-Sardinia, was separated from Europe owing to opening of the Bay of Biscay–Valaisan Ocean. By this time, Iberia was flanked to the southeast by the Alpine-Tethys that had opened during the Middle Jurassic, and to the west by the North Atlantic that had started to open during the Early Cretaceous (Stampfli *et al.*, 1998, 2001, 2002). With the Late Cretaceous onset of Africa–Europe convergence (Rosenbaum *et al.*, 2002), the Pyrenean and Betic–Balearic orogens evolved along the northern and southeastern margins of Iberia, respectively. Closure of the Pyrenean rift commenced during the Late Senonian and involved northward subduction of the continental Iberian lithosphere beneath Europe and southward subduction of the oceanic Bay of Biscay beneath Iberia. Evolution of the Pyrenean–Cantabrian orogen, in which crustal shortening persisted until end-Oligocene times, was accompanied by a gentle clockwise rotation of Iberia, causing reactivation of fault systems along its Atlantic margin (Munoz, 1992; Vergés *et al.*, 1998; Vergés and Garcia-Senez, 2001). Northwestward subduction of the oceanic Alpine-Tethys beneath Iberia was initiated during the latest Cretaceous–Paleocene. During the Late Oligocene–Early Miocene, roll-back of the Alpine-Tethys slab commenced, giving rise to back-arc extension in the Gulf of Lions and the domain of the Valencia Trough, culminating in Burdigalian separation of Corsica-Sardinia from Iberia and the opening of the oceanic Ligurian–Provençal Basin (Roca, 2001). At the same time, separation of the Kabylian block from the Balearic promontory resulted in opening of the oceanic Algerian Basin. Crustal shortening in the evolving Betic–Balearic Orogen persisted until mid-Miocene times, when the Kabylian–Alboran terrane collided with the African margin (Frizon de Lamotte *et al.*, 2000). Minor late Miocene to Pleistocene extensional reactivation of the Valencia Trough (Roca, 2001) was accompanied by the extrusion of mantle-derived partial melts in NE Iberia (Olot-Gerona-La Selva), on the Colombretes Island and in the Calatrava province (Wilson and Bianchini, 1999).

During the late Eocene and Oligocene, the cratonic parts of Iberia were subjected to intraplate compressional stresses, originating at the Pyrenean

and Betic–Balearic collision zones, causing inversion of the Mesozoic rifted Catalan Coastal Ranges and the Central Iberian basins and up-thrusting of the Central Spanish basement block. During the Late Oligocene and Early Miocene extensional stresses controlled subsidence of the Valencia Trough that was associated with thermal thinning of the lithosphere (Banda and Santanach, 1992). Regarding the latter, it is noteworthy that the NE Atlantic mantle plume was activated during the Campanian–Maastrichtian, as evidenced by magmatic activity in southern Portugal (Hoernle *et al.*, 1995; Tavares Martins, 1998). Similarly, Late Miocene to Pleistocene magmatic activity along the eastern margin of Iberia may be plume related.

Seismic tomography indicates that the subducted Alpine-Tethys slab is still attached to the African lithosphere in the area of the Rif fold belt but that a slab window gradually opened eastward (Wortel and Spakman, 2000). This is compatible with Late Miocene slab detachment-related magmatic activity in the Maghrebian domain (Wilson and Bianchini, 1999). Subduction activity apparently ceased in the Pyrenean and Betic collision zones at end Oligocene and mid-Miocene times, respectively, with remnant deep seismicity being restricted to the southeastern margin of Iberia (Blanco and Spakman, 1993). Nevertheless, continued convergence of Africa with Europe is held responsible for still ongoing intraplate deformation of Iberia that is manifested, amongst others, by earthquake activity concentrated on the Pyrenees, the Betic Orogen, the Central Iberian and Catalan Coastal Ranges, and the Atlantic coastal domain. Controlling stresses are related to collisional coupling between the African and European plates and the intervening Iberian microplate and to Atlantic ridge-push forces (**Figures 83** and **84**).

Figure 85 shows the main Neogene structural features of Iberia and the magnitude of Plio-Pleistocene uplift of its different parts. Although mechanisms underlying the observed vertical motions are not fully resolved, processes such as slab detachment and/or lithospheric delamination appear to play a minor role (Janssen *et al.*, 1993; Docherty and Banda, 1995; Seber *et al.*, 1996), whereas mantle plume-related thermal thinning of the lithosphere cannot be excluded, for example, NE Iberia. This is compatible with available geophysical data on the upper mantle structure (Blanco and Spakman, 1993; Seber *et al.*, 1996). On the other hand, along the eastern margin of Iberia, rift shoulder uplift, related to the Late Neogene extensional reactivation of the Valencia Trough (Janssen *et al.*, 1993) and the Alboran Sea (Docherty and Banda, 1995; Cloetingh *et al.*, 1992) may be a contributing factor. However, recent analyses of the stress field,

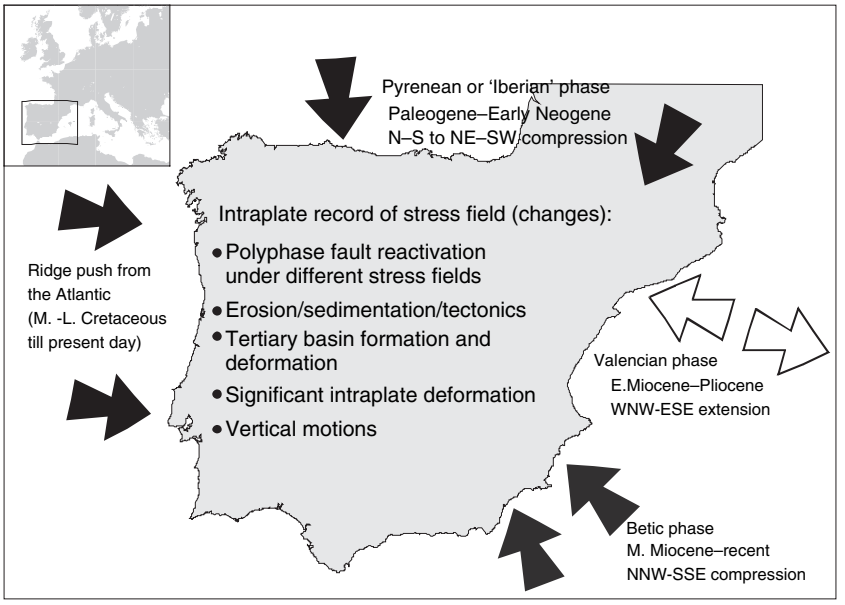

Figure 83 Plate-tectonic setting of Iberia and timing of Alpine to recent plate boundary reorganizations, their impact on intraplate deformation of the Iberian microcontinent and related basin (de)formation processes within Iberian and along its Atlantic and West Mediterranean margins. Modified from Cloetingh S, Burov E, Beekman F, Andeweg B, Andriessen PAM, Garcia-Castellanos D, de Vince G, and Vegas R (2002) Lithospheric folding in Iberia. *Tectonics* 21(5): 1041 (doi:10.1029/2001TC901031).

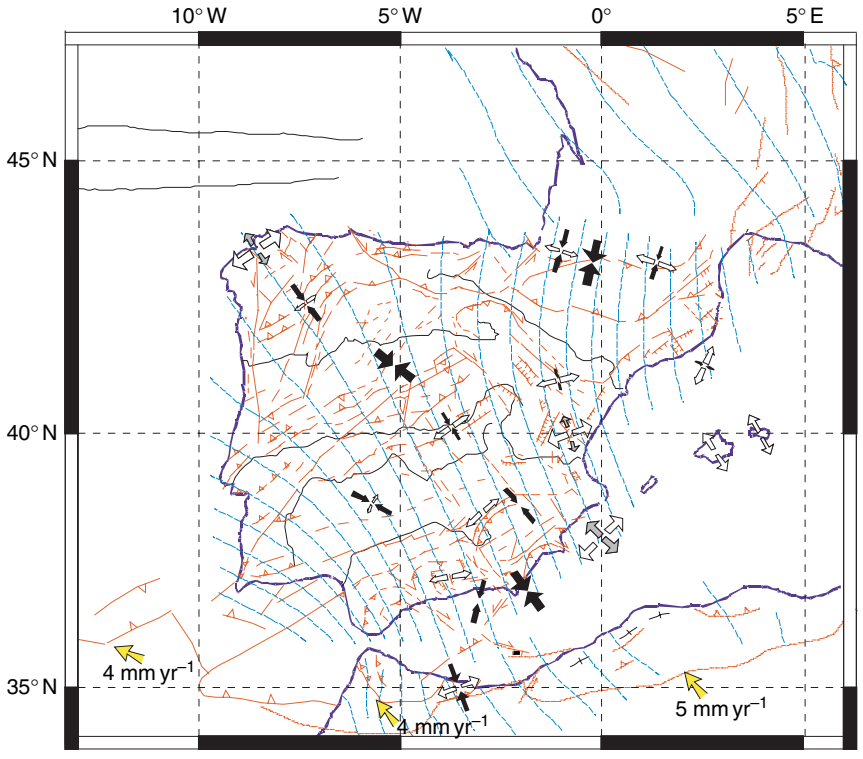

Figure 84 Present-day stress trajectories (thin blue lines) in Iberia and the western Mediterranean, based on fault slip data, borehole breakout data, and focal mechanisms (black and white arrows). Thin redlines: major tectonic structures and lineaments. The spatial orientation ('fanning') of the first-order present-day stress regime suggests a strong control by plate boundary processes (Africa/Eurasia collision, Atlantic ridge push) and large-scale weakness zones, such as formerly active plate boundaries (Pyrenees, Betics). Modified from Andeweg B, De Vincente G, Cloetingh S, Giner J, and Muñoz Martin A (1999) Local stress fields and intraplate deformation of Iberia: variations in spatial and temporal interplay of regional stress sources. *Tectonophysics* 305: 153–164.

topography evolution, and gravity data indicate that folding of the continental lithosphere of Iberia played an important, if not the dominant, role in its Late Neogene and Quaternary deformation. Indeed, recent studies provide increasing evidence for a strong contribution of crustal-scale kinematics on the record of vertical motions of the Iberian Peninsula (e.g., Friend and Dabrio, 1996; Casas-Sainz *et al.*, 2000).

In the following, novel concepts are presented on the control of lithospheric deformation on the development of drainage patterns, crustal topography, and intracontinental basins that are based on an integrated approach, linking structural field studies, thermogeochronology and modeling of lithospheric and surface processes (see Cloetingh *et al.*, 2002, 2005).

6.11.7.1 Constraints on Vertical Motions

Palaeogeographic constraints indicate that during Late Cretaceous times much of Iberia was located close to sea level with the West Iberian Massif and the area of the future Ebro Basin forming low-relief highs (Stampfli *et al.*, 2001, 2002). However, today large parts of cratonic Iberia are located at elevations of 750–1000 m, with areas affected by Late Eocene to Oligocene intraplate compression forming up to 1500 m high mountain chains (**Figure 86**).

In order to determine the timing of uplift of cratonic Iberia to its present elevation, apatite fission track studies were carried out on its Mediterranean (Stapel *et al.*, 1996) and Atlantic margins (Stapel, 1999), on the Spanish Central System (De Bruijne and Andriessen, 2000, 2002), on the Betics (Zeck *et al.*, 1992), and on the Pyrenees (Fitzgerald *et al.*, 1999). These studies evidence a rapid post-Miocene cooling phase (uplift and erosion) for topographically high areas along the western and eastern margin of Iberia (**Figure 87**), as well as for the Spanish Central System (**Figure 88**). For the latter, results indicate that an initial Late Eocene to Early Oligocene uplift phase, associated with compressional deformations,

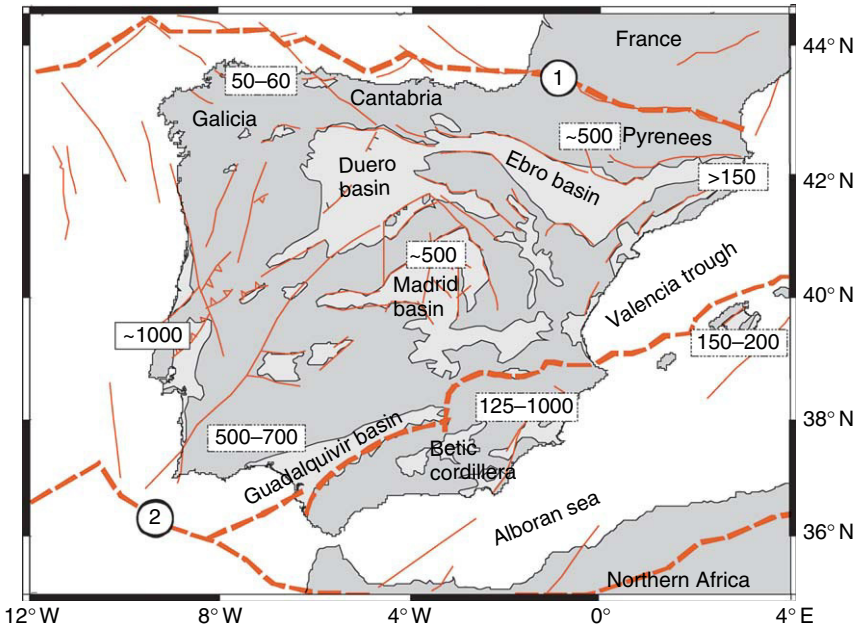

Figure 85 Tectonic map of Iberia, showing main structural features and sedimentary basins, its northern [1] and southern [2] plate boundaries, and Pliocene–Quaternary uplift patterns (numbers in boxes give estimated magnitude of uplift in meters). Modified from Cloetingh S, Burov E, Beekman F, Andeweg B, Andriessen PAM, Garcia-Castellanos D, de Vince G, and Vegas R (2002). Lithospheric folding in Iberia. *Tectonics* 21(5): 1041 (doi:10.1029/2001TC901031).

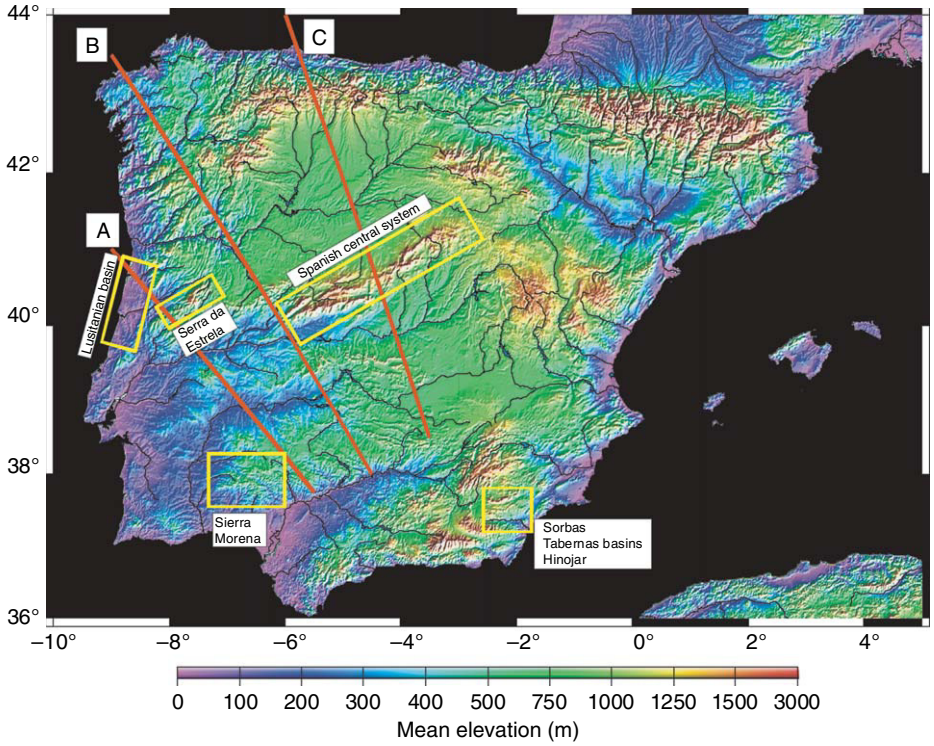

Figure 86 Digital elevation model of Iberia (data from GTOPO30). Yellow boxes refer to location of sites sampled for quantitative subsidence analyses and fission-track analyses for exhumation quantification (see also **Figures 87** and **88**). A, B, and C mark the location of profiles given in **Figure 90**. Modified from Cloetingh S, Burov E, Beekman F, Andeweg B, Andriessen PAM, Garcia-Castellanos D, de Vince G, and Vegas R (2002) Lithospheric folding in Iberia. *Tectonics* 21(5): 1041 (doi:10.1029/2001TC901031).

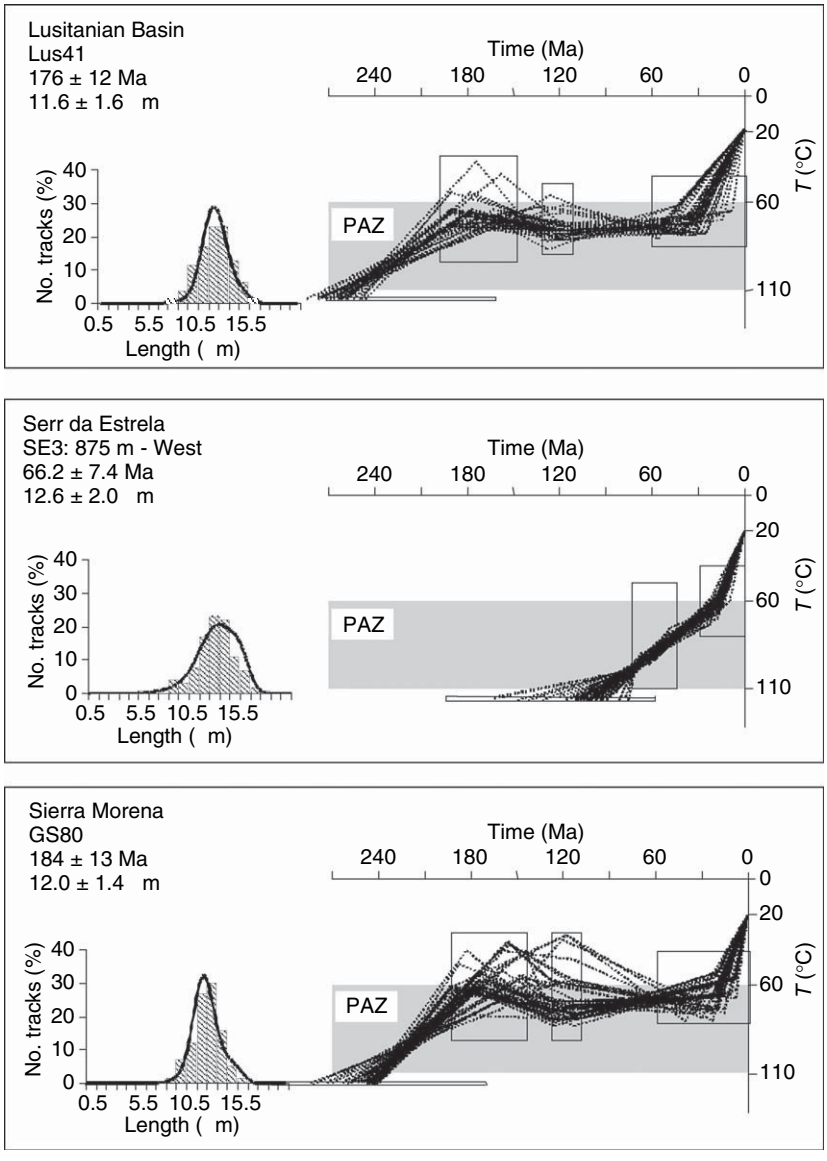

Figure 87 Constraints on timing and magnitude of Late Neogene vertical motions derived from quantitative subsidence and fission-track analyses for samples from western Iberia (LB Lusitanian Basin, SE Serra da Estrela) and from southern–western Iberia (SM Sierra Morena). Plotted is a range of cooling histories that fit the fission-track age and track length distribution. Also shown are Monte-Carlo boxes based on information from fission-track data and geologic observations. The gray-shaded area is the partial annealing zone (PAZ). Modified from Stapel G (1999) *The Nature of Isostasy in Western Iberia*. PhD thesis, Vrije Universiteit, Amsterdam, 148p.

was followed by significant cooling during Middle Miocene times (15 Ma) and a pronounced cooling acceleration from the Early Pliocene (5 Ma) onward (De Bruijne and Andriessen, 2000). In the eastern part of the Spanish Central System, the Sierra de Guadarrama, Pliocene uplift and erosion amounted to up to 6 km (Ter Voorde et al, 2004; De Bruijne and Andriessen, 2000). Results of precision levelling and VLBI laser ranging (Rutigliano *et al.*, 2000) indicate present vertical uplift rates of about 1 mm yr^{-1} for the Spanish Central System.

For the Betics, thermal modeling of fission track data supports a scenario of enhanced uplift and erosion from Pliocene times onward until the present (Ter Voorde *et al.*, 2004). This is further supported by the results of backstripping analyses and forward modeling of the sedimentary record of Neogene pull-apart basins that are superimposed on the Betic

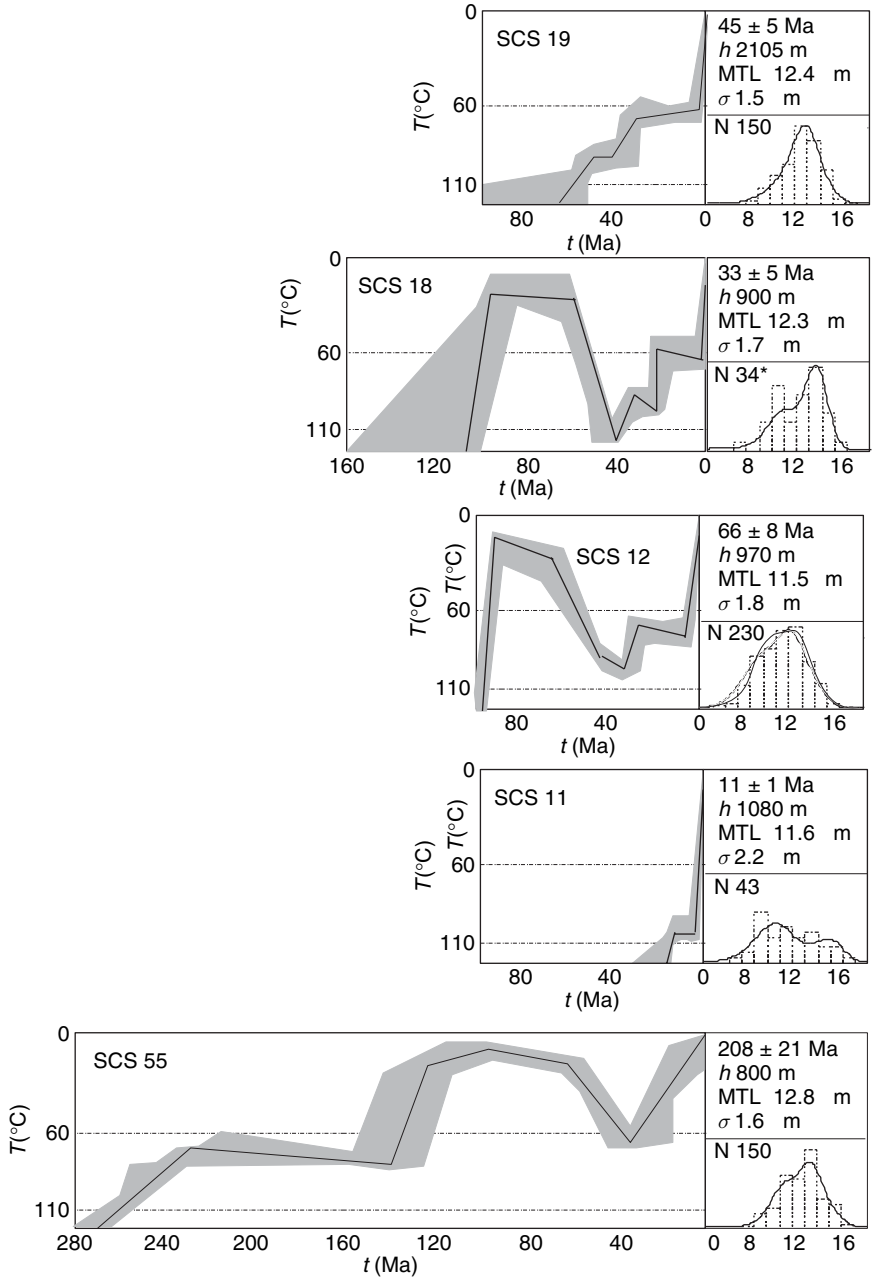

Figure 88 Constraints on timing and magnitude of Late Neogene vertical motions derived from quantitative subsidence and fission-track analyses. .Fission-track ages, track length distributions, and thermal histories giving the best-fit data for five samples from the Spanish Central System (SCS). Thermal histories were obtained with the Monte Trax program and are shown as black lines within the 100-best-fit envelopes (gray shaded). The modeled track length distributions are projected on the measured track length distribution. Modified from De Bruijne and Andriessen (2000, 2002).

Cordillera (**Figure 89**), revealing that they were uplifted and eroded during the Pliocene–Quaternary by some 500 m (Cloetingh *et al.*, 2002; Janssen *et al.*, 1993; Docherty and Banda, 1995). Moreover, on the base of Late Miocene marine sediments that were uplifted by more than 1200 m in intramontane basins of the Betic Cordillera, Plio-Pleistocene shortening and related uplift is documented (Andeweg and Cloetingh, 2001).

Initial results of GPS surveys point toward a consistently northwest directed horizontal motion of Iberia at rates of about 5 mm yr^{-1} (Fernandes *et al.*,

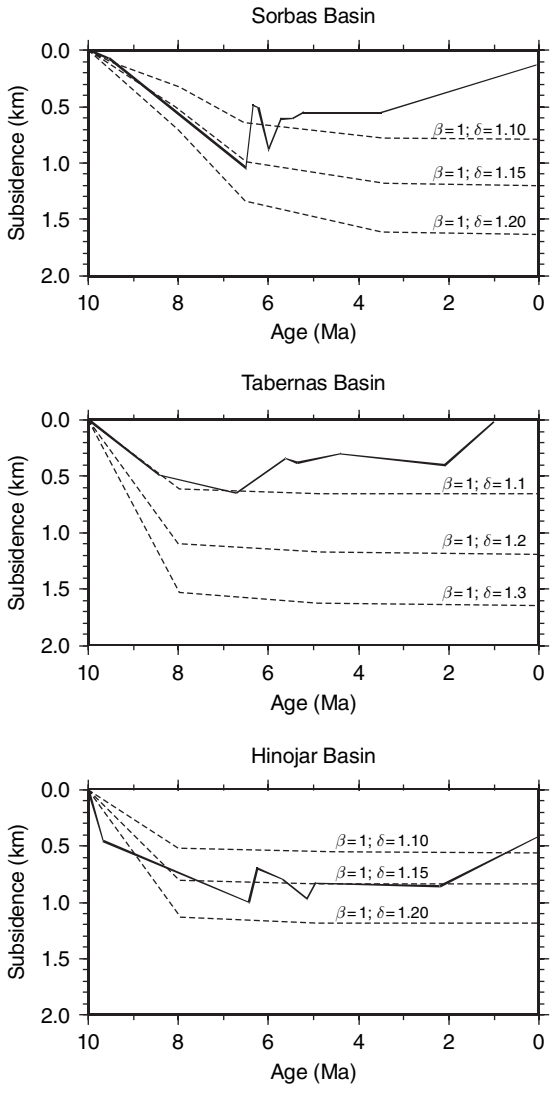

Figure 89 Tectonic subsidence curves (bold lines) for three Late Neogene pull-apart basins in the internal zone of the Betic Cordilleras (SE Spain). Thin lines are theoretical subsidence curves calculated for differential stretching of the crust ($\delta \neq 1$) and in the absence of mantle stretching ($\beta = 1$). Note that all basins show accelerated Late Plio-Quaternary uplift that strikingly deviates from prediction of thermal basin subsidence models. Modified from Cloetingh S, Ziegler PA, Beekman F, Andriessen PAM, Matenco L, Bada G, Garcia-Castellanos D, Hardebol N, Dézes P, and Sokoutis D (2005) Lithospheric memory, state of stress and rheology: Neotectonic controls on Europe's intraplate continental topography. *Quaternary Science Reviews* 24: 241–304.

2000). This raises the question whether the observed Plio-Quaternary vertical motions are related to folding of the Iberian lithosphere (Andeweg and Cloetingh, 2001), thus differentially amplifying its topography.

6.11.7.2 Present-Day Stress Regime and Topography

The present-day stress map of Iberia, given in **Figure 84**, is based on borehole break-out data, earthquake focal mechanisms and microtectonic stress indicators (Zoback, 1992; Ribeiro *et al.*, 1996; De Vicente *et al.*, 1996; Andeweg *et al.*, 1999). Iberia is characterized by a consistent horizontal compressional stress field that is dominated by northwest-directed stress trajectories fanning out in Portugal into a more westerly direction and in northeastern Spain into a northerly direction. This stress field reflects a combination of forces related to collisional coupling between Africa, Iberia and continental Europe, and Atlantic ridge-push. Northwestward movement of Africa at rates of 4–5 mm yr^{-1} is apparently compensated by crustal shortening in the seismically active Maghrebian, Betic, and Pyrenean zones, as well as by deformation of cratonic Iberia.

The topography of cratonic Iberia is characterized by a succession of roughly NE–SW trending highs and intervening lows (**Figure 90**). From northwest to southeast, these are the river Miño, the mountains of Cantabria/Leon, the Duero-Douro river basin, the Spanish Central System, the Tajo river basin, the Toledo Mountains, the river Guadiana, the Sierra Morena, and the Guadalquivir Basin. These topographic highs and lows trend normal to the present-day intraplate compressional stress trajectories, and essentially run parallel to similar trending Bouguer gravity anomalies (Cloetingh *et al.*, 2002).

The magnitude of Plio-Pleistocene vertical motions and the results of precision leveling suggest that processes controlling topography development are still ongoing and exert a first-order control on the present topographic configuration of Iberia. The observed Bouguer gravity anomalies reflect long-wavelength undulations of deep intralithospheric density interfaces, such as the crust–mantle boundary (Cloetingh and Burov, 1996), and thus mirror deformation of the entire lithosphere. Whereas a correlation between long-wavelength Bouguer gravity and topographic anomalies (**Figure 90**) speaks for coupled crustal and lithospheric mantle folding, the lack of such a correlation speaks for their decoupled folding (Cloetingh *et al.*, 1999). As so far there is no conclusive evidence from seismic tomography for a thermally perturbed upper mantle underlying most of Iberia (Wortel and Spakman, 2000), apart from its NE region (Spakman and Wortel, 2004; Sibuet *et al.*, 2004), the question remains open whether its high

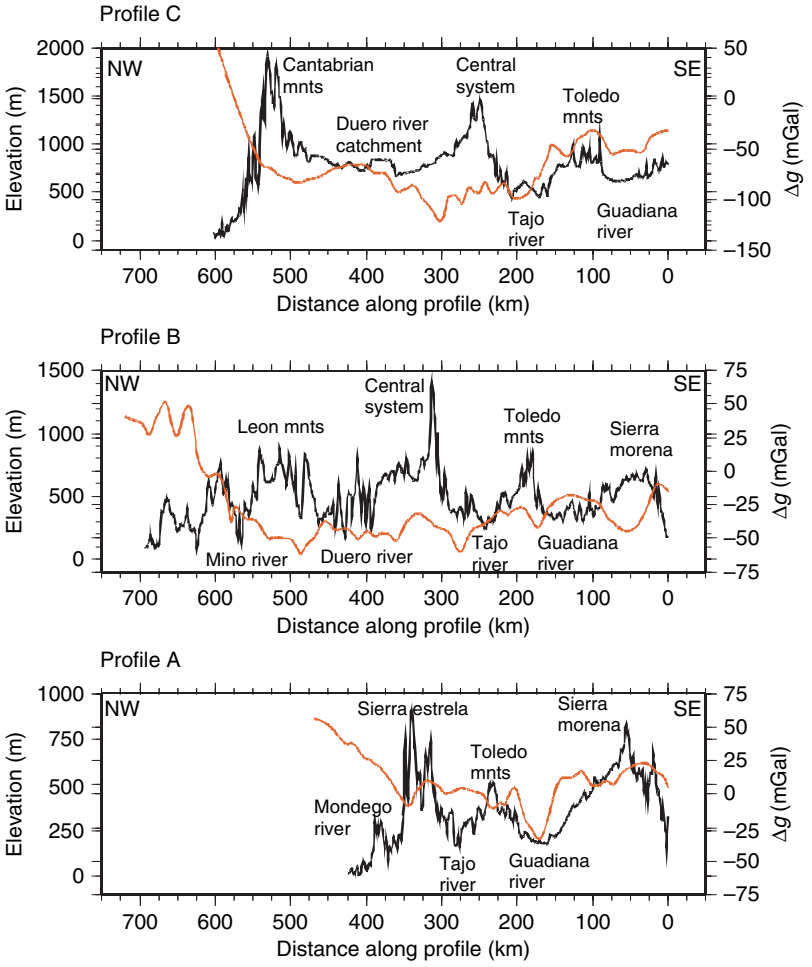

Figure 90 Topographic profiles across Iberia (black curves) compared to Bouguer gravity anomalies (red curves). For location see **Figure 86**. Modified from Cloetingh S, Burov E, Beekman F, Andeweg B, Andriessen PAM, Garcia-Castellanos D, de Vicente G, and Vegas R (2002) Lithospheric folding in Iberia. *Tectonics* 21(5): 1041(doi:10.1029/2001TC901031).

average elevation is caused by a large-scale asthenospheric thermal anomaly, giving rise to a gravity signal with a wavelength of over 500 km.

6.11.7.3 Lithospheric Folding and Drainage Pattern

For central Iberia, thermal modeling of fission track data favours a Plio-Pleistocene phase of uplift and erosion rather than a Miocene uplift phase followed by erosion (Ter Voorde *et al.*, 2004). In response to lithospheric folding, elevated areas will be subjected to erosion whereas sediments will accumulate in topographic lows. Whereas erosional unroofing of structural highs causes their isostatic uplift, sedimentary loading causes flexural subsidence of structural lows. However, the drainage pattern of Iberia removes all erosion products and deposits them on the Atlantic and Mediterranean continental shelves. Numerical modeling of the evolution of drainage networks (Garcia-Castellanos, 2002; Garcia-Castellanos *et al.*, 2003) shows that surface transport processes can effectively enhance the tectonically induced large-scale continental topography. Despite the intrinsic nonlinear nature of drainage networks, moderate vertical movements appear also to be able to organize drainage patterns in relatively flat areas where drainage is not well-organized or incised (Garcia-Castellanos, 2002).

Under the temperate climatic conditions, which characterized Iberia during most of the Cenozoic, rivers accounted for most of the surface mass transport. River catchments have typically strong 3-D asymmetries since their drainage is hierarchically organized to collect the waters and sediment from a

widespread area and channel them into a single outlet. This implies that whereas erosion affects large headwater catchment areas, deposition is localized along the lower riverbeds, around the river mouths in the Atlantic Ocean and Mediterranean and in possible intermediate lakes (**Figure 86**). Modeling also permits to analyze possible feedback mechanisms between this asymmetric surface transport and lithospheric folding (Cloetingh *et al.*, 2002, 2005).

To further evaluate the interplay between surface transport and lithospheric folding, fluvial transport can be simulated via a drainage network in which runoff water flows along the maximum slope with a sediment transport capacity proportional to the slope and water discharge (Garcia-Castellanos *et al.*, 2003). Implementation of this approach, which intrinsically predicts planform hierarchical organization of drainage networks, is based on the relationships established by Beaumont *et al.*, (1992) that were adopted in several subsequent studies (e.g., Kooi and Beaumont, 1996; Braun and Sambridge, 1997; Van der Beek and Braun, 1998). Analyses focused on the first-order features of the interplay between fluvial transport and folding, rather than on the properties of fluvial transport. Furthermore, the applied model incorporated sediment deposition in topographic minima (lakes) and in the Atlantic Ocean, thus allowing for modeling of closed transport systems in which virtually all eroded material is deposited within the model (for details see Garcia-Castellanos, 2002).

Lithospheric folding was calculated as the response of a thin homogeneous viscoelastic 2-D (plan form) thin-plate to tectonic loading (horizontal load) and surface mass redistribution (vertical load). The equation governing deformation of this plate was derived by applying the principle of correspondence between elasticity and viscoelasticity (Lambeck, 1983) to the equivalent elastic equation (e.g., Van Wees and Cloetingh, 1994). The 3D response of this plate to lithosphere shortening was calculated, adopting an EET of 30 km. This value corresponds to a mechanically coupled crust and lithospheric mantle with a thermotectonic age of 350 Ma that is consistent with results of a flexural analysis on the Ebro Basin of northeastern Spain (Gaspar-Escribano *et al.*, 2001). A viscous relaxation time of 1.2 My was adopted from a recent flexural analysis of the Guadalquivir Basin (southern margin of the Iberian Massif) (Garcia-Castellanos *et al.*, 2002). The initial configuration of the synthetic models is a flat, square continent elevated to 400 m above sea level with a random perturbation between −10 and +10 m.

Figure 91(a) shows the drainage network that developed after a period of 12 My of N–S directed horizontal compression (see Appendix 2 for a detailed description of the modeling approach). The main axes of topographic linear highs and lows predicted by the plan-view synthetic models are perpendicular to the main axes of shortening. This corresponds with the actually observed relationship between topography and stress field, with large-scale topographic linear highs and lows perpendicular to the main axis of present-day intraplate compression in Iberia (**Figure 84**). In this figure the smooth patterns of vertical motions indicate that river sediment transport plays a key role in defining the location of subsequent folding vertical motions. Note that these models illustrate the conceptual link between intraplate compression, lithospheric folding, and surface processes; an NW–SE oriented main axis of shortening (**Figure 84**) would rotate the main axis of drainage and erosion and sedimentation into an NE–SW orientation, more closely corresponding to the topography of Iberia (**Figure 86**). The drainage pattern is clearly controlled by the ~350 km wavelength of lithospheric folds. A reduction of the EET to 18 km, closer to the values found in the Guadalquivir Basin (Garcia-Castellanos *et al.*, 2002), reduces this characteristic wavelength to 220 km. During the initial stages of compression, the peneplain geometry limits erosion and deposition to the vicinity of the shoreline, whereas the interior of the continent remains almost unperturbed. Interestingly, vertical isostatic movements associated with this initial mass transport near the shoreline play a role as perturbations that trigger folding. Consequently, maximum uplift occurs along the N and S shores, as they trend normal to the compression axis.

Inversely, the organization of drainage system has also important effects on vertical motions. This is illustrated by a comparison of **Figures 91(a)** and **91(b)** with an identical model in which transport is diffusive (**Figure 91(c)**), adopting a value of $k_e = 33.0$ $m^2\,yr^{-1}$. Although the chosen diffusive constant to produce a total transport of sediments is similar to the previous model ($71.9 \times 10^3\,km^3$), the spatial organization of the drainage pattern strongly influenced the spatial mass redistribution. Deposition is localized near the main river mouths and in phase with vertical motions, since drainage is forced along the E–W trending folding-induced depressions (**Figure 91(a)**). This accentuates the folding pattern off the W shore, at $x < -420$ km. By contrast, a diffusive approach to surface transport does not introduce

relevant asymmetries in the folding pattern (**Figure 91(c)**), apart from some overprinting along the western, Atlantic margin of Iberia.

6.11.7.4 Interplay between Tectonics, Climate, and Fluvial Transport during the Cenozoic Evolution of the Ebro Basin (NE Iberia)

Endorheic drainage basins, also referred to as landlocked, internally drained or closed drainage basins, are essential for understanding the evolution of sedimentary basins because they do not fit the notion that erosion products of orogens are par force carried to the oceans. Particularly in intraorogenic settings, such as the Altiplano or the Tibetan Plateau, endorheic basins can trap important sediment volumes at high elevations above sea level (e.g., Sobel *et al.*, in press). Endorheic basins occupy, 20% of the Earth's land surface but collect only about 2% of the global river runoff, reflecting that they develop mostly under arid conditions. The Ebro Basin is a well-documented example of a long-lasting intraorogenic endorheic basin, the deposits of which are presently located at more than 1000 m above sea level. Because the sedimentary fill of the Ebro Basin has been heavily incised and exposed

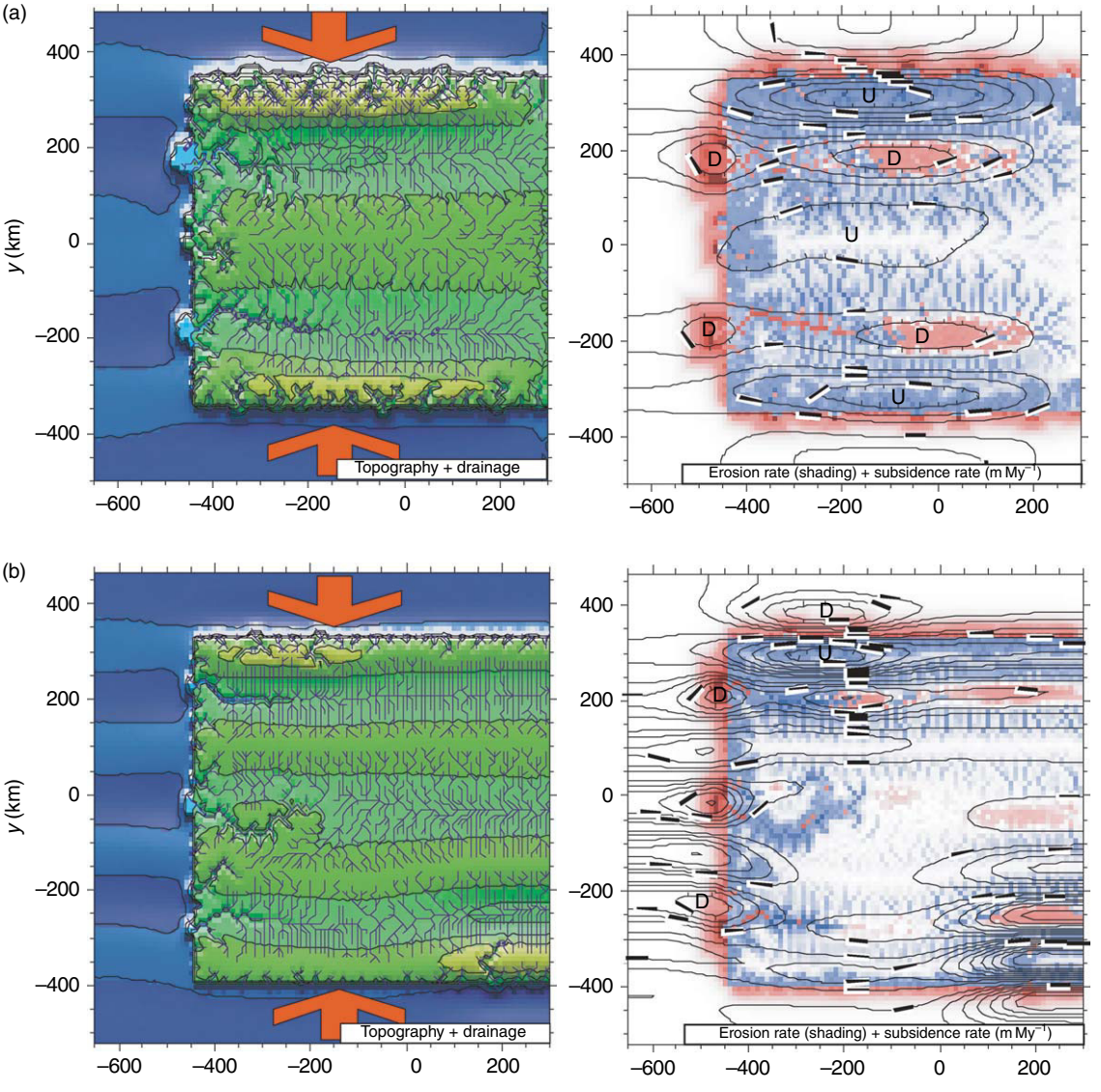

Figure 91 (*Continued*)

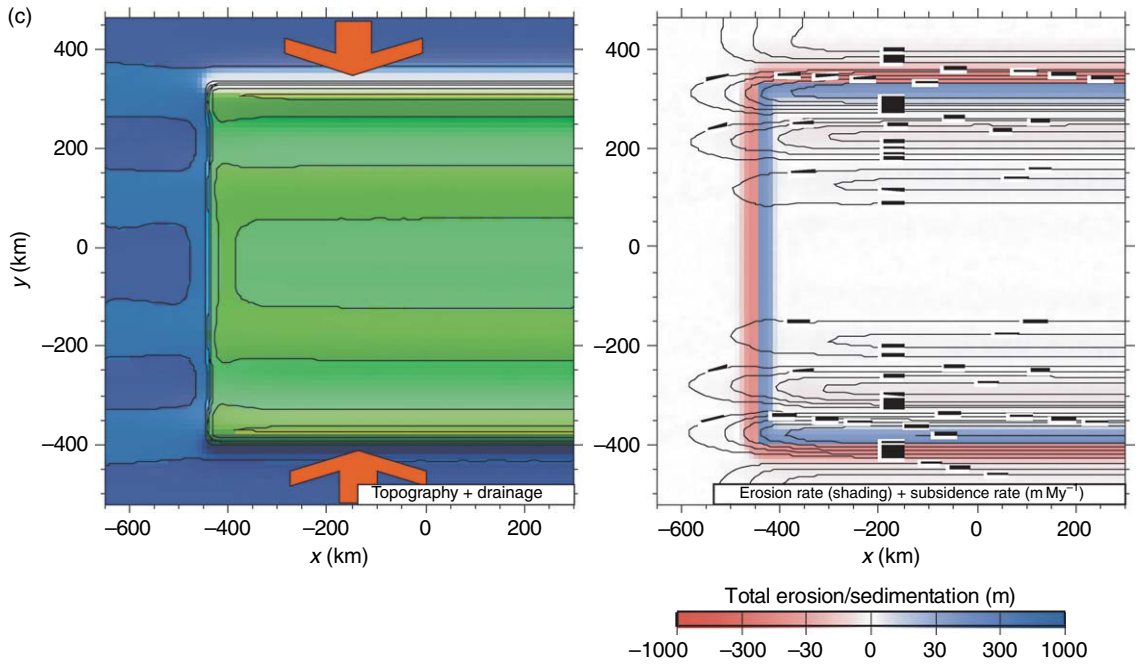

Figure 91 Synthetic models (map view) for the interplay between lithospheric folding, surface erosion, and sedimentation. An initially flat, square continent with dimensions representative for Iberia was adopted. The thickness of rivers is plotted proportional to their water discharge. Contours indicate vertical motions (m) induced by N–S directed compression during 12 My and the resulting isostatic response of the model to surface mass transport. Upper panels show topography and drainage networks. Lower panels show cumulative erosion/deposition (shading) and vertical motions (contours in m). For details and model parameter specifications, see Appendix 2. (a) Model incorporating superimposed lithospheric folding and fluvial transport through a drainage network adopting an EET of 30 km. (b) Same as (a) but adopting an EET of 18 km. (c) Same as (b) but adopting a diffusive model for mass redistribution. Modified from Cloetingh S, Ziegler PA, Beekman F, Andriessen PAM, Maţenco L, Bada G, Garcia-Castellanos D, Dèzes P, and Sokoutis D (2005) Lithospheric memory, state of stress and rheology: Neotectonic controls on Europe's intraplate continental topography. *Quaternary Science Reviews* 24: 241–304.

owing to late-stage opening of its drainage toward the Mediterranean (**Figure 92**), it serves as a natural laboratory to study the interplay between tectonics, climate, and sediment transport (e.g., Arenas *et al.*, 2001).

The Ebro Basin is rimmed by three Alpine mountain ranges (**Figure 92**), namely by the collisional Pyrenees to the N and the Catalan Coastal Ranges and the Iberian Range to the SE and SW, respectively, that represent inverted Mesozoic rifted basins. Development of the Ebro Basin began during the Paleocene in response to its flexural subsidence in the prowedge foreland of the evolving Pyrenees (Vergés *et al.*, 1998). Inversion of the Catalan Coastal Ranges and the Iberian Range commenced during the early Middle Eocene and persisted until the Late Oligocene (Roca *et al.*, 1999). Uplift of these ranges resulted in earliest Late Eocene closure of connections between oceanic domains and the Ebro Basin. With this, its endorheic stage commenced that lasted through Oligocene and most of Miocene times (Riba *et al.*, 1983). During this stage, syn- and postorogenic conglomerate fans prograded from the Iberian Range, the Catalan Coastal Ranges and the rapidly rising Pyrenees into the tectonically silled Ebro Basin, burying the frontal Pyrenean thrust elements, and giving way to distal lacustrine sediments (Coney *et al.*, 1996).

During the latest Oligocene and Early Miocene rifting phase of the Valencia Trough, tensional reactivation of reverse faults of the Catalan Coastal Ranges resulted in their gradual breakdown. By late Middle Miocene times the deltaic complex of the Castellón Group (Serravallian–early Messinian) began to prograde into the Valencia Trough, reflecting the gradual development of the modern Ebro drainage system (Bartrina *et al.*, 1992; Banda and Santanach, 1992; Vergés and Sàbat, 1999; Roca, 2001). The internal drainage of the Ebro Basin was open to the Mediterranean in the course of the Late Miocene in response to progressive incision and backcutting of the evolving river Ebro, exposing

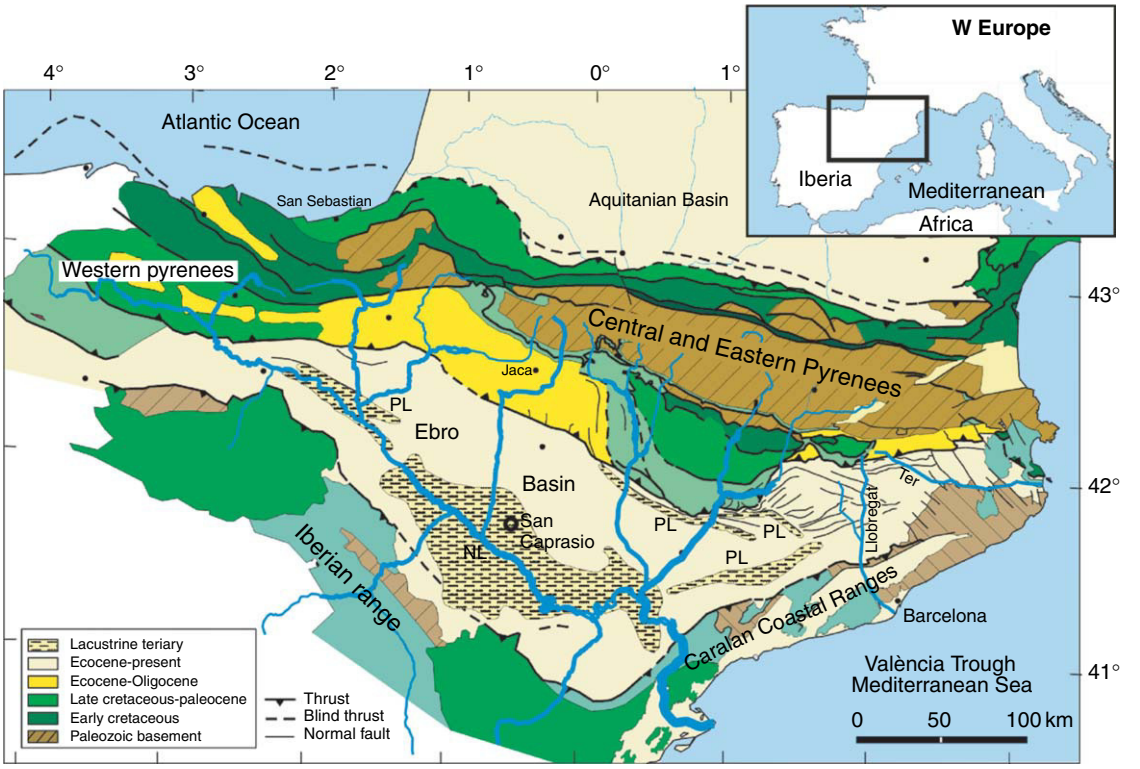

Figure 92 Geological map of the Ebro Basin and the bounding Pyrenees, Catalan Coastal Range and Iberian Range, showing the present river network and the approximate extent of Neogene lacustrine deposits (PL Paleogene, NL, Neogene). Modified from Garcia-Castellanos D, Vergés J, Gaspar-Escribano JM, and Cloetingh S (2003) Interplay between tectonics, climate and fluvial transport during the Cenozoic evolution of the Ebro Basin (NE Iberia). *Journal of Geophysical Research* 108: 2347.

impressive compressional structures in syn-tectonic Eocene sediments at the boundary between the Catalan Coastal Ranges and the Ebro Basin. With this, clastic influx into the Valencia Trough increased, as evidenced by the rapid progradation of the Castellón Group delta and the modern post-Messinian Ebro Group delta (Dañobeitia *et al.*, 1990; Ziegler, 1988).

6.11.7.4.1 Ebro Basin evolution: a modeling approach

In order to gain a better understanding of processes underlying the drainage evolution of the Ebro Basin, a numerical model was applied that integrates a surface transport model with quantitative approaches to the tectonic processes of thrusting and isostasy (for details see Garcia-Castellanos *et al.*, 2003).

Quantitative studies on the interplay between lithosphere dynamics and drainage networks in sedimentary basins are scarce. Since the early models of foreland basin development in the 1980s, the flexural response of the lithosphere to orogenic thrust loading has been accepted as the key process generating accommodation space and sediment accumulation in front of orogens (e.g., Beaumont, 1981; Flemings and Jordan, 1989; Sinclair and Allen, 1992; Ford *et al.*, 1999; Garcia-Castellanos *et al.*, 2002). However, these studies used simplistic approaches to surface mass transport, neglecting the dynamics and 3-D nature of fluvial networks. Later numerical experiments showed that the spatial and temporal distribution of sediment facies is strongly influenced by the 3-D character of fluvial transport (Johnson and Beaumont, 1995), and that the coupled tectonic–fluvial network system may control the evolution of sediment supply from orogens (Tucker and Slingerland, 1996). In turn, drainage networks in foreland basins can be under certain conditions controlled by the flexural behaviour of the lithosphere (Burbank, 1992; Garcia-Castellanos, 2002).

The numerical model applied to study the drainage and sedimentary evolution of the Ebro Basin was based on the approach developed by Garcia-Castellanos (2002) and incorporates planform numerical solutions

to the following processes (**Figures 93** and **94**): (1) tectonic deformation is mainly driven by upper crustal thrust stacking and normal faulting, (2) surface transport is driven by the fluvial network, and (3) mass redistribution resulting from (1) and (2) is compensated by regional isostasy (lithospheric flexure).

The interplay between lithospheric and surface processes is explicit in two ways. First, surface processes determine the way mass is redistributed in space and time, thus inducing isostatic vertical movements. Second, crustal and lithospheric-scale tectonics control and organize the nonlinear, chaotic nature of drainage networks. In zones affected by folding and thrusting, the long-term drainage evolution is controlled by the deformation kinematics (e.g., Tucker and Slingerland, 1996; Kühni and Pfiffner, 2001), but the second-order role of lithospheric flexure can also become relevant in undeformed areas such as the distal margin of a foreland basin (Burbank, 1992; Garcia-Castellanos, 2002) or during posttectonic erosion-induced isostatic rebound of an escarpment (Tucker and Slingerland, 1994).

Tectonic deformation was simulated with units (or blocks) moving relative to the foreland. These units preserve their vertical thickness during movement (vertical shear approach) simulating a noninstantaneous tectonic deformation. As modeling did not intend to reproduce the internal geometry of the orogenic wedge and the kinematic details of its evolution (Beaumont *et al.*, 2000), and for the sake of simplicity, crustal shortening in each mountain range was represented in the model by the least number of blocks necessary and at constant shortening rates.

Isostatic subsidence and uplift were calculated assuming that the lithosphere behaves as a 2-D thin elastic plate (e.g., Van Wees and Cloetingh, 1994) that is loaded by the large-scale mass redistribution and rests on a fluid asthenosphere.

Erosion and sedimentation were calculated (see Appendix 2) by defining the drainage network on top of a time-dependent topography resulting from tectonic deformation and isostasy. To account for the endorheic stage of the Ebro Basin, and as evaporation can eliminate excess water in a lake reducing its level below the outlet, thus causing closure of the basin, evaporation was incorporated in the model as an improvement on the algorithm of Garcia-Castellanos (2002). (See **Figure 95**.) The amount of lake evaporation was calculated by multiplying the lake surface with a constant evaporation rate and by subtracting results from the lake discharge.

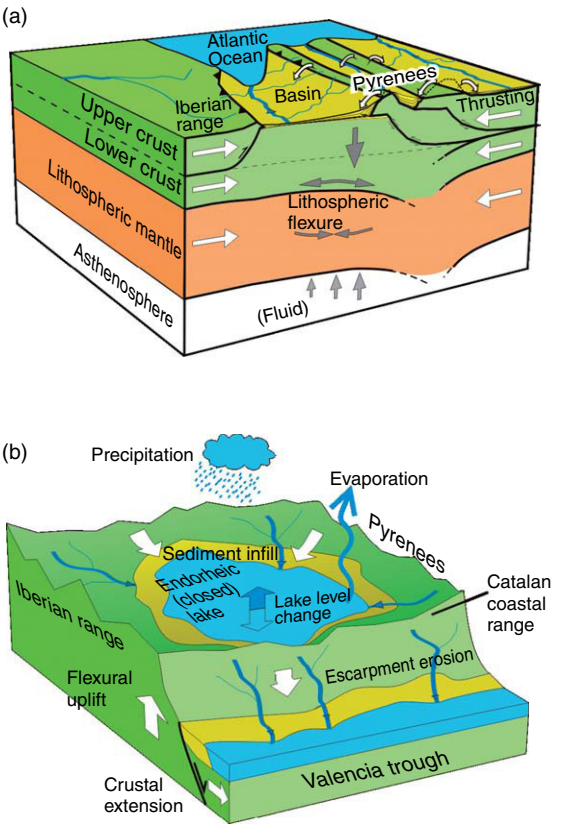

Figure 93 (a) Lithospheric-scale block diagram showing tectonic setting of the flexural Ebro Basin in the pro-wedge foreland of the Pyrenees and the Iberian Range bounding it to the SW. White arrows indicate tectonic transport direction. (b) Endorheic stage of the Ebro Basin prior to capture of its closed lake in response to erosional breakdown of the Catalan Coastal Range. Modified from Garcia-Castellanos *et al.*, (2003).

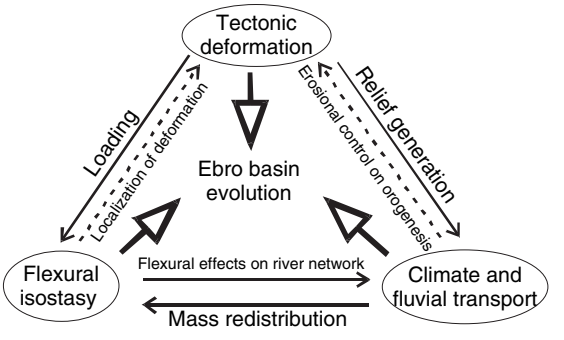

Figure 94 Interaction of processes controlling drainage evolution and large-scale sediment transport in the Ebro Basin and surrounding mountain ranges. Solid arrows: interactions addressed in the text. Stippled arrows: interactions not explicitly addressed in models presented. Modified from Garcia-Castellanos D, Vergés J, Gaspar-Escribano JM, and Cloetingh S (2003). Interplay between tectonics, climate and fluvial transport during the Cenozoic evolution of the Ebro Basin (NE Iberia). *Journal of Geophysical Research* 108: 2347.

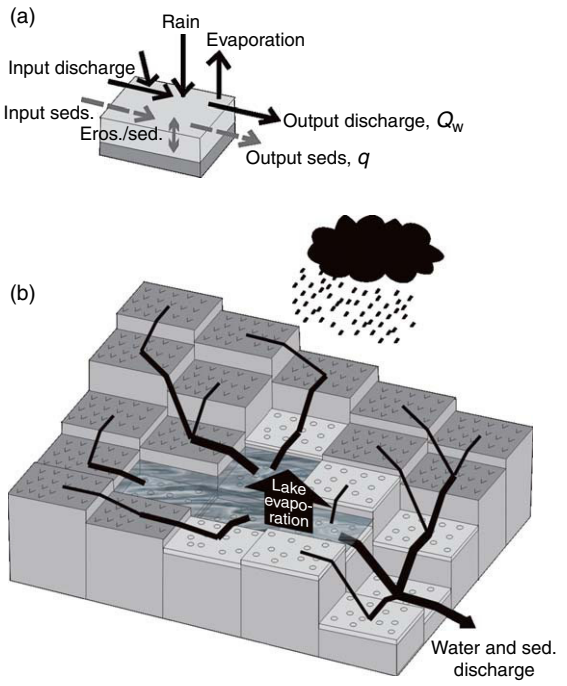

Figure 95 Cartoon illustrating the numerical surface processes model. (a) Water and sediment input and output at each cell of the model. (b) Rivers follow the maximum slope of the discretised topography, taking into account evaporation at lakes forming in local topographic minima. Modified from Garcia-Castellanos D, Vergés J, Gaspar-Escribano JM, and Cloetingh S (2003) Interplay between tectonics, climate and fluvial transport during the Cenozoic evolution of the Ebro Basin (NE Iberia). *Journal of Geophysical Research* 108: 2347.

Owing to the coupled response of these processes, the numerical model simulated the 3-D evolution of the geometry of the orogen/basin system, including topography, drainage networks, sediment horizons, erosion patterns, and vertical isostatic movements.

Results demonstrate the importance of the interplay between climatic, fluvial, and tectonic processes in shaping long-term landscape evolution and mass transport from mountain ranges to sedimentary basins. Most coupled tectonic-landscape evolution models have disregarded the role of lakes and their climate-controlled hydrographic balance (e.g., their endorheic/closed or exorheic/open character) in the evolution of continental topography and surface sediment transport. This aspect is of central importance for the Ebro Basin, in which the presence of a closed Oligocene–Miocene lake appears to have played a major role in the landscape evolution and sediment budget of the south Pyrenean area.

6.11.7.4.1.(i) Endorheic period: interplay between tectonics and climate Modeling shows that tectonic closure of the Ebro Basin transformed it into a trap for debris derived from the surrounding mountain ranges with increasing sedimentation rates giving it its singular architecture (Garcia-Castellanos *et al.*, 2003). Models validate the hypothesis formulated by Coney *et al.*, (1996) that thick syn- and posttectonic conglomerates buried the frontal, presently outcropping Pyrenean thrusts during the endorheic stage of basin evolution. Vitrinite reflectance studies in the eastern Ebro Basin suggest burial depths of the presently outcropping sediments ranging between 2750 ± 250 m near the Pyrenean front and 950 ± 150 m near the Catalan Coastal Ranges (Clavell, 1992; Waltham *et al.*, 2000). Model predictions agree with these observations, indicating that the removed sediment cover was up to 1500 m thick and that the maximum basin fill prior to drainage opening amounted to about 140 000 km^3.

Moreover, the models explain the presence of a single lake body with a very asymmetric sediment distribution, both in facies and thickness, as inferred by geological field studies (Arenas and Pardo, 1999). Modeling provides a quantitative framework for the understanding of these asymmetries that resulted from differences in the tectonic evolution of the surrounding mountain ranges: The greater tectonic shortening and catchment areas in the Pyrenees and the Iberian Chain as compared to the Catalan Coastal Ranges underlay the increased sediment supply to the basin from the N and SW, slowly shifting the lake and depocentre toward the SE.

6.11.7.4.1.(ii) Opening and incision of the Ebro Basin: interplay of lithospheric and surface processes Models predict that reworking of at least 30 000 km^3 of the Cenozoic Ebro Basin fill requires that opening of its drainage toward the Mediterranean has occurred long before the Messinian, probably between 13 and 8.5 Ma (middle Serravallian to middle Tortonian). This is compatible with the occurrence of the large-scale pre-Messinian prograding Castellón Group clastic wedge that advanced into the Valencia Trough (Ziegler, 1988; Roca and Desegaulx, 1992; Roca, 2001). Progradation of these clastics, starting in the middle Serravallian (Martínez del Olmo, 1996) can be interpreted as reflecting the opening of the endorheic Ebro paleo-lake. This is also consistent with an important increase in sedimentation rate in the Valencia Trough (Dañobeitia *et al.*, 1990; Martínez

del Olmo, 1996) that may be associated with a lake overflow during a coeval transition to a wetter climate (Alonso-Zarza and Calvo, 2000; Sanz de Siria Catalan, 1993).

In addition to the classical concept of opening of the Ebro Basin by escarpment erosion driven by Neogene Mediterranean streams, modeling suggests that four additional large-scale processes played a contributing and possibly major role (**Figure 93(b)**): (1) extensional partial breakdown of the Catalan Coastal Ranges topographic barrier; (2) extension-induced flexural flank uplift of the Catalan Coastal Range; (3) sediment overfill of the Ebro lake; and (4) lake level rise related to a long-term climate change toward wetter conditions.

Development of the Valencia Trough had two opposing effects on the opening of the Ebro Basin drainage system. First, it facilitated its opening by extensionally disrupting and narrowing the topographic barrier presented by the Eocene intraplate Catalan Coastal Ranges and by increasing the topographic gradient and erosion capacity of short streams that developed on the new Mediterranean margin. Second, it delayed its opening by flexural uplift of the flanks of the Catalan Coastal Ranges (a process similar to that described by Tucker and Slingerland, 1994). This uplift, and related exhumation, is compatible with numerical modeling (Gaspar-Escribano *et al.*, 2004) and thermogeochronological results (Juez-Larré and Andriessen, 2002, 2006), indicating that the Catalan Coastal Ranges were exhumed during the Neogene by as much as 2 km.

The combination of well-dated episodes of basin evolution, long-term denudation rates, and sediment delivery rates, together with numerical modeling provides a process-based approach to determine how tectonics and river dynamics shaped the present landscape of the NE parts of the Iberian Peninsula.

Foreland basins are generally regarded as sedimentary accumulations whose evolution depends mainly on the tectonic history of the adjacent orogen and the mechanical response of the foreland lithosphere. Studies carried out on the Ebro Basin demonstrate that the drainage history and the organization of the fluvial–lacustrine network are additional major factors controlling its evolution. The interaction between surface processes (climate, erosion, and transport) and lithospheric tectonic deformation (e.g., Avouac and Burov, 1996; Willet, 1999; Beaumont *et al.*, 2000; Garcia-Castellanos, 2002; Cloetingh *et al.*, 2002; *see also* Avouac, this volume (Chapter 6.09)) apparently controlled the end of the ~25 My long period of endorheic drainage and sediment entrapment in the Ebro Basin. Aridity, probably enhanced by an intramontane orographic position, appears to have prolonged sediment entrapment and the closure of this basin. This feedback between aridity and basin closure appears to have been preconditioned by a favourable and unique tectonic setting.

In the case of the Ebro Basin, the role of isostasy is enhanced as by the time of lake capture, a dramatic drainage change affected a catchment area of nearly 85 000 km^2 that was very sensitive to vertical movements in the domain of its eastern drainage divide.

6.11.8 Conclusions and Future Perspectives

Sedimentary basin systems are sensitive recorders of dynamic processes controlling the deformation of the lithosphere and its interaction with the deep mantle and surface processes. The thermomechanical structure of the lithosphere exerts a prime control on its response to basin-forming mechanisms, such as rifting and its deflection under vertical loads, as well as its compressional deformation. Polyphase deformation is a common feature of some of Europe's best-documented sedimentary basin systems. The relatively weak lithosphere of intraplate Europe renders many of its sedimentary basins prone to neotectonic reactivation. Tectonic processes operating during basin formation and during the subsequent deformation of basins can generate significant differential topography in basin systems. As there is a close link between erosion of topographic highs and sedimentation in subsiding areas, constraints are needed on uplift and coeval subsidence to validate quantitative process-oriented models for the evolution of sedimentary basins. Integration of analog and numerical modeling provides a novel approach to assess the feedback mechanisms between deep mantle, lithospheric, and surface processes. The analysis of European basin systems demonstrates the importance of preorogenic extension of the lithosphere in the evolution of flexural foreland basins. Furthermore, compressional reactivation of extensional basins during their postrift phase appears to be a common feature of Europe's intraplate rifts and passive-margins, reflecting temporal and spatial changes in the orientation and magnitude of the intraplate stress regime. Moreover, in the intraplate domain of continental Europe, that was thermally perturbed by

Cenozoic upper mantle plume activity, lithospheric folding plays an important role and strongly affects the pattern of vertical motions, both in terms of basin subsidence and the uplift of broad arches.

The development of sedimentary basins is, therefore, the intrinsic result of the interplay between lithospheric stresses and rheology and thermal perturbations of the lower lithosphere–upper mantle. The elucidation of palaeo-stresses, palaeo-temperatures and palaeo-rheologies of the lithosphere is vital for the reconstruction of dynamically supported palaeo-topography. Rift shoulder topography and flexural topography in compressional systems are directly linked to the thermomechanical properties and rheological stratification of the underlying lithosphere. The temporal evolution of the strength of continents and the spatial variations in stress and strength at continental margins, rifts, and orogenic belts govern the mechanics of basin development and destruction in time and space. Structural discontinuities and preexisting weakness zones are prone to reactivation in response to the buildup of extensional stresses and thus play an important role in the localization of rifts and related transfer zones. Similarly, their reactivation in response to the buildup of compressional stresses propagating from plate boundaries into continental platform areas controls the inversion of extensional basins and the upthrusting of basement blocks and contributes to the localization of lithospheric folding. The timing and nature of underlying changes in the controlling stress field and the resulting deformation processes can be unravelled by quantitative analyses of the stratigraphic record and the architecture of such complex polyphase sedimentary basins. This permits to assess systematic differences in the timing of the transition from rifting to intraplate compression and the development of foreland fold–thrust belts and lithospheric folds and vice versa.

The study of sedimentary basins demands added focus on surrounding highs that act as sediment sources as it is recognized that also uplifted/uplifting areas contain valuable information concerning, for instance, underlying deep-seated processes. State-of-the art geothermochronology and the study of erosion and river pattern evolution provide major constraints on uplift histories.

To elucidate the contribution of internal lithospheric processes and external forcing toward rates of erosion and sedimentation presents, therefore, a major challenge for sedimentary basin studies. This is particularly so as the sedimentary cover of the lithosphere provides a high-resolution record of the changing environment and of deformation and mass transfer at the surface and at different depth levels in the crust, lithosphere, and mantle system.

Monitoring lithospheric deformation and its sedimentary record provides constraints on past and present-day structures and on deformation rates. Whereas in sedimentary basin analyses tectonics, eustasy, and sediment supply have been commonly treated as separate factors, an integrated approach constrained by fully 3D quantitative subsidence and uplift history analyses in carefully selected natural laboratories is now possible and ought to be further pursued.

Recent deformation, involving tectonic reactivation, has strongly affected the structure and fill of many sedimentary basins. The long-lasting memory of the lithosphere appears to play a far more important role in basin reactivation than hitherto assumed. A better understanding of the 3D linkage between basin formation and basin deformation is, therefore, an essential step in research aiming at linking lithospheric forcing and upper-mantle dynamics to crustal uplift and erosion and their effects on the dynamics of sedimentary systems. Structural analysis of the basin architecture, including palaeo-stress assessment, provides important constraints on the transient nature of intraplate stress fields and their effects on the evolution of sedimentary basins.

Reconstruction of the basin history is a prerequisite for identifying transient processes having a bearing on basin (de)formation. A full 3D reconstruction, including the use of sophisticated 3D visualization and geometric construction techniques, is required for sedimentary basin with a faulted architecture. 3D backstripping, including the effects of flexural isostasy and faulting, allows a thorough assessment of sedimentation and faulting rates, as well as changing facies and geometries through time. The established transient architecture of the preserved sedimentary record serves as key input for process quantification.

We have presented results of several studies integrating geothermochronology, analyses of material properties of the lithosphere and the reconstruction of the geological past from the sedimentary record. As such, we have trespassed traditional boundaries between endogene and exogene geology. During the last decades, basin analysis has been at the forefront of integrating the sedimentary and lithosphere components of geology and geophysics. In this context, it is essential to link neotectonics, surface processes and

lithospheric dynamics in reconstructions of the palaeo-topography of sedimentary basins and their surrounding areas. Combining dynamic topography and sedimentary basin dynamics is also important, especially when considering the key societal role sedimentary basins play as hosts of major resources. Moreover, most of the human population is concentrated in sedimentary basins, often close to the coastal zone and deltas that are vulnerable to geological hazards inherent to activity of the Earth system.

Acknowledgments

The authors thank the Netherlands Research Centre for Integrated Solid Earth Sciences (ISES) for funding the integrated numerical/analog tectonic modeling laboratory (NUMLAB/TECLAB).

Appendix 1: Dynamic Model for Slow Lithospheric Extension

To study lithosphere extension, a 2-D finite element model is used. The program is based on a Lagrangian formulation, which makes it possible to track (material) boundaries, like the Moho, in time and space. A drawback of the Lagrangian method is that it is not suitable for solving very large grid deformation problems. This is a problem in analyzing of extension of the lithosphere, which is often accompanied by large deformations. The elements might become too deformed to yield accurate or stable solutions. In order to overcome this problem the finite element grid is periodically remeshed (see Van Wijk and Cloetingh (2002) and references therein).

In the numerical model the base of the lithosphere is defined by the 1300°C isotherm. Under such conditions, approximately the upper half of the thermal lithosphere behaves elastically on geological time scale, while in the lower half stresses are relaxed by viscous deformation. This viscoelastic behaviour is well described by a Maxwell body, resulting in the following constitutive equation for a Maxwell viscoelastic material:

$$\dot{\varepsilon} = \frac{1}{2\mu}\sigma + \frac{1}{E}\frac{\mathrm{d}\sigma}{\mathrm{d}t} \qquad [1]$$

in which $\dot{\varepsilon}$ is strain rate, μ is dynamic viscosity, σ is stress, and E is Young's modulus. For a Newtonian fluid the dynamic viscosity μ is constant. In the lithosphere, however, nonlinear creep processes prevail and the relation between stress and strain rate can be described by

$$\dot{\varepsilon} = A\sigma^n \exp\frac{-Q}{RT} \qquad [2]$$

where A, n, and Q are experimentally derived material constants, n is the power law exponent, Q is activation energy, R is the gas constant, and T is temperature.

The state of stress is constrained by the force balance:

$$\nabla \cdot \sigma + \rho g = 0 \qquad [3]$$

where g is gravity and ρ is density.

In this model it is assumed that mass is conserved and the material is incompressible. The continuity equation following from the principle of mass conservation for an incompressible medium is

$$\nabla \mathbf{v} = 0 \qquad [4]$$

In the model, the density is dependent on the temperature following a linear equation of state:

$$\rho = \rho_0(1 - \alpha T) \qquad [5]$$

where ρ_0 is the density at the surface, α is the thermal expansion coefficient, and T is temperature.

Besides viscoelastic behaviour, processes of fracture and plastic flow play an important role in deformation of the lithosphere. This deformation mechanism is active when deviatoric stresses reach a critical level. Here the Mohr–Coulomb criterion is used as a yield criterion to define this critical stress level. The Mohr–Coulomb strength criterion is defined as

$$|\tau_n| \leq c - \sigma_n \cdot \tan\vartheta \qquad [6]$$

where τ_n is the shear stress component, σ_n is the normal stress component, c is the cohesion of the material, and ϑ is the angle of internal friction. Stresses are adjusted at each time step at which this criterion is reached. Frictional sliding and fault movement are not explicitly described by this criterion.

The displacement field is obtained by solving eqns [1]–[6]. A total of 2560 straight-sided seven-node triangular elements were used with a 13-point Gaussian integration scheme. As the time discretization schemes used are fully implicit, the system is unconditionally stable. However, as the accuracy of the solution remains dependent on the dimension of the time steps, the Courant criterion was implemented.

Processes like sedimentation and erosion are not incorporated in the modeling, although they affect the evolution of a rift basin and rift shoulders, and can change the strength of the lithosphere.

The temperature field in the lithosphere is calculated for each time step using the heat flow equation:

$$\rho c_p \frac{\mathrm{d}T}{\mathrm{d}t} = \partial_j k \partial_j T + H \qquad [7]$$

where the density ρ is defined by eqn [5], c_p is specific heat, k is conductivity, and H is crustal heat production. Temperatures are calculated on the same grid as the velocity field, and advection of heat is accounted for by the nodal displacements.

Appendix 2: Surface Transport Model

Following the formulation by Beaumont *et al.*, (1992) and Kooi and Beaumont (1994), the surface transport numerical model adopted here assumes that the main agent of basin-scale incision and transport is the fluvial network. Although there is an ongoing discussion on the optimal empirical relationships governing these processes (e.g., Willgoose *et al.*, 1991; Howard *et al.*, 1994; Whipple and Tucker, 1999), this is of secondary importance here, as our analysis focuses on the large-scale, first-order features of the interplay between fluvial transport and lithospheric deformation, rather than on the properties of fluvial transport itself. According to the approach by Beaumont *et al.*, (1992), the equilibrium transport capacity q_{eq} of a river (defined as the amount of mass transported by a river producing no net erosion or sedimentation) is proportional to the mean water discharge Q_{w} and the slope S along the river profile:

$$q_{\mathrm{eq}}(x, y, t) = K_{\mathrm{f}} S(x, y, t) Q_{\mathrm{w}}(x, y, t) \qquad [8]$$

where K_{f} is the fluvial transport coefficient, for which we adopt a standard value of $60\,\mathrm{kg\,m^{-3}}$ (e.g., Kooi and Beaumont, 1996; van der Beek and Braun, 1999). For comparison with these works, note that here the sediment load has units of [mass]/[time] and K_{f} has units of [mass]/[volume]. In general, rivers are out of equilibrium such that the amount of material $\mathrm{d}q$ eroded/deposited along a river segment of length dl is proportional to the difference between the actual transported sediment q and q_{eq} following the relation

$$\frac{\mathrm{d}q(x, y, t)}{\mathrm{d}l} = \frac{1}{l_{\mathrm{f}}} \left[q(x, y, t) - q_{\mathrm{eq}}(x, y, t) \right] \qquad [9]$$

where l_f is the length scale of erosion/deposition. Under these conditions a river can change from incision to deposition by a reduction in q_{eq}, that is, by a decrease in discharge and/or slope. As water flows down the river, fluvial transport typically evolves from supply-limited to transport-limited.

The main difference between this and previous models is the explicit treatment of lakes forming in local topographic minima and their implied water losses by evaporation (**Figure 95**). When a river reaches a lake or the sea, transported sediments are distributed in all directions from the river mouth, assuming zero transport capacity in eqn [9]. This implies exponentially decreasing deposition rates with increasing distance from the river mouth. This approach overlooks other processes affecting the pattern of deposition in deltas and must be regarded as the simplest possible approach that eventually produces lake/basin overfilling by localizing deposition in the vicinity of the river mouth. Lake overfilling by sediment accumulation, together with erosion at the lake outlet (decreasing the water level of the lake), ensures that lakes behave in the model as transitory or ephemeral phenomena that tend to disappear in the absence of tectonic relief generation.

References

Aichroth B, Prodehl C, and Thybo H (1992) Crustal structure along the central segment of the EGT from seismic-refraction studies. *Tectonophysics* 207: 43–64.

Alonso-Zarza AM and Calvo JP (2000) Palustrine sedimentation in an episodically subsiding basin: The Miocene of the northern Teruel Graben (Spain). *Palaeogeography, Palaeoclimatology, Palaeoecology* 160: 1–21.

Anderson DL, Zang Y-S, and Tanimoto T (1992) Plume heads, continental lithosphere, flood basalts and tomography. In: Storey BC, Alabaster T, and Pankhurst RJ (eds.) *Geological Society, London, Special Publications,* 68: *Magmatism and the Causes of Continental Break-up*, pp. 99–124. London: Geological Society, London.

Andeweg B and Cloetingh S (1998) Flexure and 'unflexure' of the North Alpine German–Austrian Molasse Basin: Constraints from forward tectonic modelling. In: Mascle A, Puigdefàbregas C, Luterbacher HP, and Fernandez M (eds.) *Geological Society, London, Special Publications,* 134: *Cenozoic Foreland Basins of Western Europe*, pp. 403–422. London: Geological Society, London.

Andeweg B and Cloetingh S (2001) Evidence for an active sinistral shear zone in the Western Alboran region. *Terra Nova* 13: 44–50.

Andeweg B, De Vicente G, Cloetingh S, Giner J, and Muñoz Martin A (1999) Local stress fields and intraplate deformation of Iberia: variations in spatial and temporal interplay of regional stress sources. *Tectonophysics* 305: 153–164.

Arenas C and Pardo G (1999) Latest Oligocene–late Miocene lacustrine systems of the north-central part of the Ebro Basin (Spain): Sedimentary facies model and palaeogeographic

synthesis. *Palaeogeography, Palaeoclimatology, Palaeoecology* 151: 127–148.
Arenas C, Millán H, Pardo G, and Pocoví A (2001) Ebro Basin continental sedimentation associated with late compressional Pyrenean tectonics (north-eastern Iberia): Controls on basin margin fans and fluvial system. *Basin Research* 13: 65–89.
Argus DF and Heflin MB (1995) Plate motion and crustal deformation estimated with geodetic data from the Global Positioning System. *Geophysical Research Letter* 22: 1973–1976.
Artemieva IM (2006) Global $1^0 \times 1^0$ thermal model TC1 for the continental lithosphere: Implications for lithosphere secular evolution. *Tectonophysics* 416: 245–277.
Artemieva IM and Mooney WD (2001) Thermal thickness and evolution of Precambrian lithosphere. A global study. *Journal of Geophysical Research* 106: 16387–16414.
Artemieva IM and Mooney WD (2002) On the relationship between cratonic lithosphere thickness, plate motions, and basal drag. *Tectonophysics* 358: 211–231.
Artemieva IM, Thybo H, and Kaban MK (2006) Deep Europe today: Geophysical synthesis of upper mantle structure and lithospheric processes over 3.5 Ga. In: Gee DG and Stephenson RA (eds.) London: Geological Society, London. 32: European Lithosphere Dynamics, pp. 11–42.
Arthaud F and Matte P (1977) Late Paleozoic strike-slip faulting in Southern Europe and North Africa: results of a right-lateral shear between the Appalachians and Urals. *Geological Society of America Bulletin* 88: 1305–1320.
Artyushkov EV and Baer MA (1990) Formation of hydrocarbon basins: Subsidence without stretching in West Siberia. In: Pinet B and Bois C (eds.) *The Potential of Deep Seismic Reflection Profiling for Hydrocarbon Exploration*, pp. 45–61. Paris: Technip.
Avouac JP and Burov EB (1996) Erosion as a driving mechanism of intracontinental mountain growth. *Journal of Geophysical Research* 101: 17747–17769.
Babuska V and Plomerova J (1992) The lithosphere in central Europe – seismological and petrological aspects. *Tectonophysics* 207: 141–163.
Babuska V and Plomerova J (1993) Lithospheric thickness and velocity anisotropy – seismological and geothermal aspects. *Tectonophysics* 225: 79–89.
Babuska V and Plomerova J (2001) Subcrustal lithosphere around the Saxothuringian–Moldanubian Suture Zone – a model derived from anisotropy of seismic wave velocities. *Tectonophysics* 332: 185–199.
Bada G and Horváth F (2001) On the structure and tectonic evolution of the Pannonian basin and surrounding orogens. *Acta Geologica Hungarica* 44: 301–327.
Bada G, Gerner P, Cloetingh S, and Horváth F (1998) Sources of recent tectonic stress in the Pannonian region: inferences from finite element modelling. *Geophysical Journal International* 134: 87–102.
Bada G, Horvath F, Gerner P, and Fejes I (1999) Review of the present-day geodynamics of the Pannonian Basin; progress and problems. *Journal of Geodynamics* 27: 501–527.
Bada G, Horváth F, Cloetingh S, Coblentz DD, and Tóth T (2001) The role of topography induced gravitational stresses in basin inversion: The case study of the Pannonian basin. *Tectonics* 20: 343–363.
Bala A, Radulian M, and Popescu E (2003) Earthquakes distribution and their focal mechanism in correlation with the active tectonic zones of Romania. *Journal of Geodynamics* 36: 129–145.
Balla Z (1986) Paleotectonic reconstruction of the central Alpine-Mediterranean belt for the Neogene. *Tectonophysics* 127: 213–243.
Bally AW and Snelson S (1980) Realms of subsidence. In: Miall AD (ed.) *Bulletin Du Centre De Recherches Exploration Production Elf Aquitaine, 6: Facts and Principles of World Petroleum Occurrence.* Mem. Can. Soc. Pet. Geol. 6, pp. 9–94.
Banda E and Santanach P (1992) The Valencia trough (western Mediterranean): an overview. *Tectonophysics* 208: 183–202.
Barbier F, Duvergé J, and le Pichon X (1986) Structure profonde de la marge Nord-Gascogne. Implications sur le mechanism de rifting et la formation de la marge continentale. *Bulletin Du Centre De Recherches Exploration Production Elf Aquitaine* 10: 105–121.
Barton P and Wood R (1984) Tectonic evolution of the North Sea basin: crustal stretching and subsidence. *Geophysical Journal of the Royal Astronomical Society* 79: 987–1022.
Bartrina MT, Cabrera L, Jurado MJ, Guimerá J, and Roca E (1992) Evolution of the central Catalan margin of the Valencia Trough (western Mediterranean). *Tectonophysics* 203: 219–247.
Bassi G (1995) Relative importance of strain rate and rheology for the mode of continental extension. *Earth and Planetary Science Letters* 122: 195–210.
Bayer U, Scheck M, and Rabbel W (1999) An integrated study of the NE German Basin. *Tectonophysics* 314: 285–307.
Beaumont C (1981) Foreland basins. *Geophysical Journal of the Royal Astronomical Society* 65: 291–329.
Beaumont C, Keen CE, and Boutillier R (1982) On the evolution of rifted continental margins: comparison of models and observations for the Nova Scotian Margin. *Geophysical Journal of the Royal Astronomical Society* 70: 667–715.
Beaumont C, Fullsack Ph, and Hamilton W (1992) Erosional control of active compressional orogens. In: McClay KR (ed.) *Thrust Tectonics*, pp. 1–18. London: Chapman & Hall.
Beaumont C, Muñoz JA, Hamilton J, and Fullsack P (2000) Factors controlling the Alpine evolution of the central Pyrenees inferred from a comparison of observations and geodynamical models. *Journal of Geophysical Research* 105: 8121–8145.
Beekman F, Bull JM, Cloetingh S, and Scrutton RA (1996) Crustal fault reactivation as initiator of lithospheric folding in the Central Indian Ocean. *Geological Society, London, Special Publications* 99: 251–263.
Behr HJ and Heinrichs T (1987) Geological interpretation of DEKORP 2 –S: A deep seismic reflection profile across the Saxothuringian and possible implications for late Variscan structural evolution of Central Europe. *Tectonophysics* 142: 173–202.
Benek R, Kramer W, McCann T, Scheck M, Negendank JFW, Kronich D, Huebscher H-D, and Bayer U (1996) Permo-Carboniferous magmatism of the Northeast German Basin. *Tectonophysics* 266: 379–404.
Bergerat F (1987) Stress fields in the European platform at the time of Africa–Eurasia collision. *Tectonics* 6: 99–132.
Bertotti G and Ter Voorde M (1994) Thermal effects of normal faulting during rifted basin formation 2. The Lugano–Val Grande normal fault and the role of preexisting thermal anomalies. *Tectonophysics* 240: 145–157.
Bertotti G, ter Voorde M, Cloetingh S, and Picotti V (1997) Thermomechanical evolution of the South Alpine rifted margin (North Italy): constraints on the strength of passive continental margins. *Earth and Planetary Science Letters* 146: 181–193.
Bertotti G, Podlachikov Y, and Daehler A (2000) Dynamic link between the level of ductile crustal flow and style of normal faulting of brittle crust. *Tectonophysics* 320: 195–218.
Bertotti G, Maţenco L, and Cloetingh S (2003) Vertical movements in and around the SE Carpathian foredeep: Lithospheric memory and stress field control. *Terra Nova* 15: 299–305.
Bijwaard H and Spakman W (1999a) Fast kinematic ray tracing of first- and later-arriving global seismic phases. *Geophysical Journal International* 139: 359–369.
Bijwaard H and Spakman W (1999b) Tomographic evidence for a narrow whole mantle plume below Iceland. *Earth and Planetary Science Letters* 166: 121–126.

Blanco M-J and Spakman W (1993) The P-wave velocity structure of the mantle below the Iberian Peninsula; evidence for subducted lithosphere below southern Spain. *Tectonophysics* 221: 13–34.

Blundell D, Freeman R, and Mueller S (eds.) (1992) *A Continent Revealed, The European Geotraverse*, 275p. Cambridge: Cambridge University Press.

Bond GC and Kominz M (1984) Construction of tectonic subsidence curves for the early Paleozoic miogeocline southern Canadian Rocky Mountains: Implications for subsidence mechanisms age of break up and crustal thinning. *Geological Society of America Bulletin* 95: 155–173.

Bonin B (1990) From orogenic to anorogenic settings: evolution of granitoids suits after a major orogenesis. *Geological Journal* 25: 260–270.

Bonin B, Brändlin P, Bussy F, Desmons J, Eggenberger U, Finger F, Graf K, Marro C, Mercolli L, Oberhänsli R, Ploquin A, von Quadt A, von Raumer J, Schaltegger U, and Steyer HP (1993) Late Variscan magmatic evolution of the Alpine basement. In: von Raumer JF and Neubauer F (eds.) *Pre-Mesozoic Geology of the Alps*, pp. 171–201. New York: Springer.

Bonjer KP (1997) Seismicity pattern and style of seismic faulting at the eastern borderfault of the southern Rhine Graben. *Tectonophysics* 275: 41–69.

Bonnet S, Guillocheau F, and Brun J-P (1998) Relative uplift measured using river incision: The case of the Armorican basement (France). *Comptes Rendus Academie des Sciences, Earth and Planetary Sciences* 327: 245–251.

Bonnet S, Guillocheau F, Brun J-P, and Van den Driessche J (2000) Large-scale relief development related to Quaternary tectonic uplift of a Proterozoic–Paleozoic basement: The Armorican Massif, NW France. *Journal of Geophysical Research* 105: 19273–19288.

Bousquet R, Goffé B, Henry P, and Chopin Ch (1997) Kinematic, thermal and petrological model of the Central Alps: Lepontine metamorphism in the upper crust and eclogitisation of the lower crust. *Tectonophysics* 273: 105–127.

Bott MHP (1992) Modelling the loading stresses associated with continental rift systems. *Tectonophysics* 215: 99–115.

Bott MHP (1993) Modelling of plate-driving mechanisms. *Journal of the Geological Society* 150: 941–951.

Bott MHP and Kusznir NJ (1979) Stress distribution associated with compensated plateau uplift structures with application to the continental splitting mechanism. *Geophysical Journal of the Royal Astronomical Society* 56: 451–459.

Braathen A, Osmundsen P-T, Nordgulen O, Roberts D, and Meyer GB (2002) Orogen-parallel extension of the Caledonides in northern central Norway: An overview. *Norwegian Journal of Geology* 82: 225–242.

Braun J and Beaumont C (1989) A physical explanation of the relationship between flank uplifts and the breakup unconformity at rifted continental margins. *Geology* 17: 760–764.

Braun J and Sambridge M (1997) Modelling landscape evolution on geological time scales: A new method based on irregular spatial discretization. *Basin Research* 9: 27–52.

Breitkreuz C and Kennedy A (1999) Magmatic flare-up at the Carboniferous/Permian boundary in the NE German basin revealed by SHRIMP zircon ages. *Tectonophysics* 302: 307–326.

Brun JP and Nalpas T (1996) Graben inversion in nature and experiments. *Tectonics* 15: 677–687.

Brunet M-F and Cloetingh S (eds.) (2003) *Sedimentary Geology,* 156: *Integrated Peri-Tethyan Basins Studies (Peri-Tethys Programme),* 288p.

Buck WR (1991) Modes of continental lithospheric extension. *Journal of Geophysical Research* 96: 20161–20178.

Bukovics C and Ziegler PA (1985) Tectonic development of the Mid-Norway continental margin. *Marine and Petroleum Geology* 2: 2–22.

Burbank D (1992) Causes for recent uplift deduced from deposited patterns in the Ganges basin. *Nature* 357: 48–50.

Burg J-P, van den Driesschen J, and Brun J-P (1994) Syn- to post-thickening extension in the Variscan Belt of Western Europe: Modes and structural consequences. *Géologie de la France* 3: 33–51.

Burov EB and Cloetingh S (1997) Erosion and rift dynamics: new thermo-mechanical aspects of postrift evolution of extensional basins. *Earth and Planetary Science Letters* 150: 7–26.

Burov E and Diament M (1995) The effective elastic thickness of continental lithosphere: What does it really mean? (constraints from rheology, topography and gravity). *Journal of Geophysical Research* 100: 3905–3927.

Burov EB and Molnar P (1998) Gravity Anomalies over the Ferghana Valley (central Asia) and intracontinental Deformation. *Journal of Geophysical Research* 103: 18137–18152.

Burov EB, Nikishin AM, Cloetingh S, and Lobkovsky LI (1993) Continental lithosphere folding in central Asia (Part II): Constraints from gravity and tectonic modelling. *Tectonophysics* 226: 73–87.

Burton R, Kendall CGStC, and Lerche I (1987) Out of our depth: on the impossibility of fathoming eustasy from the stratigraphic record. *Earth Science Reviews* 24: 237–277.

Calcagnile G and Panza GF (1987) Properties of the lithosphere–asthenosphere system in Europe with a view toward Earth conductivity. *Pure and Applied Geophysics* 125: 241–254.

Carswell DA (1990) Eclogite and eclogite facies: definitions and classification. In: Carswell DA (ed.) *Eclogite Facies Rocks*, pp. 1–13. New York: Blackie.

Carter NL and Tsenn MC (1987) Flow properties of continental lithosphere. *Tectonophysics* 136: 27–63.

Casas-Sainz AM, Cortés-Gracia AL, and Maestro-Gonzáles A (2000) Intraplate deformation and basin formation during the Tertiary within the northern Iberian plate: origin and evolution of the Almazán Basin. *Tectonics* 19: 258–289.

Chalot-Prat F and Gîrbacea R (2000) Partial delamination of continental mantle-lithosphere, uplift-related crust-mantle decoupling, volcanism and basin formation: a new model for the Pliocene-Quaternary evolution of the southern East-Carpathians, Romania. *Tectonophysics* 327: 83–107.

Chang HK, Kowsmann RO, Figueiredo AMF, and Bender AA (1992) Tectonics and Stratigraphy of the East Brazil Rift System: an overview. *Tectonophysics* 213: 97–138.

Ciulavu D, Dinu C, and Cloetingh S (2002) Late Cenozoic tectonic evolution of the Transylvanian Basin and northeastern part of the Pannonian Basin (Romania): Constraints from seismic profiling and numerical modelling. In: Cloetingh S, Horváth F, Bada G, and Lankreijer A (eds.) *EGU St. Mueller Special Publication Series, 3: Neotectonics and Surface Processes: The Pannonian Basin and Alpine/ Carpathian System,* pp. 105–120. EGU.

Clavell E (1992) *Geologia del petroli de les conques terciaries de Catalunya*. Ph.D. thesis, University of Barcelona, Barcelona.

Cloetingh S (1988) Intra-plate stress: a new element in basin analysis. In: Kleinspehn KL and Paola C (eds.) *Frontiers in Sedimentary Geology – New Perspectives in Basin Analysis*, pp. 205–230. New York: Springer Verlag.

Cloetingh S and Kooi H (1992) Intraplate stresses and dynamical aspects of rift basins. *Tectonophysics* 215: 167–185.

Cloetingh S and Burov E (1996) Thermomechanical structure of European continental lithosphere: constraints from rheological profiles and EET estimates. *Geophysical Journal International* 124: 695–723.

Cloetingh S and Wortel R (1986) Stress in the Indo-Australian plate. *Tectonophysics* 132: 49–67.

Cloetingh S, McQueen H, and Lambeck K (1985) On a tectonic mechanism for regional sea level fluctuations. *Earth and Planetary Science Letters* 75: 157–166.

Cloetingh S, Lambeck K, and McQueen H (1987) Apparent sealevel fluctuations and a paleo-stress field for the North Sea region. In: Brooks J and Glennie K (eds.) *Petroleum Geology of North West Europe*, pp. 49–55. London: Graham and Trotman.

Cloetingh S, Wortel R, and Vlaar NJ (1989) On the initiation of subduction zones. *Pure and Applied Geophysics* 129: 7–25.

Cloetingh S, Gradstein F, Kooi H, Grant A, and Kaminski M (1990) Plate reorganization: a cause of rapid late Neogene subsidence and sedimentation around the North Atlantic? *Journal of the Geological Society* 147: 495–506.

Cloetingh S, Van der Beek PA, Van Rees D, Roep TB, Biermann C, and Stephenson RA (1992) Flexural interaction and the dynamics of Neogene extensional basin formation in the Alboran–Betic region. *Geo-Marine Letters* 12: 66–75.

Cloetingh S, Sassi W, and Horváth F (eds.) (1993) The origin of sedimentary basins; inferences from quantitative modelling and basin analyses. *Tectonophysics* 226, 518p.

Cloetingh S, Sassi W, and Task Force Team (1994) The origin of sedimentary basins: a status report from the task force of the International Lithosphere Program. *Marine and Petroleum Geology* 11: 659–683.

Cloetingh S, d'Argenio B, Catalano R, Horvath F, and Sassi W, (eds.) (1995a) Interplay of extension and compression in basin formation. *Tectonophysics* 252: pp. 1–484.

Cloetingh S, Van Wees JD, Van der Beek PA, and Spadini G (1995b) Role of pre-rift rheology in kinematics of basin formation: constrains from thermo-mechanical modelling of Mediterranean basins and intracratonic rifts. *Marine and Petroleum Geology* 12: 793–808.

Cloetingh S, Durand B, and Puigdefabregas C (eds.) (1995c) *Special Issue on Integrated Basin Studies (IBS) – A European Commission (DGXII) project. Marine and Petroleum Geology,* 12(8): 787–963.

Cloetingh S, Ben-Avraham Z, Sassi W, and Horváth F, (eds.) (1996) *Dynamics of strike slip tectonics and basin formation.* Tectonophysics 266: 1–523.

Cloetingh S, Van Balen RT, Ter Voorde M, Zoetemeijer BP, and Den Bezemer T (1997) Mechanical aspects of sedimentary basin formation: development of integrated models for lithospheric and surface processes. *International Journal of Earth Sciences* 86: 226–240.

Cloetingh S, Burov E, and Poliakov A (1999) Lithosphere folding: primary response to compression? (from Central Asia to Paris Basin). *Tectonics* 18: 1064–1083.

Cloetingh S, Burov E, Beekman F, Andeweg B, Andriessen PAM, Garcia-Castellanos D, de Vicente G, and Vegas R (2002) Lithospheric folding in Iberia. *Tectonics* 21(5): 1041 (doi:10.1029/2001TC901031).

Cloetingh S, Spadini G, van Wees JD, and Beekman F (2003) Thermo-mechanical modelling of Black Sea Basin (de)formation. *Sedimentary Geology* 156: 169–184.

Cloetingh S, Burov E, Maţenco L, Toussaint G, Bertotti G, Andriessen P, Wortel MJR, and Spakman W (2004) Thermo-mechanical controls on the mode of continental collision in the SE Carpathians (Romania). *Earth and Planetary Science Letters* 218: 57–76.

Cloetingh S, Ziegler PA, Beekman F, Andriessen PAM, Maţenco L, Bada G, Garcia-Castellanos D, Hardebol N, Dèzes P, and Sokoutis D (2005) Lithospheric memory, state of stress and rheology: Neotectonic controls on Europe's intraplate continental topography. *Quaternary Science Reviews* 24: 241–304.

Cloetingh S, Bada G, Maţenco L, Lankreijer A, Horváth F, and Dinu C (2006) Thermo-mechanical modelling of the Pannonian-Carpathian system: Modes of tectonic deformation, lithospheric strength and vertical motions. In: Gee D and Stephenson R (eds.) *Geological Society, London, Memoirs, 32: European Lithosphere Dynamics*, pp. 207–221. London: Geological Society, London.

Cobbold PR, Davy P, Gapais EA, Rossello EA, Sadybasakov E, Thomas JC, Tondji Biyo JJ, and De Urreiztieta M (1993) Sedimentary basins and crustal thickening. *Sedimentary Geology* 86: 77–89.

Coney PJ, Muñoz JA, McKlay KR, and Evenchick CA (1996) Syntectonic burial and post-tectonic exhumation of the Southern Pyrenees foreland fold-thrust belt. *Journal of the Geological Society* 153: 9–16.

Cortesogno L, Dallagiovanna A, Gaggero L, Oggiano G, Ronchi A, Seno S, and Vanossi M (1998) The Variscan post-collisional volcanism in Late Carboniferous-Permian sequences of Ligurian Alps, Southern Alps and Sardinia (Italy): a synthesis. *Lithos* 45: 305–328.

Coward MP (1993) The effects of Late Caledonian and Variscan escape tectonics on basement structure, Paleozoic basin kinematics and subsequent Mesozoic basin development in NW Europe. In: Parker J (ed.) *Petroleum Geology of Northwest Europe; Proceedings of the 4th Conference*, pp. 1095–1108. London: Geological Society.

Csontos L (1995) Tertiary tectonic evolution of the Intra-Carpathian area: A review. *Acta Vulcanologica* 7: 1–13.

Csontos L, Nagymarosy A, Horváth F, and Kováč M (1992) Tertiary evolution of the Intra-Carpathian area: a model. *Tectonophysics* 208: 221–241.

Curray JR and Moore DG (1971) Growth of the Bengal deep-sea fan and denudation of the Himalayas. *Geological Society of America Bulletin* 82: 563–572.

Dalmayrac P and Molnar B (1981) Parallel thrust and normal faulting in Peru and constraints on the state of stress. *Earth and Planetary Science Letters* 55: 473–481.

Dañobeitia J, Alonso B, and Maldonado A (1990) Geological framework of the Ebro continental margin and surrounding areas. *Marine Geology* 95: 265–287.

Davies JH and von Blanckenburg F (1996) Slab breakoff: a model of lithosphere detachment and its test in the magmatism and deformation of collisional orogens. *Earth and Planetary Science Letters* 129: 85–102.

De Bruijne CH and Andriessen PAM (2000) Interplay of intraplate tectonics and surface processes in the Sierra de Guadarrama (central Spain), assessed by apatite fission track analysis. *Physics and Chemistry of the Earth (A)* 25: 555–563.

De Bruijne CH and Andriessen PAM (2002) Far field effects of Alpine plate tectonism in the Iberian microplate recorded by fault-related denudation in the Spanish Central System (central Spain). *Tectonophysics* 349: 161–184.

De Vicente G, Giner JL, Muñoz Martin A, Gonzalez-Casado JM, and Lindo R (1996) Determination of present-day stress tensor and neotectonic interval in the Spanish Central System and Madrid Basin, central Spain. *Tectonophysics* 266: 405–424.

Decker K, Lillie B, and Tomek Č, (eds.) p. 293 (1998) PANCARDI: The lithospheric structure and evolution of the Pannonian/Carpathian/Dinarides region. *Tectonophysics* 297: 293p.

Desegaulx P, Kooi H, and Cloetingh S (1991) Consequences of foreland basin development on thinned continental lithosphere: application to the Aquitaine basin (SW France). *Earth and Planetary Science Letters* 106: 116–132.

Dewey JF (1988) Extensional collapse of orogens. *Tectonics* 7: 1123–1139.

Dewey JF and Burke K (1975) Hot-spots and continental break-up. *Geology* 2: 57–60.

Dèzes P, Schmid SM, and Ziegler PA (2004) Evolution of the European Cenozoic Rift System: Interaction of the Alpine and Pyrenean orogens with their foreland lithosphere. *Tectonophysics* 389: 1–33.

Dèzes P and Ziegler PA (2004) Moho depth map of western and central Europe. EUCOR-URGENT homepage: http://www.unibas.ch/eucor-urgent (acessed Jul 2007).

Dèzes P, Schmid SM, and Ziegler PA (2005) Reply to comments on 'Evolution of the European Cenozoic Rift System: Interaction of the Alpine and Pyrenean orogens with their foreland lithosphere. *Tectonophysics* 401: 257–262.

Dicea O (1996) Tectonic setting and hydrocarbon habitat of the Romanian external Carpathians. In: Ziegler PA and Horváth F (eds.) *Mémoires du Museum National d'Histoire Naturelle, 170, Peri-Tethys Memoir 2: Structure and Prospects of Alpine Basins and Forelands*, pp. 403–425. Paris: Commission for the Geological Map of the World.

Diehl T, Ritter JRR, and the CALIXTO group, (2005) The crustal structure beneath SE Romania from teleseismic receiver functions. *Geophysical Journal International* 163: 238–251.

Docherty C and Banda E (1995) Evidence for the eastward migration of the Alboran Sea based on regional subsidence analysis; a case for basin delamination of the subcrustal lithosphere? *Tectonics* 14: 804–814.

Doglioni C (1993) Comparison of subduction zones versus the global tectonic pattern: A possible explanation for the Alps-Carpathians system. *Geophysical Transaction* 37: 253–264.

Doré AG and Jensen LN (1996) The impact of late Cenozoic uplift and erosion on hydrocarbon exploration: offshore Norway and some other uplifted basins. *Global and Planetary Change* 12: 415–436.

Doré AG and Lundin ER (1996) Cenozoic compressional structures on the NE Atlantic margin: nature, origin and potential significance for hydrocarbon exploration. *Petroleum Geosciences* 2: 299–311.

Doré A, Augustson JH, Hermanrud C, Steward DJ, and Sylta O, (eds.) (1993) Basin modelling: Advances and applications. *Norwegian Petroleum Society, Special Publications* 3: 1–675.

Doré AG, Lundin ER, Birkeland O, Eliassen PE, and Jensen LN (1997) The NE Atlantic margin: implications of late Mesozoic and Cenozoic events for hydrocarbon prospectivity. *Petroleum Geoscience* 3: 117–131.

Doust H and Omatsola E (1989) Niger Delta. In: Edwards JD and Santogrossi PA (eds.) *American Association of Petroleum Geologists Memoirs, 48: Divergent Passive Margin Basins*, pp. 201–238. Tulsa: American Association of Petroleum Geologists.

Du ZJ, Michelini A, and Panza GF (1998) EurID, a regionalized 3-D seismological model of Europe. *Physics of the Earth and Planetary Interiors* 105: 31–62.

Dumitrescu I, Săndulescu M, and Bandrabur T (1970) Geological map scale 1:200,000, Sheet 29 Covasna. Bucharest: Geological Institute of Romania.

Dunbar JA and Sawyer DS (1989) How preexisting weaknesses control the style of rifting. *Journal of Geophysical Research* 94: 7278–7292.

Durand B, Jolivet L, Horváth F, and Séranne M (eds.) (1999) *Geological Society, London, Special Publications, 156: The Mediterranean basins: Tertiary extension within the Alpine orogen*, 570p. London: Geological Society, London.

Eide EA, Osmundsen PT, Meyer GB, Kendrick MA, and Corfu F (2002) The Nesna Shear zone, north-central Norway: An $^{40}Ar/^{39}Ar$ record of Early Devonian–Early Carboniferous ductile extension and unroofing. *Norwegian Journal of Geology* 82: 317–339.

Eisbacher GH, Lüschen E, and Wickert F (1989) Crustal-scale thrusting and extension in the Hercynian Schwarzwald and Vosges, Central Europe. *Tectonics* 8: 1–21.

Eldholm O, Thiede J, and Taylor E (1989) Evolution of the Vøring volcanic margin. In: Eldholm O, Thiede J, and Taylor E (eds.) *Proceedings of the Ocean Drilling Program, Scientific Results, 104*, pp. 1033–1065. College Station: Ocean Drilling Program.

Elfrink NM (2001) Quaternary groundwater avulsions: Evidence for large-scale midcontinent folding? *Association of Engineering Geologists News* 44: 60.

England P (1983) Constraints on extension of continental lithosphere. *Journal of Geophysical Research* 88: 1145–1152.

England P (1986) Comment on 'Brittle failure in the upper mantle during extension of the continental lithosphere' by DW Sawyer. *Journal of Geophysical Research* 91: 10487–10490.

Favre P and Stampfli GM (1992) From rifting to passive margin: the Red Sea, Central Atlantic and Alpine Tethys. *Tectonophysics* 215: 69–97.

Fernandes R, Ambrosius B, Noomen R, Basos L, and Davila J (2000) Analysis of a permanent GPS Iberian network (GIN). *10th General Assembly Wegener Project*, Extended Abstract.

Finetti I, Bricchi G, Del Ben A, Pipan M, and Xuan Z (1988) Geophysical study of the Black Sea basin. *Bollettino di Geofisica Teorica ed Applicata* 30: 197–324.

Fitzgerald PG, Munoz JA, Coney PJ, and Baldwin SL (1999) Asymmetric exhumation across the Pyrenean orogen: Implications for the tectonic evolution of a collisional orogen. *Earth and Planetary Science Letters* 173: 157–170.

Fleitout L and Froidevaux C (1982) Tectonics and topography for lithosphere containing density heterogeneities. *Tectonics* 1: 21–56.

Flemings PB and Jordan TE (1989) A synthetic stratigraphic model of foreland basins development. *Journal of Geophysical Research* 94: 3851–3866.

Fodor L, Csontos L, Bada G, Benkovics L, and Györfi I (1999) Tertiary tectonic evolution of the Carpatho-Pannonian region: A new synthesis of paleostress data. In: Durand B, Jolivet L, Horváth F, and Séranne M (eds.) *Geological Society, London, Special Publications, 156: The Mediterranean basins: Tertiary extension within the Alpine orogen*, pp. 295–334. London: Geological Society, London.

Fodor L, Bada G, Csillag G, *et al.* (2005) An outline of neotectonic structures and morphotectonics of the western and central Pannonian Basin. *Tectonophyiscs* 410: 15–41.

Ford M, Lockorish WH, and Kusznir NJ (1999) Tertiary foreland sedimentation in the Southern Subalpine Chains, SE France: A geodynamic appraisal. *Basin Research* 11: 315–336.

Forsyth D and Uyeda S (1975) On the relative importance of the driving forces of plate motions. *Geophysical Journal of the Royal Astronomical Society* 43: 163–200.

Franke W (2000) The Mid-European segment of the Variscides: tectonostratigraphic units, terrane boundaries and plate tectonic evolution. In: Franke W, Haak V, Oncken O, and Tanner D (eds.) *Geological Society, London, Special Publications, 179: Orogenic processes: Quantification and modelling in the Variscan Belt*, pp. 35–62. London: Geological Society, London.

Friend PF and Dabrio CJ, (eds.) (1996) Tertiary Basins of Spain. The stratigraphic record of crustal kinematics. In: *World and Regional Geology*, vol. 6, 418p. Cambridge: Cambridge University Press.

Frizon de Lamotte D, Mercier E, Saint Bezar B, and Bracène R (2000) Two step Atlas building and geodynamics of the West Mediterranean. *Tectonics* 19: 740–761.

Gabrielsen RH, Odinsen T, and Grunnaleite I (1999) Structuring of the Northern Viking Graben and the Møre Basin; the influence of basement structural grain, and the particular role of the Møre-Trøndelag Fault Complex. *Marine and Petroleum Geology* 16: 443–465.

Garcia-Castellanos D (2002) Interplay between lithospheric flexure and river transport in foreland basins. *Basin Research* 14: 89–104.

Garcia-Castellanos D, Cloetingh SAPL, and Van Balen RT (2000) Modeling the Middle Pleistocene uplift in the Ardennes–Rhenish Massif: thermo-mechanical weakening under the Eifel? *Global and Planetary Change* 27: 39–52.

Garcia-Castellanos D, Fernàndez M, and Torné M (2002) Modeling the evolution of the Guadalquivir foreland basin (southern Spain). *Tectonics* 21(3): 1018 (doi:10.1029/2001TC001339).

Garcia-Castellanos D, Vergés J, Gaspar-Escribano JM, and Cloetingh S (2003) Interplay between tectonics, climate and fluvial transport during the Cenozoic evolution of the Ebro Basin (NE Iberia). *Journal of Geophysical Research* 108: 2347.

Gaspar-Escribano JM, Van Wees J-D, Ter Voorde M, *et al.* (2001) 3D flexural modeling of the Ebro Basin (NE Iberia). *Geophysical Journal International* 145: 349–368.

Gaspar-Escribano JM, Garcia-Castellanos D, Roca D, and Cloetingh S (2004) Cenozoic vertical motions of the Catalan Coastal Ranges (NE Spain): The role of tectonics, isostasy, and surface transport. *Tectonics* 23: doi:10.1029/2003TC001511.

Genser J, Van Wees JD, Cloetingh S, and Neubauer F (1996) Eastern Alpine tectonometamorphic evolution: Constraints from two-dimensional P–T–t modeling. *Tectonics* 15: 584–604.

Gerbault M, Burov E, Poliakov ANB, and Daignieres M (1998) Do faults trigger folding in the lithosphere? *Geophysical Research Letter* 26: 271–274.

Gerner P, Bada G, Dövényi P, Müller B, Oncescu MC, Cloetingh S, and Horváth F (1999) Recent tectonic stress and crustal deformation in and around the Pannonian basin: Data and models. In: Durand B, Jolivet L, Horváth F, and Séranne M (eds.) *Geological Society, London, Special Publications, 156: The Mediterranean basins: Tertiary extension within the Alpine orogen*, pp. 269–294. London: Geological Society, London.

Gîrbacea R and Frisch W (1998) Slab in the wrong place Lower lithospheric mantle delamination in the last stage of the Eastern Carpathian subduction retreat. *Geology* 26: 611–614.

Goes S, Spakman W, and Bijwaard H (1999) A lower mantle source for Central European volcanism. *Science* 286: 1928–1930.

Goes S, Govers R, and Vacher P (2000a) Shallow upper mantle temperatures under Europe from P and S wave tomography. *Journal of Geophysical Research* 105: 11153–11169.

Goes S, Loohuis JJP, Wortel MJR, and Govers R (2000b) The effect of plate stresses and shallow mantle temperatures on tectonics of northwestern Europe. *Global and Planetary Change* 27: 23–39.

Gölke M and Coblentz DD (1996) Origin of the European regional stress field. *Tectonophysics* 266: 11–24.

Gölke M, Cloetingh S, and Coblentz DD (1996) Patterns of stress at the mid-Norwegian margin 62–68°N. *Tectonophysics* 266: 48–62.

Govers R and Wortel MJR (1993) Initiation of assymetric extension in continental lithosphere. *Tectonophysics* 223: 75–96.

Gradstein FM and Ogg JG (1996) A Phanerozoic time-scale. *Episodes* 19: 3–5.

Granet M, Wilson M, and Achauer U (1995) Imaging a mantle plume beneath the French Massif Central. *Earth and Planetary Science Letters* 136: 281–296.

Griffin WL, O'Reilly SY, and Pearson NY (1990) Eclogite stability near the crust–mantle boundary. In: Carswell DA (ed.) *Eclogite Facies Rocks*, pp. 291–314. New York: Blackie.

Grünthal G (1999) Seismic hazard assessment for Central, North and Northwest Europe: GSHAP Region 3. *Annali di Geophisica* 42: 999–1011.

Guggisberg B, Kaminski W, and Prodehl C (1991) Crustal structure of the Fennoscandian Shield: A traveltime interpretation of the long-range Fennolora seismic refraction profile. *Tectonophysics* 195: 105–137.

Harland WB, Armstrong RB, Cox AV, Craig LE, Smith AG, and Smith DG (1990) *A Geologic Time Scale*, 263p. Cambridge: Cambridge University Press.

Hauser F, Raileanu V, Fielitz W, Bala A, Prodehl C, Polonic G, and Schulze A (2001) VRANCEA99 – The crustal structure beneath the southeastern Carpathians and the Moesian Platform from a seismic refraction profile in Romania. *Tectonophysics* 340(3/4): 233–256.

Hegner F, Chen F, and Hann HP (2001) Chronology of basin closure and thrusting in the internal zone of the Variscan belt in the Schwarzwald, Germany: Evidence from zircon ages, trace element geochemistry, and Nd isotopic data. *Tectonophysics* 332: 169–184.

Hellinger SJ and Sclater JG (1983) Some comments on two-layer extensional models for sedimentary basins. *Journal of Geophysical Research B* 88: 8251–8269.

Hendriks BWH and Andriessen PAM (2002) Pattern and Timing of the Post-Caledonian Denudation of Northern Scandinavia Constrained by Apatite Fission Track Thermochronology. *Geological Society, London, Special Publication* 196: 117–137.

Henk A (1999) Did the Variscides collapse or were they torn apart? a quantitative evaluation of the driving forces for postconvergent extension in central Europe. *Tectonics* 18: 774–792.

Henk A, Von Blanckenburg F, Finger F, Schaltegger U, and Zulauf G (2000) Syn-convergent high-temperature metamorphism and magmatism in the Variscides: A discussion of potential heat sources. In: Franke W, Haak V, Oncken O, and Tanner D (eds.) *Geological Society, London, Special Publications, 179: Orogenic processes: Quantification and modelling in the Variscan belt*, pp. 387–399. London: Geological Society, London.

Hippolyte J-C, Badescu D, and Constantin P (1999) Evolution of the transport direction of the Carpathian belt during its collision with the east European Platform. *Tectonics* 18(6): 1120–1138.

Hoernle K, Zhang Y, and Graham D (1995) Seismic and geochemical evidence for large-scale mantle upwelling beneath the eastern Atlantic and western and central Europe. *Nature* 374: 34–39.

Holtedahl O (1953) On the oblique uplift of some northern lands. *Norges Geologiske Undersøkelse Bulletin* T14: 132–139.

Horváth F (1993) Towards a mechanical model for the formation of the Pannonian basin. *Tectonophysics* 226: 333–357.

Horváth F (1995) Phases of compression during the evolution of the Pannonian basin and its bearing on hydrocarbon exploration. *Marine and Petroleum Geology* 12: 837–844.

Horváth F and Cloetingh S (1996) Stress-induced late-stage subsidence anomalies in the Pannonian basin. *Tectonophysics* 266: 287–300.

Horváth F and Tari G (1999) IBS Pannonian basin project: a review of the main results and their bearings on hydrocarbon exploration. In: Durand B, Jolivet L, Horváth F, and Séranne M (eds.) *Geological Society, London, Special Publications, 156: The Mediterranean basins: Tertiary extension within the Alpine orogen*, pp. 195–213. London: Geological Society, London.

Horváth F, Stegena L, and Géczy B (1975) Ensimatic and ensialic interarc basins. *Journal of Geophysical Research* 80: 281–283.

Horváth F, Szalay Á, and Royden LH (1988) Subsidence, thermal and maturation history of the Great Hungarian Plain. In: Royden LH and Horváth F (eds.) *American Association of Petroleum Geologists Memoirs, 45: The Pannonian Basin: A case study in basin evolution*, pp. 355–372. Tulsa: American Association of Petroleum Geologists.

Horváth F, Bada G, Szafián P, Tari G, Ádám A, and Cloetingh S (2006) Formation and deformation of the Pannonian basin:

Constraints from observational data. In: Gee D and Stephenson R (eds.) *Geological Society, London, Memoirs, 32: European Lithosphere Dynamics*, pp. 191–206. London: Geological Society, London.

Houseman G and England P (1986) A dynamical model for lithosphere extension and sedimentary basin formation. *Journal of Geophysical Research* 91: 719–729.

Howard AD, Dietrich EW, and Seidl AM (1994) Modeling fluvial erosion on regional to continental scales. *Journal of Geophysical Research* 99: 13971–13986.

Huismans RS, Podlachikov YY, and Cloetingh S (2001a) The transition from passive to active rifting: relative importance of asthenospheric doming and passive extension of the lithosphere. *Journal of Geophysical Research* 106: 11271–11291.

Huismans R, Podladchikov Y, and Cloetingh S (2001b) Dynamic modeling of the transition from passive to active rifting, application to the Pannonian basin. *Tectonics* 20: 1021–1039.

Izotova TS and Popadyuk, IV (1996) Oiland gas accumulations in the Late Jurassicreefal complex of the West Ukrainian Carpathian fore deep. In: Ziegler PA and Horvàth F (eds.) *Mémoires du Museum National d'Histoire Naturelle, 170, Peri-Tethy Memoir 2: Structure and Prospects of Alpine Basins and Forelands*, pp. 375–390. Paris: Commission for the Geological Map of the World.

Janssen ME (1996) *Intraplate Deformation in Africa as a Consequence of Plate Boundary Changes*. PhD thesis, Vrije Universiteit, Amsterdam, 161p.

Janssen ME, Torne M, Cloetingh S, and Banda E (1993) Pliocene uplift of the eastern Iberian margin: inferences from quantitative modelling of the Valencia Trough. *Earth and Planetary Science Letters* 119: 585–597.

Janssen ME, Stephenson RA, and Cloetingh S (1995) Temporal and spatial correlations between changes in plate motions and the evolution of rifted basins in Africa. *Geological Society of America Bulletin* 107: 1317–1332.

Jarvis GT and McKenzie DP (1980) Sedimentary basin formation with finite extension rates. *Earth and Planetary Science Letters* 48: 42–52.

Johnson DD and Beaumont C (1995) Preliminary results from a planform kinematic model of orogen evolution, surface processes and the development of clastic foreland basin stratigraphy. In: Dorobek SL and Ross GM (eds.) *SEPM Special Publications, 52: Stratigraphic Evolution of Foreland Basins*, pp. 1–24. Tulsa: SEPM.

Jolivet L, Huchon P, and Rangin C (1989) Tectonic setting of Western Pacific marginal basins. *Tectonophysics* 160: 23–47.

Jones CH, Wernicke BP, Farmer LG, Coleman DS, McKenna LW, and Perry FV (1992) Variations across and along a major continental rift: an interdisciplinary study of the Basin and Range Province, Western USA. *Tectonophysics* 213: 57–96.

Jordt H, Faleide JI, Bjorlykke K, and Ibrahim MT (1995) Cenozoic sequence stratigraphy in the Central and Northern North Sea Basin: Tectonic development, sediment distribution and provenance areas. *Marine and Petroleum Geology* 12: 845–880.

Judenherc S, Granet M, Brun J-P, Poupinet G, Plomerova J, Mocquet A, and Achauer U (2002) Images of lithospheric heterogeneities in the Armorican segment of the Hercynian Range in France. *Tectonophysics* 358: 121–134.

Juez-Larré J and Andriessen PAM (2002) Post Late Paleozoic tectonism in the southern Catalan Coastal Ranges (NE Spain), assessed by apatite fission-track analysis. *Tectonophysics* 349: 367–368.

Juez-Larré J and Andriessen PAM (2006) Tectonothermal evolution of the northeastern margin of Iberia since the break-up of Pangea to present, revealed by low-temperature fission-track and (U-Th)/He thermochronology. A case history of the Catalan Coastal Ranges. *Earth and Planetary Science Letters* 243: 159–180.

Juhász E, Phillips L, Müller P, *et al.* (1999) Late Neogene sedimentary facies and sequences in the Pannonian Basin, Hungary. In: Durand B, Jolivet L, Horváth F, and Séranne M (eds.) *Geological Society, London, Special Publications, 156: The Mediterranean basins: Tertiary extension within the Alpine orogen*, pp. 335–356. London: Geological Society, London.

Kaikkonen P, Moiso K, and Heeremans M (2000) Thermomechanical lithospheric structure of the central Fennoscandian Shield. *Physics of the Earth and Planetary Interiors* 119: 209–235.

Karner GD, Egan SS, and Weissel JK (1992) Modelling the tectonic development of the Tucano and Sergipe-Alagoas rift basins, Brazil. *Tectonophysics* 215: 133–160.

Kazmin VG (1991) The position of continental flood basalts in rift zones and its bearing on models of rifting. *Tectonophysics* 199: 375–387.

Keen CE and Boutilier R (1990) Geodynamic modelling of rift basins: the syn-rift evolution of a simple half-graben. In: Pinet B and Bois C (eds.) *Collection Colloques et Séminaires,* 24: *The Potential of Deep Seismic Profiling for Hydrocarbon Exploration*, pp. 23–33. Paris: Editions Technip.

Kooi H (1991) Tectonic modelling of extensional basins: the role of lithospheric flexure, intraplate stresses and relative sea-level change. PhD Thesis, Vrije Universiteit, Amsterdam, 183p.

Kooi H and Beaumont C (1994) Escarpment evolution on high-elevation rifted margins: Insights derived from a surface processes model that combines diffusion, advection, and reaction. *Journal of Geophysical Research* 99: 12191–12209.

Kooi H and Beaumont C (1996) Large-scale geomorphology; classical concepts reconciled and integrated with contemporary ideas via a surface processes model. *Journal of Geophysical Research* 101: 3361–3386.

Kooi H and Cloetingh S (1989) Intraplate stresses and the tectono-stratigraphic evolution of the Central North Sea. In: Tankard AJ and Balkwill HR (ed.) *American Association of Petroleum Geologists Memoirs, 46: Extensional Tectonics and Stratigraphy of the North Atlantic Margins*, pp. 541–558. Tulsa: American Association of Petroleum Geologists.

Kooi H, Hettema M, and Cloetingh S (1991) Lithospheric dynamics and the rapid Pliocene-Quaternary subsidence in the North Sea basin. *Tectonophysics* 192: 245–259.

Kooi H, Cloetingh S, and Burrus J (1992) Lithospheric necking and regional isostasy at extensional basins: Part 1. Subsidence and gravity modelling with an application to the Gulf of Lions margin (SE France). *Journal of Geophysical Research* 97: 17553–17571.

Kováč M, Král J, Márton E, Plašienka D, and Uher P (1994) Alpine uplift history of the Central Western Carpathians: geochronological, paleomagnetic, sedimentary and structural data. *Geologica Carpathica* 45: 83–96.

Krzywiec P (2001) Contrasting tectonic and sedimentary history of the central and eastern parts of the Polish Carpathian Foredeep basin; results of seismic data interpretation. *Marine and Petroleum Geology* 18: 13–38.

Kühni A and Pfiffner OA (2001) Drainage patterns and tectonic forcing: A model study for the Swiss Alps. *Basin Research* 13: 169–197.

Kusznir NJ and Park RG (1987) The Extensional Strength of the Continental Lithosphere; its Dependence on Geothermal Gradient, and Crustal Composition and Thickness. *Geological Society, London, Special Publication* 28: 35–52.

Kusznir NJ and Ziegler PA (1992) Mechanics of continental extension and sedimentary basin formation: A simple-shear/

pure-shear flexural cantilever model. *Tectonophysics* 215: 117–131.

Kusznir NJ, Marsden G, and Egan SS (1991) A flexural-cantilever simple-shear/pure-shear model of continental lithosphere extension: Application to the Jeanne d'Arc Basin, Grand Banks and Viking Graben, North Sea. In: Roberts AM, Yielding G, and Freeman B (eds.) *Geological Society, London, Special Publications, 56: The Geometry of Normal Faults*, pp. 41–60. London: Geological Society, London.

Kusznir NJ, Stovba SM, Stephenson RA, and Poplavskii KN (1996) The formation of the northwestern Dniepr-Donets Basin: 2-D forward and reverse syn-rift and postrift modelling. *Tectonophysics* 268: 237–255.

Lagarde J-L, Baize S, Amorese D, Delcaillau B, and Font M (2000) Active tectonics, seismicity and geomorphology with special reference to Normandy (France). *Journal of Quaternary Science* 15: 745–758.

Lambeck K (1983) The role of compressive forces in intracratonic basin formation and mid-plate orogenies. *Geophysical Research Letters* 10: 845–848.

Lankreijer A (1998) Rheology and basement control on extensional basin evolution in Central and Eastern Europe: Variscan and Alpine-Carpathian-Pannonian tectonics. Ph.D thesis, Vrije Universiteit, Amsterdam, 158p.

Lankreijer A, Kovač M, Cloetingh S, Pitoňák P, Hlôška M, and Biermann C (1995) Quantitative subsidence analysis and forward modelling of the Vienna and Danube basins: thin-skinned versus thick-skinned extension. *Tectonophysics* 252: 433–451.

Lankreijer A, Mocanu V, and Cloetingh S (1997) Lateral variations in lithospheric strength in the Romanian Carpathians, constraints on basin evolution. *Tectonophysics* 272: 433–451.

Lankreijer A, Bielik M, Cloetingh S, and Majcin D (1999) Rheology predictions across the western Carpathians, Bohemian massif, and the Pannonian basin: Implications for tectonic scenarios. *Tectonics* 18: 1139–1153.

Lardeaux JM, Ledru P, Daniel I, and Duchène S (2001) The Variscan French Massif Central – A new addition to the ultra-high pressure metamorphic 'club': exhumation processes and geodynamic consequences. *Tectonophysics* 332: 143–162.

Larsen RM, Brekke H, Larsen BT, and Talleraas E (eds.) (1992)*Structural and tectonic modelling and its application to petroleum geology. Norwegian Petroleum Society, Special Publications*, 1: pp. 1–549.

Larsen TB, Yuen DA, and Storey M (1999) Ultrafast mantle plume and implications for flood basalt volcanism in the North Atlantic region. *Tectonophysics* 311: 31–43.

Laske G and Masters G (1997) A global digital map of sediment thickness. *EOS Transactions AGU* 78: F483.

Lawrence DT, Doyle M, and Aigner T (1990) Stratigraphic simulation of sedimentary basins: Concepts and calibration. *American Association of Petroleum Geologists Bulletin* 74: 273–295.

Le Pichon X, Henry P, and Goffé B (1997) Uplift of Tibet: from eclogite to granulite – implications for the Andean Plateau and the Variscan belt. *Tectonophysics* 273: 57–76.

Lefort J-P and Agarwal P (1996) Gravity evidence for an Alpine buckling of the crust beneath the Paris Basin. *Tectonophysics* 258: 1–14.

Lenkey L (1999) Geothermics of the Pannonian basin and its bearing on the tectonics of basin evolution. PhD thesis, Vrije Universiteit, Amsterdam, 215p.

Lenkey L, Dövényi P, Horváth F, and Cloetingh S (2002) Geothermics of the Pannonian basin and its bearing on the neotectonics. In: Cloetingh S, Horváth F, Bada G, and Lankreijer A (eds.) *EGU St. Mueller Special Publication Series, 3: Neotectonics and surface processes: The Pannonian basin and Alpine/Carpathian system* pp. 29–40. EGU.

Lenôtre N, Thierry P, Blanchin R, and Brochard G (1999) Current vertical movement demonstrated by comparative leveling in Brittany (France). *Tectonophysics* 301: 333–344.

Letouzey J (1986) Cenozoic paleo-stress pattern in the Alpine foreland and structural interpretation in a platform basin. *Tectonophysics* 132: 215–231.

Letouzey J, Werner P, and Marty A (1991) Fault reactivation and structural inversion. Backarc intraplate compressive deformations. Examples of the eastern Sunda shelf (Indonesia). *Tectonophysics* 183: 341–362.

Linzer HG (1996) Kinematics of retreating subduction along the Carpathian arc, Romania. *Geology* 24: 167–170.

Lobkovsky LI, Cloetingh S, Nikishin AM, *et al.* (1996) Extensional basins of the former Soviet Union – structure, basin formation mechanisms and subsidence history. *Tectonophysics* 266: 251–285.

Lorenz V and Nicholls IA (1984) Plate and intraplate processes of Hercynian Europe during the late paleozoic. *Tectonophysics* 107: 25–56.

Loup B and Wildi W (1994) Subsidence analysis in the Paris Basin: a key to Northwest European intracontinental basins? *Basin Research* 6: 45–62.

Lundin ER and Doré AG (1997) A tectonic model for the Norwegian passive margin with implications for the NE Atlantic: Early Cretaceous to break-up. *Journal of the Geological Society* 154: 545–550.

Manatschal G and Bernoulli D (1999) Architecture and tectonic evolution of nonvolcanic margins: present-day Galicia and ancient Adria. *Tectonics* 18: 1099–1119.

Mareschal J-C and Gliko A (1991) Lithospheric thinning, uplift, and heat flow preceding rifting. *Tectonophysics* 197: 117–126.

Marotta AM, Bayer U, and Thybo H (2000) The legacy of the NE German Basin – Reactivation by compressional buckling. *Terra Nova* 12: 132–140.

Martínez del Olmo W (1996) Depositional sequences in the Gulf of Valencia Tertiary Basin. In: Friend PF and Dabiro CJ (eds.) *Tertiary Basins of Spain, the Stratigraphic Record of Crustal Kinematics: World and Regional Geology*, pp. 55–67. New York: Cambridge University Press.

Marx J, Huebscher H-D, Hoth K, Korich D, and Kramer W (1995) Vulkanostratigraphie und Geochemie der Eruptivekomplexe. In: Plein E (ed.) *Courier Forschungsinstitut Senkenberg,* 183: *Norddeutsches Rotliegendbecken*, pp. 54–83. Devon: NHBS.

Mascle A, Puigdefàbregas C, Luterbacher HP, and Fernàandez M (eds.) (1998)*Cenozoic Foreland Basins of Western Europe. Geological Society, London, Special Publications*, 134: 427p.

Maţenco L and Bertotti G (2000) Tertiary tectonic evolution of the external East Carpathians (Romania). *Tectonophysics* 316: 255–286.

Maţenco L, Bertotti G, Dinu C, and Cloetingh S (1997a) Tertiary tectonic evolution of the external South Carpathians and the adjacent Moesian platform (Romania). *Tectonics* 16: 896–911.

Maţenco L, Zoetemeijer R, Cloetingh S, and Dinu C (1997b) Lateral variations in mechanical properties of the Romanian external Carpathians: inferences of flexure and gravity modelling. *Tectonophysics* 282: 147–166.

Maţenco L, Bertotti G, Cloetingh S, and Dinu C (2003) Subsidence analysis and tectonic evolution of the external Carpathian–Moesian Platform region during Neogene times. *Sedimentary Geology* 156: 71–94.

Maţenco L, Bertotti G, Leever K, *et al.* (2007) Large scale deformation in a locked collisional boundary: interplay between subsidence and uplift, intraplate stress and inherited lithospheric structure in the late stage of the SE Carpathians evolution. *Tectonics* submitted.

McHargue TR, Heidrick TL, and Livingston J (1992) Episodic structural development of the Central African Rift in Sudan. *Tectonophysics* 213: 187–202.

McKenzie DP (1978) Some remarks on the development of sedimentary basins. *Earth and Planetary Science Letters* 40: 25–32.

Meissner R and Bortfeld RK (eds.) (1990) *DEKORP-Atlas, Results of Deutsches Kontinentales Reflexionsseismisches Programm* 18p. and 80 plates, Berlin: Springer.

Meissner R and Rabbel W (1999) Nature of crustal reflectivity along the DEKORP profiles in Germany in comparison with reflection patterns from different tectonic units worldwide: A review. *Earth and Planetary Science Letters* 156: 7–28.

Mengel K, Sachs PM, Stosch HG, Wörner G, and Look G (1991) Crustal xenoliths from Cenozoic volcanic fields of West Germany: implication for structure and composition of the continental crust. *Tectonophysics* 195: 271–289.

Menning M (1995) A numerical time scale for the Permian and Triassic periods: an integrated time analysis. In: Scholle PA, Peryth TM, and Ulmer-Scholle DS (eds.) *The Permian of Northern Pangea*, vol. 1, pp. 77–97. Berlin: Springer.

Menning M, Weyer D, Drozodzewski G, van Ameron HWJ, and Wendt I (2000) A Carboniferous time scale, 2000: discussion and use of geological parameters as time indicators from Central and Western Europe. *Geologisches Jahrbuch A* 156: 3–44.

Mercier JL, Sebrier M, Lavenu A, *et al.* (1992) Changes in the tectonic regime above a subduction zone of Andean type: the Andes of Peru and Bolivia during the Pliocene–Pleistocene. *Journal of Geophysical Research* 97: 11945–11982.

Meulenkamp JE, Kováč M, and Cicha I (1996) On Late Oligocene to Pliocene depocentre migration and the evolution of the Carpathian–Pannonian system. *Tectonophysics* 266: 301–317.

Meyer W and Stets J (1998) Junge Tektonik in Rheinischen Schiefergebirge und ihre Quantifizierung. *Zeitschrift der Deutsches Geologisches Gesellschaft* 149: 359–379.

Millan H, Den Bezemer T, Verges J, *et al.* (1995) Paleo-elevation and EET evolution at mountain ranges: inferences from flexural modelling in the eastern Pyrenees and Ebro basin. *Marine and Petroleum Geology* 12: 917–928.

Mohr P (1992) Nature of the crust beneath magmatically active continental rifts. *Tectonophysics* 213: 269–284.

Moisio K, Kaikkonen P, and Beekman F (2000) Rheological structure and dynamical response of the DSS profile BALTIC in the SE Fennoscandian shield. *Tectonophysics* 320: 175–194.

Morgan P and Ramberg IB (1987) Physical changes in the lithosphere associated with thermal relaxation after rifting. *Tectonophysics* 143: 1–11.

Mörner N-A (2004) Active faults and palaeoseismicity in Fennoscandia, especially Sweden. Primary structures and secondary effects. *Tectonophysics* 380: 139–157.

Morton AC and Parson LM (1988) *Early Tertiary volcanism and the opening of the NE Atlantic. Geological Society, London, Special Publications* 39: 477p.

Mosar J (2003) Scandinavia's North Atlantic passive margin. *Journal of Geophysical Research* 108: 2630.

Mosar J, Lewis G, and Torsvik TH (2002) North Atlantic sea-floor spreading rates: implications for the Tertiary development of inversion structures of the Norwegian–Greenland Sea. *Journal of the Geological Society* 159: 503–515.

Munoz JA (1992) Evolution of a continental collision belt: ECORS-Pyrenees crustal balanced cross-section. In: McClay K (ed.) *Thrust Tectonics*, pp. 235–246. London: Chapman & Hall.

Nadin PA and Kusznir NJ (1995) Palaeocene uplift and Eocene subsidence in the northern North Sea basin from 2D forward and reverse stratigraphic modelling. *Journal of the Geological Society* 152: 833–848.

Nemcok M, Pospisil L, Lexa J, and Donelick RA (1998) Tertiary subduction and slab break-off model of the Carpathian–Pannonian region. *Tectonophysics* 295: 307–340.

Nemes F, Neubauer F, Cloetingh S, and Genser J (1997) The Klagenfurt Basin in the Eastern Alps: An intra-orogenic decoupled flexural basin? *Tectonophysics* 282: 189–203.

Neubauer F, Cloetingh S, Dinu C, and Mocanu V, (eds.) (1997) Tectonics of the Alpine-Carpathian–Pannonian region. *tectonophysics tectonophysics*, 272: 93–315.

Neumann E-R, Olsen KH, and Baldridge S (1995) The Oslo Rift. In: Olsen K H (ed.) *Continental Rifts: Evolution, Structure, Tectonics*, pp. 345–373. Amsterdam: Elsevier.

Neumann E-R, Wilson M, Heeremans M, *et al.* (2004) Carboniferous-Permian rifting and magmatism in southern Scandinavia, the North Sea and northern Germany: A review. In: Wilson M, Neumann E-R, Davies GR, Timmerman MJ, Heeremans M, and Larsen BT (eds.) *Geological Society, London, Special Publications, 223: Permo-Carboniferous Magmatism and Rifting in Europe*, pp. 11–40. London: Geological Society, London.

Nikishin AM, Cloetingh S, Lobkovsky L, and Burov EB (1993) Continental lithosphere folding in Central Asia (Part I): Constraints from geological observations. *Tectonophysics* 226: 59–72.

Nikishin AM, Ziegler PA, Panov DI, *et al.* (2001) Mesozoic and Cainozoic evolution of the Scythian Platform–Black Sea–Caucasus domain. In: Ziegler PA, Cavazza W, Robertson AHF, and Crasquin-Soleau S (eds.) *Peri-Tethys Mem. 6: Peri-Tethyan Rift/Wrench Basins and Passive Margins*, Mémoires du Museum National d'Histoire Naturelle, 186, pp. 295–346. Paris: Commission for the Geological Map of the World.

Nikishin AM, Ziegler PA, Abbott D, Brunet M-F, and Cloetingh S (2002) Permo-Triassic intraplate magmatism and rifting in Eurasia: implications for mantle plumes and mantle dynamics. *Tectonophysics* 351: 3–39.

Nikishin AM, Korotaev MV, Ershov AV, and Brunet M-F (2003) The Black Sea basin: tectonic history and Neogene-Quaternary rapid subsidence modelling. *Sedimentary Geology* 156: 1–10.

Nivière B and Winter T (2000) Pleistocene northwards fold propagation of the Jura within the southern Rhine Graben: seismotectonic implications. *Global and Planetary Change* 27: 263–288.

Nottvedt A, Gabrielsen RH, and Steel RJ (1995) Tectonostratigraphy and sedimentary architecture of rift basins with reference to the northern North Sea. *Marine and Petroleum Geology* 12: 881–901.

Odin GS (1994) Geologic time scale. *Comptes Rendus de l'Académie des Sciences* 318: 59–71.

Okaya N, Cloetingh S, and Mueller S (1996) A lithospheric cross section through the Swiss Alps (part II): Constraints on the mechanical structure of a continent–continent collision zone. *Geophysical Journal International* 127: 399–414.

Olesen O, Lundin ER, Nordgulen Ø, *et al.* (2002) Bridging the gap between the onshore and offshore geology in the Nordland area, northern Norway. *Norwegian Journal of Geology* 82: 243–262.

Olsen KH and Morgan P (1995) Introduction: progress in understanding continental rifts. In: Olsen KH (ed.) *Developments in Geotectonics, 25: Continental Rifts: Evolution, Structure, Tectonics*, pp. 3–26. Amsterdam: Elsevier.

Osmundsen PT, Sommaruga A, Skilbrei JR, and Olesen O (2002) Deep structure of the Norwegian Sea area, North Atlantic margin. *Norwegian Journal of Geology* 82: 205–224.

Oszczypko N (2006) Late Jurassic–Miocene evolution of the Outer Carpathian fold-and-thrust belt and its foredeep basin

(Western Carpathians, Poland). *Geological Quarterly* 50: 168–194.

Panza GF (1983) Lateral variations in the European lithosphere and seismic activity. *Physics of the Earth and Planetary Interiors* 33: 194–197.

Parnell J (*ed*.) (1994)*Geofluids: origin migration and evolution of fluids in sedimentary basins. Geological Society, London, Special Publications*, 78: 1–372.

Parsons T (1995) The Basin and Range Province. In: Olsen K H (ed.) *Developments in Geotectonics, 25: Continental Rifts: Evolution, Structure, Tectonics*, pp. 227–324. Amsterdam: Elsevier.

Pascal C and Gabrielsen RH (2001) Numerical modelling of Cenozoic stress patterns in the mid-Norwegian margin and the northern North Sea. *Tectonics* 20: 585–599.

Pavoni N (1993) Pattern of mantle convection and Pangea break-up, as revealed by the evolution of the African plate. *Journal of the Geological Society* 150: 953–964.

Peper T, Van Balen RT, and Cloetingh S (1994) Implications of orogenics wedge growth intraplates stress variations and sea level change for foreland basin stratigraphy: inferences from numerical modeling. In: Dorobek S and Ross G (eds.) *SEPM Special Publications, 52: Stratigraphic development in foreland basins*, pp. 25–35. Tulsa: SEPM.

Pérez-Gussinyé M and Watts AB (2005) The long-term strength of Europe and its implications for plate forming processes. *Nature* 436: doi:10.1038/nature03854.

Philip H (1987) Plio-Quaternary evolution of the stress field in Mediterranean zones of subduction and collision. *Annales Geophysicae* 5B: 301–320.

Plomerova J, Kouba D, and Babuska V (2002) Mapping the lithosphere-asthenosphere boundary through changes in surface-wave anisotropy. *Tectonophysics* 358: 175–185.

Posgay K, Bodoky T, Hegedüs E, *et al.* (1995) Asthenospheric structure beneath a Neogene basin in southeast Hungary. *Tectonophysics* 252: 467–484.

Price RA (1973) Large scale gravitational flow of supracrustal rocks, southern Canadian Rockies. In: de Jong K and Scholten RA (eds.) *Gravity and tectonics*, pp. 491–502. New York: Wiley.

Prijac C, Doin MP, Gaulier JM, and Guillaucheau F (2000) Subsidence of the Paris Basin and its bearing on the late Variscan lithosphere evolution: A comparison between the Plate and Chablis models. *Tectonophysics* 323: 1–38.

Quinlan G and Beaumont C (1984) Appalachian thrusting lithospheric flexure and the Paleozoic stratigraphy of the eastern interior of North America. *Canadian Journal of Earth Sciences* 21: 973–996.

Rădulescu F (1988) Seismic models of the crustal structure in Romania. *Revue Roumaine de Géologie, Géophysique et Géographie – Série de Géophysique* 32: 13–17.

Ranalli G (1995) *Rheology of the Earth*, 2nd Ed. 413p. London: Chapman and Hall.

Ranalli G and Murphy DC (1987) Rheological stratification of the lithosphere. *Tectonophysics* 132: 281–295.

Redfield TF, Osmundsen PT, and Hendriks BWH (2005) The role of fault reactivation and growth in the uplift of western Fennoscandia. *Journal of the Geological Society* 162: 1013–1030.

Reemst P (1995) Tectonic modeling of rifted continental margins; Basin evolution and tectono-magmatic development of the Norwegian and NW Australian margin. PhD thesis, Vrije Universiteit, Amsterdam, 163p.

Reemst P and Cloetingh S (2000) Polyphase rift evolution of the Vøring margin (mid-Norway): constraints from forward tectonostratigraphic modeling. *Tectonics* 19: 225–240.

Reilinger RE, McClusky SC, Oral MB, *et al.* (1997) Global positioning system measurements of present-day crustal movements in the Arabia-Africa-Eurasia plate collision zone. *Journal of Geophysical Research* 102: 9983–9999.

Reston TJ (1990) The lower crust and the extension of the continental lithosphere; kinematic analysis of BIRPS deep seismic data. *Tectonics* 9: 1235–1248.

Riba O, Reguant S, and Villena J (1983) Ensayo de síntesis estratigráfica y evolutiva de la cuenca terciaria del Ebro. *Geología de España, Libro Jubilar J. M. Rios, vol. II*, pp. 131–159. Madrid: Instituto Geológico y Minero de España.

Ribeiro A, Baptista JC, and Matias L (1996) Tectonic stress pattern in Portugal mainland and the adjacent Atlantic region (West Iberia). *Tectonics* 15: 641–659.

Richardson RM (1992) Ridge forces, absolute plate motions and the intra-plate stress field. *Journal of Geophysical Research* 97: 11739–11748.

Richter F and McKenzie D (1978) Simple plate models of mantle convection. *Journal of Geophysics* 44: 441–478.

Ritter JRR, Achauer U, and Christensen UR (2000) The teleseismic tomography experiment in the Eifel region, central Europe: design and first results. *Seismological Research Letters* 71: 437–443.

Ritter JRR, Jordan M, Christensen UR, and Achauer U (2001) A mantle plume below the Eifel volcanic fields, Germany. *Earth and Planetary Science Letters* 186: 7–14.

Roberts AM, Yielding G, Kusznir NJ, Walker I, and Don-Lopez D (1993) Mesozoic extension in the North Sea: constraints from flexural backstripping, forward modelling and fault populations. In: Parker JR (ed.) *Petroleum Geology of Northwest Europe*, Proceedings of the 4th Conference, pp. 1123–1136. London: Geological Society, London.

Robin C, Allemand P, Burov E, *et al.* (2003) Vertical movements of the Paris Basin (Triassic- Pleistocene): From 3D stratigraphic database to numerical models. In: Nieuwland DA (ed.) *Geological Society, London, Special Publications, 212: New Insights in Structural Interpretation and Modelling*, pp. 225–250. London: Geological Society, London.

Robinson A, Spadini G, Cloetingh S, and Rudat J (1995) Stratigraphic evolution of the Black Sea: Inferences from basin modelling. *Marine and Petroleum Geology* 12: 821–836.

Roca E (2001) The northwest Mediterranean Basin (Valencia Trough, Gulf of Lions and Liguro-Provencal basins): Structure and geodynamic evolution. In: Ziegler PA, Cavazza W, Robertson AHF, and Crasquin-Soleau S (eds.) *Peri-Tethys Memoir 6: Peri-Tethyan Rift/Wrench Basins and Passive Margins*, Mémoires du Museum National d'Histoire Naturelle, 186, pp. 671–706. Paris: Commission for the Geological Map of the World.

Roca E and Desegaulx P (1992) Analysis of the geological evolution and vertical movements in the Valencia Trough (western Mediterranean). *Marine and Petroleum Geology* 9: 167–185.

Roca E, Sans M, Cabrera L, and Marzo M (1999) Oligocene to middle Miocene evolution of the central Catalan margin (northwestern Mediterranean). *Tectonophysics* 315: 209–233.

Rohrman M and Van der Beek PA (1996) Cenozoic postrift domal uplift of North Atlantic margins; an asthenospheric diapirism model. *Geology* 24: 901–904.

Rohrman M, Van der Beek PA, Andriessen PAM, and Cloetingh S (1995) Meso-Cenozoic morphotectonic evolution of Southern Norway: Neogene domal uplift inferred from apatite fissiontrack thermochronology. *Tectonics* 14: 704–718.

Rohrman M, Van der Beek PA, Van der Hilst RD, and Reemst P (2002) Timing and Mechanism s of North Atlantic Cenozoic Uplift: Evidence for mantle upwelling. *Geological Society, London, Special Publications* 196: 27–43.

Rosenbaum G, Lister GS, and Duboz C (2002) Relative motion of Africa, Iberia and Europe during Alpine orogeny. *Tectonophysics* 359: 117–129.

Roure F and Sassi W (1995) Kinematics of deformation and petroleum system appraisal in Neogene foreland fold-and-thrust belts. *Petroleum Geoscience* 1: 253–269.

Roure F, Roca E, and Sassi W (1993) The Neogene evolution of the outer Carpathian flysch units (Poland, Ukraine and Romania): Kinematics of a foreland/fold-and-thrust belt system. *Sedimentary Geology* 86: 177–201.

Roure F, Brun J-P, Colletta B, and Vially R (1994) Multiphase extensional structures fold-reactivation and petroleum plays in the Alpine foreland basin of southeastern France. In: Mascle A (ed.) *Special Publication of the European Association of Petroleum Geoscientists 4: Exploration and Petroleum Geology of France*, pp. 237–260. Berlin: Springer.

Roure F, Choukroune P, and Polino R (1996a) Deep seismic reflection data and new insights on the bulk geometry of mountain ranges. *Comptes Rendus de l'Académie des Sciences* 322(IIa): 345–359.

Roure F, Shein VS, Ellouz N, and Skvortsov L (eds.) (1996b) *Geodynamic Evolution of Sedimentary Basins*, pp. 1–453. Paris: Editions Technip.

Rowley DB and Sahagian D (1986) Depth-dependent stretching: a different approach. *Geology* 14: 32–35.

Royden L (1988) Flexural behaviour of the continental lithosphere in Italy: constraints imposed by gravity and deflection data. *Journal of Geophysical Research* 93: 7747–7766.

Royden LH (1993) The tectonic expression of the slab pull at continental convergent boundaries. *Tectonics* 12: 303–325.

Royden LH and Dövényi P (1988) Variations in extensional styles at depth across the Pannonian basin system. In: Royden LH and Horváth F (eds.) *45: The Pannonian Basin: A Case Study in Basin Evolution*, pp. 235–255. Tulsa: American Association of Petroleum Geologists.

Royden LH and Horváth F (eds.) (1988)*The Pannonian Basin, A Study in Basin Evolution. American Association of Petroleum Geologists Memoirs*, 45: 394p.

Royden LH and Karner GD (1984) Flexure of lithosphere beneath the Apennine and Carpathian foredeep basins: Evidence for an insufficient topographic load. *Am Assoc Petrol Geol Buln* 68: 704–712.

Royden L and Keen CE (1980) Rifting process and thermal evolution of the continental margin of eastern Canada determined from subsidence curves. *Earth and Planetary Science Letters* 51: 343–361.

Royden L, Sclater JG, and Herzen RP (1980) Continental margin subsidence and heat flow; important parameters in formation of petroleum hydrocarbons. *American Association of Petroleum Geologists Bulletin* 62: 173–187.

Royden LH, Horváth F, Nagymarosy A, and Stegena L (1983) Evolution of the Pannonian Basin System. 2. Subsidence and thermal history. *Tectonics* 2: 91–137.

Rutigliano P and VLBI Network Team (2000) Vertical motions in the western Mediterranean area from geodetic and geological data. *Boll. Roa*, 3, *10th General Assembly Wegener Project*, Extended Abstract

Sacchi M, Horváth F, and Magyari O (1999) Role of unconformity-bounded units in the stratigraphy of the continental record: A case study from the Late Miocene of the western Pannonian Basin, Hungary. In: Durand B, Jolivet L, Horváth F, and Séranne M (eds.) *Geological Society, London, Special Publications, 156: The Mediterranean Basins: Tertiary Extension within the Alpine Orogen*, pp. 357–390. London: Geological Society, London.

Sachsenhofer RF, Lankreijer A, Cloetingh S, and Ebner F (1997) Subsidence analysis and quantitative basin modelling in the Styrian basin (Pannonian Basin System, Austria). *Tectonophysics* 272: 175–196.

Salveson JO (1976) Variations in the oil and gas geology of rift basins. *Egyptian General Petroleum Corp*, *5th Explor Sem*, *Cairo*, *Egypt*, *15–17 November*, *1976*

Sanders CAE, Andriessen PAM, and Cloetingh SAPL (1999) Life cycle of the East Carpathian orogen: Erosion history of a doubly vergent critical wedge assessed by fission track thermochronology. *Journal of Geophysical Research* 104: 29095–29112.

Săndulescu M (1984) *Geotectonics of Romania* (in Romanian) Bucharest: Editions Tehnica.

Săndulescu M (1988) Cenozoic tectonic history of the Carpathians. In: Royden LH and Horvath F (eds.) *American Association of Petroleum Geologists Memoirs, 45: The Pannonian Basin, A Study in Basin Evolution*, pp. 17–25. Tulsa: American Association of Petroleum Geologists.

Sanz de Siria Catalan A (1993) Datos sobre la paleoclimatologia y paleoecologia del Neogeno del Valles-Penedes segun las macrofloras halladas en la cuenca y zonas proximas. *Paleontologia i Evolució* 26–27: 281–289.

Sassi W, Colletta B, Bale P, and Paquereau T (1993) Modeling of structural complexity in sedimentary basins: The role of pre-existing faults in thrust tectonics. *Tectonophysics* 226: 97–112.

Sawyer DS and Harry DL (1991) Dynamic modeling of divergent margin formation: application to the US Atlantic margin. In: Meyer AW, Davies TA, and Wise SW (eds.) *Marine Geology 102: Evolution of Mesozoic and Cenozoic Continental Margins*, pp. 29–42. Amsterdam: Elsevier.

Schmid SM, Pfiffner OA, Froitzheim N, Schönborn G, and Kissling E (1996) Geophysical-geological transect and tectonic evolution of the Swiss–Italian Alps. *Tectonics* 12: 1036–1064.

Schmid SM, Berza T, Diaconescu V, Froitzheim N, and Fuegenschuh B (1998) Orogen-parallel extension in the South Carpathians during the Paleogene. *Tectonophysics* 297: 209–228.

Schmid SM, Fügenschuh B, Kissling E, and Schuster R (2004) Tectonic map and overall architecture of the Alpine orogen. *Eclogae Geologicae Helvetiae* 97: 93–117.

Schmid SM and Maţenco L (2007) An integrated cross section through the Carpathian system. *Tectonics* submitted.

Schlumberger (1991) World oil reserves – charting the future. *Middle East Well Evaluation Review* 10: 7–15.

Sclater JJG and Christie PAF (1980) Continental stretching: an explanation for the post mid-Cretaceous subsidence of the central North Sea basin. *Journal of Geophysical Research* 85: 3711–3739.

Sclater J, Royden L, Horváth F, Burchfiel B, Semken S, and Stegena L (1980) The formation of the intra-Carpathian basins as determined from subsidence data. *Earth and Planetary Science Letters* 51: 139–162.

Seber D, Barazangi M, Ibenbrahim A, and Demnati A (1996) Geophysical evidence for lithospheric delamination beneath the Alboran Sea and Rif-Betic mountains. *Nature* 379: 785–790.

Sengör AMC and Burke K (1978) Relative timing of rifting and volcanism on Earth and its tectonic implications. *Geophysical Research Letter* 5: 419–421.

Seyfert M and Henk A (2000) Deformation, metamorphism and exhumation: quantitative models for a collision zone in the Variscides. In: Franke W, Haak V, Oncken O, and Tanner D (eds.) *Orogenic Processes: Quantification and Modelling in the Variscan Belt*, Special Publication, 179, 217–230. London: Geological Society.

Shudofsky GN, Cloetingh S, Stein S, and Wortel MJR (1987) Unusually deep earthquakes in east Africa: constraints on the thermo-mechanical structure of a continental rift system. *Geophysical Research Letters* 14: 741–744.

Sibuet J-C, Srivastava SP, and Spakman W (2004) Pyrenean orogeny and plate kinematics. *Journal of Geophysical Research* 109: B08104 (doi:10.1029/2003JB002514).

Sinclair HD and Allen PA (1992) Vertical vs. horizontal motions in the Alpine orogenic wedge: Stratigraphic response in the foreland basin. *Basin Research* 4: 215–232.

Skogseid J and Eldholm O (1995) Rifted continental margin off mid-Norway. In: Banda E, Talwani E, and Torné M (eds.) *Rifted Ocean-Continent Boundaries*, pp. 147–153. Dordrecht: Kluwer Academic.

Skogseid J, Pedersen T, and Larsen VB (1992) Vøring Basin: subsidence and tectonic evolution. In: Larsen RM, Brekke H, Larsen BT, and Talleraas E (eds.) *Norwegian Petroleum Society, Special Publications 1: Structural and Tectonic Modelling and Its Application to Petroleum Geology*, pp. 55–82. Amsterdam: Elsevier.

Skogseid J, Planke S, Faleide JI, Pedersen T, Eldholm O, and Neverda FI (2000) NE Atlantic continental rifting and volcanic margin formation. *Geological Society, London, Special Publications* 167: 295–326.

Sleep NH (1971) Thermal effects of the formation of Atlantic continental margins by continental break up. *Geophysical Journal of the Royal Astronomical Society* 24: 325–350.

Sleep NH (1973) Crustal thinning on Atlantic coastal margins: evidence from old margins. In: Tarling DH and Runcorn SK (eds.) *Implications of Continental Drift to Earth Sciences*, Part 6, vol. 2, pp. 685–692. London: Academic Press.

Smolyaninova EI, Mikhailov VO, and Lyakhovsky VA (1996) Numerical modelling of regional neotectonic movements in the northern Black Sea. *Tectonophysics* 266: 221–231.

Sobel ER, Hilley GE, and Strecker MR (in press) Formation of internally drained contractional basins by aridity-limited bedrock incision. *Journal of Geophysical Research* 108(B7), 2344, doi:10.1029/2002JB001883.

Sobolev SV, Zeyen H, Granet M, *et al.* (1997) Upper mantle temperatures and lithosphere-asthenosphere system beneath the French Massif Central constrained by seismic, gravity, petrologic and thermal observations. *Tectonophysics* 275: 143–164.

Solheim A, Riis F, Elverhoi A, Faleide JJ, Jensen LN, and Cloetingh S, (eds.) (1996) Impact of glaciations on basin evolution and models for the Norwegian margin and adjacent areas. *Global Planet Change Global Planet Change*, 12: 1–450.

Sonder LJ and England PC (1989) Effects of a temperature-dependent rheology on large-scale continental extension. *Journal of Geophysical Research* 94: 7603–7619.

Spadini G (1996) Lithospheric deformation and vertical motions in back-arc Mediterranean basins: The Black Sea and the Tyrrhenian Sea. PhD Thesis, Vrije Universiteit, Amsterdam, 152p.

Spadini G and Podladchikov Y (1996) Spacing of consecutive normal faulting in the lithosphere: a dynamic model for rift axis migration. *Earth and Planetary Science Letters* 144: 21–34.

Spadini G, Bertotti G, and Cloetingh S (1995a) Tectono-stratigraphic modelling of the Sardinian margin of the Tyrrhenian Sea. *Tectonophysics* 252: 253–268.

Spadini G, Cloetingh S, and Bertotti G (1995b) Thermo-mechanical modeling of the Tyrrhenian Sea: Lithospheric necking and kinematics of rifting. *Tectonics* 14: 629–644.

Spadini G, Robinson A, and Cloetingh S (1996) Western versus eastern Black Sea tectonic evolution: Pre-rift lithospheric controls on basin formation. *Tectonophysics* 266: 139–154.

Spadini G, Robinson A, and Cloetingh S (1997) Thermo-mechanical modelling of Black Sea basin formation, subsidence and sedimentation. In: Robinson A (ed.) *American Association of Petroleum Geologists Memoirs, 68: Regional and Petroleum Geology of the Black Sea and Surrounding Areas*, pp. 19–38. Tulsa: American Association of Petroleum Geologists.

Spakman W and Wortel R (2004) A tomographoic view of the Western Mediterranean Geodynamics. In: Cavvaza W, Roure F, Spakman W, Stampfli GM, and Ziegler PA (eds.) The TRANSMED Atlas – The Mediterranean Region from Crust to Mantle and CD-ROM. pp. 31–52. Berlin: Springer.

Stampfli GM and Borel GD (2004) The TRANSMED transects in space and time: constraints on the paleotectonic evolution of the Mediterranean domain. In: Cavazza W, Roure F, Spakman W, Stampfli GM, and Ziegler PA (eds.) *The TRANSMED Atlas – The Mediterranean Region from Crust to Mantle*, pp. 53–80. Berlin: Springer.

Stampfli GM, Mosar J, Marquer D, Marchant R, Baudin T, and Borell G (1998) Subduction and obduction processes in the Swiss Alps. *Tectonophysics* 296: 159–204.

Stampfli GM, Mosar J, Favre P, Pillevuit A, and Vannay J-C (2001) Permo-Mesozoic evolution of the western Tethys realm: the Neo-Tethys East-Mediterranean connection. In: Ziegler PA, Cavazza W, Robertson AHF, and Crasquin-Soleau S (eds.) *Memoires du Museum National d'Histoire Naturelle 186: Peri-Tethys Memoir 6: Peri-Tethyan Rift/ Wrench Basins and Passive Margins*, pp. 51–108. Paris: Commission for the Geological Map of the World.

Stampfli GM, Borel GD, Marchant R, and Mosar J (2002) Western Alps geological constraints on western Tethyan reconstructions. *Journal of the Virtual Explorer* 8: 77–106.

Stapel G (1999) *The Nature of Isostasy in Western Iberia*. PhD thesis, Vrije Universiteit, Amsterdam, 148p.

Stapel G, Cloetingh S, and Pronk B (1996) Quantitative subsidence analysis of the Mesozoic evolution of the Lusitanian Basin (Western Iberian margin). *Tectonophysics* 266: 493–507.

Steckler MS and Ten Brink US (1986) Lithospheric strength variations as a control on new plate boundaries: Examples from the northern Red Sea region. *Earth and Planetary Science Letters* 79: 120–132.

Steckler MS and Watts AB (1978) Subsidence of the Atlantic-type continental margin off New York. *Earth and Planetary Science Letters* 41: 1–13.

Steckler MS and Watts AB (1982) Subsidence history and tectonic evolution of Atlantic-type continental margins. In: Scrutton RA (ed.) *Geodynamics Series 6: Dynamics of Passive Margins*, pp. 184–196. Washington, DC: Ameican Geophysical Union.

Stegena L (1967) The formation of the Hungarian basin. *Földtani Közlöny* 97: 278–285 (in Hungarian).

Stegena L, Géczy B, and Horváth F (1975) Late Cenozoic evolution of the Pannonian basin. *Földtani Közlöny* 105: 101–123 (in Hungarian).

Stel H, Cloetingh S, Heeremans M, and van Beek P (1993) Anorogenic granites, magmatic underplating and the origin of intracratonic basins in non-extensional settoing. *Tectonophysics* 226: 285–299.

Stephenson RA (1989) Beyond first-order thermal subsidence models for sedimentary basins? In: Cross TA (ed.) *Quantitative Dynamic Stratigraphy*, pp. 113–125. Englewood Cliffs, NJ: Prentice-Hall.

Stephenson RA and Cloetingh S (1991) Some examples and mechanical aspects of continental lithospheric folding. *Tectonophysics* 188: 27–37.

Stephenson RA, Stovba S, and Starostenko V (2001) Pripyat-Dniepr-Donets basin: implications for dynamics of rifting and tectonic history of the northern Peri-Tethyan platform. In: Ziegler PA, Cavazza W, Robertson AHF, and Crasquin-Soleau S (eds.) *Mémoires du Museum National d'Histoire Naturelle 186: Peri-Tethys Memoir 6, Peri-Tethyan Rift/ Wrench Basins and Passive Margins*, pp. 369–406. Paris: Commission for the Geological Map of the World.

Stockmal GS, Beaumont C, and Boutillier R (1986) Geodynamic models of convergent margin tectonics: transition from rifted margin to overthrust belt and consequences for foreland-basin development. *American Association of Petroleum Geologists Bulletin* 70: 181–190.

Straume ÅK and Austrheim H (1999) Importance of fracturing during retro-metamorphism of eclogites. *Journal of Metamorphic Geology* 7: 637–652.

Suhadolc P and Panza GF (1989) Physical properties of the lithosphere–asthenosphere system in Europe from geophysical data. In: Boriani A, Bonafede M, Piccardo GB, and Vai GB (eds.) *The Lithosphere in Italy – Advances in Earth Science Research*, vol 80, pp. 15–40. Rome: Accademia dei Lincei.

Suvorov VD, Mishenkina ZM, Petrick G, Sheludko IF, Seleznev VS, and Solovyov VM (2002) Structure of the crust in the Baikal rift zone and adjacent areas from Deep Seismic Sounding data. *Tectonophysics* 151: 61–74.

Szádeczky-Kardoss E (1967) Latest results of geological research in Hungary and its prospect in the light of international development. *Geológia és Bányászat* 1: 5–25 (in Hungarian).

Szafián P, Horváth F, and Cloetingh S (1997) Gravity constraints on the crustal structure and slab evolution along a transcarpathian transect. *Tectonophysics* 272: 233–247.

Tait JA, Bachtadse V, Franke W, and Soffel HC (1997) Geodynamic evolution of the European Variscan fold belt; paleomagnetic and geological constraints. *Geologische Rundschau* 86: 585–598.

Tărăpoancă M, Bertotti G, Maţenco L, Dinu C, and Cloetingh S (2003) Architecture of the Focsani depression: A 13 km deep basin in the Carpathians bend zone (Romania). *Tectonics* 22: 1074 (doi:10.1029/2002TC001486).

Tărăpoancă M, Garcia-Castellanos D, Bertotti G, Maţenco L, Cloetingh S, and Dinu C (2004a) Role of 3-D distributions of load and lithospheric strength in orogenic arcs: polystage subsidence in the Carpathians foredeep. *Earth and Planetary Science Letters* 221: 163–180.

Tari G, Dicea O, Faulkerson J, Georgiev G, Popov S, Stefanescu M, and Weir G (1997) Cimmerian and Alpine stratigraphy and structural evolution of the Moesian platform (Romania/Bulgaria). In: Robinson AG (ed.) *Regional and petroleum geology of the Black Sea and surrounding regions*, pp. 63–90. *Tulsa: Am Assoc Petrol Geol*.

Tari GD, övényi P, Dunkl I, *et al.* (1999) Lithospheric structure of the Pannonian basin derived from seismic, gravity and geothermal data. In: Durand B, Jolivet L, Horváth F, and Séranne M (eds.) *Geological Society London, Special Publications, 156: The Mediterranean Basins: Tertiary Extension within the Alpine Orogen*, pp. 215–250. London: Geological Society, London.

Tavares Martins L (1998) Continental tholeiitic magmatism of Algarve, southern Portugal; an examples of in situ crustal contamination. *Comunicacoes do Instituto Geologico e Mineiro, Lisbon, Portugal* 85: 99–116.

Ter Voorde M and Bertotti G (1994) Thermal effects of normal faulting during rifted basin formation, 1. A finite difference model. *Tectonophysics* 240: 133–144.

Ter Voorde M and Cloetingh S (1996) Numerical modelling of extension in faulted crust: effects of localized and regional deformation on basin stratigraphy. *Geological Society, London, Special Publications* 99: 283–296.

Ter Voorde M, Revnas ER, Faerseth R, and Cloetingh S (1997) Tectonic modelling of the Middle Jurasicsyn-rift stratigraphy in the Oseberg-Brage area, Southern Viking Graben. *Basin Research* 9: 133–150.

Ter Voorde M, Van Balen RT, Bertotti G, and Cloetingh SAPL (1998) The influence of a stratified rheology on the flexural response of the lithosphere to (un-)loading by extensional faulting. *Geophysical Journal International* 134: 721–735.

Ter Voorde M, de Bruijne K, Andriessen P, and Cloetingh S (2004) Thermal consequences of thrust faulting: simultaneous versus successive fault activation and exhumation. *Earth and Planetary Science Letters* 223(3–4): 395–413.

Torné M, Fernandez M, Wheeler W, and Karpuz R (2003) Three dimensional crustal structure of the Voring Margin (NE Atlantic): A combined seismic and gravity image. *Journal of Geophysical Research* 108: 2115.

Torsvik TH, Van der Voo R, Meert JG, Mosar J, and Walderhaug HJ (2001) Reconstructions of continents around the North Atlantic at about the 60th parallel. *Earth and Planetary Science Letters* 187: 55–69.

Tóth L, Mónus P, Zsíros T, and Kiszely M (2002) Seismicity in the Pannonian Region – earthquake data. In: Cloetingh S, Horváth F, Bada G, and Lankreijer A (eds.) *EGU St. Mueller Special Publication Series, 3: Neotectonics and Surface Processes: The Pannonian Basin and Alpine/Carpathian System* pp. 9–28. EGU.

Tucker GE and Slingerland RL (1994) Erosional dynamics, flexural isostasy, and long-lived escarpments: A numerical modeling study. *Journal of Geophysical Research* 99: 12229–12243.

Tucker GE and Slingerland RL (1996) Predicting sediment flux from fold and thrust belts. *Basin Research* 8: 329–349.

Turcotte DL and Emermann SH (1983) Mechanisms of active and passive rifting. *Tectonophysics* 94: 39–50.

Turcotte DL and Schubert G (1982) *Geodynamics.* New York: John Wiley.

Underhill JR and Partington MA (1993) Jurassic thermal doming and deflation in the North Sea: implications of the sequence stratigraphic evidence. In: Parker JR (ed.) *Petroleum Geology of Northwest Europe. Proceedings of the 4th Conference*, pp. 337–345. London: Geological Society.

Uyeda S and McCabe R (1983) A possible mechanism of episodic spreading of the Philippine Sea. In: Hashimoto M and Uyeda S (eds.) *Accretion Tectonics in the Circum-Pacific Regions*, Dordrecht: D. Reidel Publication, pp. 291–306. Tokyo: Terra Scientific Publication.

Vågnes E, Gabrielsen RH, and Haremo P (1998) Late Cretaceous-Cenozoic intraplate contractional deformation at the Norwegian continental shelf: timing, magnitude and regional implications. *Tectonophysics* 300: 29–46.

Vakarcs G, Vail PR, Tari G, Pogácsás Gy, Mattick RE, and Szabó A (1994) Third-order Miocene-Pliocene depositional sequences in the prograding delta complex of the Pannonian basin. *Tectonophysics* 240: 81–106.

Van Balen RT and Cloetingh S (1993) Intraplate stresses and fluid flow in extensional basins. *American Association of Petroleum Geologists Studies in Geology* 34: 87–98.

Van Balen RT and Cloetingh S (1994) Tectonic control of the sedimentary record and stress-induced fluid flow: constraints from basin modeling. *Geological Society, London, Special Publications* 78: 9–26.

Van Balen RT and Cloetingh S (1995) Neural network analyses of stress-induced overpressures in the Pannonian basin. *Geophysical Journal International* 121: 532–544.

Van Balen RT, Van der Beek PA, and Cloetingh S (1995) The effect of rift shoulder erosion on stratal patterns at passive margins: implications for sequence stratigraphy. *Earth and Planetary Science Letters* 134: 527–544.

Van Balen RT, Podladchikov Y, and Cloetingh S (1998) A new multi-layered model for intraplate stress-induced differential subsidence of faulted lithosphere, applied to rifted basins. *Tectonics* 17: 938–954.

Van Balen R, Lenkey L, Horváth F, and Cloetingh S (1999) Two-dimensional modelling of stratigraphy and compaction-driven fluid flow in the Pannonian basin. In: Durand B, Jolivet L, Horváth F, and Séranne M (eds.) *Geological Society, London, Special Publications, 156: The Mediterranean Basins: Tertiary Extension within the Alpine Orogen*, pp. 391–414. London: Geological Society, London.

Van Balen RT, Houtgast RF, Van der Wateren FM, Vandenberghe J, and Bogaart PW (2000) Sediment budget

and tectonic evolution of the Meuse catchment in the Ardennes and the Roer Valley Rift System. *Global and Planetary Change* 27: 113–129.

Van der Beek PA and Braun J (1998) Numerical modelling of landscape evolution on geological time-scales; a parameter analysis and comparison with the south-eastern highlands of Australia. *Basin Research* 10: 49–68.

Van der Beek P and Braun J (1999) Controls on post-Mid-Cretaceous landscape evolution in the southeastern highlands of Australia; insights from numerical surface process models. *Journal of Geophysical Research* 104: 4945–4966.

Van der Beek PA and Cloetingh S (1992) Lithospheric flexure and the tectonic evolution of the Betic Cordillers. *Tectonophysics* 203: 325–344.

Van der Beek PA, Cloetingh S, and Andriessen PAM (1994) Extensional basin formation mechanisms and vertical motion of rift flanks: Constraints from tectonic modelling and fission-track thermochronology. *Earth and Planetary Science Letters* 121: 417–433.

Van der Beek PA, Andriessen P, and Cloetingh S (1995) Morphotectonic evolution of rifted continental margins: inferences from a coupled tectonic-surface processes model and fission-track thermochronology. *Tectonics* 14: 406–421.

Van Vliet-Lanoë B, Laurent M, Everaerts M, Mansy J-L, and Manby G (2000) Evolution Neogene et quarternaire de la Somme, une flexuration tectonique active. *Comptes Rendus Academie des Sciences, Earth and Planetary Sciences* 331: 151–158.

Van Wees J-D (1994) *Tectonic Modelling of Basin Deformation and Inversion Dynamics: The Role of Pre-existing Faults and Continental Lithosphere Rheology in Basin Evolution*. PhD Thesis, Vrije Universiteit, Amsterdam, 164p.

Van Wees JD and Beekman F (2000) Lithosphere rheology during intraplate basin extension and inversion: Inferences from automated modelling of four basins in western Europe. *Tectonophysics* 320: 219–242.

Van Wees J-D and Cloetingh S (1994) A finite-difference technique to incorporate spatial variations in rigidity and planar faults into 3-D models for lithospheric flexure. *Geophysical Journal International* 117: 179–195.

Van Wees J-D and Cloetingh S (1996) 3D flexure and intraplate compression in the North Sea basin. *Tectonophysics* 266: 343–359.

Van Wees J-D and Stephenson RA (1995) Quantitative modelling of basin and rheological evolution of the Iberian Basin (Central Spain): Implications for lithosphere dynamics of intraplate extension and inversion. *Tectonophysics* 252: 163–178.

Van Wees J-D, de Jong K, and Cloetingh S (1992) Two-dimensional P-T-t modelling and dynamics of extension and inversion in the Betic Zone (SE Spain). *Tectonophysics* 203: 305–324.

Van Wees J-D, Stephenson RA, Stovba SM, and Shymanovsky VA (1996) Tectonic variation in the Dniepr–Donets Basin from automated modelling and backstripped subsidence curves. *Tectonophysics* 268: 257–280.

Van Wees JD, Arche A, Beijdorff CG, Lopez-Gomez J, and Cloetingh S (1998) Temporal and spatial variations in tectonic subsidence in the Iberian basin (eastern Spain): Inferences from automated forward modelling of high-resolution stratigraphy. (Permian–Mesozoic). *Tectonophysics* 300: 285–310.

Van Wees J-D, Stephenson RS, Ziegler PA, *et al.* (2000) On the origin of the Southern Permian Basin, Central Europe. *Marine and Petroleum Geology* 17: 43–59.

Van Wijk JW and Cloetingh S (2002) Basin migration caused by slow lithospheric extension. *Earth and Planetary Science Letters* 198: 275–288.

Van Wijk JW, Huismans RS, Ter Voorde M, and Cloetingh S (2001) Melt generation at volcanic continental margins: no need for a mantle plume? *Geophysical Research Letters* 28: 3995–3998.

Vanderhaeghe O and Teyssier C (2001) Partial melting and flow of orogens. *Tectonophysics* 342: 451–472.

Vasiliev I, Krijgsman W, Langereis CG, Panaiotu CE, Maţenco L, and Bertotti G (2004) Magnetostratigraphyc dating and astronomical forcing of the Mio-Pliocene sedimentary sequences of the Focsani basin (Eastern Paratethys – Romania). *Earth and Planetary Science Letters* 227: 231–247.

Vauchez A, Tommasi A, and Barruol G (1998) Rheological heterogeneity, mechanical anisotropy and deformation of the continental lithosphere. *Tectonophysics* 296: 61–86.

Verall P (1989) Speculations on the Mesozoic–Cenozoic tectonic history of the Western United States. In: Tankard AJ and Balkwill HR (eds.) *American Association of Petroleum Geologists Memoirs, 46: Extensional Tectonics and Stratigraphy of the North Atlantic Margins*, pp. 615–631. Tulsa: American Association of Petroleum Geologists.

Vergés JM and Garcia-Senez J (2001) Mesozoic evolution and Cainozoic inversion of the Pyrenean rift. In: Ziegler PA, Cavazza W, Robertson AHF, and Crasquin-Soleau S (eds.) *Mémoires du Museum National d'Histoire Naturelle 186: Peri-Tethys Memoir 6, Peri-Tethyan Rift/Wrench Basins and Passive Margins*, pp. 187–212. Paris: Commission for the Geological Map of the World.

Vergés J and Sàbat F (1999) Constraints on the western Mediterranean kinematics evolution along a 1000-km transect from Iberia to Africa. In: Durand B, Jolivet L, Horváth F, and Seranne M (eds.) *Geological Society, London, Special Publications, 156: The Mediterranean Basins: Tertiary Extension within the Alpine Orogen*, pp. 63–80. London: Geological Society, London.

Vergés J, Millan H, Roca E, *et al.* (1995) Evolution of a collisional orogen: eastern Pyrenees transect and petroleum potential. *Marine and Petroleum Geology* 12: 903–916.

Vergés JM, Marzo M, Santaeularia T, Serra-Kiel J, Burbank DW, Munoz JA, and Gimenez-Montsant J (1998) Quantified vertical motions and tectonic evolution of the SE Pyrenean foreland basin. *Geological Society, London, Special Publications* 134: 107–134.

Vigneresse JL (1999) Intrusion level of granitic massifs along the Hercynian belt: balancing the eroded crust. *Tectonophysics* 307: 277–295.

Vyssotski AV, Vyssotski NV, and Nezhdanov AA (2006) Evolution of the West Siberian Basin. *Marine and Petroleum Geology* 23: 93–126.

Waltham D, Docherty C, and Taberner C (2000) Decoupled flexure in the South Pyrenean foreland. *Journal of Geophysical Research* 105: 16329–16340.

Watcharanantakul R and Morley CK (2000) Syn-rift and postrift modelling of the Pattani basin, Thailand: evidence for ramp-flat detachment. *Marine and Petroleum Geology* 17: 937–958.

Watts AB (2001) *Isostasy and Flexure of the Lithosphere*, 458p. Cambridge: Cambridge University Press.

Watts AB and Burov EB (2003) Lithospheric strength and its relationship to the elastic and seismogenic layer thickness. *Earth and Planetary Science Letters* 213: 113–131.

Watts AB and Fairhead JD (1997) Gravity anomalies and magmatism along the western continental margin of the British Isles. *Journal of the Geological Society* 154: 523–529.

Watts AB, Karner GD, and Steckler MS (1982) Lithospheric flexure and the evolution of sedimentary basins. Kent P, Bott MHP, McKenzie DP, and Williams CA (eds.) *The Evolution of Sedimentary Basins. Philosophical Transactions of The Royal Society A*, 305, pp. 249–281.

Watts AB, Platt J, and Buhl P (1993) Tectonic evolution of the Alboran Sea basin. *Basin Research* 5: 153–177.

Wenzel F, Lorenz F, Sperner B, and Oncescu MC (1999) Seismotectonics of the Romanian Vrancea area. In: Wenzel F, Lungu D, and Novak O (eds.) *Vrancea Earthquakes: Tectonics, Hazard and Risk Mitigation*, pp. 15–26. Dordrecht: Kluwer Academic.

Wenzel F, Sperner B, Lorenz F, and Mocanu V (2002) Geodynamics, tomographic images and seismicity of the Vrancea region (SE-Carpathians, Romania). *EGU Stephan Mueller Special Publication Series* 3: 95–104.

Wernicke B (1985) Uniform-sense normal simple shear of the continental lithosphere. *Canadian Journal of Earth Sciences* 22: 108–125.

Wernicke B (1990) The fluid crustal layer and its implication for continental dynamics. In: Salisbury MH and Fountein DM (eds.) *Exposed Cross-Sections of the Continental Crust*, pp. 509–544. Dordrecht: Kluwer Academic.

Whipple KX and Tucker GE (1999) Dynamics of the stream-power river incision model; implications for height limits of mountain ranges, landscape response timescales, and research needs. *Journal of Geophysical Research* 104: 17661–17674.

White N and McKenzie D (1988) Formation of the 'steer's head' geometry of sedimentary basins by differential stretching of the crust and mantle. *Geology* 16: 250–253.

White RS and McKenzie DP (1989) Volcanism at rifts. *Scientific American* 201: 44–59.

Whittaker A, Bott MHP, and Waghorn GD (1992) Stresses and plate boundary forces associated with subduction plate margins. *Journal of Geophysical Research* 97: 11933–11944.

Willet SD (1999) Orogeny and orography: The effects of erosion on the structure of mountain belts. *Journal of Geophysical Research* 104: 28957–28981.

Willgoose G, Bras RL, and Rodriguez-Iturbe I (1991) A physically based coupled channel network growth and hillslope evolution model (3 sections). *Water Resources Research* 27: 1671–1702.

Wilson M (1993a) Geochemical signature of oceanic and continental basalts: a key to mantle dynamics. *Journal of the Geological Society* 150: 977–990.

Wilson M (1993b) Magmatism and the geodynamics of basin formation. *Sedimentary Geology* 86: 5–29.

Wilson M (1997) Thermal evolution of the Central Atlantic passive margins: continental break-up above a Mesozoic super-plume. *Journal of the Geological Society* 154: 491–495.

Wilson M and Bianchini G (1999) Tertiary–Quaternary magmatism within the Mediterranean and surrounding regions. In: Durand B, Jolivet L, Horváth F, and Séranne M (eds.) *Geological Society, London, Special Publication, 156: The Mediterranean Basin: Tertiary Extension within the Alpine Orogen*, pp. 141–168. London: Geological Society, London.

Wilson M and Patterson R (2001) Intraplate magmatism related to short-wavelength convective instabilities in the upper mantle: Evidence from the Tertiary-Quaternary volcanic province of western and central Europe. *Geological Society of America Special Paper* 352: 37–58.

Wilson M, Rosenbaum JM, and Dunworth EA (1995) Melilites: partial melts of the thermal boundary layer? *Journal of Petrology* 32: 181–196.

Wittenberg A, Vellmer C, Kern H, and Mengel K (2000) The Variscan lower continental crust: evidence for crustal delamination from geochemical and petrological investigations. In: Franke W, Haak V, Oncken O, and Tanner D (eds.) *Geological Society, London, Special Publication, 179: Orogenic Processes: Quantification and Modelling in the Variscan Belt*, pp. 401–414. London: Geological Society, London.

Worrall DM and Snelson S (1989) Evolution of the northern Gulf of Mexico, with emphasis on Cenozoic growth faulting and the role of salt. In: Bally AW and Palmer AR (eds.) *The Geology of North America – An Overview, The Geology of North America, A*, pp. 97–138. Boulder, CO: Geological Society of America.

Wortel R and Spakman W (2000) Subduction and slab detachment in the Mediterranean–Carpathian region. *Science* 290: 1910–1917.

Yegorova TP, Stephenson RA, Kozlenko VG, Starostenko VI, and Legostaeve OV (1999) 3-D gravity analysis of the Dniepr–Donets Basin and Donbas Foldbelt, Ukraine. *Tectonophysics* 313: 41–58.

Zeck HP, Monie P, Villa IM, and Hansen BT (1992) Very high rates of cooling and uplift in the Alpine belt of the Betic Cordilleras, southern Spain. *Geology* 20: 79–82.

Zeyen H, Volker F, Wehrle V, Fuchs K, Sobolev SV, and Altherr R (1997) Styles of continental rifting; crust-mantle detachment and mantle plumes. *Tectonophysics* 278: 329–352.

Ziegler PA (1983) Crustal thinning and subsidence in the North Sea. *Nature* 304: 561p.

Ziegler PA (1987) Compressional intra-plate deformations in the Alpine foreland – An introduction. *Tectonophysics* 137: 1–5.

Ziegler PA 1988 Evolution of the Arctic-orth Atlantic and the western Tethys, *American Association of Petroleum Geologists Memoir*, 43: 198p.

Ziegler PA (1989a) Evolution of the North Atlantic; an overview. *American Association of Petroleum Geologists Memoir* 46: 111–129.

Ziegler PA (1989b) *Evolution of Laurussia. A study in Late Palaeozic Plate Tectonics*, 102p. Dordrecht: Kluver Academic.

Ziegler PA (1990a) Collision related intraplate compression deformations in western and central Europe. *Journal of Geodynamics* 11: 357–388.

Ziegler PA (1990b) *Geological Atlas of Western and Central Europe,* 2nd edn., 239p. Bath: Shell Internationale Petroleum Maatschappij BV.

Ziegler PA (1992) Geodynamics of rifting and implications for hydrocarbon habitat. *Tectonophysics* 215: 221–253.

Ziegler PA (1993) Plate moving mechanisms: their relative importance. *Journal of the Geological Society* 150: 927–940.

Ziegler PA (1994) Cenozoic rift system of Western and Central Europe: An overview. *Geologie en Mijnbouw* 73: 99–127.

Ziegler PA (1996a) Hydrocarbon habitat in rifted basins. In: Roure F, Ellouz N, Shein VS, and Skvortsov I (eds.) *Geodynamic Evolution of Sedimentary Basins*, pp. 85–94. Paris: Editions Technip.

Ziegler PA (1996b) Geodynamic processes governing development of rifted basins. In: Roure F, Ellouz N, Shein VS, and Skvortsov L (eds.) *Geodynamic Evolution of Sedimentary Basins*, pp. 19–67. Paris: Editions Technip.

Ziegler PA and Cloetingh S (2004) Dynamic processes controlling evolution of rifted basins. *Earth-Science Reviews* 64: 1–50.

Ziegler PA and Dèzes P (2005) Evolution of the lithosphere in the area of the Rhine Rift System. Behrmann JH, Granet M, Schmid S, and Ziegler PA (eds.) *EUCOR-URGENT Special Issue. International Journal of Earth Sciences*, 94, pp. 594–614.

Ziegler PA and Dèzes P (2006) Crustal evolution of Western and Central Europe. In: Gee DG and Stephenson RA (eds.) *Geological Society, London, Memoirs, 32: European Lithosphere Dynamics*, pp. 43–56. London: Geological Society, London.

Ziegler PA and Dèzes P 2007. Cenozoic uplift of Variscan Massifs in the Alpine foreland: Timing and controlling mechanisms. *Global and Planetary Change*, 58(1-4), 237–269.

Ziegler PA and Horváth F (eds.) (1996) *Mémoires du Museum National d'Histoire Naturelle, 170: Peri-Tethys Memoir 2: Structure and Prospects of Alpine Basins and Forelands,* 547p.

Ziegler PA and Roure F (eds.) (1996) *Architecture and petroleum systems of the Alpine orogen and associated basins. Mémoires du Museum National d'Histoire Naturelle, vol 170 Peri–Tethys Mem*, vol 2. Paris: Commission for the Geological Map of the World.

Ziegler PA and Stampfli GM (2001) Late Palaeozoic–Early Mesozoic plate boundary reorganization: collapse of the Variscan orogen and opening of Neotethys. In: Cassinis G (ed.) *Natura Bresciana, Monografia 25: Permian continental deposits of Europe and other areas. Regional reports and Correlations*, pp. 17–34. Brescia: Museo Civico di Scienze Naturali di Brescia.

Ziegler PA, Cloetingh S, and van Wees J-D (1995) Dynamics of intraplate compressional deformation: the Alpine foreland and other examples. *Tectonophysics* 252: 7–59.

Ziegler PA, Van Wees J-D, and Cloetingh S (1998) Mechanical controls on collision-related compressional intraplate deformation. *Tectonophysics* 300: 103–129.

Ziegler PA, Cloetingh S, Guiraud R, and Stampfli GM (2001) Peri-Tethyan platforms: constraints on dynamics of rifting and basin inversion. In: Ziegler PA, Cavazza W, Robertson AHF, and Crasquin-Soleau S (eds.) *Peri-Tethys Memoir 6: Peri-Tethyan Rift/Wrench Basins and Passive Margins, Mémoires du Museum National d'Histoire Naturelle*, 186, pp. 9–49. Paris: Commission for the Geological Map of the World.

Ziegler PA, Bertotti G, and Cloetingh S (2002) Dynamic processes controlling foreland development—the role of mechanical (de)coupling of orogenic wedges and forelands. In: Bertotti G, Schulmann K, and Cloetingh SAPL (eds.) *EGU St. Muller Special Publication Series, 1: Continental Collision and the Tectono-Sedimentary Evolution of Forelands,* pp. 17–56. EGU.

Ziegler PA, Schumacher ME, Dèzes P, van Wees J-D, and Cloetingh S (2004) Post-Variscan evolution of the lithosphere in the Rhine Graben area: constraints from subsidence modelling. In: Wilson M, Neumann E-R, Davies GR, Timmerman MJ, Heeremans M, and Larsen BT (eds.) *Geological Society, London, Special Publications, 223: Permo-Carboniferous Magmatism and Rifting in Europe*, pp. 289–317. London: Geological Society, London.

Ziegler PA, Schumacher ME, Dézes P, van Wees J-D, and Cloetingh S (2006) Post-Variscan evolution of the lithosphere in the area of the European Cenozoic Rift System. In: Gee DG and Stephenson RA (eds.) *European Lithosphere Dynamics*, 32, pp. 97–112. London, Mem: Geol Soc.

Zoback MD, Stephenson RA, Cloetingh S, *et al.* (1993) Stresses in the lithosphere and sedimentary basin formation. *Tectonophysics* 226: 1–13.

Zoback ML (1992) First and second order patterns of stress in the lithosphere: the World Stress Map Project. *Journal of Geophysical Research* 97: 11703–11728.

Zoetemeijer R, Desegaulx P, Cloetingh S, Roure F, and Morett I (1990) Lithospheric dynamics and tectonic–stratigraphic evolution of the Ebro basin. *Journal of Geophysical Research* 95: 2701–2711.

Zoetemeijer R, Cloetingh S, Sassi W, and Roure F (1993) Modelling of piggy-back basin stratigraphy: record of tectonic evolution. *Tectonophysics* 226: 253–269.

Zoetemeijer R, Tomek C, and Cloetingh S (1999) Flexural expression of European continental lithosphere under the western outer Carpathians. *Tectonics* 18: 843–861.